FINITE ELEMENT ANALYSIS ON HEAT FLOW BASED ON HEATLINE CONCEPT FOR MHD FREE CONVECTION WITHIN TRAPEZOIDAL CAVITY

by

Muhammad Sajjad Hossain
Student No. 0409093005P
Registration No. 0409093005, Session: April-2009

MASTER OF PHILOSOPHY
IN
MATHEMATICS

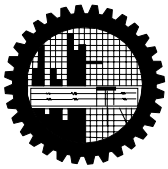

Department of Mathematics
Bangladesh University of Engineering and Technology (BUET),
Dhaka-1000
July - 2012

The thesis titled

FINITE ELEMENT ANALYSIS ON HEAT FLOW BASED ON HEATLINE CONCEPT FOR MHD FREE CONVECTION WITHIN TRAPEZOIDAL CAVITY

Submitted by

Muhammad Sajjad Hossain
Student No. 0409093005P, Registration No. 0409093005, Session: April-2009, a part time student of M. Phil. (Mathematics) has been accepted as satisfactory in partial fulfillment for the degree of

Master of Philosophy in Mathematics

On 01 July, 2012.

BOARD OF EXAMINERS

1. _____
   Dr. Md. Abdul Alim — Chairman
   Associate Professor — (Supervisor)
   Dept. of Mathematics, BUET, Dhaka-1000

2. _____
   Head
   Dr. Md. Elias — Member
   Dept. of Mathematics — (Ex-Officio)
   BUET, Dhaka-1000

3. _____
   Dr. Md. Mustafa Kamal Chowdhury — Member
   Professor
   Dept. of Mathematics, BUET, Dhaka-1000

4. _____
   Dr. Md. Abdul Maleque — Member
   Professor
   Dept. of Mathematics, BUET, Dhaka-1000

5. _____
   Dr. Md. Ashraf Uddin — Member
   Professor — (External)
   Department of Mathematics
   Shahjalal University of Science & Technology, Sylhet-3114

AUTHOR'S DECLARATION

I hereby announce that the work which is being presented in this thesis entitled

"FINITE ELEMENT ANALYSIS ON HEAT FLOW BASED ON HEATLINE CONCEPT FOR MHD FREE CONVECTION WITHIN TRAPEZOIDAL CAVITY"

submitted in partial fulfillment of the requirements for the decoration of the degree of Master of Philosophy, department of Mathematics, BUET, Dhaka, is an authentic record of my own work.

The work is also original except where indicated by and attached with special reference in the context and no part of it has been submitted for any attempt to get other degrees or diplomas.

All views expressed in the dissertation are those of the author and in no way or by no means represent those of Bangladesh University of Engineering and Technology, Dhaka. This dissertation has not been submitted to any other University for examination either in home or abroad.

(Muhammad Sajjad Hossain)
Date: 01 July, 2012

PERMIT OF RESEARCH

This is to endorse that the work presented in this thesis is carried out by the author under the supervision of Dr. Md. Abdul Alim, Associate Professor, Department of Mathematics, Bangladesh University of Engineering & Technology, Dhaka.

Dr. Md. Abdul Alim **Muhammad Sajjad Hossain**

Dedicated to,

My Parents, Wife & Beloved Daughter

ACKNOWLEDGEMENT

I would like to affirm the notable recognizance of Almighty's continual mercy, because no work would have been possible to accomplish the goal line without help of Allah. With great pleasure the author takes this opportunity to place on record her deepest respect and sincerest gratitude to his Supervisor Dr. Md. Abdul Alim, Associate Professor, Department of Mathematics, Bangladesh University of Engineering and Technology, Dhaka for his expert guidance and valuable suggestions throughout this work. It would not have been possible to carry out this study successfully without continuous inspiration, guidance, constant support, intuitive suggestions and relentless encouragement from supervisor.

I am also deeply indebted to Professor and Head Dr. Md. Elias, Head of the Department of Mathematics, Prof. Dr. Md. Mustafa Kamal Chowdhury, and Prof. Dr. Md. Abdul Maleque, Department of Mathematics, BUET for their wise and liberal co-operation in providing me all necessary help from the department during my course of M.Phil. Degree. I wish to thank to the all staff of the Department of Mathematics, Bangladesh University of Engineering and Technology, for their cooperation in this work.

I am in debt of gratitude to Md. Nasir Uddin, Aki Farhana, M.Phil. Student, Department of Mathematics, BUET, who have assisted me by providing relevant books, programming and valuable suggestions.

Finally I express my devoted affection to my wife Mrs. Niger Sultana Pami, my beloved daughter Ummay Salma Hossain and all of my family members and relatives specially my parents for creating a delightful atmosphere as well as excusing me from family duties in order to complete the courses, research studies and final production of the thesis work.

Author

ABSTRACT

Free convection or natural convection in trapezoidal cavities has received considerable attention because of its importance in several thermal engineering problems, for example, in the design of electronic devices, solar thermal receivers, uncovered flat plate solar collectors having rows of vertical strips geothermal reservoirs etc.

In this thesis under the title "Finite Element Analysis on Heat Flow Based on Heatline Concept for MHD Free Convection within Trapezoidal Cavity", two problems have been studied. The relative direction between the buoyancy force and the externally forced flow is important. In the case where the fluid is externally forced to flow as the buoyancy force, the mode of heat transfer is termed combined forced and natural convection. The studies as well as depending on various flow of uniform and non-uniform heating and geometrical conditions are abstracted below.

Initially, Numerical simulation of two-dimensional laminar steady-state on MHD free convection within trapezoidal cavity with uniformly heated bottom wall has been investigated. In this study, natural convection within a trapezoidal enclosure for uniformly heated bottom wall, insulated top wall and isothermal side walls with inclination angles (ϕ) are considered. Heat flow patterns in the presence of natural convection within trapezoidal enclosures have been analyzed with heatlines concept. The fluid is concerned for the wide range of Rayleigh number (Ra) from 10^3 to 10^7 and Prandtl number (Pr) from 0.026, 0.7, 1000 with various tilt angles $\Phi = 45^0$, 30^0 and 0^0(square)..

The properties of the fluid were presumed to be constant. The physical problems are represented mathematically by different sets of governing equations along with the corresponding boundary conditions. The non-dimensional governing equations are discretized by using Galerkin weighted residual method of finite element formulation. Results are presented in terms of streamlines, isotherms, average Nusselt number along the bottom wall for uniform heating , average Nusselt number along the side wall for uniform heating, Local Nusselt number along distance for uniform heating of the side wall, Local Nusselt number along distance for uniform heating of the bottom wall, for different combinations of the governing parameters namely Prandtl number *Pr*, Hartmann number *Ha* and at the three values of Rayleigh number *Ra*, varying from 10^3 to 10^7. This range of

Ra is selected on the basis of calculation covering free convection dominated regimes. The computational results also indicate that the average Nusselt number at the uniform heating of bottom wall and side wall of the cavity is depending on the dimensionless parameters. Comparisons with previously published work are performed and the results are found to be in excellent agreement.

Finally, Numerical simulation of two-dimensional laminar steady-state on MHD free convection within trapezoidal cavity with non-uniformly heated bottom wall has also been investigated. The cavity consists of the same condition like previous one i.e., natural convection within a trapezoidal enclosure non-uniformly heated bottom wall, insulated top wall and isothermal side walls with inclination angles (ϕ) are considered. Heat flow patterns in the presence of natural convection within trapezoidal enclosures have been analyzed with heatlines concept. The fluid is also concerned for the wide range of Rayleigh number (Ra) from 10^3 to 10^7 and Prandtl number (Pr) from 0.026, 0.7, 1000 with various tilt angles $\Phi = 45^0$, 30^0 and 0^0(square).

Results are also presented in terms of streamlines, isotherms, average Nusselt number along the bottom wall for non-uniform heating , average Nusselt number along the side wall for non-uniform heating, Local Nusselt number along distance for non-uniform heating of the side wall, Local Nusselt number along distance for non- uniform heating of the bottom wall, for different combinations of the governing parameters namely Prandtl number *Pr*, Hartmann number *Ha* and at the three values of Rayleigh number *Ra*, varying from 10^3 to 10^7. This range of *Ra* is selected on the basis of calculation covering free convection dominated regimes. The computational results also indicate that the average Nusselt number at the non-uniform heating of bottom wall and side wall of the cavity is depending on the dimensionless parameters.

CONTENTS

NOMENCLATURE

θ_{av}	average temperature
B_0	magnetic induction
C_p	Specific heat at constant pressure (J/kg K)
g	gravitational acceleration (m/s^2)
Gr	Grashof number
h	convective heat transfer coefficient (W/m^2 K)
Ha	Hartmann number
k	thermal conductivity of fluid(W/m K)
L	Height or base of trapezoidal cavity (m)
K	Thermal conductivity ratio fluid
N	Total number of nodes
Nu_{av}	Average Nusselt number
Nu_{local}	Local Nusselt number
P	non-dimensional pressure
p	pressure
Pr	Prandtl number
Ra	Rayleigh number
T	non-dimensional temperature
T_h	Temperature of hot bottom wall (k)
T_c	Temperature of cold bottom wall (k)
U	x component of dimensionless velocity
u	x component of velocity (m/s)
V	y component of dimensionless velocity
v	y component of velocity (m/s)
V_0	Lid velocity
x, y	Cartesian coordinates
X, Y	dimensionless Cartesian coordinates

Greek symbols

α	Thermal diffusivity (m^2/s)
β	Coefficient of thermal expansion (K^{-1})
ρ	Density of the fluid (kg/m^3)
$\Delta\theta$	Temperature difference
θ	Fluid temperature
μ	Dynamic viscosity of the fluid (Pa s)
Ψ	Streamfunction

Π	Heatfunction
v	Kinematic viscosity of the fluid (m^2/s)
σ	Fluid electrical conductivity($\Omega^{-1}m^{-1}$)

Subscripts

b	Bottom wall
l	Left wall
r	Right wall
s	Side wall

LIST OF TABLES

LIST OF FIGURES

CHAPTER 1

INTRODUCTION

1.1 Introduction

Heat transfer is that science which seeks to predict the energy transfer which may take place between material bodies as a result of a temperature difference. Thermodynamics teaches that this energy transfer is defined as heat. The science of heat transfer seeks not merely to explain how heat energy may be transferred, but also to predict the rate at which the exchange will take place under certain specified conditions.

The phenomenon of heat transfer was known to human being even in the primitive age when they used to use solar energy as a source of heat. Heat transfer in its initial stage was conceived with the invention of fire in the early age of human civilization. Since then its knowledge and use has been progressively increasing each day as it is directly related to the growth of human civilization. With the invention of stream engine by James watt in 1765 A. D., the phenomenon of heat transfer got its first industrial recognition and after that its use extended to a great extent and spread out in different spheres of engineering fields. In the past three decades, digital computers, numerical techniques and development of numerical models of heat transfer have made it possible to calculate heat transfer of considerable complexity and thereby create a new approach to the design of heat transfer equipment.

The study of temperature and heat transfer is of great importance to the engineers because of its almost universal occurrence in many branches of science and engineering. Although heat transfer analysis is most important for the proper sizing of fuel elements in the nuclear reactors cores to prevent burnout, the performance of aircraft also depends upon the case with which the structure and engines can be cooled. The design of chemical plants is usually done on the basis of heat transfer analysis and the analogous mass transfer processes. The transfer and conversion of energy from one form to another is the basis to all heat transfer process and hence, they are governed by the first as well as the second law

of thermodynamics. Heat transfer is commonly associated with fluid dynamics. The knowledge of temperature distribution is essential in heat transfer studies because of the fact that the heat flow takes place only wherever there is a temperature gradient in a system. The heat flux which is defined as the amount of heat transfer per unit area in per unit time can be calculated from the physical laws relating to the temperature gradient and the heat flux.

The study of the universe has led to the realization that all physical phenomena are subject to natural laws. The term natural might well be used to describe the framework or system of fundamental and universal importance within this system is the mechanisms for the transfer of heat. Heat transfer is a branch of applied thermodynamics. It estimates the rate at which heat is transferred across the system boundaries subjected to specific temperature differences and the temperature distribution of the system during the process. Whereas classical thermodynamics deals with the amount of heat transferred during the process. Heat transfer processes have always been an integral part of our environment.

1.2 Flow within an enclosure

The flow within an enclosure consisting of two walls, at different temperatures, is an important circumstance encountered quite frequently in practice. In all the applications having this kind of situation, heat transfer occurs due to the temperature difference across the fluid layer, one horizontal solid surface being at a temperature higher than the other. If the upper plate is the hot surface, then the lower surface has heavier fluid and by virtue of buoyancy the fluid would not come to the lower plate. Because in this case the heat transfer mode is restricted to only conduction. But if the fluid is enclosed between two horizontal surfaces of which the upper surface is at lower temperature, there will be the existence of cellular natural convective currents which are called as Benard cells. For fluids whose density decreases with increasing temperature, this leads to an unstable situation. Benard mentioned this instability as a “top heavy” situation. In that case fluid is completely stationary and heat is transferred across the layer by the conduction mechanism only. Rayleigh recognized that this unstable situation must break down at a certain value of Rayleigh number above which convective motion must be generated. Jeffreys calculated this limiting value of Ra to be 1708, when air layer is bounded on both sides by solid walls.

1.3 Regular and Irregular Shapes

"Regular' has both a general meaning and a specific geometric meaning. In all cases, it concerns how much the various parts of the objects are 'the same'.

Consider the rectangle:

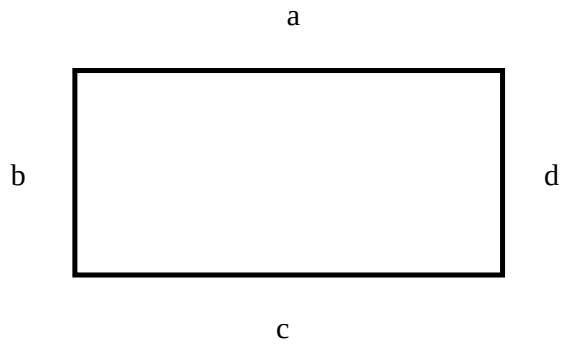

Figure 1.1: Regular shape of a rectangle

The sides a and c have the same length. The sides b and d have the same length. All the angles are the same. A sense of the regularity comes from how it pick up and turn it, and drop it back down and it still look the same. These are called symmetries of the object. If it picks up and turn it 180 degrees: a goes to c, b goes to d. The property 'same length' now means something more that can rigidly move it so those sides coincide. If it pick up and flip it over around a vertical line through the center ac.

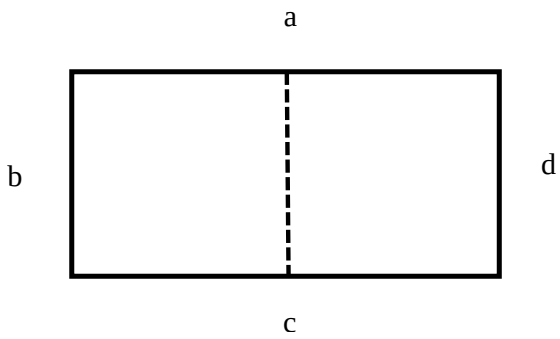

Figure 1.2: Regular shape of a rectangle through the center line ac

Side b goes to side d, sides a and d go on top of themselves. Another symmetry. A final reflection would involve turning through the line bd.

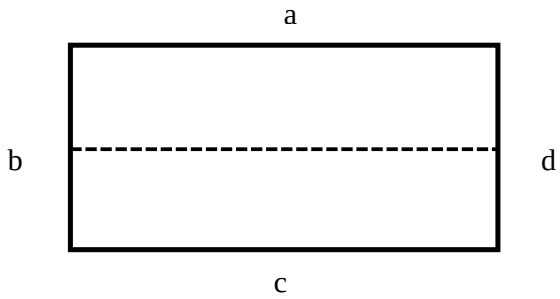

Figure 1.3: Regular shape of a rectangle through the center line bd

This takes side a to side c. In fact, trying combinations of these, you can take any corner of the rectangle onto any other corner. All the corners are sort of 'the same'.

A square would have more symmetries than a rectangle. Any side could be taken to any other side, any corner to any other corner. This has quarter turns as well as half-turns, mirrors through the corners as well as the vertical and horizontal mirrors of the rectangle. That is the square is more regular than the rectangle, because there are more symmetries. As a related fact, more parts are the same. For triangles:

1. Some have no two sides the same, so they are not regular.

2. Some have two sides the same. That also guarantees that two of the angles are the same. These are isosceles. Such triangles do have a mirror through the vertex (corner) where the equal sides meet and the middle of the edge opposite this vertex. That edge joins the two equal angles.

3. Some have all three sides the same. That goes with having all three angles the same. (Get one and the other follows.) For these 'equilateral triangles', there are lots of symmetries: taking any side to any side, any corner to any other corner. This would certainly be called regular.

1.3.1 Applications of an Irregular Trapezoidal Enclosure

In recent years, trapezoidal enclosures have received a good attention because of its applicability in various fields. For this reason the present problem is customized under trapezoidal enclosure. The important natural phenomenon of trapezoidal enclosure is such as building and thermal insulation systems (air conditioning, load calculations for pitched roofs with horizontal suspended ceiling), solar engineering applications (triangular built-in-storage solar collector), geophysical fluid mechanics (heat transfer and exchange of nutrients or pollutants from the coastal region to the interior waters of lakes or reservoirs,

pollutants diffusion in sea and also use in the Ultrasonic Grinding Machine in the industry).For Example,

Rigidal Versacor Ultima is a trapezoidal through fixed insulated composite panel which provides an extremely cost-effective and fast track construction solution for both new build and refurbishment projects. Rigidal Versacor Ultima is available in steel or aluminum with a high performance Versacor corrosion resistant coating.

This is particularly suited to heavy industry applications and coastal environments. Manufactured by CENTRIA (a partnership of HH Robertson and Smith Steelite), Versacor benefits from over 100 years experience and advanced technology in the provision of maximum protection for metal roofs and walls.The CFC-free insulation core of Rigidal Versacor Ultima provides thermal reliability over the lifetime of the building, and enhanced insulation cores using polyisocyanurate (PIR) foams are also available. Insulated composite panels offer many advantages over traditional build-up systems, including guaranteed performance, durability, reduced construction costs, excellent levels of air tightness and no risk of condensation or cold bridging within the panel.

Figure 1.4: Trapezoidal through fixed Aluminium composite panel for façade cladding Versacor Ultima

1.4 Heat Transfer Mechanism

Heat is the form of energy that can be transferred from one system to another as a result of temperature difference. A thermodynamic analysis is concerned with the amount of heat transfer as a system undergoes a process from one equilibrium state to another. The

science that deals with the determination of the rates of such energy transfers is the heat transfer. The transfer of energy as heat is always from the higher temperature medium to the lower temperature one, and heat transfer stops when the two mediums reach the same temperature.

Heat can be transferred in three different mechanisms or modes: conduction, convection and radiation. All modes of heat transfer require the existence of a temperature difference, and all modes are from the high temperature medium to a lower temperature one. In reality, the combined effect of these three modes of heat transfer control temperature distribution in a medium. A brief description of convection mode is given below.

1.4.1 Convection

Convection is the movement of molecules within fluids (i.e. liquids, gases) and rheids. It cannot take place in solids, since neither bulk current flows nor significant diffusion can take place in solids.

Convection is one of the major modes of heat transfer and mass transfer. Convective heat and mass transfer take place through both diffusion – the random Brownian motion of individual particles in the fluid – and by advection, in which matter or heat is transported by the larger-scale motion of currents in the fluid. In the context of heat and mass transfer, the term "convection" is used to refer to the sum of advective and diffusive transfer. The term "convection" may have slightly different but related usages in different contexts. The broader sense is in fluid mechanics, where "convection" refers to the motion of fluid (regardless of cause). However in thermodynamics "convection" often refers specifically to heat transfer by convection. Additionally, convection includes fluid movement both by bulk motion (advection) and by the motion of individual particles (diffusion). However in some cases, convection is taken to mean only advective phenomena. For instance, in the transport equation, which describes a number of different transport phenomena, terms are separated into "convective" and "diffusive" effects. A similar differentiation is made in the Navier–Stokes equations. In such cases the precise meaning of the term may be clear only from context. Convection occurs on a large scale in atmospheres, oceans, and planetary mantles. Fluid movement during convection may be invisibly slow, or it may be obvious and rapid, as in a hurricane. On astronomical scales, convection of gas and dust is thought to occur in the accretion disks of black holes, at speeds which may closely approach that of light.

Convective heat transfer is a mechanism of heat transfer occurring because of bulk motion (observable movement) of fluids. Heat is the entity of interest being advected (carried), and diffused (dispersed). This can be contrasted with conductive heat transfer, which is the transfer of energy by vibrations at a molecular level through a solid or fluid, and radiative heat transfer, the transfer of energy through electromagnetic waves. Heat is transferred by convection in numerous examples of naturally occurring fluid flow, such as: wind, oceanic currents, and movements within the Earth's mantle. Convection is also used in engineering practices to provide desired temperature changes, as in heating of homes, industrial processes, cooling of equipment, etc.

The rate of convective heat transfer may be improved by the use of a heat sink, often in conjunction with a fan. For instance, a typical computer CPU will have a purpose-made fan to ensure its operating temperature is kept within tolerable limits.

A **convection cell**, also known as a **Bénard cell** is a characteristic fluid flow pattern in many convection systems. A rising body of fluid typically loses heat because it encounters a cold surface; because it exchanges heat with colder liquid through direct exchange; or in the example of the Earth's atmosphere, because it radiates heat. Because of this heat loss the fluid becomes denser than the fluid underneath it, which is still rising. Since it cannot descend through the rising fluid, it moves to one side. At some distance, its downward force overcomes the rising force beneath it, and the fluid begins to descend. As it descends, it warms again and the cycle repeats itself. In Convection mechanisms convection may happen in fluids at all scales larger than a few atoms. There are a variety of circumstances in which the forces required for natural and forced convection arise, leading to different types of convection, described below. In broad terms, convection arises because of body forces acting within the fluid, such as gravity (buoyancy), or surface forces acting at a boundary of the fluid.

The causes of convection are generally described as one of either "natural" ("free") or "forced", although other mechanisms also exist (discussed below). However the distinction between natural and forced convection is particularly important for convective heat transfer.

1.4.2 Free or Natural Convection

Natural convection, or free convection, occurs due to temperature differences which affect the density, and thus relative buoyancy, of the fluid. Heavier (more dense) components will fall while lighter (less dense) components rise, leading to bulk fluid movement. Natural convection can only occur, therefore, in a gravitational field. A common example of natural convection is a pot of boiling water in which the hot and less-dense water on the bottom layer moves upwards in plumes, and the cool and denser water near the top of the pot likewise sinks.

Natural convection will be more likely and/or more rapid with a greater variation in density between the two fluids, a larger acceleration due to gravity that drives the convection, and/or a larger distance through the convecting medium. Convection will be less likely and/or less rapid with more rapid diffusion (thereby diffusing away the gradient that is causing the convection) and/or a more viscous (sticky) fluid. The onset of natural convection can be determined by the Rayleigh number (*Ra*).The differences in buoyancy within a fluid can arise for reasons other than temperature variations, in which case the fluid motion is called gravitational convection.

1.4.3 Conduction

Conduction is the mode of heat transfer in which energy exchange takes place from the region of high temperature to that of law temperature by the kinetic motion or direct impact of molecules, as in the case of fluid at rest, and by the drift of electrons, as in the case of metals. In a solid which is a good electric conductor, a large number of free electrons move about in the lattice, hence materials that are good electric conductors are generally good heat conductors (i.e. copper, silver.etc).

1.4.4 Streamfunction

The fluid motion is displayed using the streamfunction (ψ) obtained from velocity components U and V. The relationships between streamfunction (ψ) and velocity components for two-dimensional flows are

$$U = \frac{\partial \psi}{\partial Y} \qquad \text{and} \qquad V = -\frac{\partial \psi}{\partial X}$$

which yield a single equation

$$\frac{\partial^2 \psi}{\partial X^2} + \frac{\partial^2 \psi}{\partial Y^2} = \frac{\partial U}{\partial Y} - \frac{\partial V}{\partial X}$$

Using the above definition of the streamfunction, the positive sign of w denotes anti-clockwise circulation and the clockwise circulation is represented by the negative sign of ψ.

1.4.5 Heatfunction

The heat flow within the enclosure is displayed using the heatfunction (Π) obtained from conductive heat fluxes $\left(-\frac{\partial\theta}{\partial X},-\frac{\partial\theta}{\partial Y}\right)$ as well as convective heat fluxes $\left(U\theta,V\theta\right)$. The heatfunction satisfies the steady energy balance equation, such that

$\frac{\partial\Pi}{\partial Y}=U\theta-\frac{\partial\theta}{\partial X}$ and $\frac{\partial\Pi}{\partial X}=V\theta-\frac{\partial\theta}{\partial Y}$

which yield a single equation

$\frac{\partial^2\Pi}{\partial X^2}+\frac{\partial^2\Pi}{\partial Y^2}=\frac{\partial}{\partial Y}\left(U\theta\right)-\frac{\partial}{\partial X}\left(V\theta\right)$

Using the above definition of the heatfunction, the positive sign of Π denotes anti-clockwise heat flow and the clockwise heat flow is represented by the negative sign of Π.

1.4.6 Thermal Conductivity

Thermal conductivity of a material can be defined as the rate of heat transfer through a unit thickness of the material per unit area per unit temperature difference. Therefore the thermal conductivity of a material is a measure of the ability of the material to conduct heat. A high value for thermal conductivity indicates that the material is a good heat conductor, and a low value for thermal conductivity indicates that the material is a poor heat conductor or insulator. For example the materials such as copper and silver that are good electric conductors are also good heat conductors, and have high values of thermal conductivity. Materials such as rubber, wood are poor conductors of heat and have low conductivity values. The rate of heat conduction through a medium depends on the geometry of the medium, its thickness, and the material of the medium, as well as the temperature difference across the medium. The proportionality constant k is called thermal conductivity of the material.

1.4.7 Thermal Diffusivity

The time dependent heat conduction equation for constant k contains a quantity α, called the thermal diffusivity. Thermal diffusivity represents how fast heat diffuses through a material and is defined as

$$\alpha = \frac{\kappa}{\rho C_P}$$

Here the thermal conductivity κ represents how well a material conducts heat, and the heat capacity ρCp represents how much energy a material stores per unit volume. Therefore, the thermal diffusivity of a material can be viewed as the ratio of the heat conducted through the material to the heat stored per unit volume. A material that has a high thermal conductivity or a low heat capacity will obviously have a large thermal diffusivity. The larger thermal diffusivity means that the propagation of heat into the medium is faster. A small value of thermal diffusivity means the material mostly absorbs the heat and a small amount of heat is conducted further.

1.4.8 Internal and External Flows

A fluid flow is classified as being internal or external, depending on whether the fluid is forced to flow in a confined channel or over a surface. An internal flow is bounded on all sides by solid surfaces except, possibly, for an inlet and exit. Flows through a pipe or in an air-conditioning duct are the examples of internal flow. Internal flows are dominated by the influence of viscosity throughout the flow field. The internal flow configuration represents a convenient geometry for the heating and cooling of fluids used in the chemical processing, environmental control, and energy conversion areas. The flow of an unbounded fluid over a surface is external flow. The flows over curved surfaces such as sphere, cylinder, airfoil, or turbine blade are the example of external flow. In external flows the viscous effects are limited to boundary layers near solid surfaces.

1.4.9 Boundary Layer

Since fluid motion is the distinguishing feature of heat convection, it is necessary to understand some of the principles of fluid dynamics in order to describe adequately the processes of convection. When a fluid flows over a body, the velocity and temperature distribution at the immediate vicinity of the surface strongly influenced by the convective heat transfer. In order to simplify the analysis of convective heat transfer the boundary layer concept frequently is introduced to model the velocity and temperature fields near the solid surface in order to simplify the analysis of convective heat transfer. So we are concerned with two different kinds of boundary layers, the velocity boundary layer and the thermal boundary layer.

The velocity boundary layer is defined as the narrow region, near the solid surface, over which velocity gradients and shear stresses are large, but in the region outside the boundary layer, called the potential-flow region, the velocity gradients and shear stresses are negligible. The exact limit of the boundary layer cannot be precisely defined because of the asymptotic nature of the velocity variation. The limit of the boundary layer is usually taken to be at the distance from the surface, at which the fluid velocity is equal to a predetermined percentage of the free stream value, U_∞. This percentage depends on the accuracy desired, 99 or 95% being customary. Although, outside the boundary layer region the flow is assumed to be inviscid, but inside the boundary layer the viscous flow may be either laminar or turbulent. In the case of laminar boundary layer, fluid motion is highly ordered and it is possible to identify streamlines along which particles move. Fluid motion along a streamline is characterized by velocity components in both the x and y directions. Since the velocity component v is in the direction normal to the surface, it can contribute significantly to the transfer of momentum, energy or species through the boundary layer. Fluid motion normal to the surface is necessitated by boundary layer growth in the x direction. In contrast, fluid motion in the turbulent boundary layer is highly irregular and is characterized by velocity fluctuations. These fluctuations enhance the transfer of momentum, energy and species and hence increase surface friction, as well as convection transfer rates. Due to fluid mixing resulting from the fluctuations, turbulent boundary layer thicknesses are larger and boundary layer profiles are flatter than in laminar flow. The thermal boundary layer may be defined (in the same sense that the velocity boundary layer was defined above) as the narrow region between the surface and the point at which the fluid temperature has reached a certain percentage of ambient temperature T_∞. Outside the thermal boundary layer the fluid is assumed to be a heat sink at a uniform temperature of T_∞ The thermal boundary layer is generally not coincident with the velocity boundary layer, although it is certainly dependent on it. If the fluid has high thermal conductivity, it will be thicker than the velocity boundary layer, and if conductivity is low, it will be thinner than the velocity boundary layer.

1.4.10 Slanted Enclosure

The tilted enclosure geometry has received considerable attention in the heat transfer literature because of mostly growing interest of solar collector technology. The angle of tilt has a dramatic impact on the flow housed by the enclosure. Consider an enclosure heated from below is rotated about a reference axis. When the tilted angle becomes 90º,

the flow and thermal fields inside the enclosure experience the heating from side condition. Thereby convective currents may pronounce over the diffusive currents. When the enclosure rotates to 180º, the heat transfer mechanism switches to the diffusion because the top wall is heated.

1.5 Magneto-Hydrodynamics

Magneto-hydrodynamics (MHD) is the academic discipline which studies the dynamics of electrically conducting fluids. Examples of such fluids include plasmas, liquid metals and salt water. The word Magneto-hydrodynamics (MHD) is derived from “magneto-” meaning “magnetic field”, and “hydro” meaning “liquid”, and “dynamics” meaning “movement”. The field of MHD was initiated by Hannes Alfven, for which he received the Noble Prize in Physics in 1970.The idea of MHD is that magnetic fields which induce currents in a moving conducting fluid, and create forces on the fluid, and also change the magnetic field itself. The set of equations which describe MHD are a combination of the Nevier-Stokes equations of fluid dynamics and Maxwell’s equations of electromagnetism. These differential equations have to be solved simultaneously, either analytically or numerically. MHD is a continuum theory and as such it cannot treat kinetic phenomena, i.e. those in which the existence of discrete particles or of a non-thermal velocities distribution are important. The simple form of MHD, Ideal MHD, assumes that fluid has so little resistivity that it can be treated as a perfect conductor. This is the limit of infinite magnetic Reynolds number in ideal MHD, Lenz’s law dictates that the fluid is in a sense tied to the magnetic fields lines. To explain, in ideal MHD a small rope like volume of the fluid surrounding a field line will continue to lie along a magnetic field line, even as it is twisted and distorted by fluid flows in the system The connection between magnetic field lines and fluid in ideal MHD fixes the topology of the magnetic field in the fluid-for example, if a set of magnetic field lines are tied into a knot, then they will remain so as long as the fluid/plasma has negligible resistivity. This difficulty in reconnecting magnetic field lines makes it possible to store energy by moving the fluid or the source of the magnetic field. The energy can then become available if the conditions for ideal MHD break down allowing magnetic reconnection that release the stored energy from the magnetic field.

The ideal MHD equations consist of the continuity equation, the momentum equation, and Ampere's Law in the limit of no electric field and no electron diffusivity, and a

temperature evolution equation. As with any fluid description to a kinetic system, a closure approximation must be applied to highest moment of the particle distribution equation. This is often accomplished with approximations to the heat flux through a condition of adiabaticity or isothermality.

Ideal MHD is only strictly applicable when:

1. The plasma is strongly collisional, so that the time scale of collisions is shorter than the other characteristic times in the system, and the particle distributions are therefore close to Maxwellian.

2. The resistivity due to these collisions is small. In particular, the typical magnetic diffusion times over any scale length present in the system must be longer than any time scale of interest.

3. We are interested in length scales much longer than the ion skin depth and Larmor radius perpendicular to the field, long enough along the field to ignore Landau damping, and time scales much longer than the ion gyration time (system is smooth and slowly evolving).

1.5.1 Applications of MHD

Geophysics

The fluid core of the Earth and other planets is theorized to be a huge MHD dynamo that generates the Earth's magnetic field. due to the motion of liquid iron.

Astrophysics

MHD applies quite well to astrophysics since over 99% of baryonic matter content of the Universe is made up of plasma, including stars, the interplanetary medium (space between the planets), the interstellar medium (space between the stars), nebulae and jets. Many astrophysical systems are not in local thermal equilibrium, and therefore require an additional kinematic treatment to describe all the phenomena within the system. Sunspots are caused by the Sun's magnetic fields, as Joseph Larmor theorized in 1919. The solar wind is also governed by MHD. The differential solar rotation may be the long term effect of magnetic drag at the poles of the Sun, an MHD phenomenon due to the Parker spiral shape assumed by the extended magnetic field of the Sun. Previously, theories describing

the formation of the Sun and planets could not explain how the Sun has 99.87% of the mass, yet only 0.54% of the angular momentum in the solar system. In a closed system such as the cloud of gas and dust from which the Sun was formed, mass and angular momentum are both conserved.

That conservation would imply that as the mass concentrated in the center of the cloud to form the Sun, it would spin up, much like a skater pulling their arms in. The high speed of rotation predicted by early theories would have flung the proto-Sun apart before it could have formed. However, magneto hydrodynamic effects transfer the Sun's angular momentum into the outer solar system, slowing its rotation. Breakdown of ideal MHD (in the form of magnetic reconnection) is known to be the cause of solar flares, the largest explosions in the solar system. The magnetic field in a solar active region over a sunspot can become quite stressed over time, storing energy that is released suddenly as a burst of motion, X-rays, and radiation when the main current sheet collapses, reconnecting the field.

Engineering

MHD is related to engineering problems such as plasma confinement, liquid-metal cooling of nuclear reactors, and electromagnetic casting (among others).The first prototype of this kind of propulsion was built and tested in 1965 by Steward Way, a professor of mechanical engineering at the University of California, Santa Barbara. Way, on leave from his job at Westinghouse Electric, assigned his senior year undergraduate students to develop a submarine with this new propulsion system. In early 1990s, Mitsubishi built a boat, the 'Yamato,' which uses a magneto hydrodynamic drive, is driven by a liquid helium-cooled superconductor, and can travel at 15 km/h. MHD power generation fueled by potassium-seeded coal combustion gas showed potential for more efficient energy conversion (the absence of solid moving parts allows operation at higher temperatures), but failed due to cost prohibitive technical difficulties. In micro fluidic devices, the MHD pump is so far the most effective for producing a continuous, no pulsating flow in a complex micro channel design. It was used to implement a PCR protocol.

1.5.2 Fluid Mechanics Aspect

The local properties such as pressure and velocity of the fluid should strictly be defined as averages over elements large compared with the microscopic structure of matter but small enough in comparison with the scale of the macroscopic phenomena.

In MHD, the fluid is electrically conducting. It is not magnetic; it affects a magnetic field not by its mere presence but only by virtue of electric currents flowing in it. The fluid conducts because it contains free charges (ions or electrons) that can move indefinitely. According to the non-relativistic electromagnetic theory, a charged particle such as an electron suffers forces of three kinds.

1. It is repelled or attracted by other charged particles, the total force on the particle per unit of its charge due to all the other charges present being the electrostatic field, E's.

2. Charged particles in motion and also magnetic materials produce the phenomenon of magnetism or magnetic field, B.

2(a). A charge particle moving with velocity relative to a certain frame of reference suffers a magnetic force $\overline{V} \times \overline{B}$ per unit of its charge. The force is perpendicular to $\overline{V}$ and $\overline{B}$. The direction of $\overline{B}$ is that in which the particle must travel to feel no magnetic force.

2(b). If the magnetic field B, so identified, is changing with time relative to a certain frame of reference, then per unit of its charge a particle will suffer a further force Ei. The total force on a particle per unit of its charge is $f_e = \overline{E} + \overline{V} \times \overline{B}$. This is known as Lorentz force.

Electromagnetic body forces act on the fluid, and in turn the motion of the fluid in the presence of the electromagnetic field may generate an induced electromotive force and alter the fields. Implicit in this is the assumption of local quasi-equilibrium, which permits the state of the fluid at each point to be described by a few variables, related just as if the fluid were in equilibrium. Thereby the fluid may be assumed to be incompressible, homogeneous and isotropic in the mathematical and electric sense. The mathematical models have no difference from those used in conventional fluid mechanics. The only effect of the electromagnetic field is a coupling through the electromagnetic body force in the equation of motion.

1.5.3 Boussinesq Approximation

The governing equations for convection flow are coupled elliptic partial differential equations and are, therefore, of considerable complexity. The major problems in obtaining a solution to these equations lie in the inevitable variation of density with temperature, or concentration, and in their partial, elliptic nature. Several approximations are generally made to considerably simplify these equations. Among them Boussinesq approximation is considered here. In flows accompanied by heat transfer, the fluid properties are normally functions of temperature. The variations may be small and yet be the cause of the fluid motion. If the density variation is not large, one may treat the density as constant in the unsteady and convection terms, and treat it as variable only in the gravitational term. This is called the Boussinesq approximation.

1.6 Dimensionless Parameters

The dimensionless parameters can be thought of as measures of the relative importance of certain aspects of the flow. Some dimensionless parameters related to our study are discussed below:

1.6.1 Rayleigh Number, *Ra*

The Rayleigh number for a fluid is a dimensionless number associated with buoyancy driven flow (also known as free convection or natural convection).in fluid mechanics When the Rayleigh number is below than the critical value for that fluid, heat transfer is primarily in the form of conduction; when it exceeds the critical value, heat transfer is primarily in the form of convection. The Rayleigh number is named after Lord Rayleigh and is defined as the product of the Grashof number, which describes the relationship between buoyancy and viscosity within a fluid, and the Prandt number, which describes the relationship between momentum diffusivity and thermal diffusivity. Hence the Rayleigh number itself may also be viewed as the ratio of buoyancy forces and (the product of) thermal and momentum diffusivities.

For convection near a vertical wall, this number is

$$Ra_x = Gr_x \,\mathrm{Pr} = \frac{g\beta}{\nu\alpha}(T_s - T_\infty)x^3$$

where

x = Characteristic length (in this case, the distance from the leading edge)

Ra_x = Rayleigh number at position x

Gr_x = Grashof number at position x

Pr = Prandtl number

g = acceleration due to gravity

T_s = Surface temperature (temperature of the wall)

T_∞ = Quiescent temperature (fluid temperature far from the surface of the object)

v = Kinematic viscosity

α = Thermal diffusivity

β = Thermal expansion coefficient

In the above, the fluid properties Pr, v, α and β are evaluated at the film temperature, which is defined as,

$$T_f = \frac{T_s + T_\infty}{2}$$

For most engineering purposes, the Rayleigh number is large, somewhere around 10^6 and 10^8.

1.6.2 Grashof number, Gr

The flow regime in free convection is governed by the dimensionless Grashof number, which represent the ratio of the buoyancy force to the viscous forces acting on the fluid, and is defined as

$$Gr = \frac{g\,\beta\,L^3\left(T_w - T_\infty\right)}{\nu^2}$$

where g is the acceleration due to gravity, β is the volumetric thermal expansion coefficient, T_w is the wall temperature, T_∞ is the ambient temperature, L is the characteristic length and ν is the kinematics viscosity. The Grashof number Gr plays same role in free convection as the Reynolds

number *Re* plays in forced convection. As such, the Grashof number provides the main criterion in determining whether the fluid flow is laminar or turbulent in free convection. For vertical plates, the critical value of the Grashof number is observed to be about 10^9. Therefore, the flow regime on a vertical plate becomes turbulent at Grashof numbers greater than10^9.

1.6.3 Prandtl Number, *Pr*

The relative thickness of the velocity and the thermal boundary layers is best described by the dimensionless parameter Prandtl number, defined as

Pr = Molecular diffusivity of momentum / Molecular diffusivity of heat = υ/α

It is named after Ludwig Prandtl, who introduced the concept of boundary layer in 1904 and made significant contributions to boundary layer theory. The Prandtl numbers of fluids range from less than 0.01 for liquid metals to more than 100,000 for heavy oils. Note that the Prandtl number is in the order of 7 for water. The Prandtl numbers of gases are about 1, which indicates that both momentum and heat dissipate through the fluid at about the same rate. Consequently the thermal boundary layer is much thicker for liquid metals and much thinner for oils relative to the velocity boundary layer.

1.6.4 Hartmann Number, *Ha*

Hartmann number is the ratio of electromagnetic force to the viscous force first

introduced by Hartmann. It is defined by:

$$Ha = B_0 L\sqrt{\frac{\sigma}{\mu}}$$

Where, B_0 is the magnetic field, L is the characteristic length scale, σ is the electrical conductivity, μ is the viscosity. In addition, it is a dimensionless quantity characterizing flow of conducting fluid in a transverse magnetic field, being the product of the magnetic flux density, a representative length, and the square root of the ratio of electrical conductivity to viscosity.

1.6.5 Nusselt Number, *Nu*

The Nusselt number represents the enhancement of heat transfer through a fluid layer as a result of convection relative to conduction across the same fluid layer, and is defined as

$Nu = hL / k$

where k is the thermal conductivity of the fluid, h is the heat transfer coefficient and L is the characteristics length. The Nusselt number is named after Wilhelm Nusselt, who made significant contributions to convective heat transfer in the first half of the twentieth century, and it is viewed as the dimensionless convection heat transfer coefficient. The larger Nusselt number indicates a large temperature gradient at the surface and hence, high heat transfer by convection. A Nusselt number of $Nu = 1$, for a fluid layer represents heat transfer across the layer by pure conduction. To understand the physical significance of the Nusselt number, consider the following daily life problems. We remedy to forced convection whenever we want to increase the rate of heat transfer from a hot object. In free convection flow velocities are produced by the buoyancy forces hence there are no externally induced flow velocities.

1.7 Significance of Current Work

Natural convection in enclosed cavities has received significant attention due to many engineering applications . A recent investigation is also based on applications of heatlines to analyze natural convection within porous non-isothermal triangular cavities . However, visualization of heat flows via heatlines was not reported for trapezoidal enclosures. It is also essential to study the heat transfer characteristics in complex geometries in order to obtain the optimal design of the container for various industrial applications. Thus, it is important to study the energy flow using heatlines within trapezoidal enclosures. Besides, this energy flows due to natural convection within trapezoidal enclosures with hot bottom wall and cold side walls in presence of insulated top walls is analyzed by Basak et al.(March 2009). This fundamental problem is to examine thermal mixing near the central core of the cavity for various material processing applications. Besides, The effects of permeability and different thermal boundary conditions on the natural convection in a square porous cavity by using Darcy – Forchheimer model and Darcy – Brinkman-Forchheimer model have been studied numerically. The position of the enclosure has a significant influence on the natural convection. Computational study on the natural convection in an enclosure with layered porous media has been performed by using Darcy's model and Darcy-Brinkman-Forchheimer model. Mahmud and Fraser examined the flow, temperature and entropy generation fields inside a square porous cavity under the influence of magnetic field using Darcy model.But it was seen that heat flow using heatlines with magneto-hydrodynamics within trapezoidal enclosures had not been analyzed by weighted residual finite element method. Consequently as my interest I chose

a trapezoidal cavity whereas heat flow with MHD (magneto-hydrodynamics) of free convection was analyzed based on heatline concept.

1.8 Main Objectives of The Present Study

The aim of the proposed study is to present the effects on heat flow for MHD free convection within trapezoidal cavity. Results will be presented for different non-dimensional governing and physical parameters in terms of streamlines, stream functions, total heat flux, isotherms, heat transfer rate as well as the average temperature of the fluid in the cavity.

The specific objectives of the present research work are:

- To develop the mathematical models regarding the effect on heat flow for MHD free convection in a trapezoidal cavity.
- To investigate the effects of governing parameters namely Rayleigh number *Ra*, Prandtl number *Pr* and Hartmann number *Ha* on the flow and thermal field in the cavity.
- To solve the model equations using finite element method.
- To analyze effects on heat flow with heatline concept.
- To compare results with other published works.

1.9 Outline of the Thesis

This dissertation contains seven chapters. This thesis is concerned with the analysis effects on heat flow for MHD free convection within trapezoidal cavity based on heatline concept. There are many cavity configurations for the study of conjugate effect of conduction and natural convection flow. In this study we have considered a trapezoidal cavity.

In Chapter 1, a general framework for the description of convective heat transfers has been presented and discussed their properties, also relevant discussion on dimensionless parameter. In this chapter a brief introduction is presented with aim and objective and also inspiration behind the selection of current Work.

In Chapter 2, a brief discussion of literature review. of the past studies on fluid flow and heat transfer in cavities or channels is presented. In this state-of-the art review, different aspects of the previous studies have been mentioned categorically. This is followed by the

post-mortem of a recent historical event for the illustration of fluid flow and heat transfer effects in cavities

In Chapter 3, we have discussed the computational technique of the problem for viscous incompressible flow.

In Chapter 4, Mathematical modeling of the problem for both uniform and non-uniform heating have been discussed.

In Chapter 5, MHD effects of free convection for heated uniformly of bottom wall in a trapezoidal cavity have been investigated numerically. Here, results of the relevant parametric study have been performed.

In Chapter 6, MHD effects of free convection for heated non-uniformly of bottom wall in a trapezoidal cavity have been investigated numerically. Here, results of the relevant parametric study have been performed.

Finally, in Chapter 7 the main achievements and some ideas of further work have been summarized.

CHAPTER 2

LITERATURE REVIEW

Literature Review

Analysis of free convection usually induced in enclosed cavities or channels containing heating elements on one of its wall or on both walls are important from both theoretical and practical points of view. The fundamental problem of free convection in cavity has received considerable attention from researchers. Most of the cavities commonly used in industries are cylindrical, rectangular, trapezoidal and triangular etc. Trapezoidal cavities have received a considerable attention for its application in various fields. Many numerical investigations on free convection in different types of cavities have been investigated in the recent year.

Anandalakshmi and Basak (January 2012) have been carried out for the energy distribution and thermal mixing in steady laminar natural convective flow through the rhombic enclosures with various inclination angles, φ for various industrial applications. Here simulations are carried out for various regimes of Prandtl (*Pr*) and Rayleigh (*Ra*) numbers. Dimensionless streamfunctions and heatfunctions are used to visualize the flow and energy distribution, respectively.

Also a comprehensive understanding of energy flow and entropy generation is needed for an optimal process design via reducing irreversibilities in terms of 'entropy generation'. In this study, analysis on entropy generation during natural convection in a trapezoidal cavity with various inclination angles ($\varphi = 45°$, 60° and 90°) have been carried out for an efficient thermal processing of various fluids of industrial importance (Pr = 0.015, 0.7 and 1000) in the range of Rayleigh number ($10^3 - 10^5$) by Basak et. al (January 2012). Basak et al. (August 2011) studied A comprehensive heatline based approach for natural convection flows in trapezoidal enclosures with the effect of various walls heating. The present numerical study deals with natural convection flow in closed trapezoidal enclosures. The detailed analysis is carried out in two cases: (1) linearly heated side walls; (2) linearly heated left wall and cold right wall. In both the cases bottom wall is uniformly

heated and top wall is well insulated. A penalty finite element method with bi-quadratic elements is used to obtain the results in the form of isotherms, streamlines and heatlines and local and average Nusselt numbers. Numerical results are obtained for various values of Rayleigh number Ra , Prandtl number Pr and inclination angles (φ = 45°, 60° and 90°). Results signify that, at low Ra heat transfer is conduction dominant. At , multiple circulations of streamlines and heatlines results in enhanced convection. For linearly heated side walls (case 1), symmetric pattern in fluid flow and heat flow is observed. Enhanced thermal transport is observed from bottom wall to top portion of side walls via dense heatlines along the vertical center line. It is found that, less intense circulations occurs in square cavity (φ = 90°) compared to other cavities φ = 45°, 60°. In case 2, the cold right wall receives larger amount of heat from bottom wall compared to that of linearly heated left wall. The formation of boundary layer on the walls is explained based on heatlines. The local and average Nusselt numbers are also illustrated using heatlines. It is found that, Nu_b distribution exhibits sinusoidal variation at in case 1. It is also found that, Nu_l and Nu_r display wavy pattern at higher Ra for all Pr in case 2. Finally, it is concluded that, overall heat transfer rates are larger for square cavity (φ = 90°) compared to other angles (φ = 45°, φ = 60°) irrespective of heating patterns for side walls.

Basak et al. (March 2009) also investigated heat flow patterns in the presence of natural convection within trapezoidal enclosures with heatlines concept. In this study, natural convection within a trapezoidal enclosure for uniformly and non-uniformly heated bottom wall, insulated top wall and isothermal side walls with inclination angle have been investigated. Momentum and energy transfer are characterized by streamfunctions and heatfunctions, respectively, such that streamfunctions and heatfunctions satisfy the dimensionless forms of momentum and energy balance equations, respectively. Finite element method has been used to solve the velocity and thermal fields and the method has also been found robust to obtain the streamfunction and heatfunction accurately. The unique solution of heatfunctions for situations in differential heating is a strong function of Dirichlet boundary condition which has been obtained from average Nusselt numbers for hot or cold regimes. Parametric study for the wide range of Rayleigh number and Prandtl number with various tilt angles and (square) have been carried out. Heatlines are found to be continuous lines connecting the cold and hot walls and the lines are perpendicular to the isothermal wall for the conduction dominant heat transfer. The enhanced thermal mixing near the core for larger Ra is explained with dense heatlines and convective loop of

heatlines. The formation of boundary layer on the walls has a direct consequence based on heatlines. The local Nusselt numbers have also been shown for side and bottom walls and variation of local Nusselt numbers with distance have also been explained based on heatlines. It is found that average heat transfer rate does not vary significantly with for non-uniform heating of bottom wall.

Basak et al. (December 2010) also investigated the numerical investigation of natural convection in a porous trapezoidal enclosures has been performed for uniformly or non-uniformly heated bottom wall. Penalty finite element analysis with bi-quadratic elements is used for solving the Navier–Stokes and energy balance equations. The numerical solutions are studied in terms of streamlines, isotherms, heatlines, local and average Nusselt numbers for a wide range of parameters $Da(10^{-5}–10^{-3})$, *Pr(0.015–1000)* and $Ra(Ra = 10^{3}–10^{6})$. At low Darcy number ($Da = 10^{-5}$), heat transfer is primarily due to conduction for all φ's as seen from the heatlines which are normal to the isotherms.

Basak et al. (September 2009a) also presented natural convection flows in porous trapezoidal enclosures with various inclination angles. Here Simulations were carried out using penalty finite element analysis with bi-quadratic elements to investigate the influence of uniform and non-uniform heating of bottom wall within a trapezoidal enclosure of various inclination angles . Parametric study has been carried out for a wide range of Rayleigh number , Prandtl number and Darcy number . Numerical results are presented in terms of stream functions, isotherm contours and Nusselt numbers.

Natural convection in trapezoidal enclosures for uniformly heated bottom wall, linearly heated vertical wall(s) in presence of insulated top wall have been investigated numerically with penalty finite element method by Basak et. al (September 2009b). Baytaş and Pop (January 2001) studied natural convection in a trapezoidal enclosure filled with a porous medium.

Basak et al. (January 2009) also studied the phenomena of natural convection in a trapezoidal enclosure filled with porous matrix numerically. A penalty finite element analysis with bi-quadratic elements is performed to investigate the influence of uniform and non-uniform heating of bottom wall while two vertical walls are maintained at constant cold temperature and the top wall is well insulated. Parametric study for the wide range of Rayleigh number *Ra* , Prandtl number *Pr* and Darcy number shows consistent performance of the present numerical approach to obtain the solutions in terms of stream

function and isotherm contours. For parameters studied in the above range, a symmetry is observed for temperature and flow simulations. Non-uniform heating of the bottom wall produces greater heat transfer rate at the center of the bottom wall than uniform heating case for all Rayleigh and Darcy numbers but average Nusselt number shows overall lower heat transfer rate for non-uniform heating case. It is observed that the conduction is dominant irrespective of *Ra* for . As Rayleigh number increases, there is a change from conduction dominant region to convection dominant region for . The correlations between average Nusselt number and three parameters (Rayleigh number (*Ra*), Prandtl number (*Pr*) and Darcy number (*Da*)) are also obtained. Basak et al. (September 2009c) also performed the phenomena of natural convection within a trapezoidal enclosure filled with porous matrix for linearly heated vertical wall(s) with various inclination angles φ.

Besides, a study of the natural heat and mass transfer in a trapezoidal cavity heated from the bottom and cooled from the inclined upper wall is undertaken by Boussaid et al. (April 1999). He obtained results show that the flow configuration depends on the θ angle inclination of the upper wall. Baez and Nicolas (2006) also Performed 2D natural convection flows in tilted cavities: Porous media and homogeneous fluids.

Costa (1999, 2000, 2003, 2006) performed unified viewpoint in both physical and numerical aspects on the analysis of heatlines for visualizing two-dimensional transpoet problems. Heatlines analysis has been carried out for investigations in polar coordinates

by Ho C.J. et al.(1989, 1990a,b), Littlefield (1986),Chattopadhyay and Das (1995). There are few studies on the application of heatlines for natural convection by earlier workers Aggarwal and Manhapra (1989), Bello-Ochende (1988), Deng and Tang (2002), Zhao et al. (2007). Application of heatlines was shown for thermomagnetic convection in electroconductive melts.

Eyden (1988) presented some results of numerical and experimental study of turbulent double-diffusive natural convection of a mixture of two gases in a trapezoidal enclosure with imposed unstable thermal stratification.

Fusegi et al.(1992) investigated natural convection in a differentially heated square cavity with internal heat generation. Hall et al. (1988) showed transient natural convection in a rectangular enclosure with one heated side wall. Lyican and Bayazitoglu (1980) performed an analytical study of natural convective heat transfer within trapezoidal enclosure. Kuyper and Hoogendoorn (1995) investigated Laminar natural convection flow in

trapezoidal enclosures to study the influence of the inclination angle on the flow and the dependence of the average Nusselt numbers on the Rayleigh number. A critical Rayleigh number is presented depending on the tilting angle, where unicellular convection is observed. Karyakin (1989) reported two-dimensional laminar natural convection in enclosures of arbitrary cross-section. This study reported on transient natural convection in an isosceles trapezoidal cavity inclined at angle φ to the vertical line where a single circulation region is found in the steady state case. The heat transfer rate is found to increase with the increase in angle φ.

The extensive studies for rectangular and square enclosures using various numerical simulations reported by Al-Amiri et al.(2007) Hyun and Lee (1989), Lage and Bejan (1991,1993), Nicolette et al. (1985), Patterson and Imberger (1980) and Xia and Murthy (2002). They ensure that several attempts have been made to acquire a basic understanding of natural convection flows and heat transfer characteristics in an enclosure.

Peric (1993) studied Natural convection in trapezoidal cavities with a series of symmetrically refined grids 10×10 to 160×160 control volume and observed the convergence of results for grid independent solutions. Boussaid et al. (2003) investigated thermosolutal heat transfer within trapezoidal cavity heated at the bottom wall and cooled at the inclined top wall. Varol et al. (2009, 2008a,b) recently for various inclinations of trapezoidal enclosures filled with either fluid or porous medium on natural convection have been carried out.

The heatlines are introduced for visualization and analysis of heat transfer (1983,2004). Convective heat transfer processes were analyzed mainly using isotherms before introduction of the concept of ‘heatlines’. The heatline is the best way to visualize the heat transfer in two-dimensional convective transport processes. Energy flow within various regimes especially for convective heat transport processes can be best visualized by heatlines whereas isotherms are unable to give guideline for energy flows. The heatlines are mathematically represented by heatfunctions and the proper dimensionless forms of heatfunctions are closely related to overall Nusselt numbers. Kimura and Bejan (2004) proposed heatlines for visualization of convective heat transfer through an extension of heat flux line concept to include the advection terms. Further, Bejan (1983) reviewed extensively various aspects of heatlines and illustrated the use of heatline concept to visualize various physical situations.

Hooman et al.(2008) showed visualization of natural convection in a porous cavity occupied by a fluid with temperature-dependent viscocity. Mobedi (2008) made natural convection in a square cavity with finite thickness horizontal walls. Zhao et al. (2008) performed on natural convection in an enclosure with localized heating and salting. Basak et al. (2006) investigated the effects of thermal boundary conditions on natural convection flows within a square cavity. Basak and Roy (2005) also performed on natural convection flows in a square cavity with non-uniformly heated wall.

Kumar B.V. Rathish and Kumar Bipin (April 2004) performed coupled non-linear partial differential equations governing the natural convection from an isothermal wall of a trapezoidal porous enclosure have been solved numerically by finite element method (FEM) in conjunction with GMRES, a Krylov subspace based solver. In view of the enormous amount of computation, a parallel numerical algorithm for incomplete LU-conjugate gradient (ILU-CG) solver on eight-noded ANUPAM cluster under MIMD paradigm based on ANULIB message passing library has been developed. Parallel computations have been carried out for various values of flow and geometric parameters both under Darcian and non-Darcian assumptions on the porous model. Cumulative heat fluxes and Nusselt number (*Nu*) associated with convection process are presented through computer generated plots. Kumar Subodh (February 2004) presented simple thermal analysis to evaluate the natural convective heat transfer coefficient, h_{c12} for a trapezoidal absorber plate-inner glass cover enclosure of a double-glazed box-type solar cooker.

A numerical study is conducted to investigate the transport mechanism of free convection in a trapezoidal enclosure filled with water–Cu nanofluid by Nasrin and Parvin (February 2012). A penalty finite element analysis with bi-quadratic elements is performed to investigate the influence of uniform and non-uniform heating of bottom wall on natural convection flows in a trapezoidal cavity by Natarajan et. al (February 2008). In this investigation, bottom wall is uniformly and non-uniformly heated while two vertical walls are maintained at constant cold temperature and the top wall is well insulated. Parametric study for the wide range of Rayleigh number (*Ra*), and Prandtl number (*Pr*), shows consistent performance of the present numerical approach to obtain the solutions in terms of stream functions and the temperature profiles.

Natarajan et. al (May 2012) presented. a numerical study of combined natural convection and surface radiation heat transfer in a solar trapezoidal cavity absorber for Compact Linear Fresnel Reflector (CLFR) . The numerical simulation results are presented in terms

of Nusselt number correlation to show the effect of these parameters on combined natural convection and surface radiation heat loss.

Papanicolaou and Belessiotis (January 2005) performed the natural convective heat and mass transfer in an asymmetric, trapezoidal enclosure is studied numerically. Such a configuration is encountered in greenhouse-type solar stills, where natural convection in the enclosed humid air due to vertical temperature and concentration gradients between the saline water and the transparent cover, plays a decisive role. In this double-diffusion problem, the relative magnitude of the thermal and the concentration (or solutal) Rayleigh numbers, expressed by their ratio N is a key parameter. The numerical solutions yield a multi-cellular flow field, with the number of cells depending on the Rayleigh number for a fixed Lewis number and geometry. For a positive value of N ($N = 1$) the solution is qualitatively similar to the case with only thermal buoyancy present ($N = 0$). However, for negative values ($N = -1$), more complex unsteady phenomena arise, having a different nature in the laminar and the turbulent flow regime, which are both investigated.

Saleh et. al (January 2011) studied Natural convection heat transfer in a nanofluid-filled trapezoidal enclosure. Heat transfer enhancement utilizing nanofluids in a trapezoidal enclosure is investigated for various pertinent parameters. Here we also developed a new correlation for the average Nusselt number as a function of the angle of the sloping wall, effective thermal conductivity and viscosity as well as Grashof number. Saleh et. al (August 2011) also studied the effect of a magnetic field on steady convection in a trapezoidal enclosure filled with a fluid-saturated porous medium by the finite difference method . Here the results indicate that the heat transfer performance decreases by decreasing the angle of sloping wall. Optimum reducing of the heat transfer rate was obtained for an acute trapezoidal enclosure and large magnetic field in the horizontal direction.

However overall heat loss coefficients of the trapezoidal cavity absorber with rectangular and round pipe were studied in the laboratory by Singh et. al (February 2010). As there should be minimum heat loss from the absorber to achieve better efficiency of the solar collector.

Varol (February 2012) analyzed the detailed heat transfer and fluid flow within two entrapped porous trapezoidal cavities involving cold inclined walls and hot horizontal walls. Results are presented for different values of the governing parameters, such as Darcy-modified Rayleigh number, aspect ratio of two entrapped trapezoidal cavities and

thermal conductivity ratio between the middle horizontal wall and fluid medium. Heat transfer rates are estimated in terms of local and mean Nusselt numbers. Local Nusselt numbers with spatial distribution exhibit monotonic trend irrespective of all Rayleigh numbers for the upper trapezoidal whereas wavy distribution of local Nusselt number occur for the lower trapezoidal. Varol (November 2010) also studied a numerical work to determine the heat transfer and fluid flow due to buoyancy forces in divided trapezoidal enclosures filled with fluid saturated porous media. In this investigation, bottom wall was non-uniformly heated while two vertical walls were insulated and the top wall was maintained at constant cold temperature.

Entropy generation due to buoyancy induced convection and conduction in a right angle trapezoidal enclosure filled with fluid saturated porous medium has also been performed numerically by Varol et. al (June 2009). Left vertical solid wall of the trapezoidal enclosure has a finite thickness and conductivity. The outside temperature of the solid wall is higher than that of inclined wall, while horizontal walls are adiabatic. It is found that the most important parameters on heat transfer and fluid flow are thermal conductivity ratio and dimensionless thickness of the solid wall of the enclosure. Thus, these parameters also generate entropy for the whole system. It is also found that increasing the Rayleigh number decreases the Bejan number; however, heat transfer is an increasing function of Rayleigh number.A numerical study of the steady buoyancy-induced flow and heat transfer in a trapezoidal cavity filled with a porous medium saturated with cold water at a temperature around 4 °C has been performed by Varol et. al (April 2010). The analysis has been done for a cavity with different aspect ratios ranging from 0.25 to 0.75 and Rayleigh numbers ranging from 100 to 1000 using a finite-difference method. It is found that four cells are formed inside the cavity independent of the Rayleigh number and aspect ratio.

Magnetohydrodynamics (MHD) is the academic discipline which studies the dynamics of electrically conducting fluids. Examples of such fluids include plasmas, liquid metals, and salt water. The MHD was originally applied to astrophysical and geophysical problems, where it is still very important. Engineers employ MHD principles in the design of heat exchanger, pumps and flow meters, in space vehicle propulsion, control and re-entry in creating novel power generating systems and developing confinement schemes for controlled fusion.

Most existing studies are concerned with the natural convection heat transfer through a porous medium saturated by an electrically non-conducting fluid, which is the case in

most practical situations. Recently the equally important problem of hydro-magnetic convective flow of a conducting fluid motion induces an electric current and, in general, the fluid velocity is reduced due to interaction between the electric current and the motion. Very little research works has been done on the magnetohydrodynamics natural convection in porous media though its potential applications. The first experimental investigation on magnetic effects in porous media was carried out by Wallace et al. (1969, digitized 19 March 2009). They proposed a technique for studying pore size distribution in a porous medium using magnetic field. Experiments on the flow of mercury in porous media (sandstone) either with no magnetic field, or with a transverse magnetic field and in presence of crosswise electric currents were performed. When a transverse magnetic field is applied alone, there is no change of flow rate of mercury through the porous media due to the combination of low magnetic field and small characteristic pore length causing a small *Ha*. However, simultaneous application of a transverse magnetic field and an electric current cause the change of flow rate of mercury. Later, Rudraiah et al. (1975) carried out a theoretical and numerical study of Hartmann flow over a non-conducting permeable bed for the validation of the work of Wallace et al. (1969, digitized 19 March 2009). They quoted that the volume rate of flow through porous media decreases considerably on increasing the magnetic field. Also, several analytical and numerical works in the literature are devoted to the study of the MHD flow through a porous medium between two parallel fixed plates (Ram and Mishra (1977); Tawil and Kamel (1994)), or bounded by an infinitely vertical plate (Raptis and Perdikis (1985); Yih (1998)) or in a circular pipe (Ram and Mishra (1977)).

The instability problem of fluid flow down a vertical or an inclined plate are commonly seen in industrial applications, e.g. in the finishing of painting, laser cutting process and casting technology. Hung et al. (1996) made an attempt to analyze the nonlinear instability of a magnetohydrodynamics (MHD) film flow with phase change at the interface. They pointed that increasing the stability of film flow by controlling magnetic field; a film flow with optimum conditions could be obtained. Kahveci and Öztuna (2009) made on MHD natural convection flow and heat transfer in a laterally heated partitioned enclosure. Saha et al.(August 2007) studied on the effect of Hall current on the MHD laminar natural convection flow from a vertical permeable flat plate with uniform surface temperature.

CHAPTER 3

COMPUTATIONAL TECHNIQUE

3.1 Computational Technique

Computational fluid dynamics (CFD) has been rapidly gaining popularity over the past several years for technological as well as scientific interests. For many problems of industrial interest, experimental techniques are extremely expensive or even impossible due to the complex nature of the flow configuration. Analytical methods are often useful in studying the basic physics involved in a certain flow problem, however, in many interesting problems; these methods have limited direct applicability. The dramatic increase in computational power over the past several years has led to a heightened interest in numerical simulations as a cost effective method of providing additional flow information, not readily available from experiments, for industrial applications, as well as a complementary tool in the investigation of the fundamental physics of turbulent flows, where analytical solutions have so far been unattainable. It is not expected (or advocated), however, that numerical simulations replace theory or experiment, but that they be used in conjunction with these other methods to provide a more complete understanding of the physical problem at hand.

Mathematical model of physical phenomena may be ordinary or partial differential equations, which have been the subject of analytical and numerical investigations. The partial differential equations of fluid mechanics and heat transfer are solvable for only a limited number of flows. To obtain an approximate solution numerically, we have to use a discretization method, which approximated the differential equations by a system of algebraic equations, which can then be solved on a computer. The approximations are applied to small domains in space and / or time so the numerical solution provides results at discrete locations in space and time. Much as the accuracy of experimental data depends on the quality of the tools used, the accuracy of numerical solutions depend on the quality of discretizations used .Computational fluid dynamics (CFD) computation involves the formation of a set numbers that constitutes a practical approximation of a real life system. The outcome of computation process improves the understanding of the performance of a

system. Thereby, engineers need CFD codes that can make physically realistic results with good quality accuracy in simulations with finite grids. Contained within the broad field of computational fluid dynamics are activities that cover the range from the automation of well established engineering design methods to the use of detailed solutions of the Navier-Stokes equations as substitutes for experimental research into the nature of complex flows. CFD have been used for solving wide range of fluid dynamics problem. It is more frequently used in fields of engineering where the geometry is complicated or some important feature that cannot be dealt with standard methods. More details are available in Ferziger & Perić (1997) and Patankar (1980).

3.1.1 Merits and Demerits of Numerical Method

As computational power grows, the need for more advanced numerical algorithms also increases. There are many different techniques for constructing numerical solutions of fluid flow problems, e.g. finite difference methods(FD), finite volume methods (FV), and finite element methods(FE), to name a few, and all have their strengths and weaknesses. Since the goal of the present research lies in the development of methods which may ultimately be used for large-scale applications of industrial interest, finite element methods have been chosen, given their accuracy as well as their ability to approximate arbitrarily complex geometric configurations. The finite element method applied to fluid dynamics has reached level of maturity over the past two decades such that it is now being successfully applied to industrial strength problems including turbulent flows.

Finite element method is an ideal numerical approach for solving a system of partial differential equations. The finite element method produces equations for each element independently of all other elements. Only when the equations are collected together and assembled into a global matrix are the interactions between elements taken into account. Despite these ideal characteristics, the finite element method dominates in most of the computational fluid dynamics. The present research is an attempt to bring the FE technique again into light through a novel formulation of two dimensional incompressible thermal flow problems. As the formulation establishes a priority of finite element technique over the FD and FV method, the philosophy and approach of the three methods are recapitulated here in brief. The finite difference method relies on the philosophy that the body is in one single piece but the parameters are evaluated only at some selected points within the body, satisfying the governing differential equations approximately, where as the finite volume method relies on the philosophy that the body is divided into a

finite number of control volumes, On the other hand, in the finite element method, the body is divided into a number of elements. The Finite element method works when all other methods fail and it's managing complex geometrical bodies and boundaries. There are many commercial packages such as ANSYS, MATLAB and COMSOL MULTIPHYSICS for analyzing practical problems. The demerits of this method, it considers the body is not in one piece, but it is an assemblage of elements connected only at nodes and Finite element solution is highly dependent on the element type.

Accurate and reliable prediction of complex geometry is of great importance to meet the severe demand of greater reliability as well as economic challenge. It is noted that these complex geometries occurs most frequently in CFD. Presented methods have a common feature: they generate equations for the values of the unknown functions at a finite number of points in the computational domain. But there are also several differences. The finite difference and the finite volume methods generate numerical equations at the reference point based on the values at neighboring points. The finite element method takes care of boundary conditions of Neumann type while the other two methods can easily apply to the Dirichlet conditions. The finite difference method could be easily extended to multidimensional spatial domains if the chosen grid is regular (the cells must look cuboids, in a topological sense). The grid indexing is simple but some difficulties appear for the domain with a complex geometry. For the finite element method there are no restrictions on the connection of the elements when the sides (or faces) of the elements are correctly aligned and have the same nodes for the neighboring elements. This flexibility allows us to model a very complex geometry. The finite volume method could also use irregular grids like the grids for the finite element methods, but keeps the simplicity of writing the equations like that for the finite difference method. Of course, the presence of a complex geometry slows down the computational programs. Another benefit of the finite element method is that of the specific mode to deduce the equations for each element that are then assembled. Therefore, the addition of new elements by refinement of the existing ones is not a major problem. For the other methods, the mesh refinement is a major task and could involve the rewriting of the program. But for all the methods used for the discrete analogue of the initial equation, the obtained system of simultaneous equations must be solved. That is why, the present work emphasizes the use of finite element techniques to solve flow and heat transfer problems. The details of this method are explained in the following section.

3.2 Elements of Numerical Solution Methods

Several components of numerical solution methods are available in Ferziger and Perić (1997), here only the main steps will be demonstrate in the following.

3.2.1 Mathematical Model

The starting point of any numerical method is the mathematical model, i.e. the set of partial differential equations and boundary conditions. A solution method is usually designed for a particular set of equations. Trying to produce a general-purpose solution method, i.e. one which is applicable to all flows, is impractical, is not impossible and as with most general purpose tools, they are usually not optimum for any one application.

3.2.2 Discretization Process

After selecting the mathematical model, one has to choose a suitable discretization method, i.e. a method of approximating the differential equations by a system of algebraic equations for the variable at some set of discrete locations in space and time.

3.2.3 Numerical Grid

The numerical grid defines the discrete locations, at which the variables are to be calculated, which is essentially a discrete representation of the geometric domain on which the problem is to be solved. It divided the solution domain into a finite number of sub-domains (elements, control volumes etc). Some of the options available are structural (regular) grid, block structured grid, unstructured grids etc.

3.2.4 Finite Approximations

Following the choice of grid type, one has to select the approximations to be used in the discretization process. In a finite difference method, approximations for the derivatives at the grid points have to be selected. In a finite volume method, one has to select the methods of approximating surface and volume integrals. In a finite element method, one has to choose the functions and weighting functions.

3.2.5 Solution Technique

Discretization yields a large system of non-linear algebraic equations. The method of solution depends on the problem. For unsteady flows, methods based on those used for initial value problems for ordinary differential equation (marching in time) is used. At each time step an elliptic problem has to be solved. Pseudo-time marching or an equivalent

iteration scheme usually solves steady flow problems. Since the equations are non-linear, an iteration scheme is used to solve them. These methods use successive linearization of the equations and the resulting linear systems are almost always solved by iterative techniques. The choice of solver depends on the grid type and the number of nodes involved in each algebraic equation.

3.3 Discretization Approaches

The first step to numerically solve a mathematical model of physical phenomena is its numerical discretization. This means that each component of the differential equations is transformed into a "numerical analogue" which can be represented in the computer and then processed by a computer program, built on some algorithm. There are several discritization methods available for the high performance numerical computation in CFD.

- Finite difference method (FDM)
- Finite volume method (FVM)
- Finite element method (FEM)
- Boundary element method (BEM)
- Boundary volume method (BVM)

In the present numerical computation, galerkin finite element method (FEM) has been used.

3.4 Finite Element Method

The finite element method (FEM) is a powerful computational technique for solving problems which are described by partial differential equations or can be formulated as functional minimization. The basic idea of the finite element method is to view a given domain as an assemblage of simple geometric shapes, called finite elements, for which it is possible to systematically generate the approximation functions needed in the solution of partial differential equations by the variational or weighted residual method. The computational domains with irregular geometries by a collection of finite elements makes the method a valuable practical tool for the solution of boundary, initial and eigen value problems arising in various fields of engineering. The approximation functions, which satisfy the governing equations and boundary conditions, are often constructed using ideas

from interpolation theory. Approximating functions in finite elements are determined in terms of nodal values of a physical field which is sought. A continuous physical problem is transformed into a discretized finite element problem with unknown nodal values. For a linear problem, a system of linear algebraic equations should be solved. Values inside finite elements can be recovered using nodal values.

The major steps involved in finite element analysis of a typical problem are:

1. Discretization of the domain into a set of finite elements (mesh generation).
2. Weighted-integral or weak formulation of the differential equation to be analyzed.
3. Development of the finite element model of the problem using its weighted-integral or weak form.
4. Assembly of finite elements to obtain the global system of algebraic equations.
5. Imposition of boundary conditions.
6. Solution of equations.
7. Post-computation of solution and quantities of interest.

3.4.1 MESH GENERATION

In finite element method, the mesh generation is the technique to subdivide a domain into a set of subdomains, called finite elements. Figure 3.1 shows a domain, Λ is subdivided into a set of subdomains, Λ^e with boundary Γ^e.

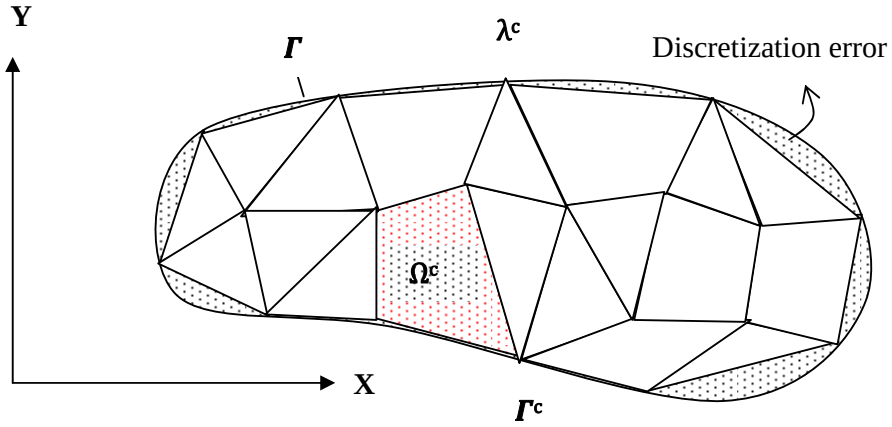

Figure 3.1: Finite element discretization of a domain

The present numerical technique will discretize the computational domain into unstructured triangles by Delaunay Triangular method. The Delaunay triangulation is a geometric structure that has enjoyed great popularity in mesh generation since the mesh generation was in its infancy. In two dimensions, the Delaunay triangulation of a vertex set maximizes the minimum angle among all possible triangulations of that vertex set.

Figure 3.2 shows the mesh mode for the present numerical computation. Mesh generation has been done meticulously.

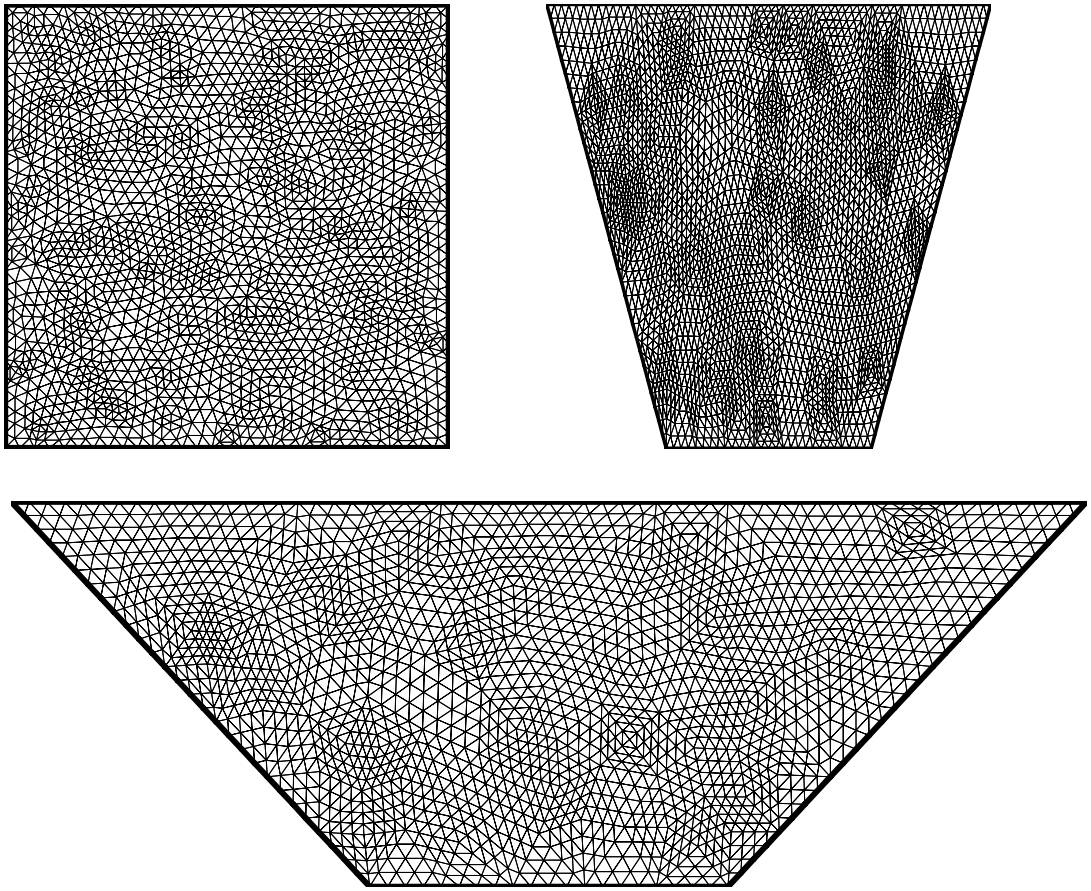

Figure 3.2: Current mesh structure of elements for trapezoidal cavity where $\phi = 0^o$,$\phi = 30^o$, $\phi = 45^o$

3.4.2 Finite Element Formulation and Computational Technique

Viscous incompressible thermal flows have been the subject of our investigation. The problem is relatively complex due to the coupling between the energy equation and the Navier-Stokes equations, which govern the fluid motion. These equations comprise a set of coupled nonlinear partial differential equations, which is difficult to solve especially with complicated geometries and boundary conditions. The finite element formulation and computational procedure for Navier-Stokes equations along with energy equations will be discuss in the chapter 4 and chapter5.

3.5 Algorithm

The algorithm was originally put forward by the iterative Newton-Raphson algorithm; the discrete forms of the continuity, momentum and energy equations are solved to find out the value of the velocity and the temperature. It is essential to guess the initial values of the variables. Then the numerical solutions of the variables are obtained while the convergent criterion is fulfilled. The simple algorithm is shown by the flow chart below.

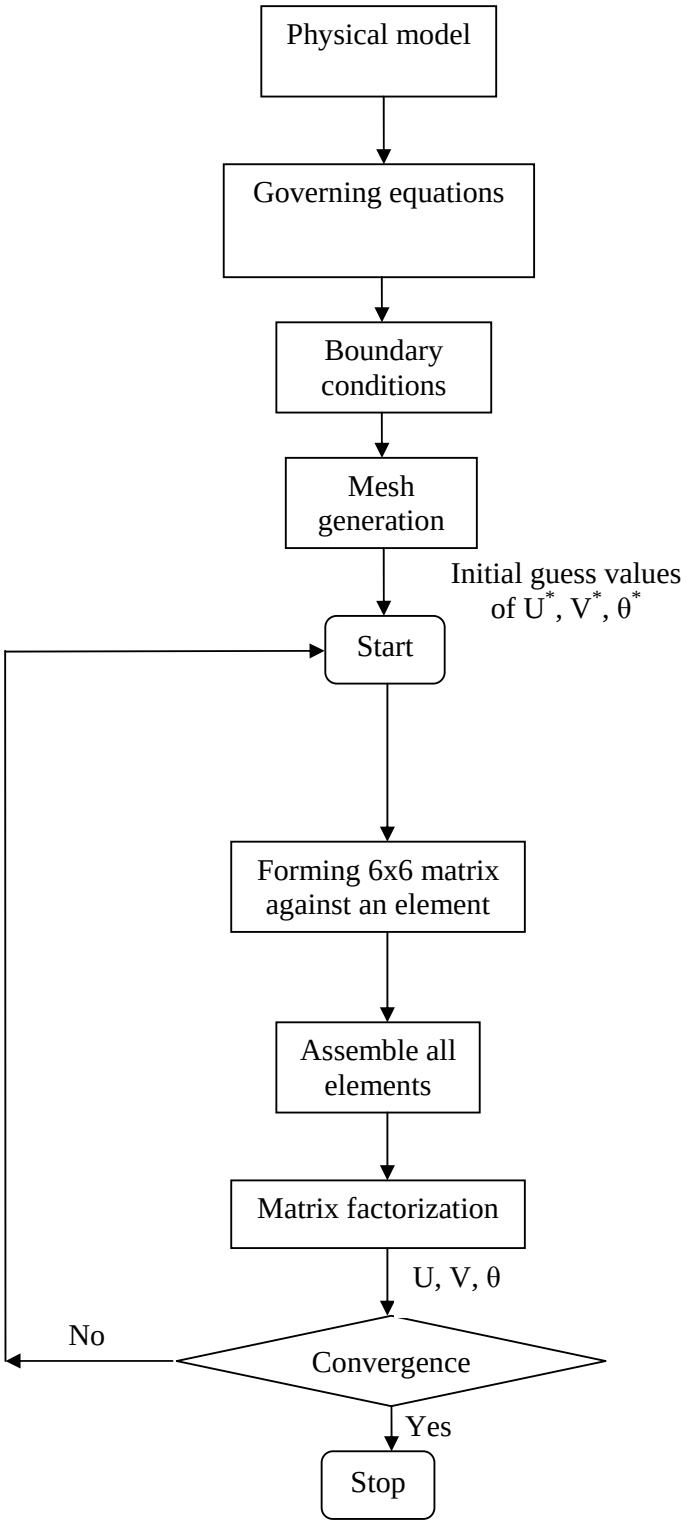

Figure 3.3: Flow chart of the computational procedure

3.5.1 Solution of System of Equations

A system of linear algebraic equations has been solved by the UMFPACK with MATLAB interface. UMFPACK is a set of routines for solving asymmetric sparse linear systems Ax = b, using the Asymmetric MultiFrontal method and direct sparse LU factorization. Five primary UMFPACK routines are required to factorize A or Ax = b:

1. Pre-orders the columns of A to reduce fill-in and performs a symbolic analysis.
2. Numerically scales and then factorizes a sparse matrix.
3. Solves a sparse linear system using the numeric factorization.
4. Frees the Symbolic object.
5. Frees the Numeric object.

Additional routines are:

1. Passing a different column ordering
2. Changing default parameters
3. Manipulating sparse matrices
4. Getting LU factors
5. Solving the LU factors
6. Computing determinant

UMFPACK factorizes PAQ, PRAQ, or $PR^{-1}AQ$ into the product LU, where L and U are lower and upper triangular, respectively, P and Q are permutation matrices, and R is a diagonal matrix of row scaling factors (or R = I if row-scaling is not used). Both P and Q are chosen to reduce fill-in (new nonzeros in L and U that are not present in A). The permutation P has the dual role of reducing fill-in and maintaining numerical accuracy (via relaxed partial pivoting and row interchanges). The sparse matrix A can be square or rectangular, singular or non-singular, and real or complex (or any combination). Only square matrices A can be used to solve Ax = b or related systems. Rectangular matrices can only be factorized. UMFPACK first finds a column pre-ordering that reduces fill-in, without regard to numerical values. It scales and analyzes the matrix, and then automatically selects one of three strategies for pre-ordering the rows and columns: asymmetric, 2-by-2 and symmetric. These strategies are described below.

One notable attribute of the UMFPACK is that whenever a matrix is factored, the factorization is stored as a part of the original matrix so that further operations on the matrix can reuse this factorization. Whenever a factorization or decomposition is

calculated, it is preserved as a list (element) in the factor slot of the original object. In this way a sequence of operations, such as determining the condition number of a matrix and then solving a linear system based on the matrix, do not require multiple factorizations of the intermediate results.

Conceptually, the simplest representation of a sparse matrix is as a triplet of an integer vector **i** giving the row numbers, an integer vector **j** giving the column numbers, and a numeric vector **x** giving the non-zero values in the matrix. The triplet representation is row-oriented if elements in the same row were adjacent and column-oriented if elements in the same column were adjacent. The compressed sparse row (csr) or compressed sparse column (csc) representation is similar to row-oriented triplet or column-oriented triplet respectively. These compressed representations remove the redundant row or column in indices and provide faster access to a given location in the matrix.

3.6 Chapter Summary

This chapter has presented a tutorial introduction to computational method with advantages of numerical investigation, because numerical method has played a central role in this thesis. Various components of numerical method have been also explained. Finally, the major steps involved in finite element analysis of a typical problem have been discussed.

CHAPTER 4

MATHEMATICAL MODELING OF THE PROBLEM

4.1 Mathematical Modeling

The convection heat transfer occurs due to temperature differences which affect the density, and thus relative buoyancy of the fluid is referred to as free convection (natural convection). The starting point of any numerical method is the mathematical model, i.e. the set of partial differential equations and boundary conditions. A solution method is usually designed for a particular set of equations. Trying to produce a general-purpose solution method, i.e. one which is applicable to all flows, is impractical, is not impossible and as with most general purpose tools, they are usually not optimum for any one application.

The generalized governing equations are used based on the conservation laws of mass, momentum and energy. As the heat transfer depends upon a number of factors, a dimensional analysis is presented to show the important non-dimensional parameters which will influence the dimensionless heat transfer parameter, i.e. Nusselt number.

4.2 Physical Model

The physical model is shown in Fig. 4.1, along with the important geometric parameters. A trapezoidal cavity of height L with the left wall inclined at an angle $\phi = 45^0, 30^0, 0^0$ with Y axis is considered. The heat transfer and the fluid flow for uniform heating in a two-dimensional trapezoidal cavity with a fluid whose left wall and right wall (i.e. side walls) are subjected to cold T_c temperature, bottom wall is subjected to hot T_h temperature while the top wall is kept insulated. The heatlines and thermal mixing will be illustrated for commonly used fluid with Pr = 0:026 – 1000 and Ra = 10^3 - 10^7 in various industrial applications. The fluid is considered as incompressible, Newtonian and the flow is assumed to be laminar. The boundary conditions for velocity are considered as no-slip on solid boundaries.

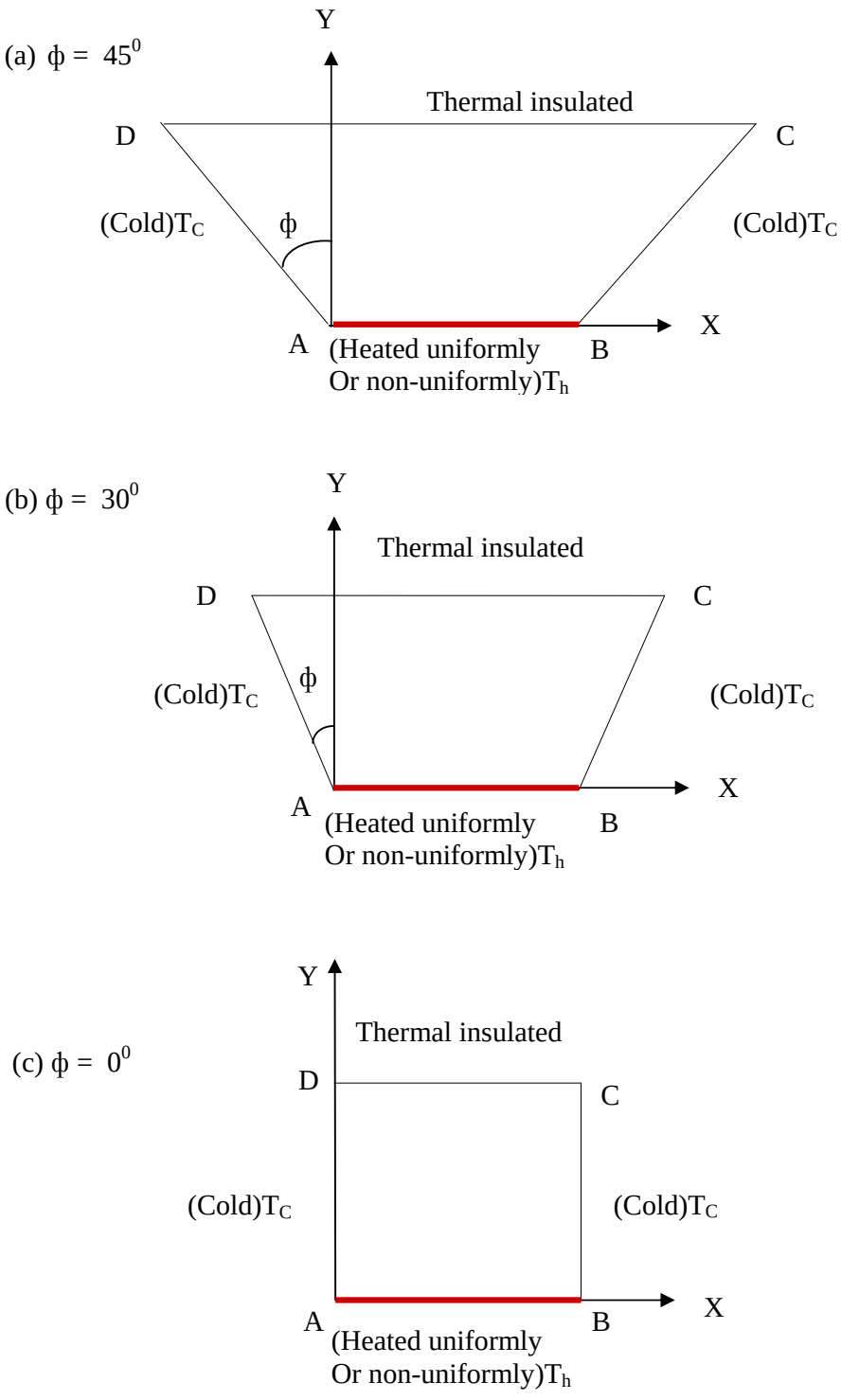

Figure: 4.1. Schematic diagram of the physical system for (a) ϕ = 45^0 , (b) ϕ = 30^0 and (c) ϕ = 0^0

4.3 Mathematical Formulation

The several steps of the mathematical formulation for the above physical configurations are shown as follows

4.3.1 Governing Equations

The fundamental laws used to solve the fluid flow and heat transfer problems, which are the conservation of mass (continuity equations), conservation of momentums (momentum equations), and conservation of energy (energy equations and constitute a set of coupled, nonlinear, partial differential equations. The viscous dissipation term in the energy equation is neglected. For the treatment of the buoyancy term in the momentum equation, Boussinesq approximation is employed to account for the variations of density as a function of temperature, and to couple in this way the temperature field to the flow field. Also for laminar incompressible thermal flow, the buoyancy force is included here as a body force in the *v*-momentum equation. The governing equations for steady natural convection flow can be written as:

Continuity Equation

$$\frac{\partial u}{\partial x}+\frac{\partial v}{\partial y}=0 \tag{4.1}$$

Momentum Equations

$$u\frac{\partial u}{\partial x}+v\frac{\partial u}{\partial y}=-\frac{1}{\rho}\frac{\partial p}{\partial x}+\nu\left(\frac{\partial^2 u}{\partial x^2}+\frac{\partial^2 u}{\partial y^2}\right) \tag{4.2}$$

$$u\frac{\partial v}{\partial x}+v\frac{\partial v}{\partial y}=-\frac{1}{\rho}\frac{\partial p}{\partial y}+\nu\left(\frac{\partial^2 v}{\partial x^2}+\frac{\partial^2 v}{\partial y^2}\right)+g\beta(T-T_c)-\frac{\sigma B_0^2 v}{\rho} \tag{4.3}$$

Energy Equations

$$u\frac{\partial T}{\partial x}+v\frac{\partial T}{\partial y}=\frac{k}{\rho c_p}\left(\frac{\partial^2 T}{\partial x^2}+\frac{\partial^2 T}{\partial y^2}\right) \tag{4.4}$$

where x and y are the distances measured along the horizontal and vertical directions respectively; u and v are the velocity components in the x and y directions respectively; T denote the fluid temperature, T_c denotes the reference temperature for which buoyant force

vanishes, p is the pressure and ρ is the fluid density, g is the gravitational constant, β is the volumetric coefficient of thermal expansion, c_p is the fluid specific heat, k is the thermal conductivity of fluid.

4.3.2 Boundary Conditions

The boundary conditions for the present problem are specified as follows:

Case – I (Uniform heating):

At the bottom wall:

$$u(x,0)=0,\quad v(x,0)=0,\quad T=T_h(\text{Heated uniformly}),\qquad \forall\ y=0,\quad 0\le x\le L$$

At the left wall:

$$u(0,y)=0,\quad v(0,y)=0,\quad T=T_c,\qquad \forall\ x\cos\phi+y\sin\phi=0,\quad 0\le y\le L$$

At the right wall:

$$u(0,y)=0,\quad v(0,y)=0,\quad T=T_c,\qquad \forall\ x\cos\phi-y\sin\phi=L\cos\phi,\quad 0\le y\le L$$

At the top wall:

$$u(x,L)=0,\quad v(x,L)=0,\quad \frac{\partial}{\partial y}\left(\frac{T-T_c}{T_h-T_c}\right)=0,\qquad \forall\ y=L,\quad -L\tan\phi\le x\le L\left(1+\tan\phi\right)$$

Case – II (Non-Uniform heating):

At the bottom wall:

$$u(x,0)=0,\quad v(x,0)=0,\quad T=T_h(\text{Heated Non-uniformly}),\qquad \forall\ y=0,\quad 0\le x\le L$$

At the left wall:

$$u(0,y)=0,\quad v(0,y)=0,\quad T=T_c,\qquad \forall\ x\cos\phi+y\sin\phi=0,\quad 0\le y\le L$$

At the right wall:

$$u(0,y)=0,\quad v(0,y)=0,\quad T=T_c,\qquad \forall\ x\cos\phi-y\sin\phi=L\cos\phi,\quad 0\le y\le L$$

At the top wall:

$$u(x,L)=0,\quad v(x,L)=0,\quad \frac{\partial}{\partial y}\left(\frac{T-T_c}{T_h-T_c}\right)=0,\qquad \forall\ y=L,\quad -L\tan\phi\le x\le L\left(1+\tan\phi\right)$$

where x and y are the distances measured along the horizontal and vertical directions, respectively; u and v are the velocity components in the x- and y-direction, respectively; L is the height of trapezoidal cavity with left wall inclined at an angle ϕ = 45^0, 30^0, 0^0 with y axis; T denotes the temperature; T_h and Tc are heated uniformly or non-uniformly and cold temperatures respectively.

The local Nusselt number at the heated surface of the cavity which is defined by the following expression:

$$Nu_l = Nu_r = Nu_s = Nu_b - \frac{h(x)L}{k}$$

Such local values have been further averaged over the entire heated surface to obtain the surface averaged or overall mean Nusselt number at the bottom, left and right walls are

$$Nu=\int_0^L Nu_l dx=\int_0^L Nu_r dx=\int_0^L Nu_s dx=\int_0^L Nu_b dx$$

Where *L* and *h(x)* are the length and the local convection heat transfer coefficient of the heated wall respectively. The average Nusselt number can be used in process engineering design calculations to estimate the rate transfer from the heated surface.

4.3.3 Non-Dimensional Variables

Non-dimensional variables or numbers are used for making the governing equations (4.1−4.4) into dimensionless form are stated as follows:

$$X=\frac{x}{L},\quad Y=\frac{y}{L},\quad U=\frac{uL}{\alpha},\quad V=\frac{vL}{\alpha},\quad P=\frac{pL^2}{\rho\alpha^2},\quad \theta=\frac{T-T_c}{T_h-T_c},\quad \mathrm{Pr}=\frac{\nu}{\alpha},$$

$$Gr=\frac{g\beta L^3\left(T_h-T_c\right)}{\nu^2},\quad Ra=\frac{g\beta L^3\left(T_h-T_c\right)\mathrm{Pr}}{\nu^2},\quad Ha^2=\frac{\sigma B_0^2 L^2}{\rho\alpha},\quad \alpha=\frac{k}{\rho C_p}$$

Where X and Y are the coordinates varying along horizontal and vertical directions, respectively, U and V are the velocity components in the X and Y directions, respectively, θ is the dimensionless temperature and P is the dimensionless pressure and also $\Delta T = T_h - T_c$ and α are the temperature difference and thermal diffusivity of the fluid respectively.

The dimensionless parameters are the Grashof number *Gr*, Prandtl number *Pr*, Hartmann number and Rayleigh number *Ra*.

4.3.4 Non-Dimensional Governing Equations

The non-dimensional governing equations for steady two-dimensional free convection flow in the trapezoidal cavity after substitution the Non-dimensional variables or numbers into the equations (4.1-4.4), we get,

Continuity Equation

$$\frac{\partial U}{\partial X} + \frac{\partial V}{\partial Y} = 0 \tag{4.5}$$

Momentum Equations

$$U\frac{\partial U}{\partial X} + V\frac{\partial U}{\partial Y} = -\frac{\partial P}{\partial X} + \Pr\left(\frac{\partial^2 U}{\partial X^2} + \frac{\partial^2 U}{\partial Y^2}\right) \tag{4.6}$$

$$U\frac{\partial U}{\partial X} + V\frac{\partial U}{\partial Y} = -\frac{\partial P}{\partial Y} + \frac{1}{\mathrm{Re}}\left(\frac{\partial^2 V}{\partial X^2} + \frac{\partial^2 V}{\partial Y^2}\right) + Ra\,\Pr\theta - Ha^2 V \tag{4.7}$$

Energy Equations

$$U\frac{\partial \theta}{\partial X} + V\frac{\partial \theta}{\partial Y} = \left(\frac{\partial^2 \theta}{\partial X^2} + \frac{\partial^2 \theta}{\partial Y^2}\right) \tag{4.8}$$

4.3.5 Non-Dimensional Boundary Conditions

The non- dimensional boundary conditions under consideration can be written as:

Case – I (Uniform heating):

At the bottom wall:

$$U = 0, \quad V = 0, \quad \theta = 1 \qquad \forall\ Y = 0, \quad 0 \le X \le 1$$

At the left wall:

$$U = 0, \quad V = 0, \quad \theta = 0, \qquad \forall\ X\cos\phi + Y\sin\phi = 0, \quad 0 \le Y \le 1$$

At the right wall:

$$U = 0, \quad V = 0, \quad \theta = 0, \qquad \forall\ X\cos\phi - Y\sin\phi = \cos\phi, \quad 0 \le Y \le 1$$

At the top wall:

$$U = 0, \quad V = 0, \quad \frac{\partial\theta}{\partial Y} = 0, \qquad \forall\ Y = 1, \quad -\tan\phi \le X \le (1 + \tan\phi)$$

Case – II (Non-Uniform heating):

At the bottom wall:

$$U = 0, \quad V = 0, \quad \theta = \sin(\pi X) \qquad \forall\ Y = 0, \quad 0 \le X \le 1$$

At the left wall:

$$U = 0, \quad V = 0, \quad \theta = 0, \qquad \forall\ X\cos\phi + Y\sin\phi = 0, \quad 0 \le Y \le 1$$

At the right wall:

$$U = 0, \quad V = 0, \quad \theta = 0, \qquad \forall\ X\cos\phi - Y\sin\phi = \cos\phi, \quad 0 \le Y \le 1$$

At the top wall:

$$U = 0, \quad V = 0, \quad \frac{\partial\theta}{\partial Y} = 0, \qquad \forall\ Y = 1, \quad -\tan\phi \le X \le (1 + \tan\phi)$$

where X and Y are dimensionless coordinates varying along horizontal and vertical directions, respectively; U and V are dimensionless velocity components in X and Y directions, respectively; θ is the dimensionless temperature.

The local Nusselt number at the heated surface of the cavity which is defined by the following expression:

$$Nu_l = Nu_r = Nu_b = Nu_s = -\frac{\partial \theta}{\partial n}$$

where n denotes the normal direction on a plane.

According to Singh and Sharif (2003), the average Nusselt number at the heated bottom wall, cooled left and right walls and insulated top walls of the cavity based on the non-dimensional variables may be expressed as,

$$Nu = \int_0^1 Nu_l \, dX = \int_0^1 Nu_r \, dX = \int_0^1 Nu_s \, dX = \int_0^1 Nu_b \, dX$$

.

4.4 Numerical Analysis

The governing equations along with the boundary conditions are solved numerically, employing Galerkin weighted residual finite element techniques discussed below.

4.4.1 Finite Element Formulation

The numerical procedure used to solve the governing equations for the present work is based on the Galerkin weighted residual method of finite-element formulation. The non-linear parametric solution method is chosen to solve the governing equations. This approach will result in substantially fast convergence assurance. A non-uniform triangular mesh arrangement is implemented in the present investigation especially near the walls to capture the rapid changes in the dependent variables.

The velocity and thermal energy equations (4.5)-(4.8) result in a set of non-linear coupled equations for which an iterative scheme is adopted. To ensure convergence of the numerical algorithm the following criteria is applied to all dependent variables over the solution domain

$$\sum \left| \psi_{ij}^{n} - \psi_{ij}^{n-1} \right| \leq 10^{-5}$$

where Ψ represents a dependent variable U, V, P, and T; the indexes i, j indicate a grid point; and the index n is the current iteration at the grid level. The six node triangular element is used in this work for the development of the finite element equations. All six nodes are associated with velocities as well as temperature; only the corner nodes are associated with pressure. This means that a lower order polynomial is chosen for pressure and which is satisfied through continuity equation. The velocity component and the temperature distributions and linear interpolation for the pressure distribution according to their highest derivative orders in the differential Eqs (4.5)-(4.8) as

$$U(X,\ Y) = N_\alpha U_\alpha \tag{4.9}$$

$$V(X,\ Y) = N_\alpha V_\alpha \tag{4.10}$$

$$\theta(X,Y) = N_\alpha\ \theta_\alpha \tag{4.11}$$

$$P(X,\ Y) = H_\lambda P_\lambda \tag{4.12}$$

where α = 1, 2, … …, 6; λ= 1, 2, 3; N_α are the element interpolation functions for the velocity components and the temperature, and H_λ are the element interpolation functions for the pressure.

To derive the finite element equations, the method of weighted residuals Zienkiewicz (1991) is applied to the equations (4.5) – (4.8) as

$$\int_A N_\alpha \left(\frac{\partial U}{\partial X} + \frac{\partial V}{\partial Y} \right)\ dA = 0 \tag{4.13}$$

$$\int_A N_\alpha \left(U \frac{\partial U}{\partial X} + V \frac{\partial U}{\partial Y} \right) dA = -\int_A H_\lambda \left(\frac{\partial P}{\partial X} \right) dA + \mathrm{Pr} \int_A N_\alpha \left(\frac{\partial^2 U}{\partial X^2} + \frac{\partial^2 U}{\partial Y^2} \right) dA \tag{4.14}$$

$$\begin{aligned} &\int_A N_\alpha (U \frac{\partial V}{\partial X} + V \frac{\partial V}{\partial Y}) dA = -\int_A H_\lambda (\frac{\partial P}{\partial Y}) dA + \\ &\mathrm{Pr} \int_A N_\alpha (\frac{\partial^2 V}{\partial X^2} + \frac{\partial^2 V}{\partial Y^2}) dA + Ra\,\mathrm{Pr} \int_A N_\alpha \theta dA - Ha^2 \int_A N_\alpha V dA \end{aligned} \tag{4.15}$$

$$\int_A N_\alpha \left(U \frac{\partial \theta}{\partial X} + V \frac{\partial \theta}{\partial Y} \right) dA = \int_A N_\alpha \left(\frac{\partial^2 \theta}{\partial X^2} + \frac{\partial^2 \theta}{\partial Y^2} \right) dA \tag{4.16}$$

Where *A* is the element area.

Gauss's theorem is then applied to equations (4.14)-(4.16) to generate the boundary integral terms associated with the surface tractions and heat flux. Then equations (4.14)-(4.16) becomes,

$$\begin{aligned} &\int_A N_\alpha \left(U \frac{\partial U}{\partial X} + V \frac{\partial U}{\partial Y} \right) dA + \int_A H_\lambda \left(\frac{\partial P}{\partial X} \right) dA \\ &\quad + \Pr \int_A \left(\frac{\partial N_\alpha}{\partial X} \frac{\partial U}{\partial X} + \frac{\partial N_\alpha}{\partial Y} \frac{\partial U}{\partial Y} \right) dA = \int_{S_0} N_\alpha S_x dS_0 \end{aligned} \tag{4.17}$$

$$\begin{aligned} &\int_A N_\alpha (U \frac{\partial V}{\partial X} + V \frac{\partial V}{\partial Y}) dA + \int_A H_\lambda (\frac{\partial P}{\partial Y}) dA + \Pr \int_A (\frac{\partial N_\alpha}{\partial X} \frac{\partial V}{\partial X} + \frac{\partial N_\alpha}{\partial Y} \frac{\partial V}{\partial Y}) \\ &- Ra \Pr \int_\alpha N_\alpha \theta dA + Ha^2 \int_\alpha N_\alpha V dA = \int_{S_0} N_\alpha S_y dS_0 \end{aligned} \tag{4.18}$$

$$\int_\alpha N_\alpha (U \frac{\partial \theta}{\partial X} + V \frac{\partial \theta}{\partial Y}) dA + \int_\alpha (\frac{\partial N_\alpha}{\partial X} \frac{\partial \theta}{\partial X} + \frac{\partial N_\alpha}{\partial Y} \frac{\partial \theta}{\partial Y}) dA = \int_{S_w} N_\alpha q_{lw} dS_w \tag{4.19}$$

Here (4.14)-(4.15) specifying surface tractions (S_x, S_y) along outflow boundary S_0 and (4.16) specifying velocity components and fluid temperature or heat flux (q_w) that flows into or out from domain along wall boundary S_w. Substituting the element velocity component distributions, the temperature distribution, and the pressure distribution from equations (4.9)-(4.12), the finite element equations can be written in the form,

$$K_{\alpha\ \beta}{}^x U_\beta + K_{\alpha\ \beta}{}^y V_\beta = 0 \tag{4.20}$$

$$K_{\alpha\beta\gamma}{}^x U_\beta U_\gamma + K_{\alpha\beta\gamma}{}^y V_\gamma U_\gamma + M_{\alpha\mu}{}^x P_\mu + \Pr \left(S_{\alpha\beta}{}^{xx} + S_{\alpha\beta}{}^{yy} \right) U_\beta = Q_\alpha{}^u \tag{4.21}$$

$$\begin{aligned} &K_{\alpha\beta\gamma}{}^x U_\beta V_\gamma + K_{\alpha\beta\gamma}{}^y V_\gamma V_\gamma + M_{\alpha\mu}{}^y P_\mu + \\ &\Pr(S_{\alpha\beta}{}^{xx} + S_{\alpha\beta}{}^{yy} + Ha^2 K_{\alpha\beta}) V_\beta - Ra \Pr K_{\alpha\beta} \theta_\beta = Q_\alpha{}^v \end{aligned} \tag{4.22}$$

$$K_{\alpha\beta\gamma^x} U_\beta \theta_\gamma + K_{\alpha\beta\gamma^y} V_\beta \theta_\gamma + \left(S_{\alpha\beta^{xx}} + S_{\alpha\beta^{yy}} \right) \theta_\beta = Q_{\alpha^\theta} \tag{4.23}$$

where the coefficients in element matrices are in the form of the integrals over the element area and along the element edges S_0 and S_w as

$$K_{\alpha\beta^x} = \int_A N_\alpha N_{\beta,x} dA \tag{4.24a}$$

$$K_{\alpha\beta^y} = \int_A N_\alpha N_{\beta,y} dA \tag{4.24b}$$

$$K_{\alpha\beta\gamma^x} = \int_A N_\alpha N_\beta N_{\gamma,x} dA \tag{4.24c}$$

$$K_{\alpha\beta\gamma^y} = \int_A N_\alpha N_\beta N_{\gamma,y} dA \tag{4.24d}$$

$$K_{\alpha\beta} = \int_A N_\alpha N_\beta dA \tag{4.24e}$$

$$S_{\alpha\beta^{xx}} = \int_A N_{\alpha,x} N_{\beta,x} dA \tag{4.24f}$$

$$S_{\alpha\beta^{yy}} = \int_A N_{\alpha,y} N_{\beta,y} dA \tag{4.24g}$$

$$M_{\alpha\mu^x} = \int_A H_\alpha H_{\mu,x} dA \tag{4.24h}$$

$$M_{\alpha\mu^y} = \int_A H_\alpha H_{\mu,y} dA \tag{4.24i}$$

$$Q_{\alpha^u} = \int_{S_0} N_\alpha S_x dS_0 \tag{4.24j}$$

$$Q_{\alpha^v} = \int_{S_0} N_\alpha S_y dS_0 \tag{4.24k}$$

$$Q_{\alpha^\theta} = \int_{S_w} N_\alpha \, q_{1w} dS_w \tag{4.24l}$$

$$Q_{\alpha^{\theta_s}} = \int_{S_w} N_\alpha \, q_{2w} dS_w \tag{4.24m}$$

These element matrices are evaluated in closed form ready for numerical simulation. Details of the derivation for these element matrices are omitted herein.

The derived finite element equations (4.20)-(4.23) are nonlinear. These nonlinear algebraic equations are solved by applying the Newton-Raphson iteration technique by first writing the unbalanced values from the set of the finite element equations (4.20)-(4.23) as,

$$F_{\alpha p} = K_{\alpha\beta^x} U_\beta + K_{\alpha\beta^y} V_\beta \tag{4.25a}$$

$$F_{\alpha u} = K_{\alpha\beta\gamma^x} U_\beta U_\gamma + K_{\alpha\beta\gamma^y} V_\gamma U_\gamma + M_{\alpha\mu^x} P_\mu + \Pr\left(S_{\alpha\beta^{xx}} + S_{\alpha\beta^{yy}} \right) U_\beta - Q_{\alpha u} \tag{4.25b}$$

$$F_{\alpha v} = K_{\alpha\beta\gamma^x} U_\beta V_\gamma + K_{\alpha\beta\gamma^y} V_\gamma V_\gamma + M_{\alpha\mu^y} P_\mu + \Pr\left(S_{\alpha\beta^{xx}} + S_{\alpha\beta^{yy}} + Ha^2 K_{\alpha\beta} \right) V_\beta - Ra \Pr K_{\alpha\beta} \theta_\beta - Q_{\alpha\theta} \tag{4.25c}$$

$$F_{\alpha\theta} = K_{\alpha\beta\gamma^x} U_\beta \theta_\gamma + K_{\alpha\beta\gamma^y} V_\beta \theta_\gamma + \left(S_{\alpha\beta^{xx}} + S_{\alpha\beta^{yy}} \right) \theta_\beta - Q_{\alpha\theta} \tag{4.25d}$$

This leads to a set of algebraic equations with the incremental unknowns of the element nodal velocity components, temperatures, and pressures in the form,

$$\begin{bmatrix} K_{pu} & K_{pv} & 0 & 0 \\ K_{uu} & K_{uv} & 0 & K_{up} \\ K_{\theta u} & K_{\theta v} & K_{\theta\theta} & 0 \\ K_{vu} & K_{vv} & K_{v\theta} & K_{vp} \end{bmatrix} \begin{bmatrix} \Delta p \\ \Delta u \\ \Delta\theta \\ \Delta v \end{bmatrix} = - \begin{bmatrix} F_{\alpha p} \\ F_{\alpha u} \\ F_{\alpha\theta} \\ F_{\alpha v} \end{bmatrix} \tag{4.26}$$

Where $K_{uu} = K_{\alpha\beta\gamma^x} U_\beta + K_{\alpha\gamma\beta^x} U_\gamma + K_{\alpha\beta\gamma^y} V_\beta + \Pr\left(S_{\alpha\beta^{xx}} + S_{\alpha\beta^{yy}} \right)$

$K_{uv} = K_{\alpha\beta\gamma^y} U\gamma$

$K_{u\theta} = 0; \qquad K_{up} = M_{\alpha\mu^x}$

$K_{vu} = K_{\alpha\beta\gamma^x} V\gamma$

$K_{vv} = K_{\alpha\beta\gamma^x} U_\gamma + K_{\alpha\beta\gamma^y} V_\gamma + K_{\alpha\beta\gamma^y} V_\gamma + \Pr\left(S_{\alpha\beta^{xx}} + S_{\alpha\beta^{yy}} + Ha^2 K_{\alpha\beta} \right)$

$K_{v\theta} = -Ra \Pr K_{\alpha\beta}; \qquad K_{vp} = M_{\alpha\mu^y}$

$$K_{\theta u} = K_{\alpha\beta\gamma^x}\theta\gamma; \qquad K_{\theta v} = K_{\alpha\beta\gamma^y}\theta\gamma$$

$$K_{\theta\theta} = K_{\alpha\beta\gamma^x}U_\beta + K_{\alpha\beta\gamma^y}V_\beta + (S_{\alpha\beta^{xx}} + S_{\alpha\beta^{yy}})$$

$$K_{\theta p} = 0$$

$$K_{pu} = K_{\alpha\beta^x}; \qquad K_{pv} = K_{\alpha\beta^y} \quad , \quad \text{and} \quad K_{p\theta} = 0 = K_{pp}$$

The iteration process is terminated if the percentage of the overall change compared to the previous iteration is less than the specified value.

To solve the sets of the global nonlinear algebraic equations in the form of matrix, the Newton-Raphson iteration technique has been adapted through PDE solver with MATLAB interface.

CHAPTER 5

MHD FREE CONVECTION WITHIN TRAPEZOIDAL CAVITY WITH UNIFORMLY HEATED BOTTOM WALL

The heat transfer and the fluid flow for uniform heating of bottom wall in a two-dimensional trapezoidal cavity of height L with the left wall inclined at an angle ϕ = 45^0, 30^0, 0^0 with Y axis was considered as shown in a schematic diagram of figure 4.1 in section 4.2 of chapter 4. In this physical system, dimensional governing equations (4.1 – 4.4) and non-dimensional governing equations (4.5 -4.8) are solved in section 4.3.1 and 4.3.4 respectively in previous chapter 4. For boundary conditions, left wall and right wall (i.e. side walls) are subjected to cold temperature *(T_c)* and the top wall is thermal insulated and also the bottom wall is heated uniformly as shown in section 4.3.2 and 4.3.5(case –I : uniform heating). Numerical technique of finite element formulation has also been discussed in section 4.4.1.In this chapter grid independence test, code validation, comparisons and results have been discussed.

5.1 Grid Independence Test for Uniform Heating

Test for the accuracy of grid fineness has been carried out to find out the optimum grid number.

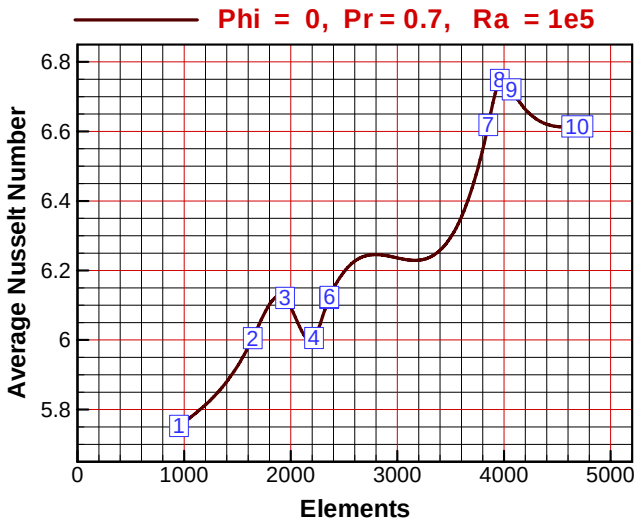

Figure 5.1: Convergence of average Nusselt number with grid refinement for *Pr* = 0.7, *Ha* = 50, ϕ = 0^0 and *Ra* = 10^5 in presence of uniform heating.

In order to obtain grid independent solution, a grid refinement study is performed for a trapezoidal cavity with *Pr* = 0.7, *phi* = 0 and $Ra = 10^5$. Figure 4.2 shows the convergence of the average Nusselt number, Nu_{av} at the heated surface with grid refinement. It is observed that grid independence is achieved with 2363 elements where there is insignificant change in Nu with further increase of mesh elements. Six different non-uniform grids with the following number of nodes and elements were considered for the grid refinement tests: 6402 nodes, 952 elements; 10981 nodes, 1643 elements; 12922 nodes, 1947 elements; 14729 nodes, 2218 elements; 15635 nodes, 2359 elements; 15731 nodes, 2363 elements, 25462 nodes, 3852 elements, 26185 nodes, 3960 elements, 26903 nodes, 4071 elements, 30970 nodes, 4687 elements, . From these values, 15731 nodes, 2363 elements elements can be chosen throughout the simulation to optimize the relation between the accuracy required and the computing time.

Nodes (elements)	6402 (952)	10981 (1643)	12922 (1947)	14729 (2218)	15635 (2359)	15731 (2363)	25462 (3852)	26185 (3960)	26903 (4071)	30970 (4687)
Nu	5.753017	6.005381	6.120885	6.005761	6.121049	6.123839	6.618788	6.74774	6.721055	6.614218
Time (s)	3.563	5.313	6.813	7.235	7.875	7.875	13.781	14.0	14.266	16.656

Table 5.1: Grid Sensitivity Check at *Pr* = 0.7 , *Phi* = 0 , *Ha* = 50 *and Ra* = 10^5.

5.2 Code Validation

For the validation of the code, a trapezoidal cavity without MHD is considered with a fluid by finite element weighted residual method whose left wall and right wall (i.e. side walls) are subjected to cold T_c temperature, bottom wall is subjected to uniformly hot T_h temperature while the top wall is kept insulated. Average Nusselt number is calculated for three different Rayleigh numbers ($Ra = 10^3$, 10^4 and 10^5) and three different angles ϕ = 45^0, 30^0, 0^0 , while the prandtl number is fixed i.e. Pr = 0.7 for uniform heating of bottom and side wall respectively. The results were compared with those reported by Basak et al. (March 2009). In Table 5.2 and Table 5.3, for code validation, average Nusselt numbers is presented for different Rayleigh numbers of uniform heating of bottom and side wall respectively with fixed Prandtl number. For code validation, in Table 5.2 and also in the

figure (5.2 – 5.4) of uniform bottom heating 14060 nodes and 2121 elements, 12673 nodes and 1906elements, 5858 nodes and 864 elements have been used for $\phi = 0^0$, $\phi = 30^0$, $\phi = 45^0$ and $Ra = 10^5$ respectively. In table 5.3, to bring the results of uniform heating of side wall 14060 nodes and 2121 elements, 8434 nodes and 1256 elements, 1527 nodes and 216 elements have also been used for $\phi = 0^0$, $\phi = 30^0$, $\phi = 45^0$ respectively. The results of the figure (5.2 – 5.4) of uniform bottom heating were also compared with those reported by Basak et al. (2009) with streamlines, isotherms (temperature) and Heat function or total heat flux for Pr =0.7 and . $Ra = 10^5$. The results from the present experiment are almost same as Basak et.al.

Ra	Average Nusselt Number, (Nu_{av})					
	Present work without MHD			Basak et al. (2009) without MHD		
	$\phi = 0^0$	$\phi = 30^0$	$\phi = 45^0$	$\phi = 0^0$	$\phi = 30^0$	$\phi = 45^0$
10^3	6.055778	4.714051	3.894428	5.31956	3.93605	3.34577
10^4	6.09068	4.935452	4.19254	6.4311	5.37306	4.90481
10^5	7.558405	6.633036	5.952502	8.71198	7.80227	7.37514

Table 5.2: Code validation for uniform heating of bottom wall with Pr = 0.7.

Ra	Average Nusselt Number, (Nu_{av})					
	Present work without MHD			Basak et al. (2009) without MHD		
	$\phi = 0^0$	$\phi = 30^0$	$\phi = 45^0$	$\phi = 0^0$	$\phi = 30^0$	$\phi = 45^0$
10^3	3.134102	2.240473	1.672972	2.65347	1.74006	1.27778
10^4	3.151073	2.354613	1.842988	3.19866	2.37812	1.83453
10^5	3.887594	3.213328	2.797346	4.31809	3.43934	2.71105

Table 5.3: Code validation for uniform heating of side wall with Pr = 0.7

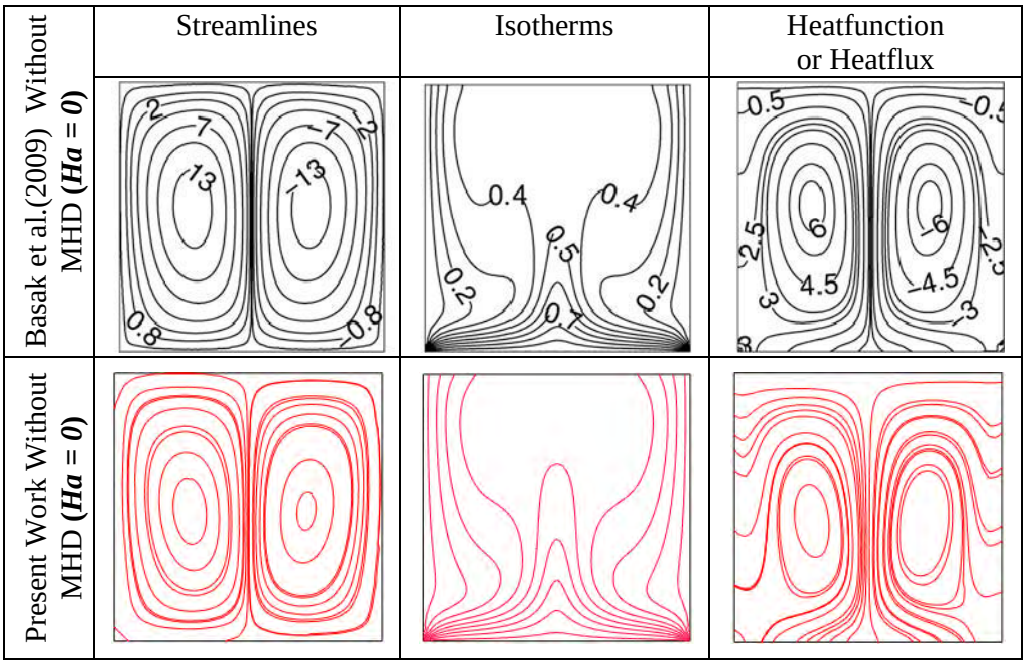

Figure 5.2: Code validation for uniform bottom heating at *Ra* = 10^5, ϕ = 0^0 with Pr = 0.7.

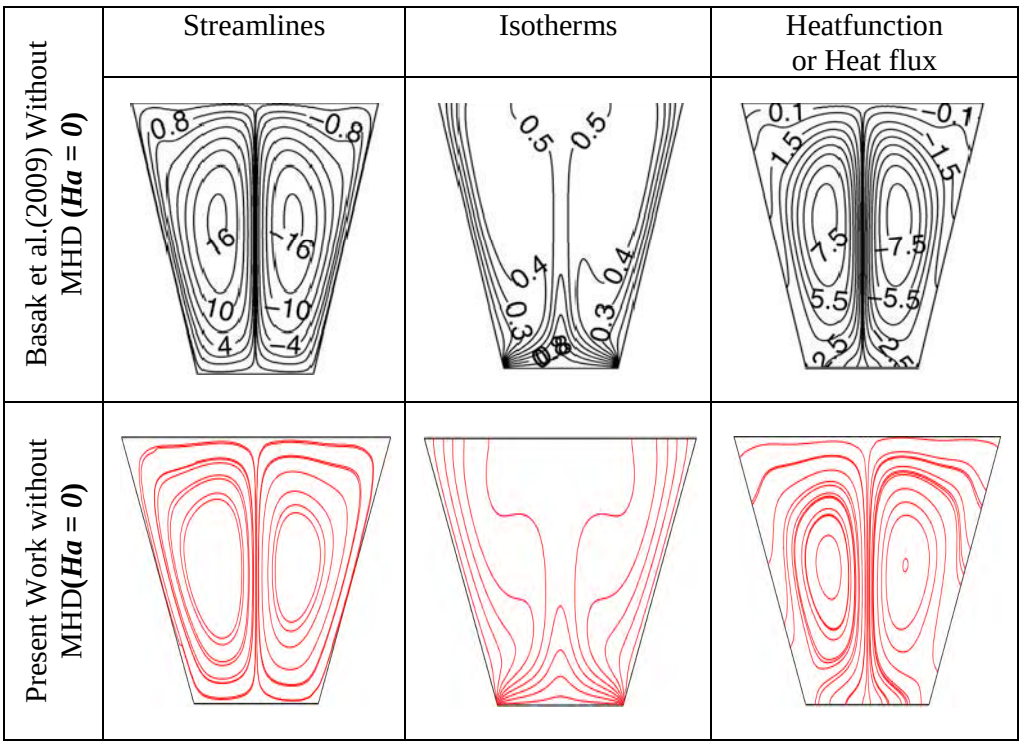

Figure 5.3: Code validation for uniform bottom heating at *Ra* = 10^5, ϕ = 30^0 with Pr = 0.7

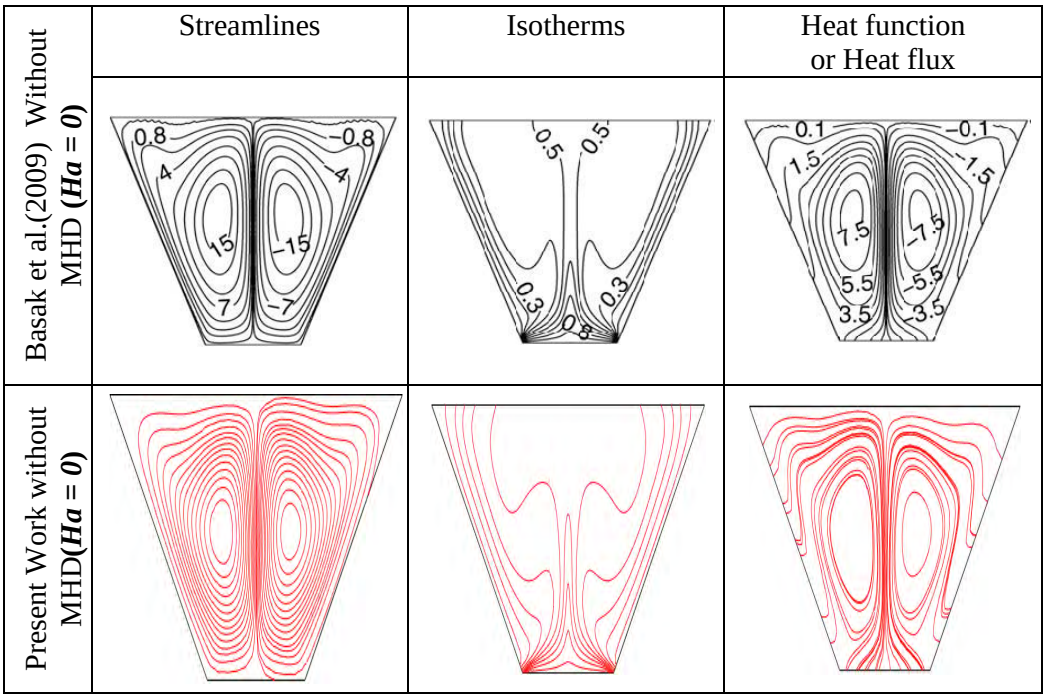

Figure 5.4: Code validation for uniform bottom heating at $Ra = 10^5$, $\phi = 45^0$ with Pr = 0.7.

5.3 Comparisons between without and with MHD

After validation of the code, a trapezoidal cavity with MHD is considered with a fluid whose left wall and right wall (i.e. side walls) are subjected to cold T_c temperature, bottom wall is subjected to uniformly hot T_h temperature while the top wall is kept insulated . Average Nusselt number is calculated for three different Rayleigh numbers ($Ra = 10^3$, 10^4 and 10^5) and three different angles $\phi = 45^0$, 30^0, 0^0, while the prandtl number is fixed i.e. Pr = 0.7 for uniform heating of bottom and side wall respectively. The results were compared with the present work where magneto-hydrodynamic effect is not applied. In Table 5.4 and Table 5.5, for comparison, average Nusselt number is presented for different Rayleigh numbers of uniform heating of bottom and side wall respectively with fixed Prandtl number. Here average Nusselt number of uniform heating of bottom and side wall is enhancing for different Rayleigh numbers. When Rayleigh numbers increase then average Nusselt number increase is seen. This is happening because of heat transfer. Also magnitudes of average Nusselt number of uniform heating of bottom wall is higher than magnitudes of average Nusselt number of uniform heating of side wall for various

Rayleigh numbers. The results of the figure (5.5 – 5.7) with magneto-hydrodynamics (MHD) effect of uniform bottom heating for $\phi = 0^0$, $\phi = 30^0$, $\phi = 45^0$ and $Ra = 10^5$ were also compared to the present work with streamlines, isotherms (temperature) and heat function or total heat flux where magneto-hydrodynamics (MHD) is not applied. Here from the present work of the figure it is seen that heat flow suppressed out for magnetic effect. Comparisons of the results without and with MHD of the current research work are given below.

Ra	Average Nusselt Number, (Nu_{av})					
	Present work With MHD			Present work without MHD		
	$\phi = 0^0$	$\phi = 30^0$	$\phi = 45^0$	$\phi = 0^0$	$\phi = 30^0$	$\phi = 45^0$
10^3	5.685321	4.46249	3.892641	6.055778	4.714051	3.894428
10^4	5.686197	4.463856	3.893894	6.09068	4.935452	4.19254
10^5	5.753017	4.666547	4.2141	7.558405	6.633036	5.952502

Table 5.4: Comparison of the results for uniform heating of bottom wall with Pr = 0.7.

Ra	Average Nusselt Number, (Nu_{av})					
	Present work With MHD			Present work without MHD		
	$\phi = 0^0$	$\phi = 30^0$	$\phi = 45^0$	$\phi = 0^0$	$\phi = 30^0$	$\phi = 45^0$
10^3	2.859967	2.239549	1.96883	3.134102	2.240473	1.672972
10^4	2.859702	2.240199	1.970905	3.151073	2.354613	1.842988
10^5	2.88603	2.341693	2.148533	3.887594	3.213328	2.797346

Table 5.5: Comparison of the results for uniform heating of side wall with Pr = 0.7

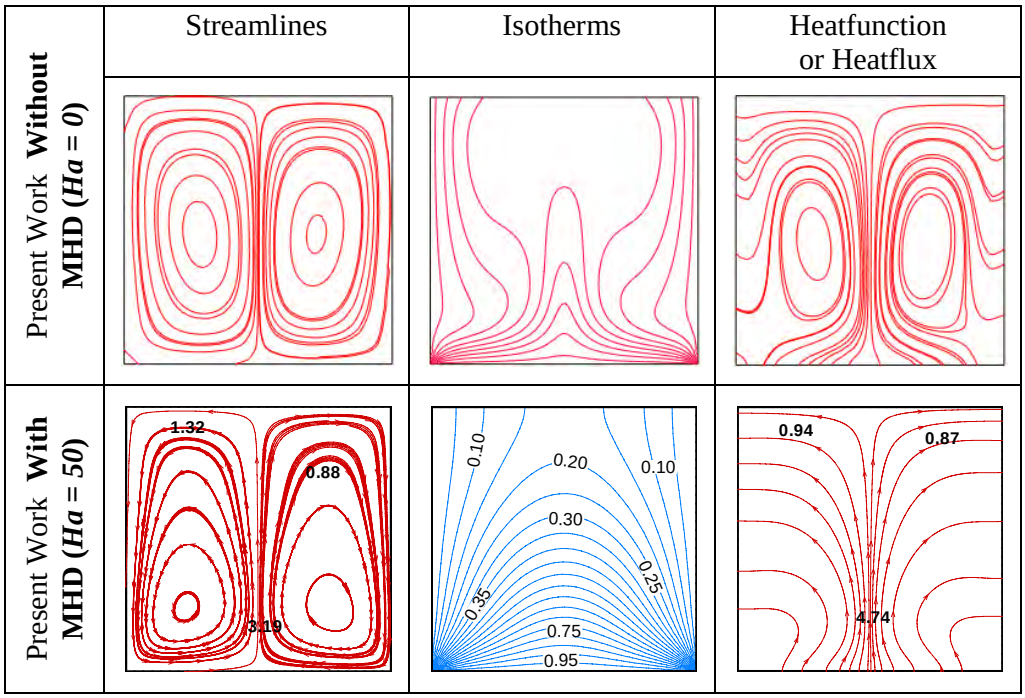

Figure 5.5: Comparison for uniform bottom heating at $Ra = 10^5$, $\phi = 0^0$ with Pr = 0.7 when *Ha* = 0 and *Ha* = 50.

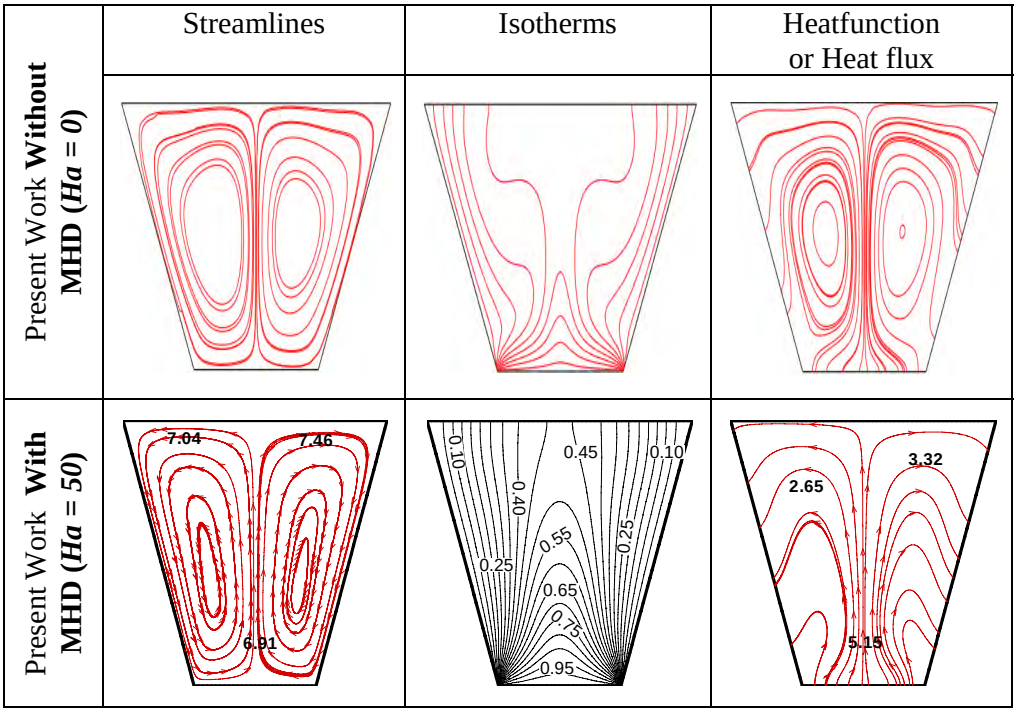

Figure 5.6: Comparison for uniform bottom heating at $Ra = 10^5 \phi = 30^0$ with Pr = 0.7 when *Ha* = 0 and *Ha* = 50.

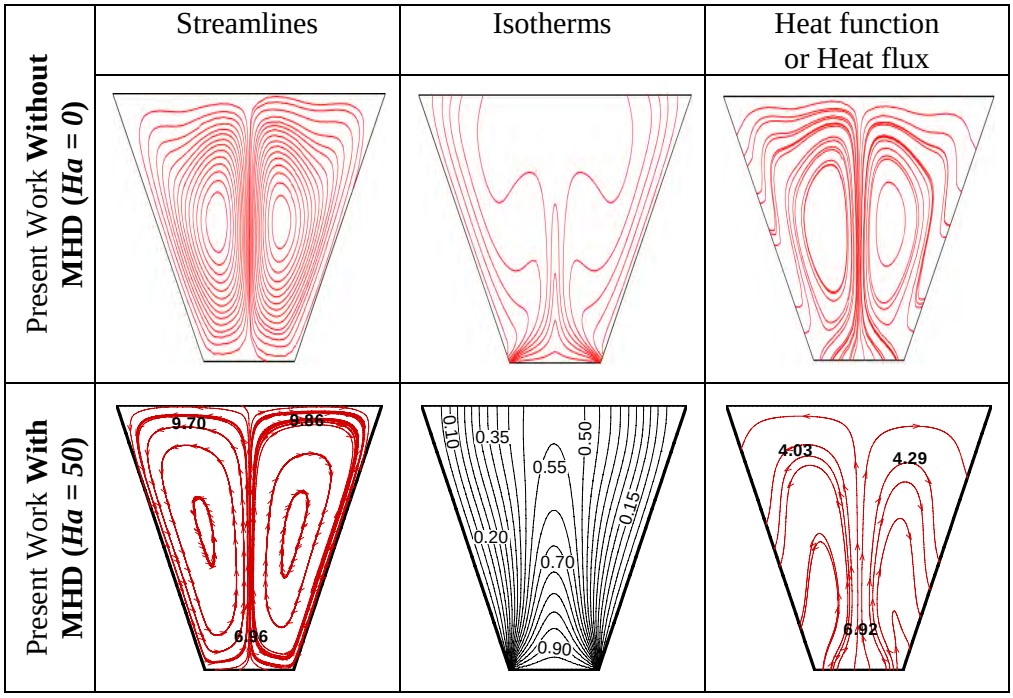

Figure 5.7: Comparison for uniform bottom heating at $Ra = 10^5 \phi = 45^0$ with Pr = 0.7 when $Ha = 0$ and $Ha = 50$.

5.4 Results and Discussion

After completing the code validation with those reported Basak et al. (March 2009), two dimensional laminar steady state on MHD free convection within trapezoidal cavity with uniformly heated bottom wall have been studied numerically. In this endorsement uniformly heated bottom wall, thermal insulation of top wall and cooled side (left or right) walls have been analyzed. Two-dimensional form of Navier-stoke equations along with the energy equations are solved by Galerkin finite element method. Results are obtained on uniform heating for parametric study for the wide range of Rayleigh number, Ra = 10^3-10^7 and Prandtl number, Pr = 0.026, 0.7, 1000 with various angles, $\phi = 45^0, 30^0, 0^0$(square cavity).

5.4.1 Uniform Heating of Bottom Wall

Figure 5.8 -5.19 display the effects of streamline (stream function), isotherms (temperature) and heatlines for Pr = 0.026, 0.7, 1000 when bottom wall is uniformly heated and side walls is maintained as cold. Here we see that from the middle portion of

the bottom wall fluid rise up and the fluid near the hot of bottom wall has lower density. So it moves upward relatively heavy fluid along two vertical side walls moves downwards (flow down) forming using symmetric rolls with clockwise and anticlockwise rotations inside the cavity and the fluid is heated up. Thus fluid completes circulation.

Figure 5.8 illustrate that the magnitudes of streamfunction contours are considerably smaller which express that, at low Rayleigh number the flow is primarily due to conduction. For Ra = 10^3, Pr = 0.026 and $\phi = 0^0$(square cavity) isotherms (temperature) with $\theta = 0.05 - 0.10$ occur symmetrically along side (left or right) walls and with $\theta \geq 0.15$ are smooth curves symmetric with respect to vertical symmetrical line (Fig. 5.8a). For Ra = 10^3, Pr = 0.026 and $\phi = 30^0$ the temperature contours with $\theta = 0.05 – 0.25$ occur symmetrically near the side walls of the enclosure and with $\theta \geq 0.30$ are smooth curves symmetric with respect to central symmetrical line (Fig. 5.8b). Again for Ra = 10^3, Pr = 0.026 and $\phi = 45^0$ isotherms (temperature) with $\theta = 0.05 – 0.30$ occur symmetrically near the side walls of the enclosure and with $\theta \geq 0.35$ are smooth curves symmetric with respect to vertical symmetrical line (Fig. 5.8c).

The presence of significant convection is also exhibited with temperature distribution for various ϕ in trapezoidal cavity. It can be explained with distribution of heat energy is governed by heat function or heat flux. Heatlines or total heat flux are shown in panels of fig.5.8a-c. Heatlines illustrate that heat energy from the bottom wall symmetrically distributed to side walls for various tilt angles of ϕ especially for smaller Ra. It is important to note that two bottom corner edges have infinite heat flux as the cold wall is directly in contact with the hot bottom wall and sign of heat functions are depend on boundary conditions at two bottom corners. Our sign convection is based on fact that heat flow occurs from hot to cold walls and the positive heat flow correspond to anticlockwise heat flow. It may be noted that the magnitudes of heat functions decrease from the bottom edges to the central symmetric line where no heat flux condition is valid due to symmetric boundary conditions for temperature.

It is interesting to note that at the bottom corner point $\phi = 0^0$(square cavity) is larger than for $\phi = 45^0$ and 30^0. It is evident that heatlines near the bottom portion of side walls are more dense for $\phi = 45^0$ and less dense for $\phi = 0^0$(square cavity). The dense heatlines is also indicating enhanced rate of heat transfer from the bottom to the side walls. Therefore isotherms with $\theta = 0.05 – 0.35$ are shifted for $\phi = 45^0$ toward the side walls. It ios also

observed that heat transfer at the top portion of the cavity for $\phi = 45^0$ and 30^0 is higher compressed to $\phi = 0^0$(square cavity) based on value of heatfunction (Π). As the heat transfer is quite large at the corners of bottom wall, the thermal boundary layer was found to develop near the bottom edges and thickness of boundary layer is larger at the top portion of the cold wall signifying less heat transfer to the top portion. The stratification zone of temperature contours occur near the center of the bottom wall as vertical heatlines occur near the central heatlines.

Figure 5.9 and 5.10 point up that the magnitudes of streamfunction are smaller for Ra = 10^4, 10^5, Pr = 0.026 and isotherms (temperature) with $\theta = 0.05 – 0.15$, $\theta = 0.05 – 0.30$, $\theta = 0.05 – 0.35$ occur symmetrically near the side walls of the enclosure and with $\theta \geq 0.25$, $\theta \geq 0.30$, $\theta \geq 0.35$ are smooth curves symmetric with respect to central symmetrical line for Ra = 10^4, 10^5, Pr = 0.026 and $\phi = 45^0$, 30^0, 0^0(square cavity) (Fig 5.9a-c, 5.10a-c) and heatlines enhanced the rate of heat transfer from the bottom to side walls for Ra = 10^4, 10^5, Pr = 0.026. It is observed that at critical Ra the middle portion of isotherms starts getting deformed and the maximum value of ψ is at the eye of vortices. As Ra increases, the buoyancy driven circulation inside the cavity is also increased as seen from greater magnitudes of stream function (fig. 5.9and 5.10). It is also observed that the greater circulation in bottom regime follows a progressive wrapping and isotherms are more compressed towards the side wall as can be seen fig 5.9 and 5.10.

Figure 5.11 illustrate that effect of buoyancy force is compared to viscous forces and the intensity of fluid motion has been increased by larger magnitudes of streamfunction for Ra = 10^7, Pr = 0.026. The enhance convection causes larger heat energy to flow from the bottom wall to the top portion of the vertical wall and large regime of the top portion of the cavity remains at uniform temperature for $\phi = 45^0$ and 30^0.It is interesting to note that isotherms are more compressed near to corners of bottom wall. Therefore the deformation occurs in the streamfunction near to the corners of bottom wall. As a result secondary circulations are also developed near to the intersection of uniformly heated bottom wall and center of the cold side walls for $\phi = 0^0$ and for $\phi = 30^0$, 45^0 symmetric multiple circulations near to corner appear. These secondary vortices push the eye of the primary vortices toward the axis of symmetry as shown in fig 5.11.

It is interesting to detect that the stratification zone of temperature at the center vertical line near the bottom wall for Ra = 10^7 is suppressed whereas stratification zone of

temperature is larger for Ra = 10^3 due to increased convection. It is also noted that stratification zone of temperature at bottom wall is thicker for $\phi = 0^0$(square cavity) due to less intense circulation near the top portion of the cavity. Isotherms (temperature) with $\theta = 0.05 – 0.55$, $\theta = 0.05 – 0.70$, $\theta = 0.05 – 0.65$ occur symmetrically near the side walls of the enclosure and with $\theta \geq 0.60$, $\theta \geq 0.75$, $\theta \geq 0.70$ are smooth curves symmetric with respect to central symmetrical line for Ra = 10^7, Pr = 0.026 and $\phi = 45^0$, 30^0, 0^0(square cavity) respectively. It is also observed that the shapes of streamlines almost circular except near the side wall. Heatlines indicate the heat transfer from the hot wall to cold side walls and uniform heat flow circulation due to fluid circulation cells. Heatlines near the top portion of the side walls are oscillatory due to secondary circulation for $\phi = 45^0$ and 30^0. It is also observed that heatlines are quite dense near the central regime for $\phi = 45^0$ and 30^0 and implies enhance thermal mixing near the central to top portion of the cavity.It may also be identify that the ignifcant convection causes distortion of heatlines especially near the side walls as compared with conduction heat transfer(see fig 5.8).

Figure 5.12 – 5.15 exemplify that the magnitudes of streamfunction are circular or elliptical near the core but the streamlines near the wall is almost parallel to wall exhibiting large intensity of flow for Pr = 0.7 and Ra = $10^3 – 10^7$. Also for Pr = 0.7 and Ra = 10^3 isotherms with $\theta = 0.05 – 0.10$, $\theta = 0.05 – 0.25$, $\theta = 0.05 – 0.30$ and also $\theta = 0.05 – 0.10$, $\theta = 0.05 – 0.25$, $\theta = 0.05 – 0.35$ for Pr = 0.7 and Ra = 10^4 and also $\theta = 0.05 – 0.15$, $\theta = 0.05 – 0.45$, $\theta = 0.05 – 0.50$ for 0.7 and Ra = 10^5 and also $\theta = 0.05 – 0.50$, $\theta = 0.05 – 0.55$, $\theta = 0.05 – 0.45$ for 0.7 and Ra = 10^7 occur symmetrically near the side walls of the enclosure and $\theta \geq 0.15$, $\theta \geq 0.30$, $\theta \geq 0.35$ and $\theta \geq 0.15$, $\theta \geq 0.30$, $\theta \geq 0.40$ and also $\theta \geq 0.20$, $\theta \geq 0.50$, $\theta \geq 0.55$ and $\theta \geq 0.55$, $\theta \geq 0.60$, $\theta \geq 0.50$ are smooth curves symmetric with respect to central symmetrical line for Ra = 10^3 - 10^7, Pr = 0.7 and $\phi = 45^0$, 30^0, 0^0(square cavity) respectively. It is interesting to detect that the intensity of flow have been increased for irrespective of ϕ as seen fig 5.9 – 5.11. Although streamlines are circular or elliptical near the core but streamlines near the wall is almost parallel to wall for intensity of flow (see fig 5.12 – 5.15). It is also fascinating that multiple correlations are absent for Pr = 0.7 and Ra = 10^7 wherwas multiple heat circulation loops were observed for Pr = 0.026(see fig 5.15). Due to enhanced flow circulations the isotherms are highly compressed near the side walls except near the bottom wall especially for $\phi = 45^0$ and 30^0.The thermal energy is further analyzed with heatlines. The large temperature gradient near the side walls are due to significant number of heatlines with a large variation of heatfunction as seen in

figure 5.12a-c to 5.15a-c whereas the heatlines along the side walls are less dense leading to less thermal gradient and also near corners irrespective of ϕ s.

Figure 5.16 – 5.19 show streamline. Isotherms (temperature) and heatlines for Ra = 10^3 - 10^7, Pr =1000 and ϕ = 45^0, 30^0, 0^0(square cavity) respectively. Also for Pr = 1000 and Ra = 10^3 isotherms with θ = 0.05 – 0.10, θ = 0.05 – 0.25, θ = 0.05 – 0.35 and also θ = 0.05 – 0.15, θ = 0.05 – 0.45, θ = 0.05 – 0.50 for Pr = 1000 and Ra = 10^4 and also θ = 0.05 – 0.50, θ = 0.05 – 0.60, θ = 0.05 – 0.55 for 1000 and Ra = 10^5 and also θ = 0.05 – 0.45, θ = 0.05 – 0.40, θ = 0.05 – 0.40 for 1000 and Ra = 10^7 occur symmetrically near the side walls of the enclosure and θ ≥ 0.15, θ ≥ 0.30, θ ≥ 0.40 and θ ≥ 0.20, θ ≥ 0.50, θ ≥ 0.55 and also θ ≥ 0.55, θ ≥ 0.60, θ ≥ 0.60 and θ ≥ 0.50, θ ≥ 0.45, θ ≥ 0.45 are smooth curves symmetric with respect to central symmetrical line for Ra = 10^3 - 10^7, Pr = 0.7 and ϕ = 45^0, 30^0, 0^0(square cavity) respectively. Comparative studies on figures (5.12 – 5.15) and figures (5.16 -5.19) show that as Pr increases from 0.7 to 1000 for various Ra, the values of stream function on the core cavity increase because of highly viscous. It is exemplify that the greater circulations due to higher Pr leads to elliptical stream function in the core. At larger Ra = 10^7 and Pr =1000 (Fig. 5.19a-c), it is seen that the intensity of flow circulations are increased from the values of stream functions. Streamlines near the side walls take the shape of container or circular and signify enhance mixing effects. The isotherms θ ≤ 0.40 are highly compressed near the side walls and isotherms with θ ≥ 0.50 are also confined within a small regime near the bottom wall. The heatlines are highly dense at the central regime. The enhanced thermal mixing due to convection as well as heat transfort from the bottom wall to uniform temperature near the central regime.

It is also significant that at high Pr the streamline except at the central regime are almost circular indicating higher insity of flows. Also the signififcant number of heatlines are observed along the side walls leading to large thermal gradient for ϕ = 45^0 and 30^0 and heatlines are more less dense along the side vertical walls. Besides this, the effects of heat transfer for various Ra and inclination angles ϕ = 45^0, 30^0, 0^0 for different Pr on local and average Nusselt number are discussed later in detail.

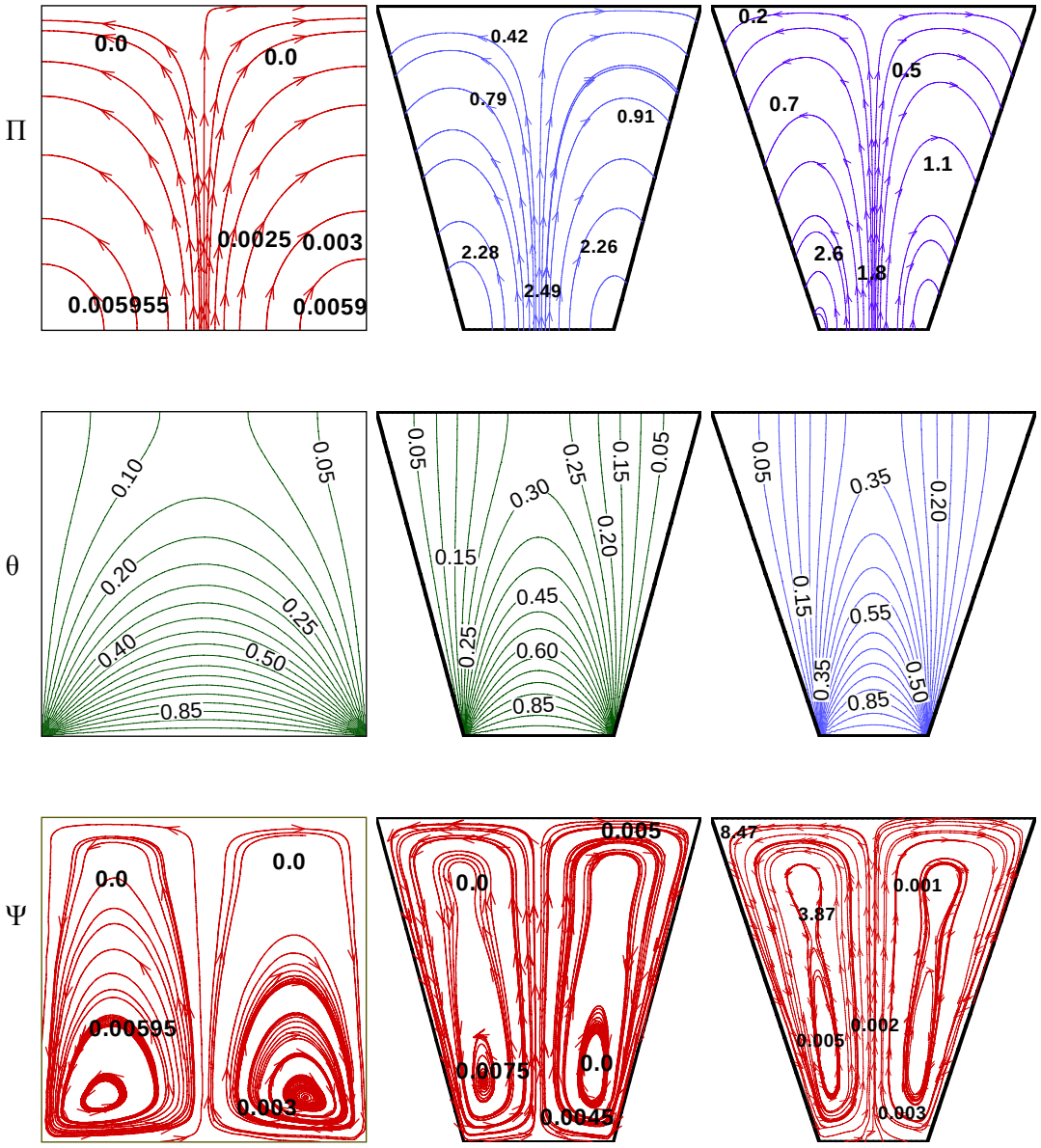

Figure 5.8: Stream function (Ψ), temperature (θ), heat function or total heat flux(Π) contours for uniform bottom heating θ(X,0) = 1 with Pr = 0.026, Ha = 50 and Ra = 103 (a) Φ = 0o (b) Φ = 30o (c) Φ = 45o

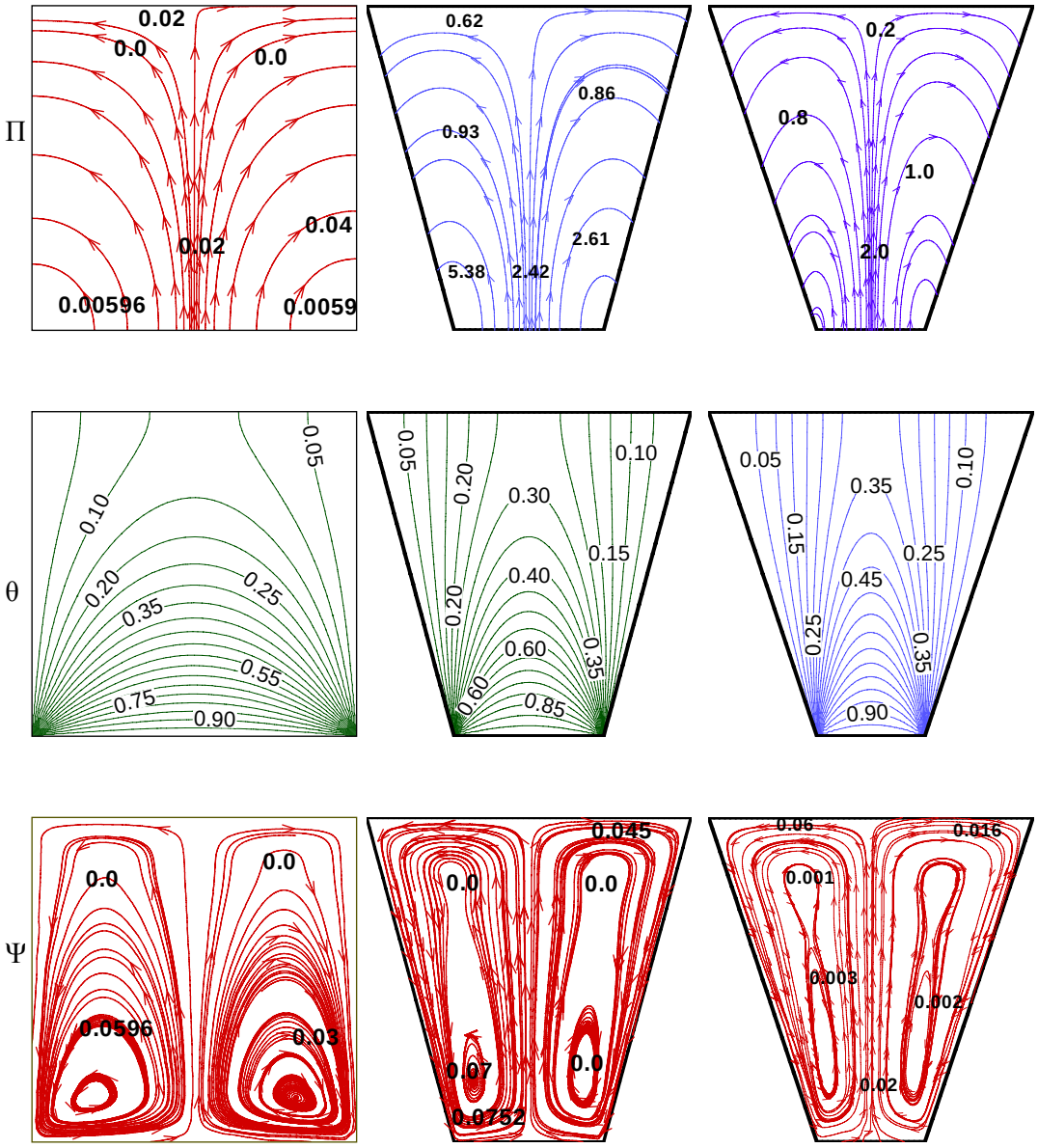

Figure 5.9: Stream function (Ψ), temperature (θ), heat function or total heat flux(Π) contours for uniform bottom heating θ(X,0) = 1 with Pr = 0.026, Ha = 50 and Ra = 10^4 (a) Φ = 0^o (b) Φ = 30^o (c) Φ = 45^o

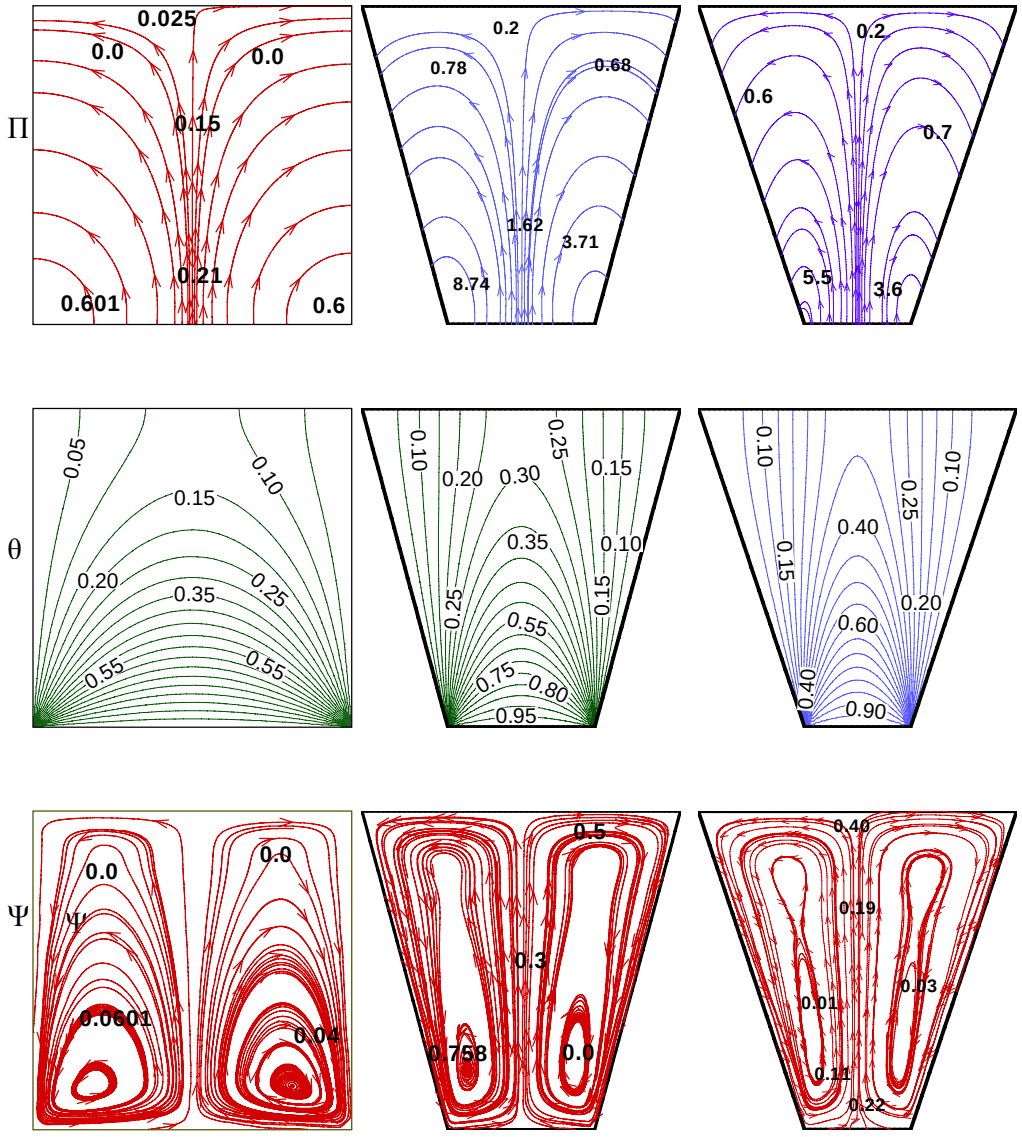

a b c

Figure 5.10: Stream function (Ψ), temperature (θ), heat function or total heat flux(Π) contours for uniform bottom heating θ(X,0) = 1 with Pr = 0.026, Ha = 50 and Ra = 10^5 (a) Φ = 0^o (b) Φ = 30^o (c) Φ = 45^o

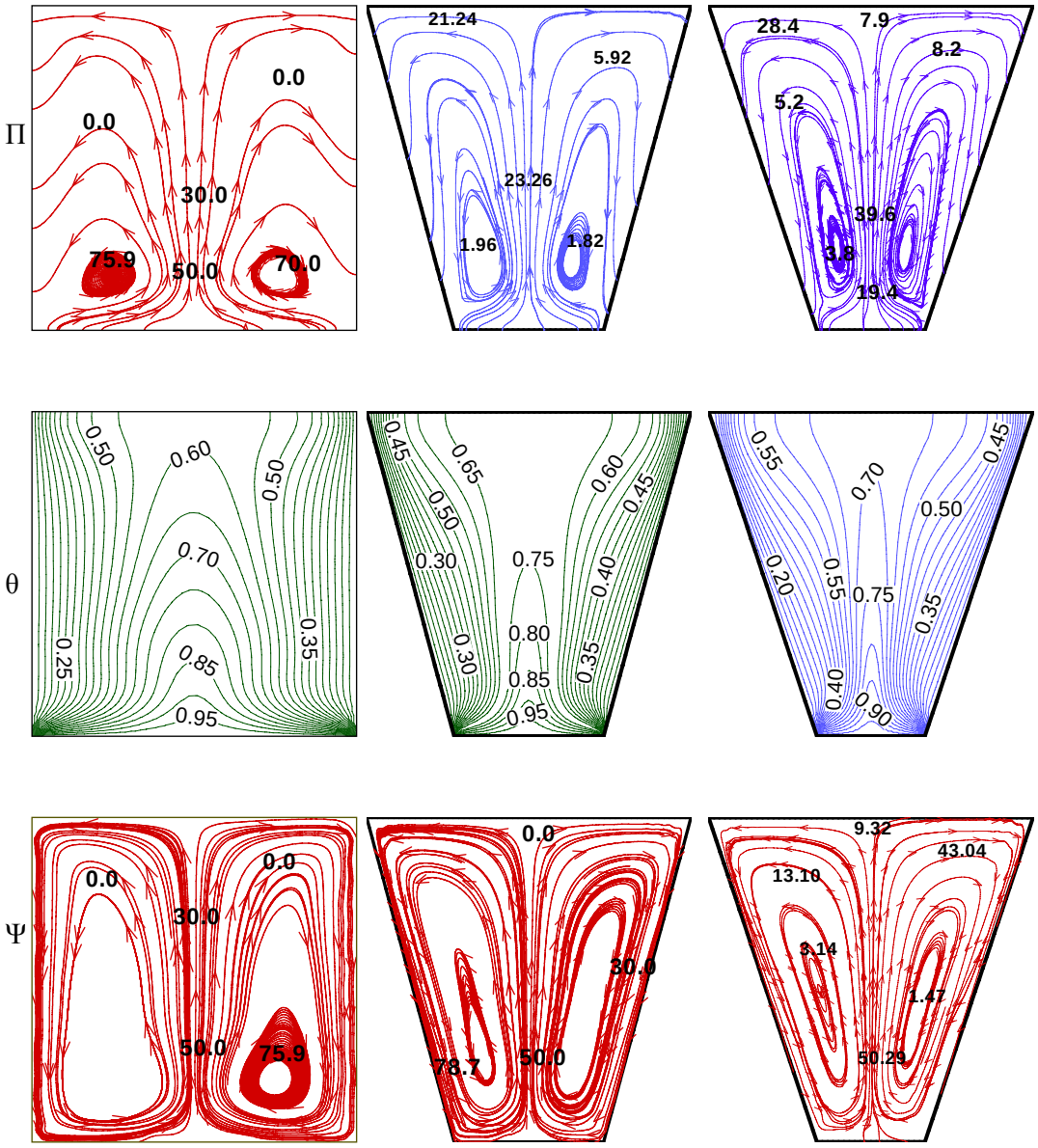

a b c

Figure 5.11: Stream function (Ψ), temperature (θ), heat function or total heat flux(Π) contours for uniform bottom heating θ(X,0) = 1 with Pr = 0.026, Ha = 50 and Ra = 10^7 (a) Φ = 0^o (b) Φ = 30^o (c) Φ = 45^o

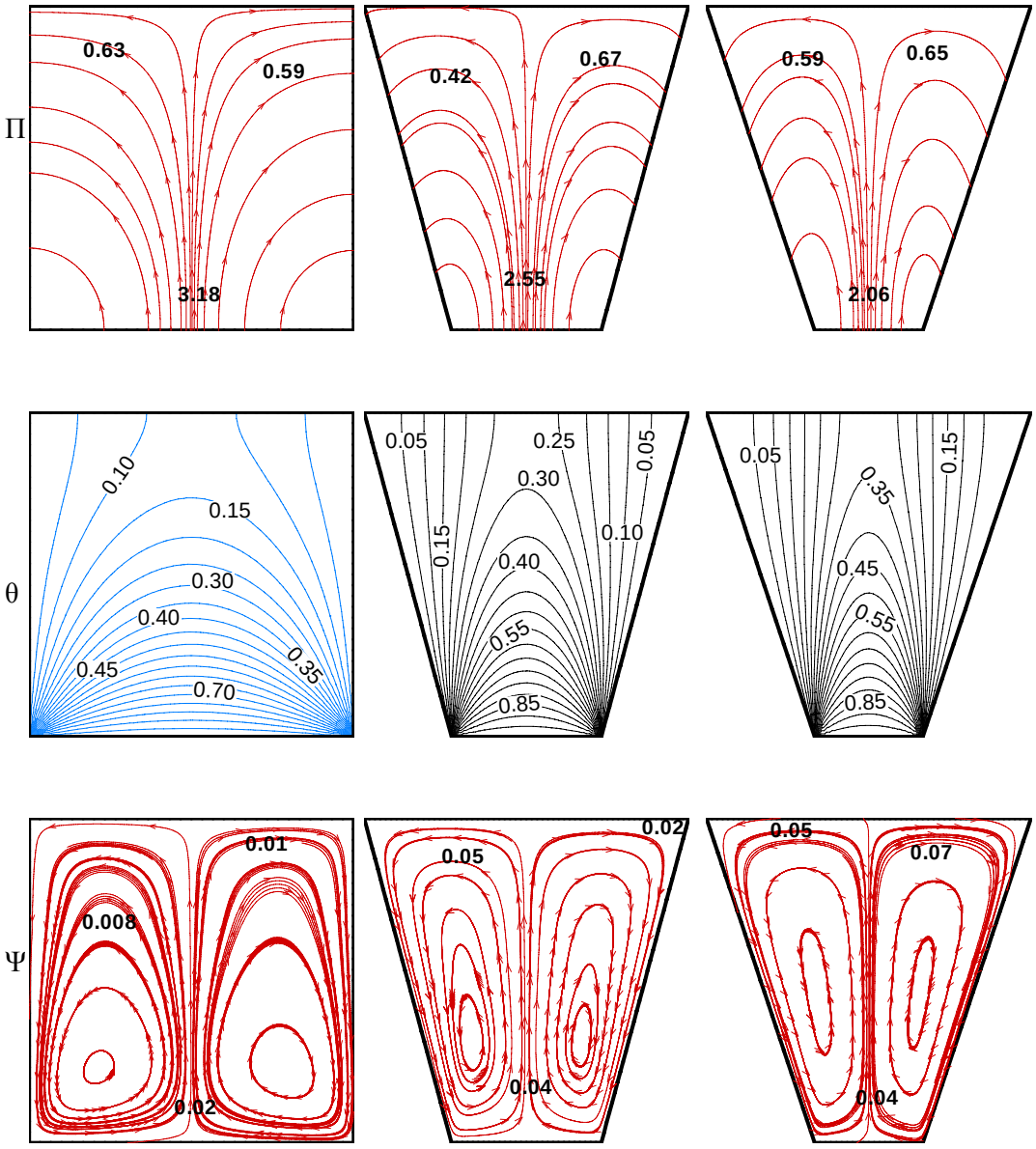

Figure 5.12: Stream function (Ψ), temperature (θ), heat function or total heat flux(Π) contours for uniform bottom heating θ(X,0) = 1 with Pr = 0.7, Ha = 50 and Ra = 10^3 (a) Φ = 0^o (b) Φ = 30^o (c) Φ = 45^o

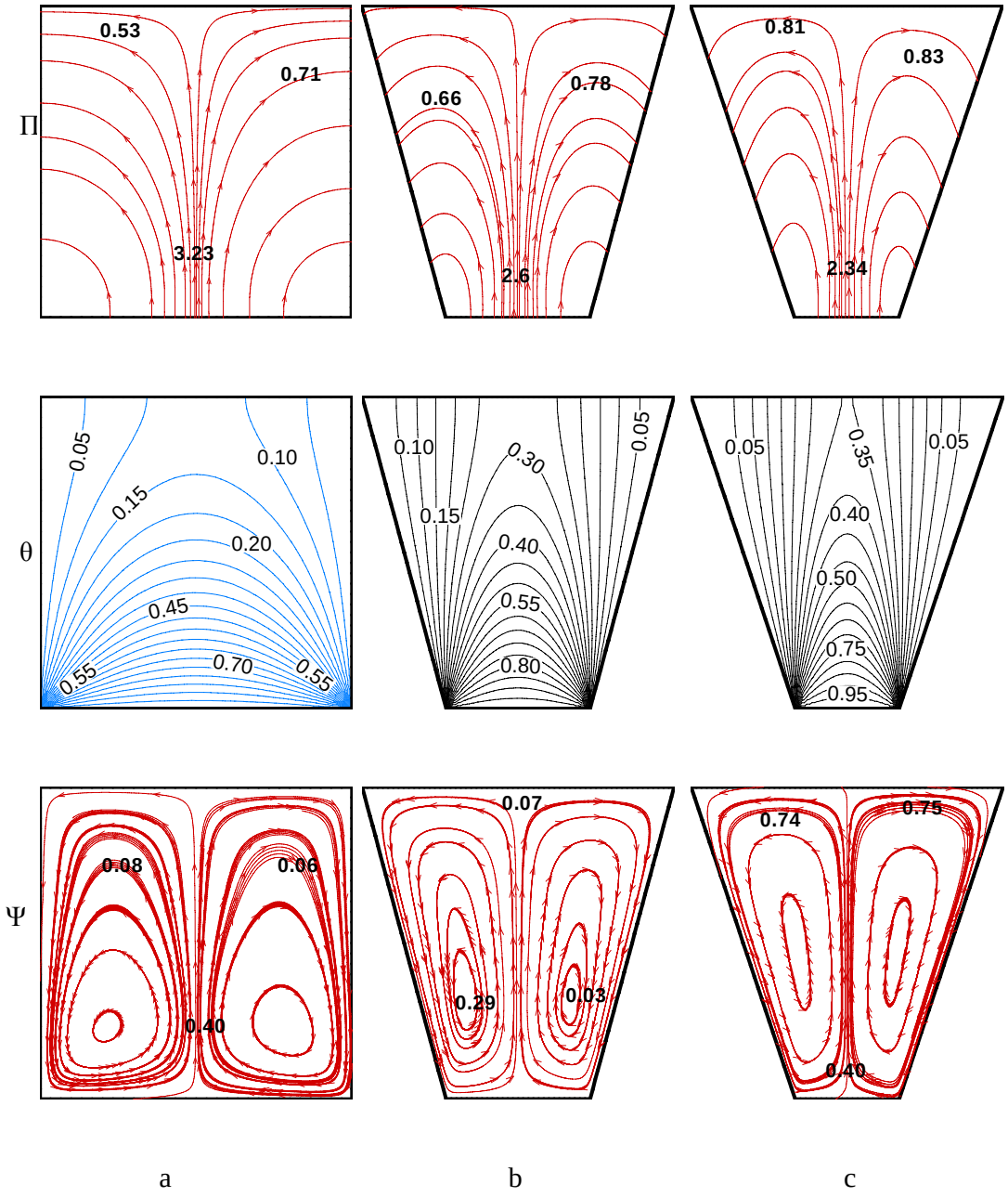

Figure 5.13: Stream function (Ψ), temperature (θ), heat function or total heat flux(Π) contours for uniform bottom heating θ(X,0) = 1 with Pr = 0.7, Ha = 50 and Ra = 10^4 (a) Φ = 0^o (b) Φ = 30^o (c) Φ = 45^o

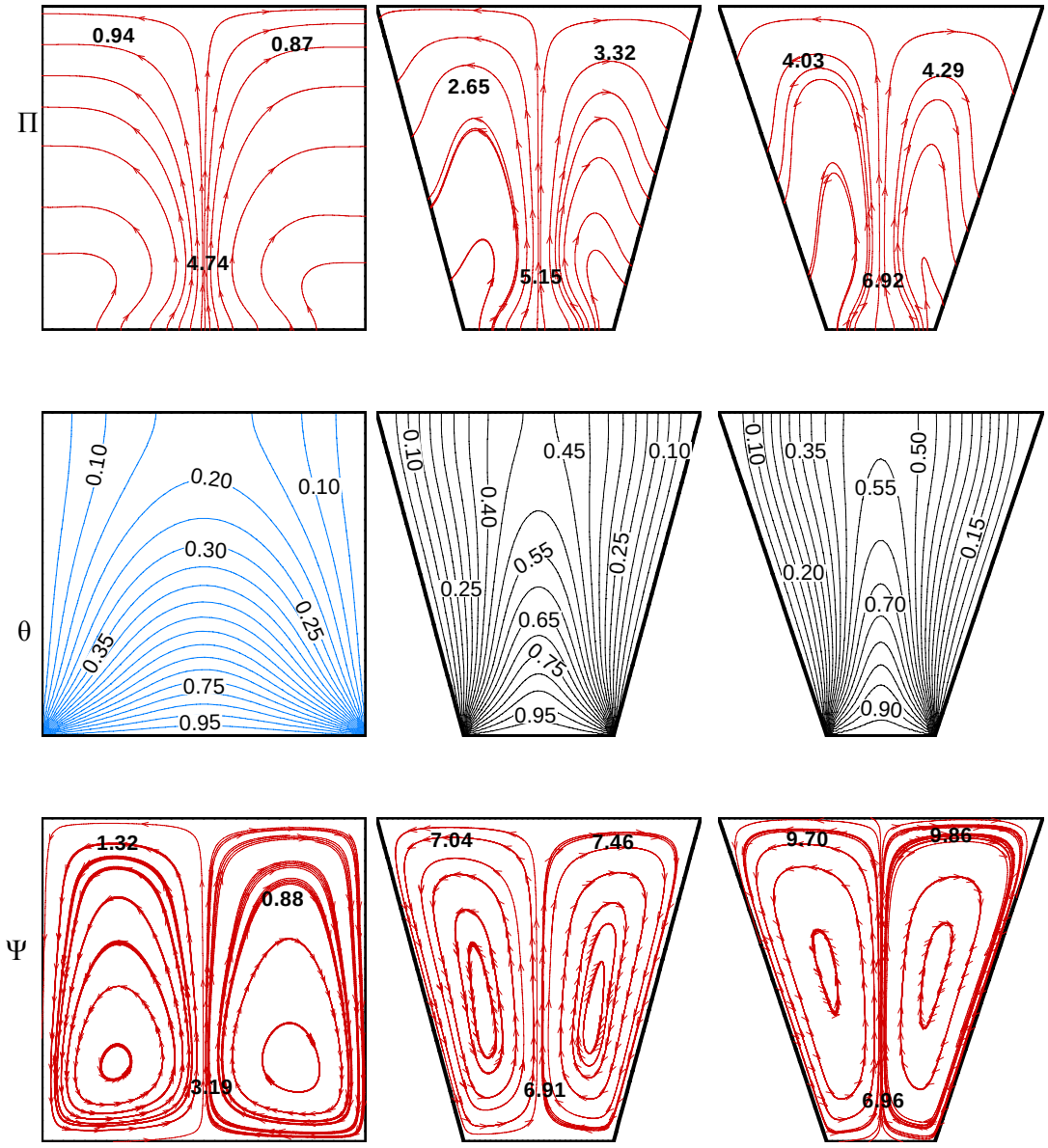

Figure 5.14: Stream function (Ψ), temperature (θ), heat function or total heat flux(Π) contours for uniform bottom heating θ(X,0) = 1 with Pr = 0.7, Ha = 50 and Ra = 10^5 (a) Φ = 0^o (b) Φ = 30^o (c) Φ = 45^o

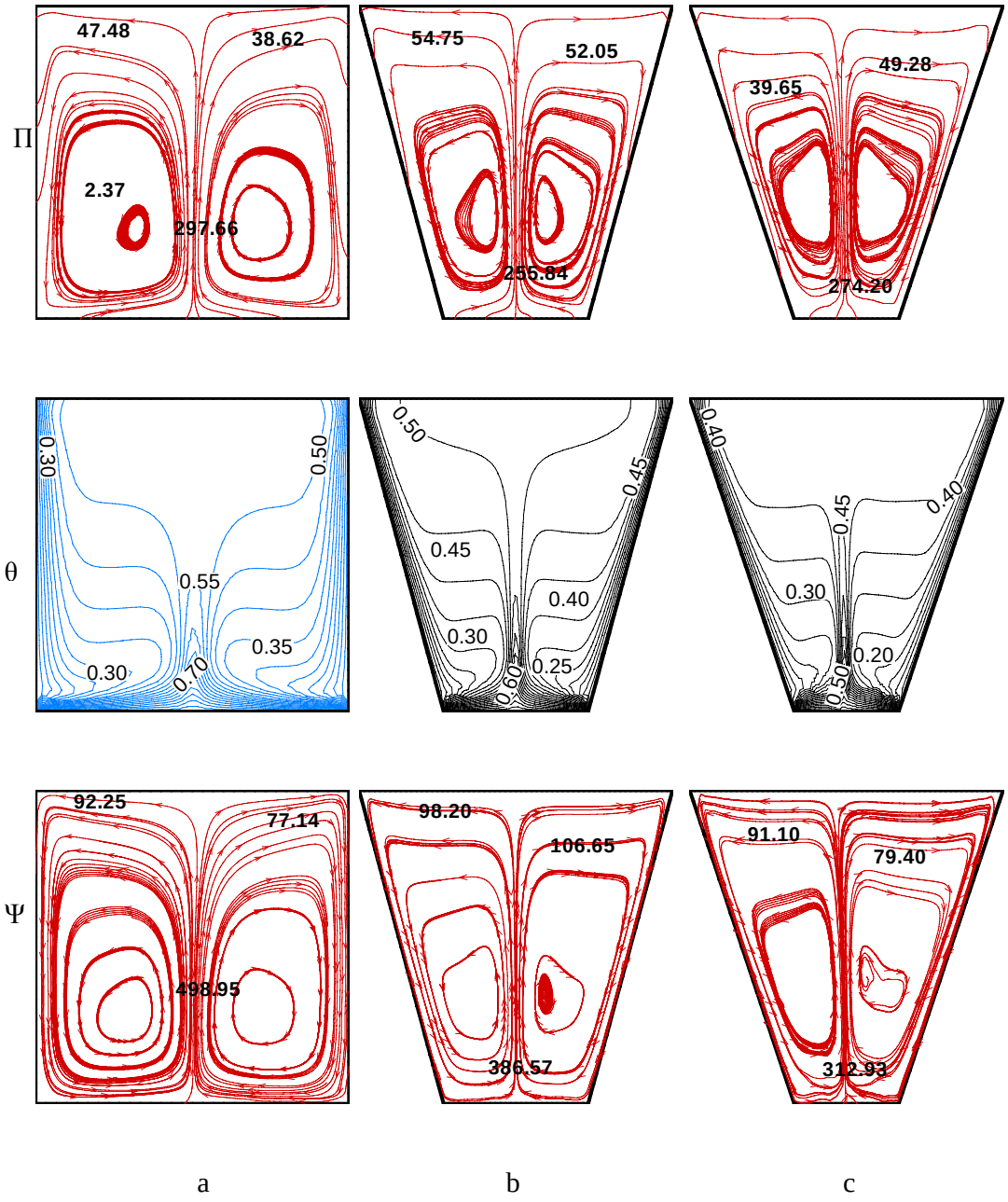

Figure 5.15: Stream function (Ψ), temperature (θ), heat function or total heat flux(Π) contours for uniform bottom heating θ(X,0) = 1 with Pr = 0.7, Ha = 50 and Ra = 10^7 (a) Φ = 0^o (b) Φ = 30^o (c) Φ = 45^o

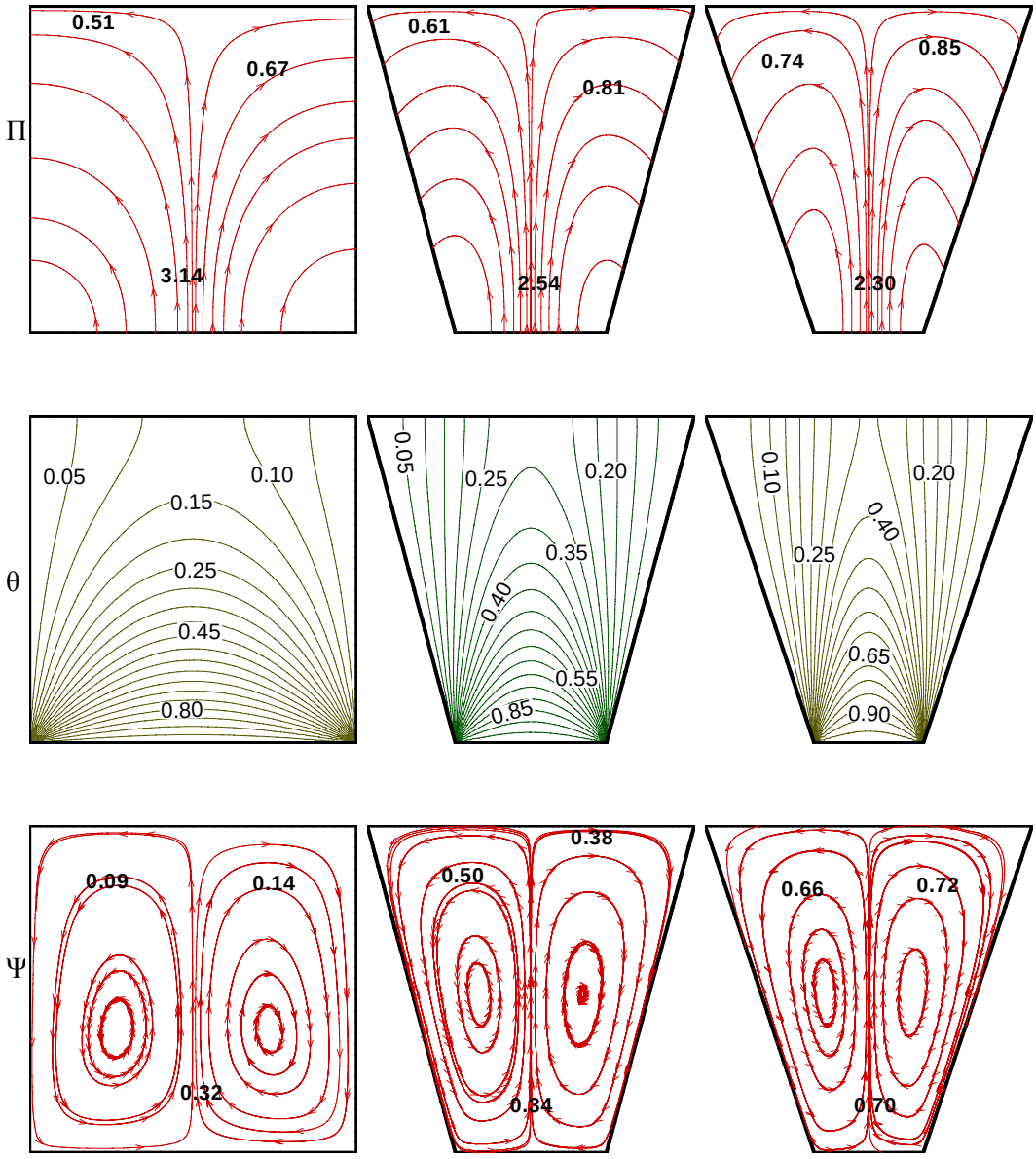

Figure 5.16: Stream function (Ψ), temperature (θ), heat function or total heat flux(Π) contours for uniform bottom heating θ(X,0) = 1 with Pr = 1000, Ha = 50 and Ra = 10^3 (a) Φ = 0^o (b) Φ = 30^o (c) Φ = 45^o

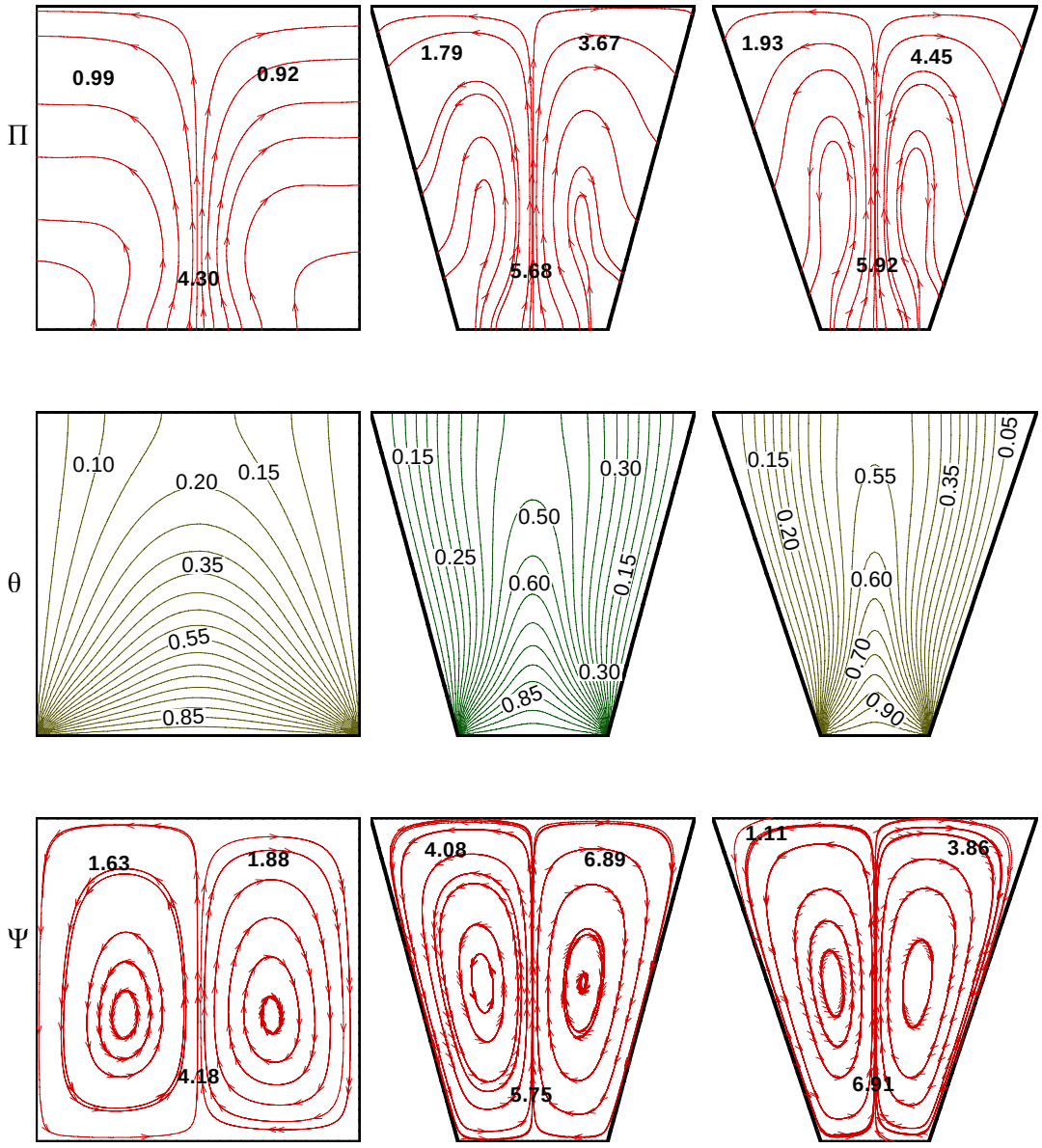

Figure 5.17: Stream function (Ψ), temperature (θ), heat function or total heat flux(Π) contours for uniform bottom heating θ(X,0) = 1 with Pr = 1000, Ha = 50 and Ra = 10^4 (a) Φ = 0^o (b) Φ = 30^o (c) Φ = 45^o

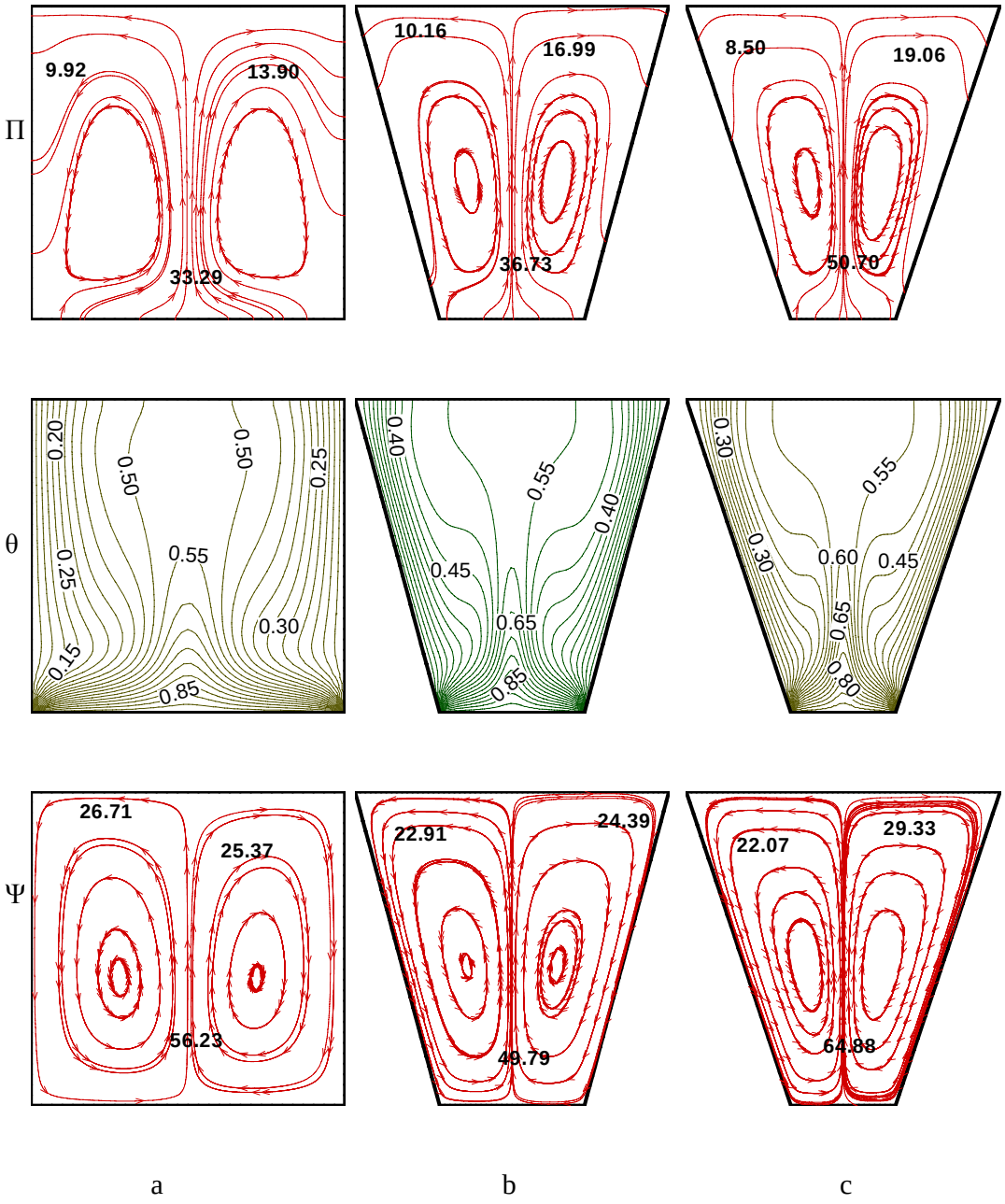

Figure 5.18: Stream function (Ψ), temperature (θ), heat function or total heat flux(Π) contours for uniform bottom heating θ(X,0) = 1 with Pr = 1000, Ha = 50 and Ra = 10^5 (a) Φ = 0^o (b) Φ = 30^o (c) Φ = 45^o

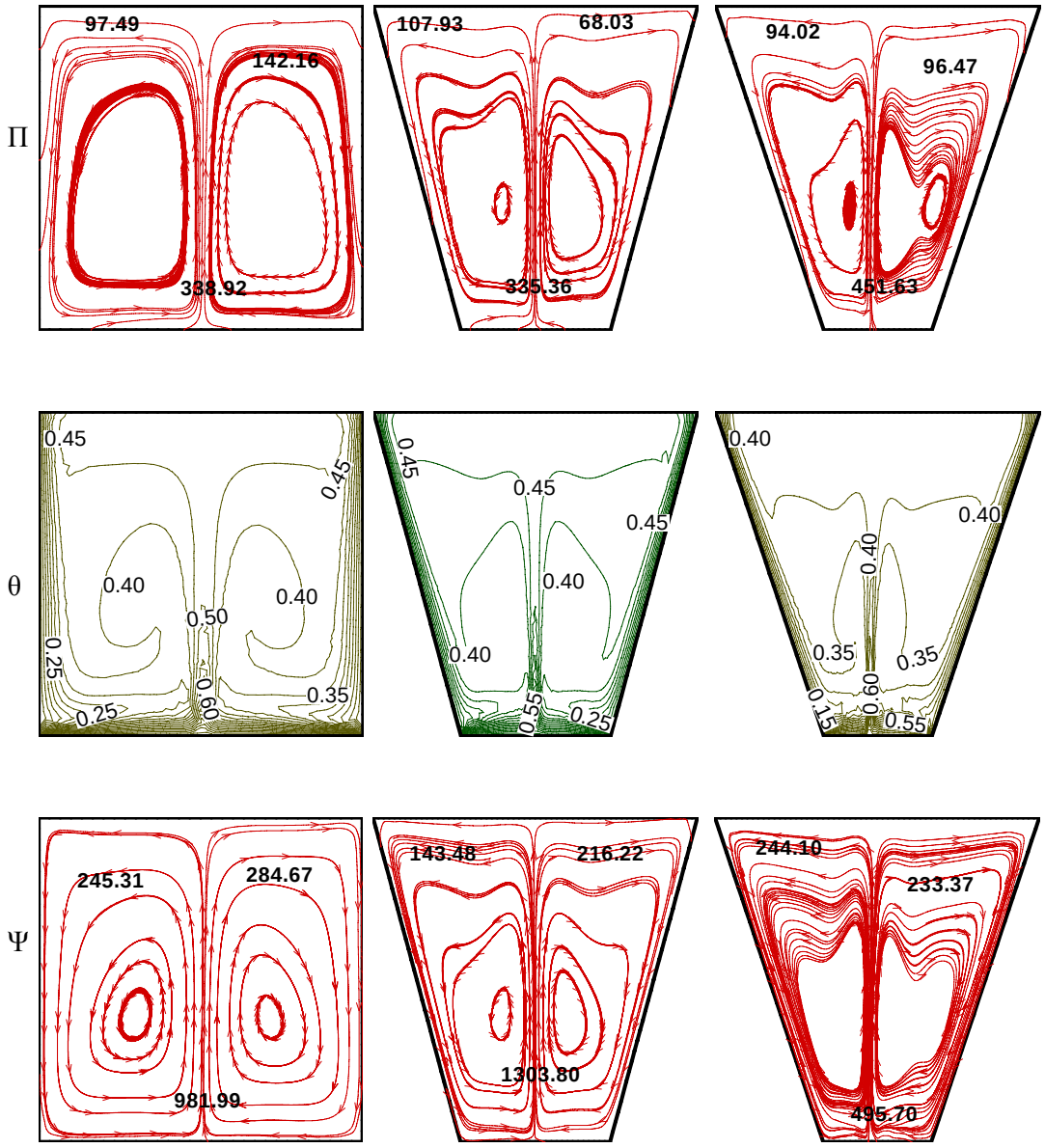

Figure 5.19: Stream function (Ψ), temperature (θ), heat function or total heat flux(Π) contours for uniform bottom heating θ(X,0) = 1 with Pr = 1000, Ha = 50 and Ra = 10^7 (a) Φ = 0^o (b) Φ = 30^o (c) Φ = 45^o

5.4.2 Heat Transfer Rates: Local Nusselt Number vs distance for various Prandtl Number, Rayleigh Number and inclination angles in case of uniform heating

Figure 5.20 display the effects of local Nusselt number vs distance for various inclinations of angles i.e. i) $\phi = 0^0$,ii) $\phi = 30^0$, iii) $\phi = 45^0$, for uniform heating of bottom wall with Pr = 0.026. Here the heat transfer rates are shown for $Ra = 10^3$. As bottom wall is heated and side wall is cold and top wall is insulated so that for adjacent wall it is observed that heat transfer rate is maximum near edge of the left wall and the rate is step down from left side and the it is straightly moving and then also it goes up to right side. Here the heat transfer rates are almost same for $\phi = 30^0, 45^0$ except $\phi = 0^0$ [square cavity].

Figure 5.21 and figure 5.22 also display similar effects of local Nusselt number with distance for various inclination tilt angles for Pr = 0.026 in case of uniform heating. But here the values of heat transfer rate increase a little. Here the heat transfer rates are shown for $Ra = 10^3, 10^4$.

Figure 5.23 detects the variation of local Nusselt number with distance for various inclination tilt angles i.e. i) $\phi = 0^0$,ii) $\phi = 30^0$, iii) $\phi = 45^0$,with Pr = 0.026 for uniform heating of bottom wall. Here heat transfer rates are discussed for $Ra = 10^7$. It is observed that heat transfer rates is very high at corners and it reduce the heat transfer rates toward the middle of bottom wall as the comparison of temperature contours is minimum at the center of wall irrespective of ϕs with Pr = 0.026.

Figure 5.24 show the effects for various inclination angles when Ra = 103 and Pr = 0.7 in presence of uniform heating of bottom walls. Here it is seen that the value of heat transfer rates increases as Pr increases. It is also interesting to observe that the heat transfer rates (Nu_b) for $\phi = 30^0$, and $\phi = 45^0$ are almost identical except $\phi = 0^0$. It is also observed that thermal gradient is minimum at the center of bottom wall as seen from dispersed isotherm contours at the center of the wall for irrespective of ϕs.

Figure 5.25 – 5.27 exemplify that similar effects of various inclination angles $\phi = 45^0, 30^0, 0^0$ for $Ra = 10^4, 10^5, 10^7$ with Pr = 0.7 in presence of uniform bottom heating. Here we also see that, in case of uniform heating the heat transfer rate of left wall is very high at the top edge of left wall is very high and heat transfer rate is almost uniform near the bottom edge of hot vertical wall. As Ra increases then the magnitudes of heat transfer rates increases. It

is seen that the thermal gradient is minimum at the center of bottom wall for dispersed isothermal contour for irrespective of ϕ. The larger heat transfer rate for $\phi = 0^0$ occurs due to highly compressed isotherms as seen figure 5.12a-c to figure 5.15a-c. Here it is also seen that the heat transfer rates for $\phi = 30^0$ and 45^0 are almost same except $\phi = 0^0$. But at larger $Ra = 10^7$ it is experiential that the oscillation of local heat transfer rates occur due to presence of secondary circulations which result of isotherm contours at various places of bottom wall of uniform heating.

Fig 5.28 – 5.31 illustrate that local heat transfer rate (Nu_b) vs distance for various inclination tilt angles i.e. for i) $\phi = 0^0$,ii) $\phi = 30^0$, iii) $\phi = 45^0$ when Pr = 1000 and for different Rayleigh numbers in presence of uniform heating of bottom wall. From figure 5.28, it is seen that heat transfer rates (Nu_b) are almost identical for $\phi = 30^0$, 45^0whereas $\phi = 0^0$ are larger. The larger heat transfer rates (Nu_b) are compressed due to strong circulations. The similar effects is shown in figure 5.29 – 5.31.But it is that when Ra increases then the magnitudes of local heat transfer rates (Nu_b) increases. As Ra increases then the strength of circulations is increased and consequently isotherm lines are compressed towards the hot wall. Hence the gradient increases near the wall. It is also seen the heat transfer rate is maximum near the edge of side wall and minimum near the center of bottom wall (See figure 5.28 – 5.31).

Figure 5.32 represent local heat transfer rates vs distance for different Rayleigh numbers i.e. for $Ra = 10^3 - 10^7$ when Pr = 0.026 and $\phi = 0^0$ (square cavity).Here it is demonstrate that heat transfer rates are almost same for $Ra = 10^3 – 10^5$ except $Ra = 10^7$. When $Ra = 10^7$ the local heat transfer rates (Nu_b) is larger and isotherms are uniformly distributed throughout the domain except near the center of bottom wall

Figure 5.33 – 5.34 show the similar effects of local hea transfer rates (Nu_b) for different Rayleigh numbers with $\phi = 0^0$ and Pr = 0.7, 1000 respectively. Here it is shown that when Pr increases from 0.026 to 0.7 (see figure 5.33) then the magnitudes of heat transfer rates (Nu_b) increases. It is also happen when Pr increase to 1000 (see figure 5.34). At higher Pr (Pr = 0.7 - 1000) the isotherms near the center of bottom wall are highly compressed due to strong circulations.

Figure 5.35 – 5.37 illustrates the same effects of local heat transfer rates vs distance for different Ra with $\phi = 30^0$ and Pr = 0.026 – 1000 respectively. Here we see that hat transfer

rate are almost same (figure 5.35) for Ra = 10^3 – $10^5$and is more larger for Ra = 107 when Pr = 0.026. When Pr increases (see figure 5.36 and 5.37) then the magnitudes of local heat transfer rates is also increased.

Figure 5.38 – 5.40 exemplify that the effects of local heat transfer rates for various Ra when $\phi = 45^0$ and Pr = 0.026 – 1000 is considered. Figure 5.38 display that the effects of local heat transfer rates (Nu_b) are identical for Ra = 10^3 and $10^4$with Pr = 0.026. As Ra increases then the heat transfer rates increases. When Pr [Pr = 0.7] increases (figure 5.39) then it is seen that the magnitudes of heat transfer rates increases. Here we also see that local Nusselt numbers have wavy distribution for Pr = 0.7. This is due to strong primary circulations. When Pr also increases (Pr = 1000 and see figure 5.40) then it is shown that the heat transfer rates are not almost identical for different Ra. As Ra increases then the strength of circulations is increased and local heat transfer rate (Nu_b) is also larger. Here also we see that local Nusselt numbers have also more wavy distributions (figure 5.40) for Pr = 1000. It is interesting to note that local Nusselt number has a high value for Pr = 1000 due to large temperature gradient resulting increased intensity of circulations for uniform hating case of bottom wall.

Figure 5.41 – 5.44 show the effect of local heat transfer rates (Nu_s) vs distance for various inclination tilt angles i.e. for $\phi = 0^0$, 30^0, 45^0 when Ra = 10^3 and Pr = 0.026for uniform heating of side wall. It is observed that local heat transfer rate is maximum at the bottom edge of side wall and thereafter decreases sharply upto a point which is very near to the bottom edge. It is seen that Nu_s increase upto a point near to the top wall and also decreases with distance near to the bottom wall. The boundary layer starts to form at the bottom edge of the side wall and the boundary layer thickness is quite large near the bottom wall for all ϕs. Due to large intensity of convection at Ra = 10^3 the thickness of the boundary layers are small at the middle portions of side walls and is found to be larger near the top portion. But also figure 5.42-5.43 shows the similar effects of local heat transfer rates (Nu_s) with distance for same Pr and different Ra respectively. As Ra increases then the magnitudes of local heat transfer rates become smaller and maximum heat transfer occur near the top portion. It is also seen from figure 5.44 that the magnitude of heat transfer rate becomes quite smaller due to dominant heat conduction mode. It may be mentioned that the larger degree of compression of isotherms for uniform heating case results in larger and Nu_s is quite large near to the bottom wall.

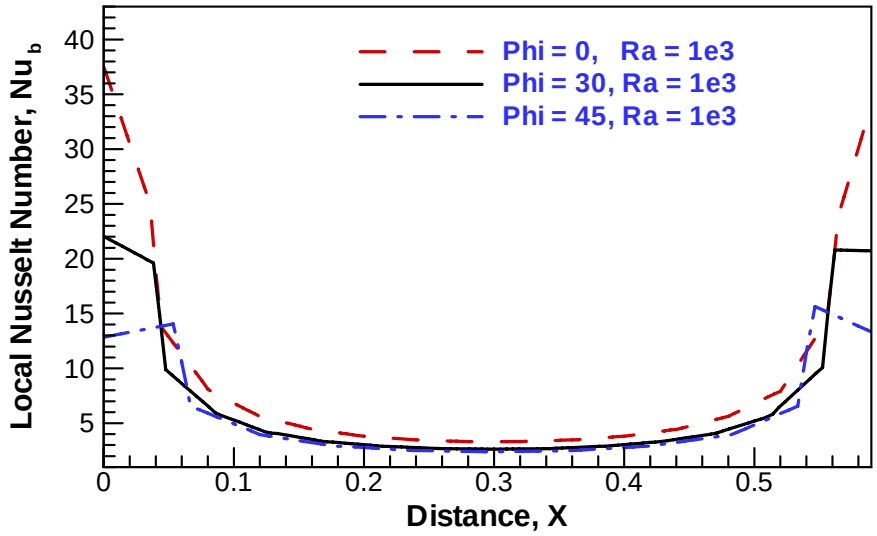

Figure 5.20: Variations of local Nusselt numbers (Nu_b) with distance for Pr = 0.026, Ra = 10^3 and for various inclination of angles (a) $\Phi = 0^o$ (b) $\Phi = 30^o$ (c) $\Phi = 45^o$ in presence of uniform heating of bottom walls.

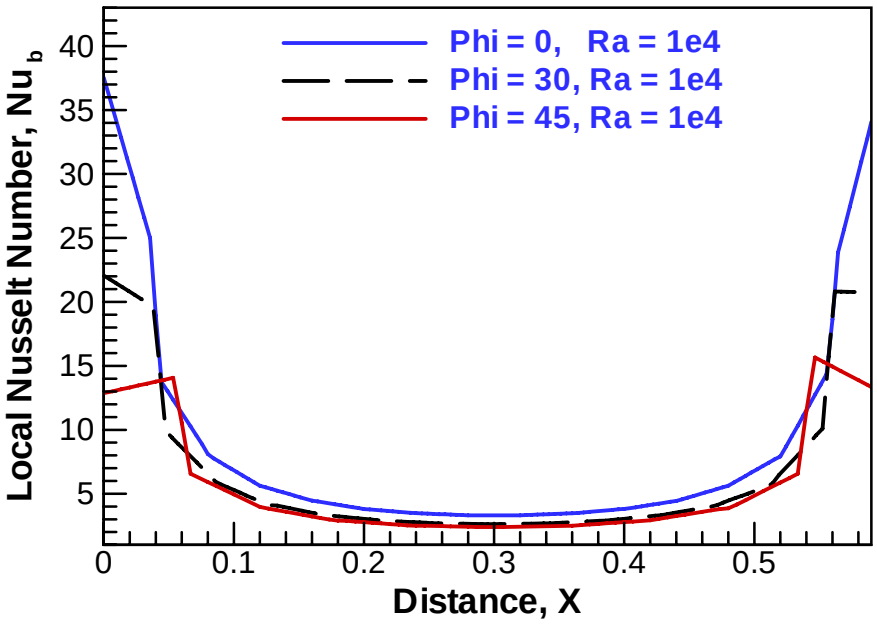

Figure 5.21: Variations of local Nusselt numbers (Nu_b) with distance for Pr = 0.026, Ra = 10^4 and for various inclination of angles (a) $\Phi = 0^o$ (b) $\Phi = 30^o$ (c) $\Phi = 45^o$ in presence of uniform heating of bottom walls.

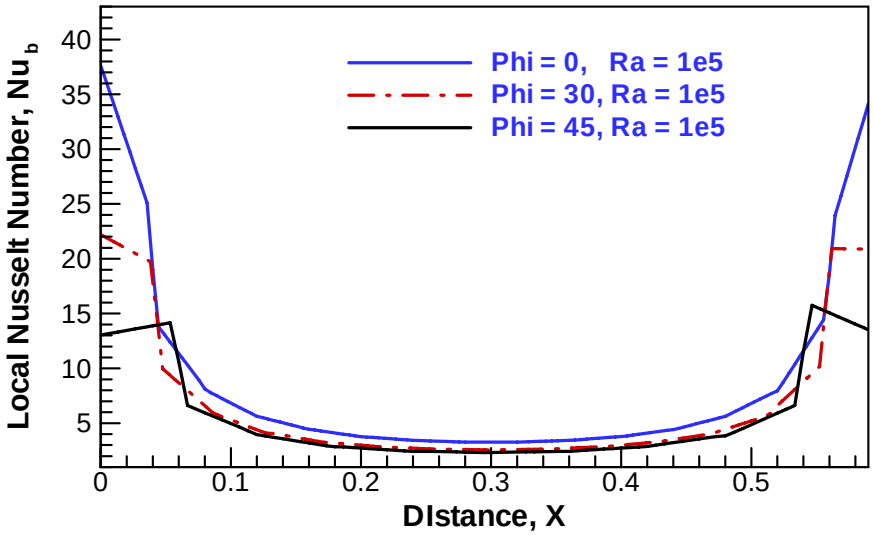

Figure 5.22: Variations of local Nusselt numbers (Nu_b) with distance for Pr = 0.026, Ra = 10^5 and for various inclination of angles (a) $\Phi = 0^o$ (b) $\Phi = 30^o$ (c) $\Phi = 45^o$ in presence of uniform heating of bottom walls.

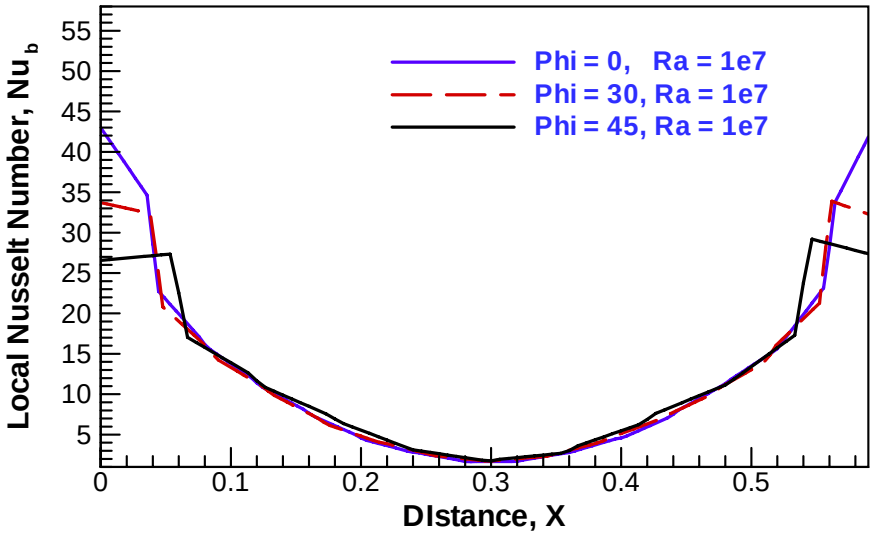

Figure 5.23: Variations of local Nusselt numbers (Nu_b) with distance for Pr = 0.026, Ra = 10^7 and for various inclination of angles (a) $\Phi = 0^o$ (b) $\Phi = 30^o$ (c) $\Phi = 45^o$ in presence of uniform heating of bottom walls.

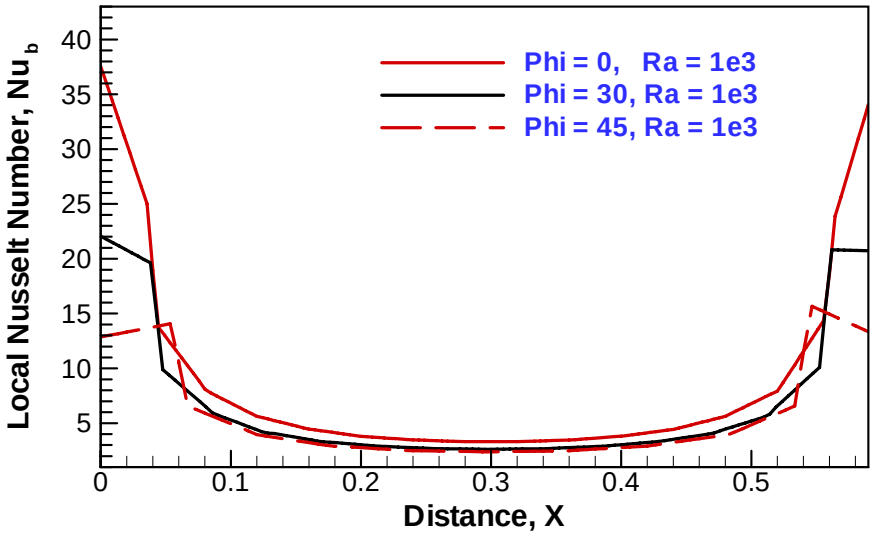

Figure 5.24: Variations of local Nusselt numbers (Nu_b) with distance for Pr = 0.7, Ra = 10^3 and for various inclination of angles (a) $\Phi = 0^o$ (b) $\Phi = 30^o$ (c) $\Phi = 45^o$ in presence of uniform heating of bottom walls.

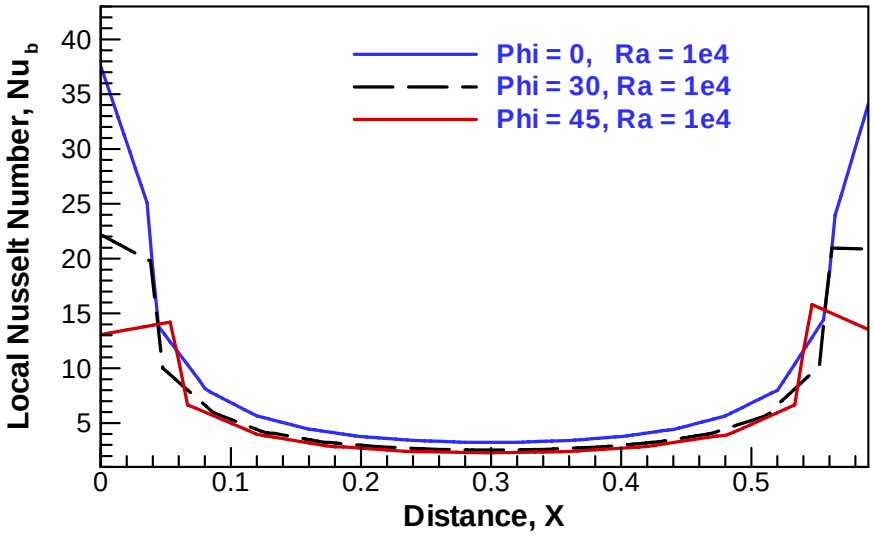

Figure 5.25: Variations of local Nusselt numbers (Nu_b) with distance for Pr = 0.7, Ra = 10^4 and for various inclination of angles (a) $\Phi = 0^o$ (b) $\Phi = 30^o$ (c) $\Phi = 45^o$ in presence of uniform heating of bottom walls.

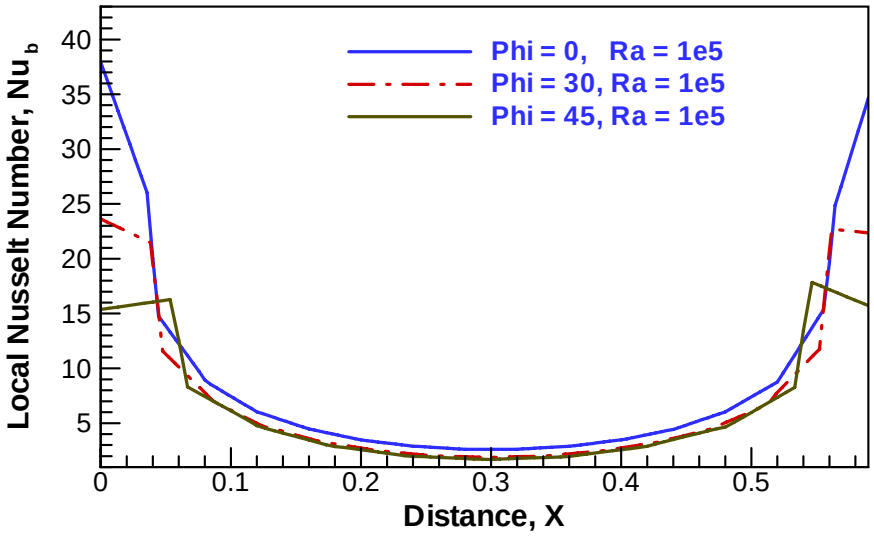

Figure 5.26: Variations of local Nusselt numbers (Nu_b) with distance for Pr = 0.7, Ra = 10^5 and for various inclination of angles (a) $\Phi = 0^o$ (b) $\Phi = 30^o$ (c) $\Phi = 45^o$ in presence of uniform heating of bottom walls.

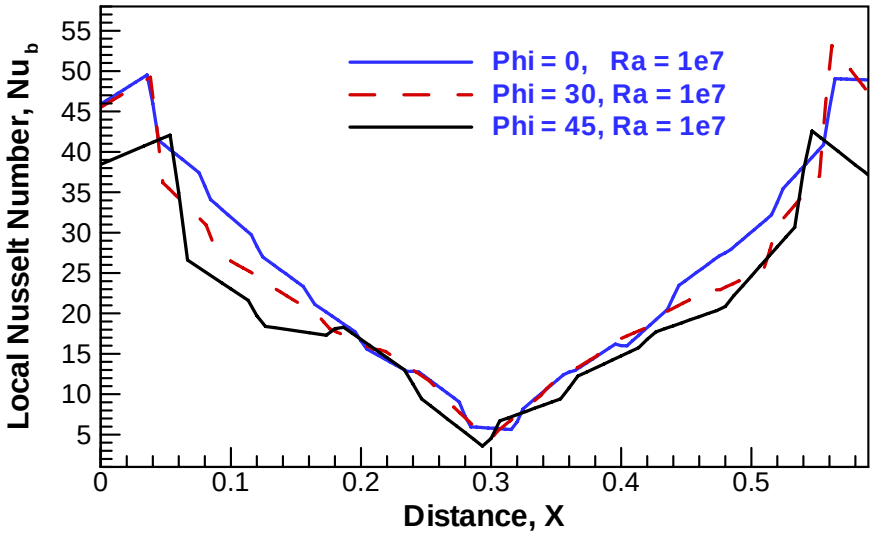

Figure 5.27: Variations of local Nusselt numbers (Nu_b) with distance for Pr = 0.7, Ra = 10^7 and for various inclination of angles (a) $\Phi = 0^o$ (b) $\Phi = 30^o$ (c) $\Phi = 45^o$ in presence of uniform heating of bottom walls.

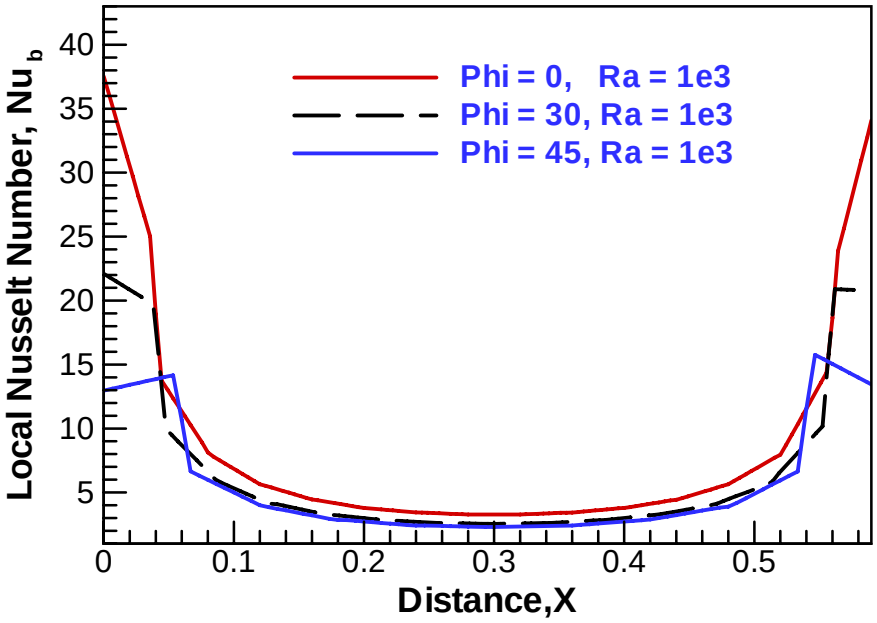

Figure 5.28: Variations of local Nusselt numbers (Nu_b) with distance for Pr = 1000, Ra = 10^3 and for various inclination of angles (a) $\Phi = 0^o$ (b) $\Phi = 30^o$ (c) $\Phi = 45^o$ in presence of uniform heating of bottom walls.

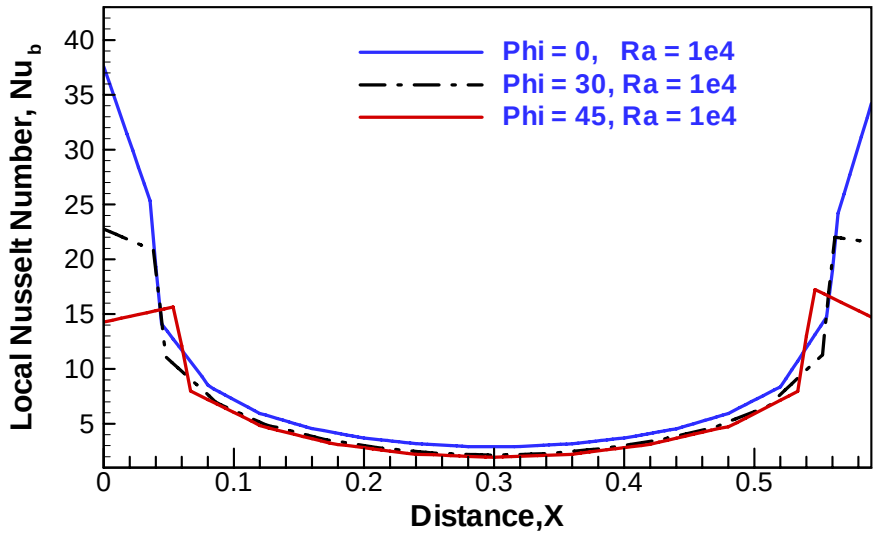

Figure 5.29: Variations of local Nusselt numbers (Nu_b) with distance for Pr = 1000, Ra = 10^4 and for various inclination of angles (a) $\Phi = 0^o$ (b) $\Phi = 30^o$ (c) $\Phi = 45^o$ in presence of uniform heating of bottom walls.

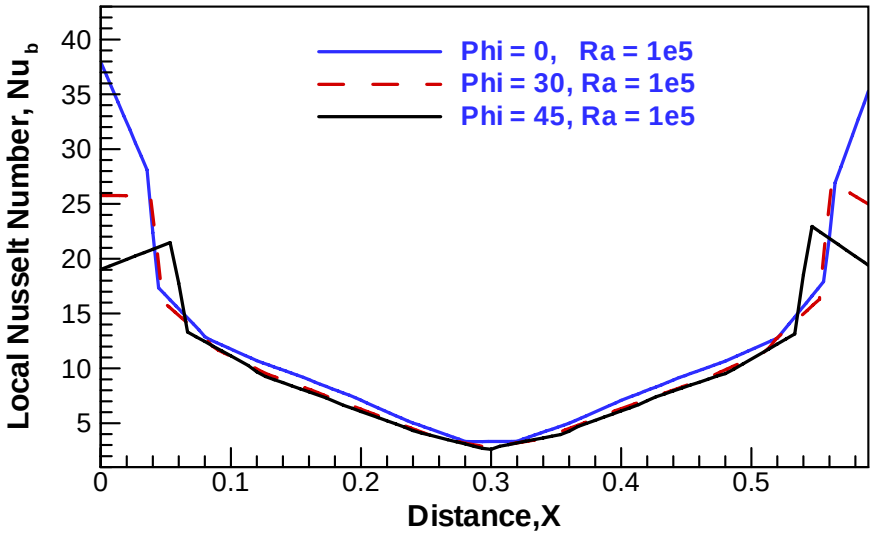

Figure 5.30: Variations of local Nusselt numbers (Nub) with distance for Pr = 1000, Ra = 10^5 and for various inclination of angles (a) $\Phi = 0^o$ (b) $\Phi = 30^o$ (c) $\Phi = 45^o$ in presence of uniform heating of bottom walls.

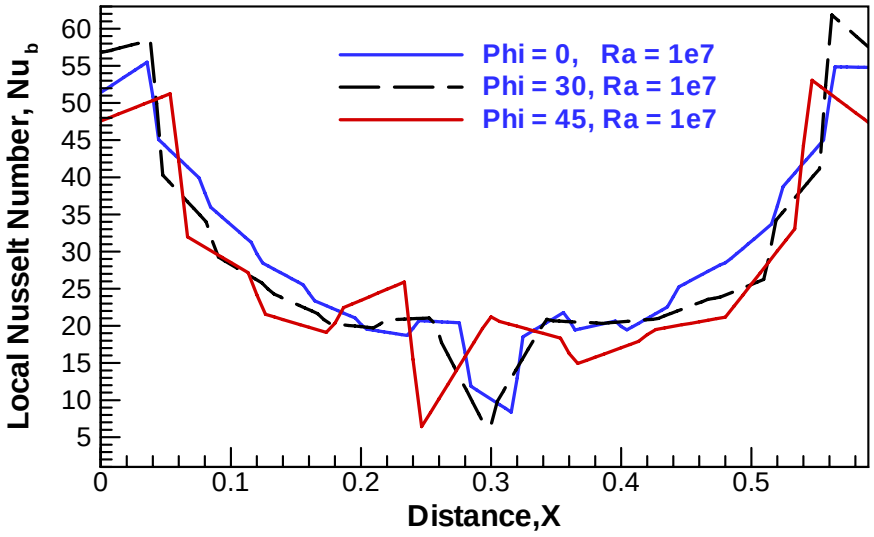

Figure 5.31: Variations of local Nusselt numbers (Nu_b) with distance for Pr = 1000, Ra = 10^7 and for various inclination of angles (a) $\Phi = 0^o$ (b) $\Phi = 30^o$ (c) $\Phi = 45^o$ in presence of uniform heating of bottom walls.

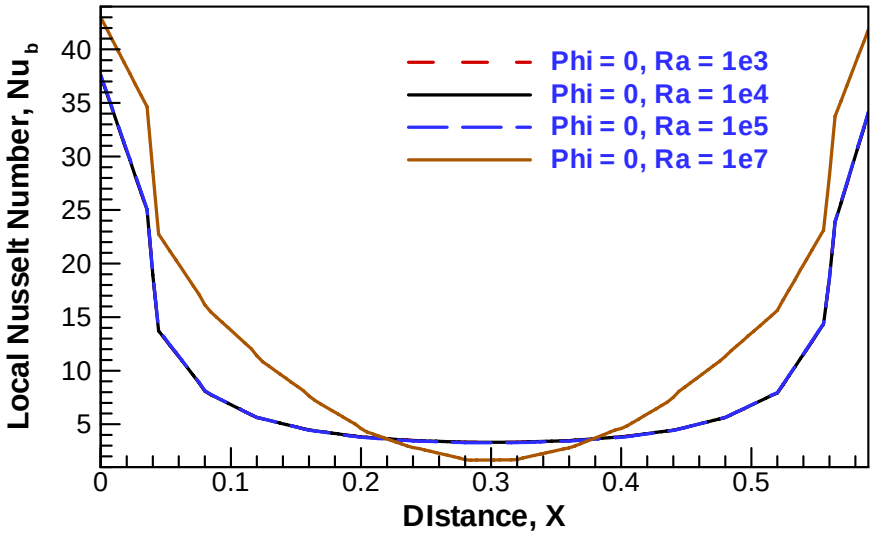

Figure 5.32: Variations of local Nusselt numbers (Nu_b) with distance for Pr = 0.026, $\Phi = 0^o$ and for various Rayleigh numbers (a) Ra = 10^3 (b) Ra = 10^4 (c) Ra = 10^5 (d) Ra = 10^7 in presence of uniform heating of bottom walls.

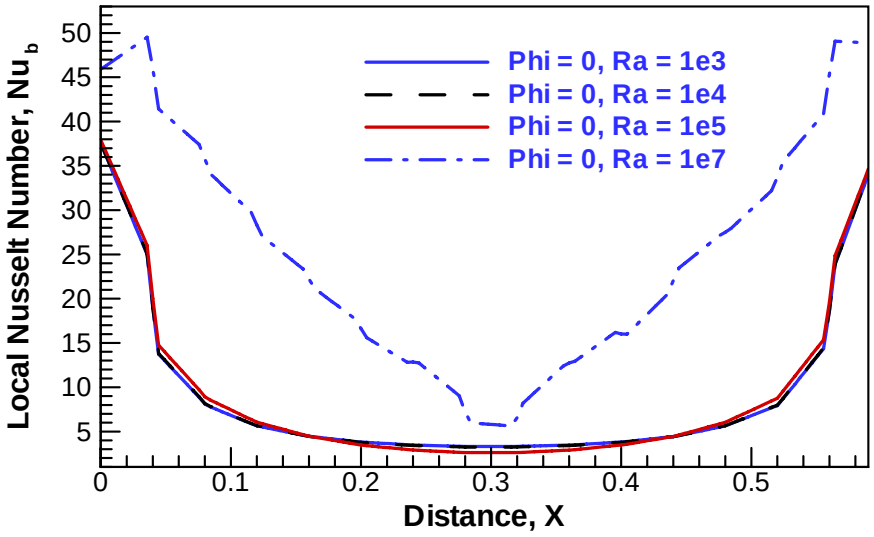

Figure 5.33: Variations of local Nusselt numbers (Nu_b) with distance for Pr = 0.7, $\Phi = 0^o$ and for various Rayleigh numbers (a) Ra = 10^3 (b) Ra = 10^4 (c) Ra = 10^5 (d) Ra = 10^7 in presence of uniform heating of bottom walls.

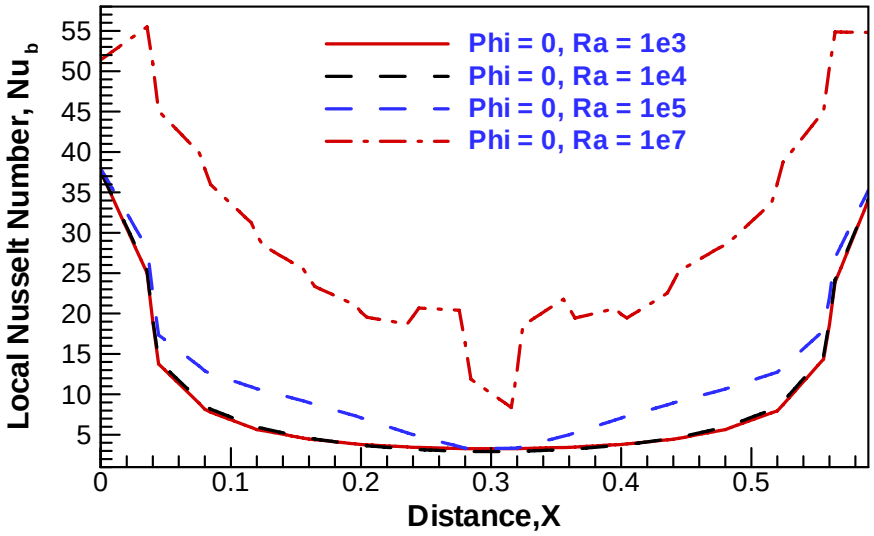

Figure 5.34: Variations of local Nusselt numbers (Nu_b) with distance for Pr = 1000, $\Phi = 0^o$ and for various Rayleigh numbers (a) $Ra = 10^3$ (b) $Ra = 10^4$ (c) $Ra = 10^5$ (d) $Ra = 10^7$ in presence of uniform heating of bottom walls.

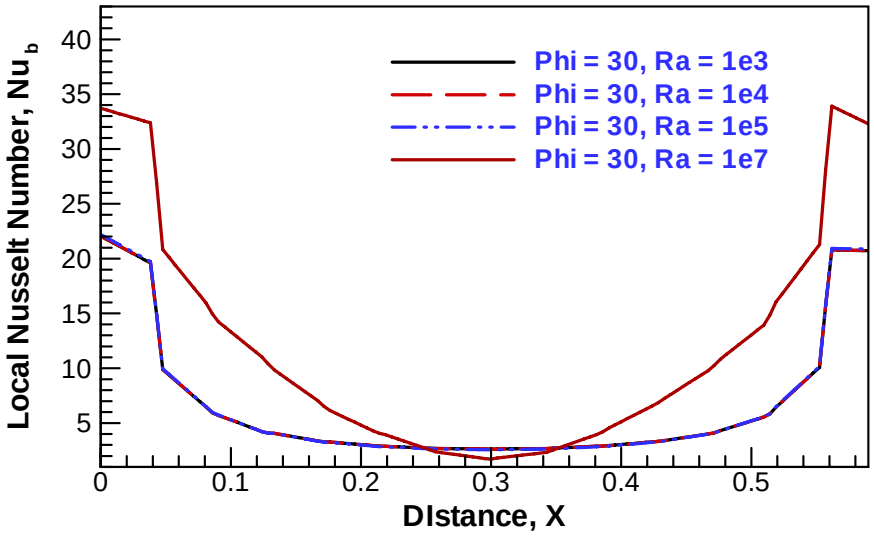

Figure 5.35: Variations of local Nusselt numbers (Nu_b) with distance for Pr = 0.026, $\Phi = 30^o$ and for various Rayleigh numbers (a) $Ra = 10^3$ (b) $Ra = 10^4$ (c) $Ra = 10^5$ (d) $Ra = 10^7$ in presence of uniform heating of bottom walls.

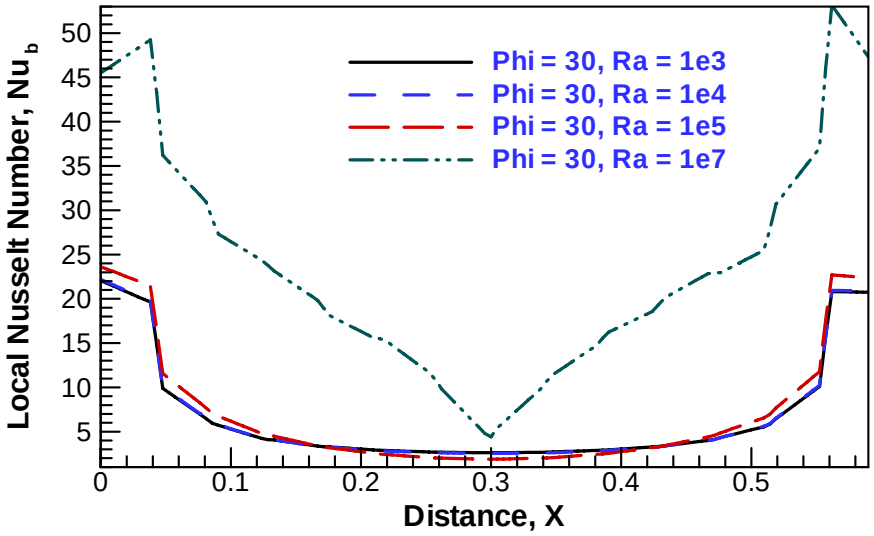

Figure 5.36: Variations of local Nusselt numbers (Nu_b) with distance for Pr = 0.7, Φ = 30^o and for various Rayleigh numbers (a) Ra = 10^3 (b) Ra = 10^4 (c) Ra = 10^5 (d) Ra = 10^7 in presence of uniform heating of bottom walls.

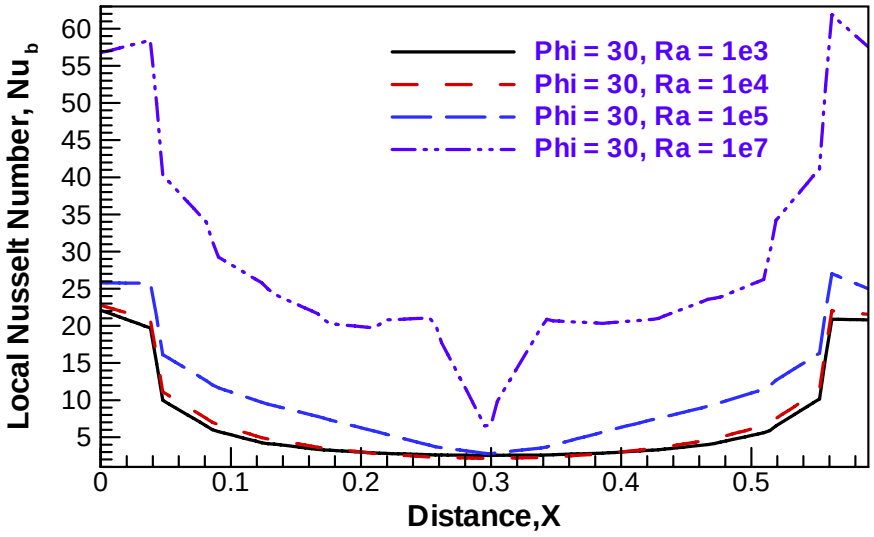

Figure 5.37: Variations of local Nusselt numbers (Nu_b) with distance for Pr = 1000, Φ = 30^o and for various Rayleigh numbers (a) Ra = 10^3 (b) Ra = 10^4 (c) Ra = 10^5 (d) Ra = 10^7 in presence of uniform heating of bottom walls.

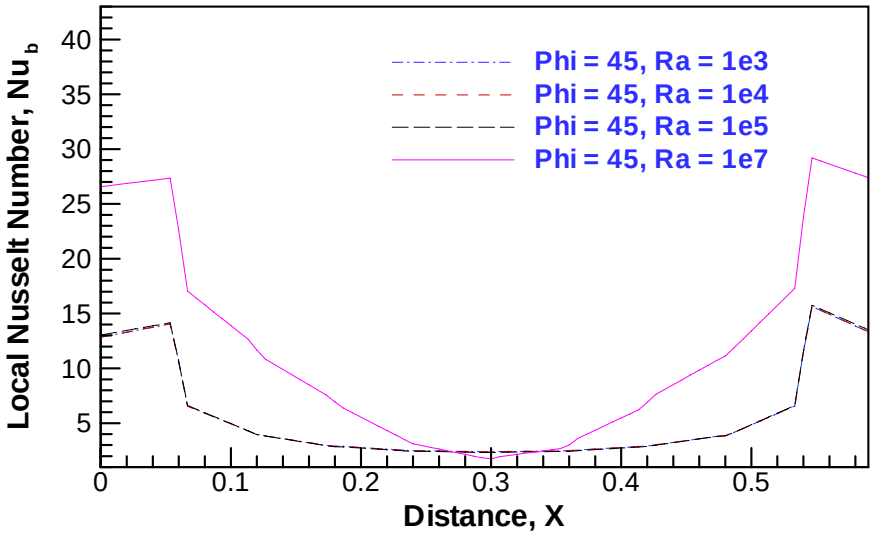

Figure 5.38: Variations of local Nusselt numbers (Nu_b) with distance for Pr = 0.026, Φ = 45^o and for various Rayleigh numbers (a) Ra = 10^3 (b) Ra = 10^4 (c) Ra = 10^5 (d) Ra = 10^7 in presence of uniform heating of bottom walls.

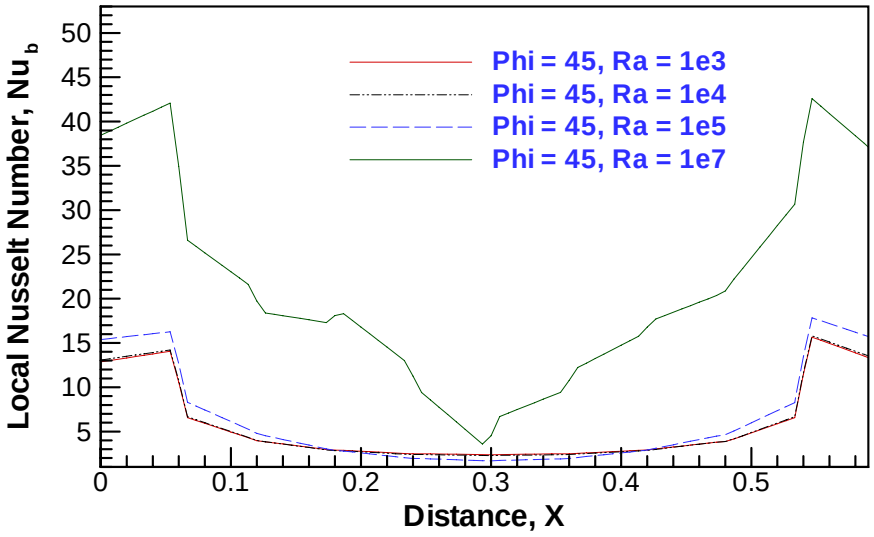

Figure 5.39: Variations of local Nusselt numbers (Nu_b) with distance for Pr = 0.7, Φ = 45^o and for various Rayleigh numbers (a) Ra = 10^3 (b) Ra = 10^4 (c) Ra = 10^5 (d) Ra = 10^7 in presence of uniform heating of bottom walls.

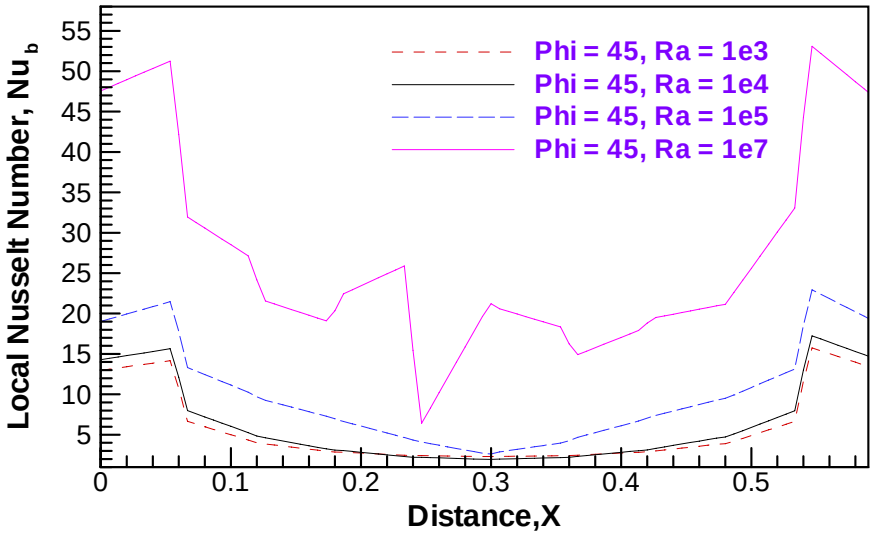

Figure 5.40: Variations of local Nusselt numbers (Nu_b) with distance for Pr = 1000, Φ = 45^o and for various Rayleigh numbers (a) Ra = 10^3 (b) Ra = 10^4 (c) Ra = 10^5 (d) Ra = 10^7 in presence of uniform heating of bottom walls.

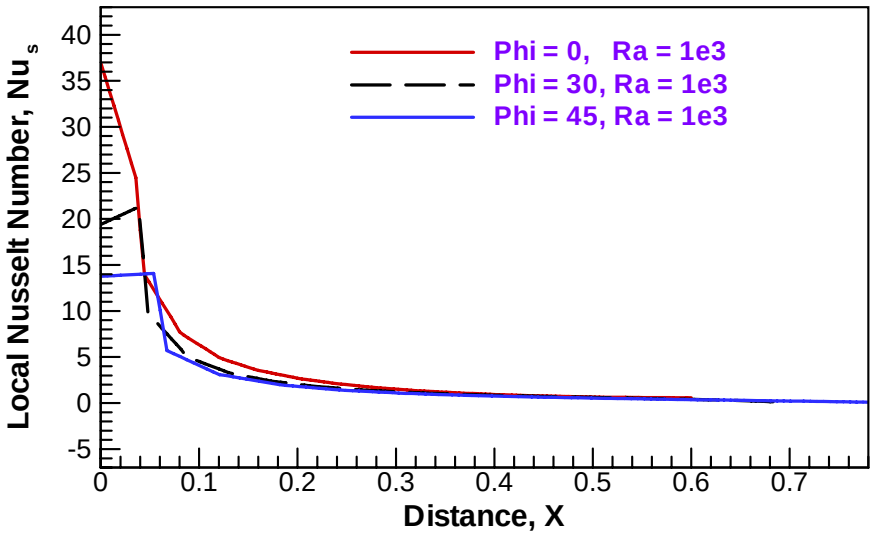

Figure 5.41: Variations of local Nusselt numbers (Nu_s) with distance for Pr = 0.026, Ra = 10^3 and for various inclination of angles (a) Φ = 0^o (b) Φ = 30^o (c) Φ = 45^o in presence of uniform heating of side walls.

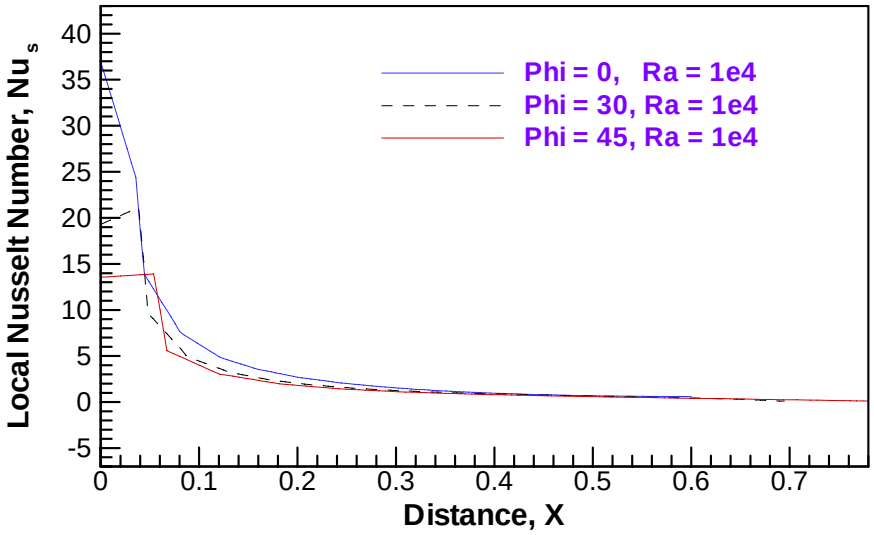

Figure 5.42: Variations of local Nusselt numbers (Nu_s) with distance for Pr = 0.026, Ra = 10^4 and for various inclination of angles (a) $\Phi = 0^o$ (b) $\Phi = 30^o$ (c) $\Phi = 45^o$ in presence of uniform heating of side walls.

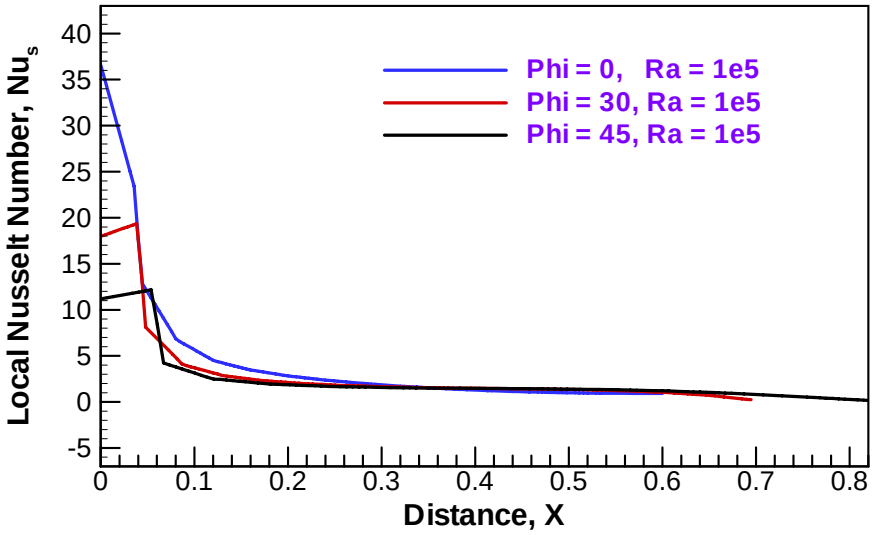

Figure 5.43: Variations of local Nusselt numbers (Nu_s) with distance for Pr = 0.026, Ra = 10^5 and for various inclination of angles (a) $\Phi = 0^o$ (b) $\Phi = 30^o$ (c) $\Phi = 45^o$ in presence of uniform heating of side walls.

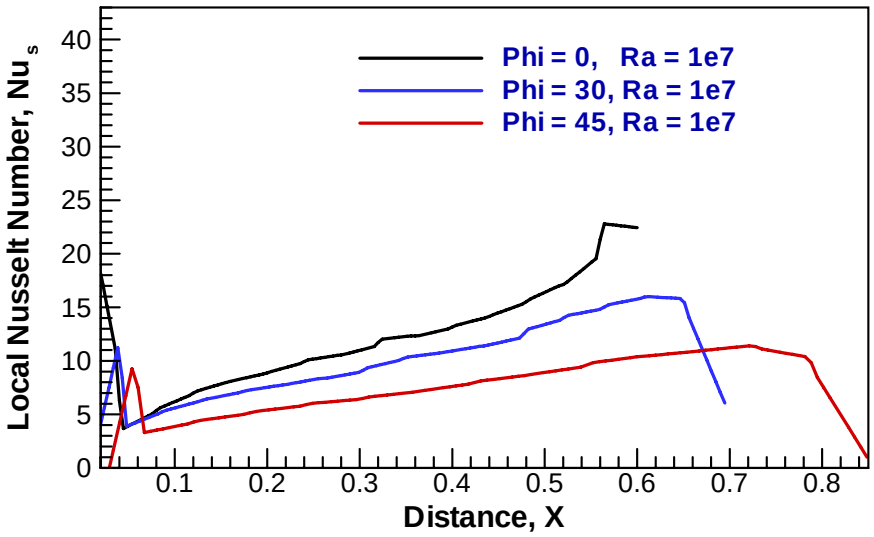

Figure 5.44: Variations of local Nusselt numbers (Nu_s) with distance for Pr = 0.026, Ra = 10^7 and for various inclination of angles (a) $\Phi = 0^o$ (b) $\Phi = 30^o$ (c) $\Phi = 45^o$ in presence of uniform heating of side walls.

5.4.3 Heat Transfer Rates: Average Nusselt Number vs Rayleigh Number for different Prandtl Number, and inclination angles in case of uniform heating

The overall effects upon the heat transfer rates are displayed in figure 5.45-5.47 and 5.48-5.50, where distributions of average Nusselt number of bottom and side wall respectively are plotted vs the logarithmic Rayleigh number. Note that figure 5.45-5.47 illustrate uniform heating of bottom wall and figure 5.48-5.50 illustrate uniform heating of side wall. It may be noted that average Nusselt number is obtained by considering temperature gradient. It also be noted that as Ra increases then the average Nusselt number increases. It is seen in figure 5.45 that as Ra increases from 10^3-10^6 then average Nusselt number is straightly moving but as Ra increases more, then average Nusselt number is increasing for Pr = 0.026. As Pr increases (figure 5.46) then conduction dominant heat transfer is narrowed down. It also seen from figure 5.47 that, as Pr increases more than from uniform heating case it is analyzed that average Nusselt number for bottom wall remain constant during the entire Rayleigh number regime. This illustrates that the conduction dominant heat transfer for different Prandtl number regime irrespective of Ra. As Pr increases then for conduction dominant heat transfer, the average Nusselt number is generally constant irrespective of Ra. It is observed that Nub at the middle portion of bottom wall for $\Phi = 0^o$

is larges for uniform heating case whereas for $\Phi = 30^o$ and 45^o heat transfer rates are identical. It is also seen that Nu_s is largest near the bottom corner of side walls for $\Phi = 0^o$. At larges Pr (Pr= 1000) of uniform bottom heating it is seen that as Ra increase from 10^3 to 10^6, then average heat transfer rates (Nu_b) increases. After crossing $Ra = 10^6$ then it is also seen average heat transfer rates are decreasing. After that when Ra goes to 10^7 then average heat transfer rate is also increasing because of highly viscous of Pr. Figure 5.48-5.50 show the similar effects of average Nusselt number with uniform heating of side walls. Here it is interesting to note that the heat transfer rates (Nu_{av})of side wall is less than uniform heating of bottom wall and it effects only for highly viscous of Prandtl number. Besides this, the average Nusselt number with Rayleigh number are also shown in table (5.6 – 5.8) and table (5.9 – 5.11) for uniform heating of bottom wall and side walls respectively.

Ra	Average Nusselt Number, (Nu_{av})		
	$\phi = 0^0$	$\phi = 30^0$	$\phi = 45^0$
10^3	5.685279	4.462485	3.892755
10^4	5.6854	4.462547	3.892687
10^5	5.686727	4.463427	3.892576
10^6	5.713755	4.511001	3.963368
10^7	7.865817	7.490336	7.380522

Table 5.6: Average Nusselt Number vs Rayleigh number for uniform heating of bottom wall with Pr = 0.026

Ra	Average Nusselt Number, (Nu_{av})		
	$\phi = 0^0$	$\phi = 30^0$	$\phi = 45^0$
10^3	5.685321	4.46249	3.892641
10^4	5.686197	4.463856	3.893894
10^5	5.753017	4.666547	4.2141
10^6	8.796366	8.230399	8.011008
10^7	15.497432	14.561562	12.946846

Table 5.7: Average Nusselt Number vs Rayleigh number for uniform heating of bottom wall with Pr = 0.7

Ra	Average Nusselt Number, (Nu_{av})		
	$\phi = 0^0$	$\phi = 30^0$	$\phi = 45^0$
10^3	5.685541	4.463759	3.894383
10^4	5.720275	4.685459	4.195594
10^5	7.502485	6.77423	6.38686
10^6	11.336868	10.787012	10.630463
10^7	18.04662	17.318061	16.436009

Table 5.8: Average Nusselt Number vs Rayleigh number for uniform heating of bottom wall with Pr = 1000

Ra	Average Nusselt Number, (Nu_{av})		
	$\phi = 0^0$	$\phi = 30^0$	$\phi = 45^0$
10^3	2.86001	2.239547	1.968798
10^4	2.85994	2.23954	1.968841
10^5	2.859301	2.239628	1.969558
10^6	2.859966	2.259666	2.013594
10^7	3.867217	3.743934	3.821934

Table 5.9: Average Nusselt Number vs Rayleigh number for uniform heating of side wall with Pr = 0.026

Ra	Average Nusselt Number, (Nu_{av})		
	$\phi = 0^0$	$\phi = 30^0$	$\phi = 45^0$
10^3	2.859967	2.239549	1.96883
10^4	2.859702	2.240199	1.970905
10^5	2.88603	2.341693	2.148533
10^6	4.39259	4.125596	4.102104
10^7	7.742302	7.407918	6.794414

Table 5.10: Average Nusselt Number vs Rayleigh number for uniform heating of side wall with Pr = 0.7

Ra	Average Nusselt Number, (Nu_{av})		
	$\phi = 0^0$	$\phi = 30^0$	$\phi = 45^0$
10^3	2.860026	2.240455	1.970969
10^4	2.876289	2.35496	2.137091
10^5	3.76617	3.400206	3.253002
10^6	5.668432	5.358906	5.358472
10^7	9.092274	9.06801	8.918795

Table 5.11: Average Nusselt Number vs Rayleigh number for uniform heating of side wall with Pr = 1000

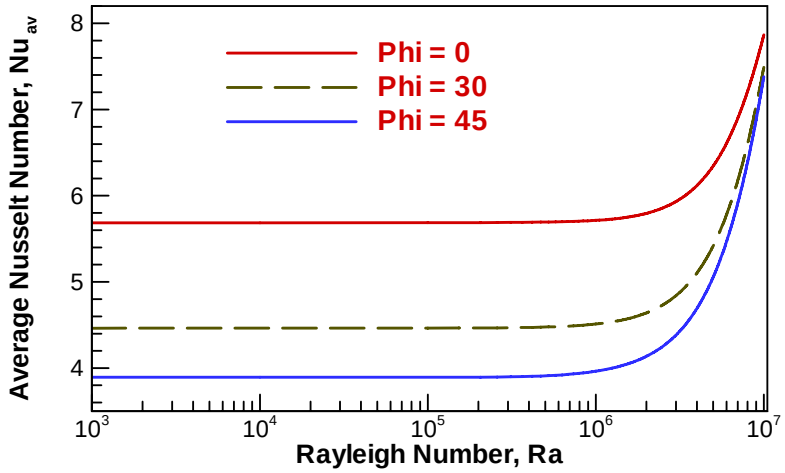

Figure 5.45: Average Nusselt Number vs Rayleigh number for uniform heating of bottom wall with Pr = 0.026

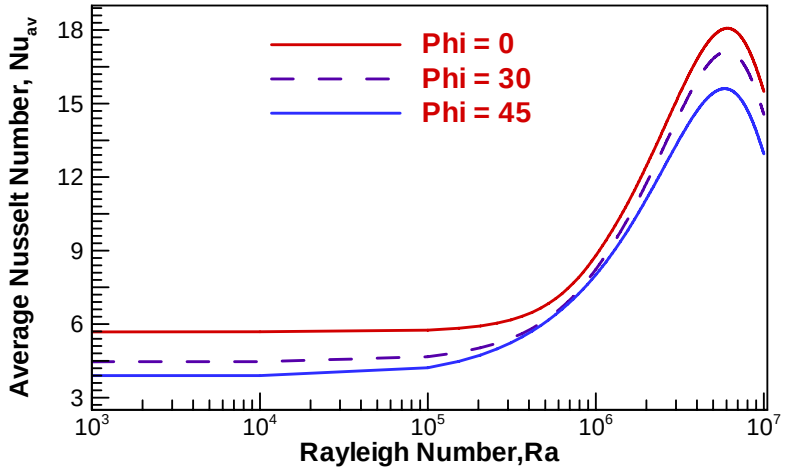

Figure 5.46: Average Nusselt Number vs Rayleigh number for uniform heating of bottom wall with Pr = 0.7

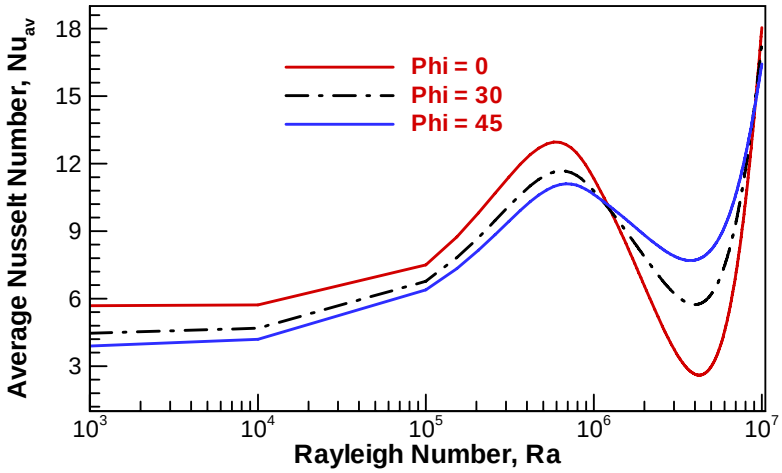

Figure 5.47: Average Nusselt Number vs Rayleigh number for uniform heating of bottom wall with Pr = 1000

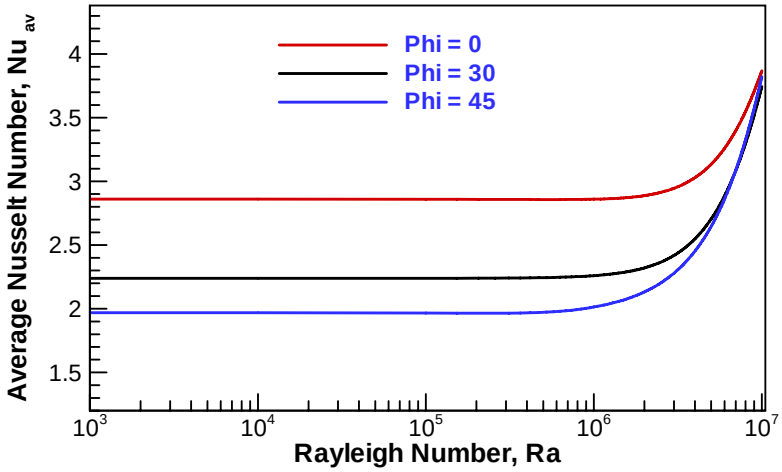

Figure 5.48: Average Nusselt Number vs Rayleigh number for uniform heating of side wall with Pr = 0.026

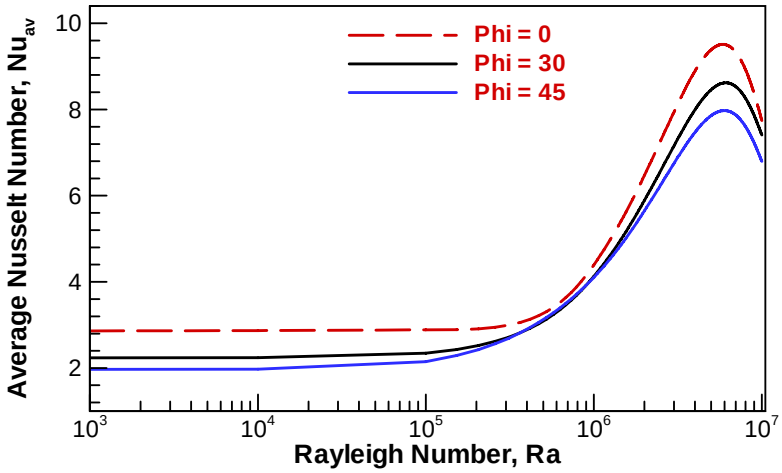

Figure 5.49: Average Nusselt Number vs Rayleigh number for uniform heating of side wall with Pr = 0.7

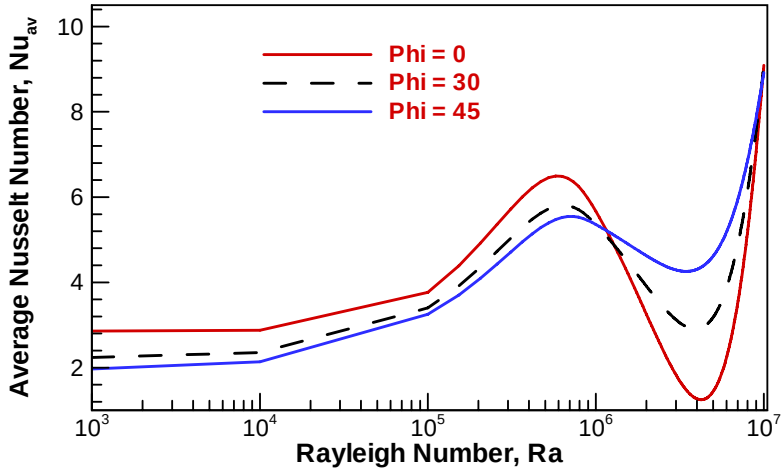

Figure 5.50: Average Nusselt Number vs Rayleigh number for uniform heating of side wall with Pr = 1000

5.5 Chapter Summary

Two-dimensional laminar steady state MHD free or natural convection within trapezoidal cavity for uniformly heated of bottom wall has been analyzed with heatlines concept. A finite element method for steady-state incompressible MHD free convection flow is presented. The finite element equations were derived from the governing flow equations that consist of the conservation of mass, momentum, and energy equations. The derived finite element equations are nonlinear requiring an iterative technique solver. The Newton-Raphson iteration method has applied to solve these nonlinear equations for solutions of the nodal velocity component, temperature, and pressure by considering Prandtl numbers of 0.026, 0.7, 1000, Hartman numbers of 50 and also Rayleigh numbers of 10^3 to 10^7. The results show that,

- The heat transfer rate is maximum near the edge of the wall and the rate is minimum near the center of the wall irrespective of all angles (ϕ) for uniform heating of the bottom wallfor Rayleigh number 10^3 to 10^7 gradually.

- Heat transfer depends on Prandtl number and heat transfer rate is maximum near the edge of the wall and the rate is minimum near the center of the wall irrespective of all angles (ϕ) for uniform heating of the bottom wall.

- Thermal boundary layer thickness is thinner for increasing of Rayleigh number due to upsurge of convective heat transfer rate.
- Local Nusselt number for uniform bottom heating is largest at the bottom edge of the side wall, and thereafter that decreases sharply upto a point which is very near to the bottom edge.
- The heat transfer rate average Nusselt Number, Nu_{av} increases with the increase of Rayleigh number, Ra, for uniform heating of bottom wall.
- The heat transfer rate average Nusselt Number, Nu_{av} increases with the increase of Rayleigh number, Ra, for uniform heating of side wall.
- Various vortices entering into the flow field and secondary vortex at the vicinity boundary wall and bottom wall of the cavity is seen in the streamlines.

CHAPTER 6

MHD FREE CONVECTION WITHIN TRAPEZOIDAL CAVITY WITH NON-UNIFORMLY HEATED BOTTOM WALL

A two-dimensional trapezoidal cavity of height L with the left wall inclined at an angle ϕ = 45^0, 30^0, 0^0 with Y axis was considered for non-uniform heating of bottom wall as shown in a schematic diagram of figure 4.1 in section 4.2 of chapter 4. In physical system, dimensional governing equations (4.1 – 4.4) and non-dimensional governing equations (4.5 -4.8) are solved in section 4.3.1 and 4.3.4 respectively in previous chapter 4. For boundary conditions, left wall and right wall (i.e. side walls) are subjected to cold temperature *(T_c)* and the top wall is thermal insulated and also the bottom wall is heated non-uniformly as shown in section 4.3.2 and 4.3.5 (case –II : non-uniform heating). Numerical technique of finite element formulation has also been discussed in section 4.4.1.In this chapter grid independence test, code validation, comparisons and results have been discussed.

6.1 Grid Independence Test for Non-Uniform Heating

Test for the accuracy of grid fineness has been carried out to find out the optimum grid number.

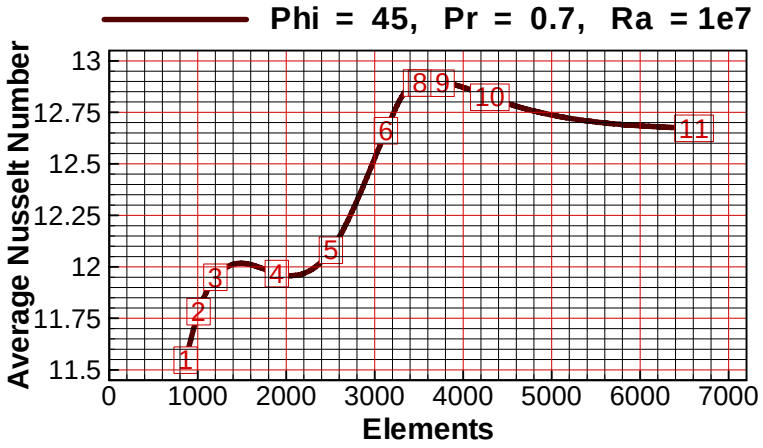

Figure 6.1: Convergence of average Nusselt number with grid refinement for *Pr* = 0.7, *Ha* = 50, ϕ = 45^0 and *Ra* = 10^7 in presence of non-uniform heating.

In order to obtain grid independent solution, a grid refinement study is performed for a trapezoidal cavity with *Pr* = 0.7, *phi* = 45^0 and *Ra* = 10^7. Figure 5.2 shows the convergence of the average Nusselt number, Nu_{av} at the heated surface with grid refinement. It is observed that grid independence is achieved with 3456 elements where there is insignificant change in Nu with further increase of mesh elements. Six different non-uniform grids with the following number of nodes and elements were considered for the grid refinement tests: 5858 nodes, 864 elements; 6849 nodes, 1010 elements; 8098 nodes, 1200 elements; 12672 nodes, 1894 elements; 16605 nodes, 2505 elements; 20781 nodes, 3127 elements, 22944 nodes, 3456 elements, 23339 nodes, 3513 elements, 25053 nodes, 3767 elements, 31479 nodes, 4301 elements, 43505 nodes, 6609 elements . From these values, 22944 nodes, 3456 elements can be chosen throughout the simulation to optimize the relation between the accuracy required and the computing time.

Nodes (lements)	5858 (864)	6849 (1010)	8098 (1200)	12672 (1894)	16605 (2505)	20781 (3127)	22944 (3456)	25053 (3767)	31479 (4301)	43505 (6609)
Nu	11.54703	11.782359	11.94927	6 11.96754	12.08048	12.66089	12.8922	12.8917	12.8233	12.6724
Time (s)	8.047	8.781	9.172	12.719	18.703	26.203	26.75	31.968	38.594	64.75

Table 6.1: Grid Sensitivity Check at *Pr* = 0.7, *Phi* =45^0, *Ha*=50 *and Ra* = 10^7.

6.2 Code Validation

For the validation of the code, a trapezoidal cavity without MHD is considered with a fluid by finite element weighted residual method whose left wall and right wall (i.e. side walls) are subjected to cold T_c temperature, bottom wall is subjected to non-uniformly hot T_h temperature while the top wall is kept insulated. Average Nusselt number is calculated for three different Rayleigh numbers (*Ra* = 10^3, 10^4 and 10^5) and three different angles ϕ = 45^0, 30^0, 0^0 , while the prandtl number is fixed i.e. Pr = 0.7 for non-uniform heating of bottom wall. The results were compared with those reported by Basak et al. (March 2009). In Table 6.2, for code validation, average Nusselt numbers is presented for different Rayleigh numbers of non-uniform heating of bottom with the above fixed Prandtl number. For code validation, in Table 6.2 for non-uniform bottom heating 6402 nodes and 952

elements, 2178 nodes and 314 elements, 1527 nodes and 216 elements have been used for $\phi = 0^0$, $\phi = 30^0$, $\phi = 45^0$ and $Ra = 10^5$ respectively. The results of the figure (6.2 – 6.4) of non-uniform bottom heating were also compared with those reported by Basak et al. (March 2009) with streamlines, isotherms (temperature) and Heat function or total heat flux for Pr =0.026 and . $Ra = 10^5$. The results from the present experiment are almost same as Basak et.al.

Ra	Average Nusselt Number, (Nu_{av})					
	Present work without MHD			Basak et al. (2009) without MHD		
	$\phi = 0^0$	$\phi = 30^0$	$\phi = 45^0$	$\phi = 0^0$	$\phi = 30^0$	$\phi = 45^0$
10^3	4.362908	3.180613	2.883518	1.97369	1.5808	1.42156
10^4	4.408955	3.39454	3.155096	2.84441	2.75579	2.87144
10^5	5.839234	5.054993	4.822457	5.12784	4.84779	4.70209

Table 6.2: Code validation for non-uniform heating of bottom wall with Pr = 0.7.

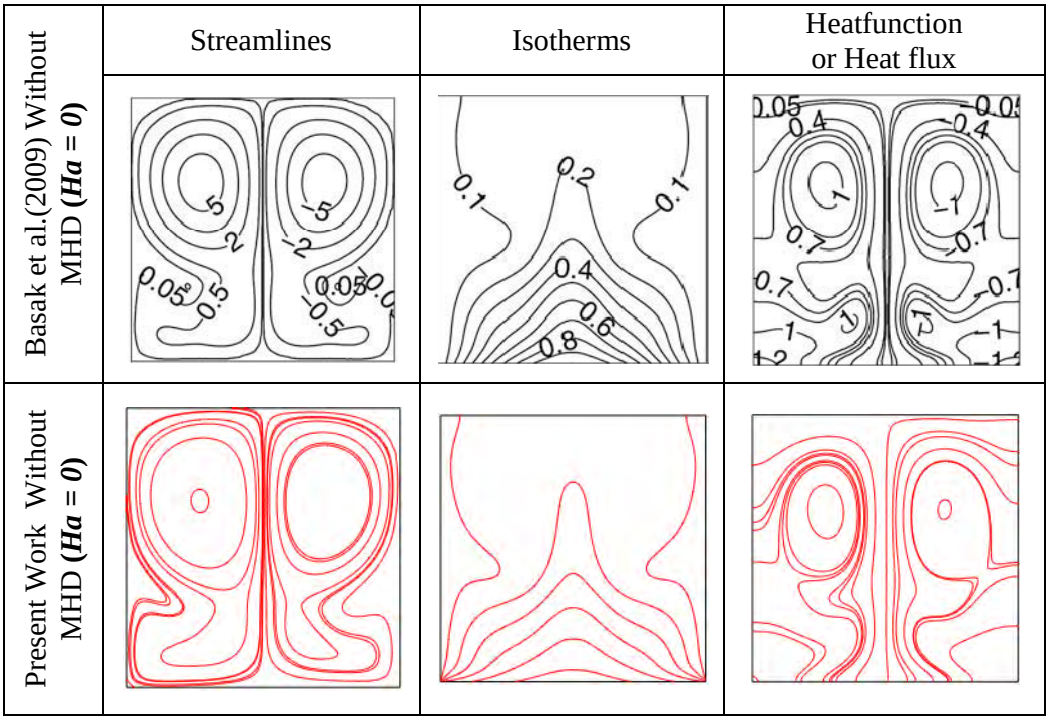

Figure 6.2: Code validation for non- uniform bottom heating at *Ra* = 10^5, $\phi = 0^0$ with Pr = 0.026.

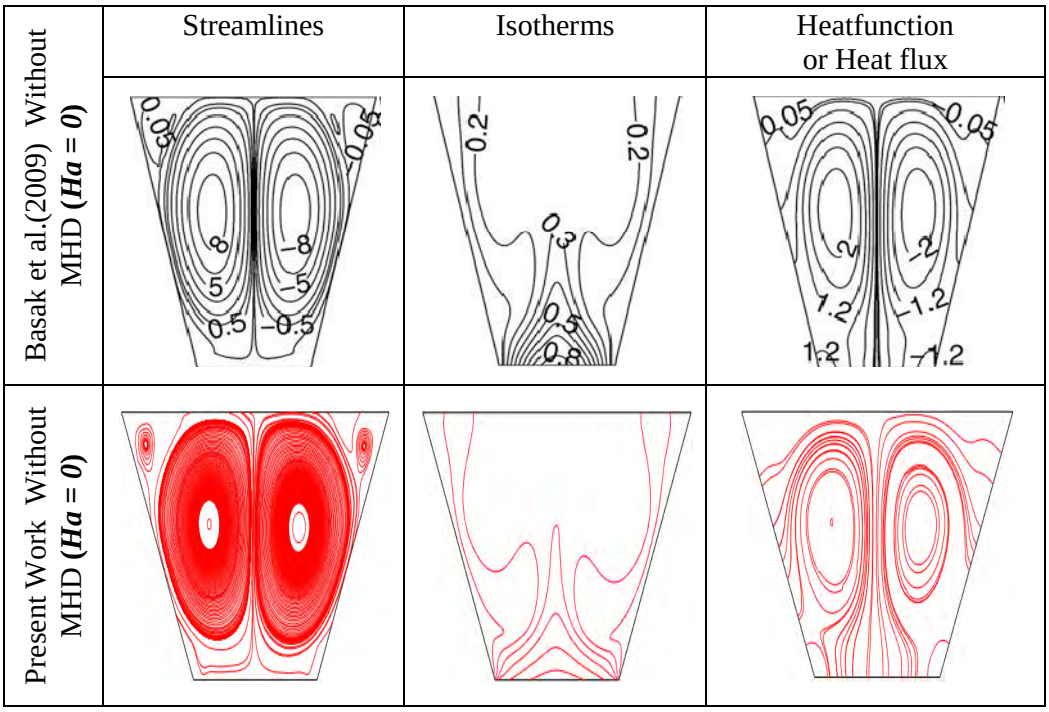

Figure 6.3: Code validation for non- uniform bottom heating at *Ra* = 10^5, ϕ = 30^0 with Pr = 0.026.

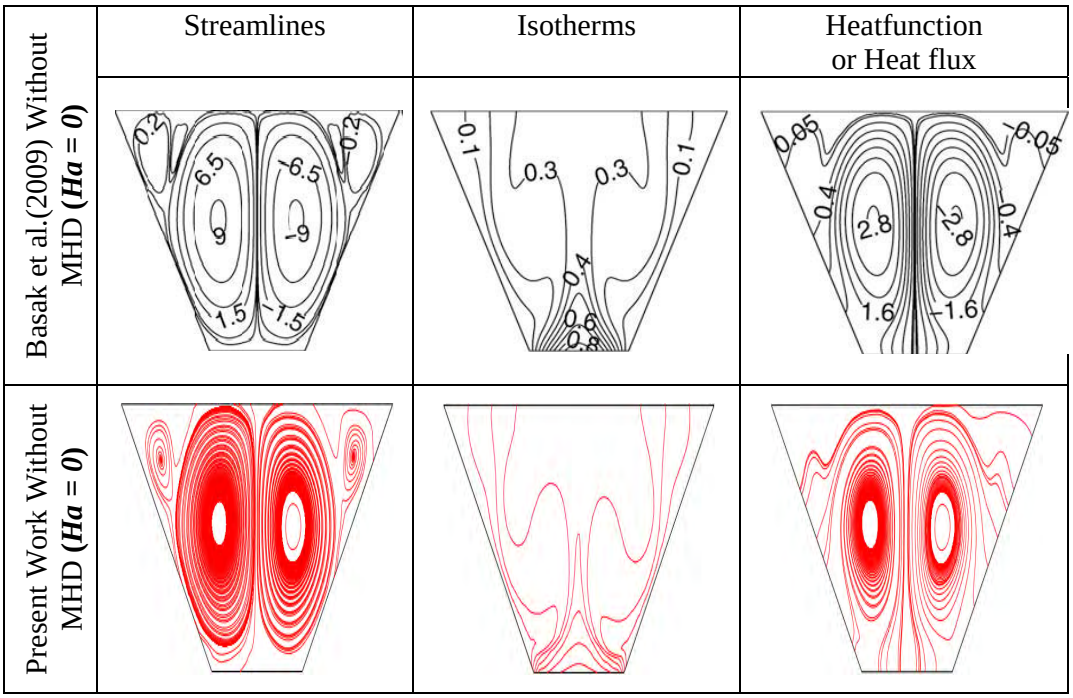

Figure 6.4: Code validation for non- uniform bottom heating at *Ra* = 10^5, ϕ = 45^0 with Pr = 0.026.

6.3 Comparisons between without and with MHD

After validation of the code, a trapezoidal cavity with MHD is considered with a fluid whose left wall and right wall (i.e. side walls) are subjected to cold T_c temperature, bottom wall is subjected to uniformly hot T_h temperature while the top wall is kept insulated. Average Nusselt number is calculated for three different Rayleigh numbers ($Ra = 10^3$, 10^4 and 10^5) and three different angles $\phi = 45^0$, 30^0, 0^0 , while the prandtl number is fixed i.e. Pr = 0.7 for non-uniform heating of bottom wall. The results were compared with the present work where magnetohydrodynamic effect is not applied. In Table 6.3, for comparison, average Nusselt number is presented for different Rayleigh numbers of non-uniform heating of bottom wall with the above fixed Prandtl number. Here average Nusselt number of non-uniform heating of bottom wall is enhancing for different Rayleigh numbers. When Rayleigh numbers increase then average Nusselt number increase is seen. This is happening because of heat transfer. The results of the figure (6.5 – 6.7) with magneto-hydrodynamics (MHD) of non-uniform bottom heating for $\phi = 0^0$, $\phi = 30^0$, $\phi = 45^0$ and $Ra = 10^5$. were also compared with the present work with streamlines, isotherms (temperature) and Heat function or total heat flux where magneto-hydrodynamics (MHD) is not applied. Here from the present work of the figure it is seen that heat flow of non-uniform heating more suppressed out than uniform heating for magnetic effect. Comparisons of the results without and with MHD of the current research work are given below.

Ra	Average Nusselt Number, (Nu_{av})					
	Present work withMHD			Present work without MHD		
	$\phi = 0^0$	$\phi = 30^0$	$\phi = 45^0$	$\phi = 0^0$	$\phi = 30^0$	$\phi = 45^0$
10^3	4.361568	3.506399	3.157268	4.362908	3.180613	2.883518
10^4	4.365658	3.51229	3.163712	4.408955	3.39454	3.155096
10^5	4.464063	3.729079	3.474017	5.839234	5.054993	4.822457

Table 6.3: Comparisons for non-uniform heating of bottom wall with Pr = 0.7.

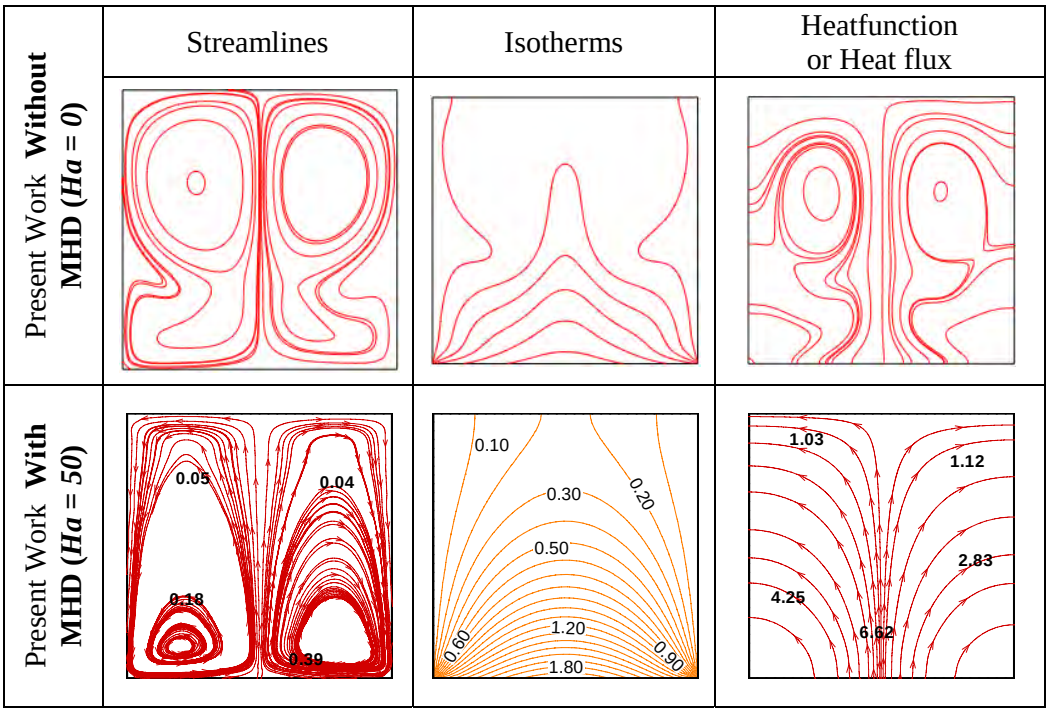

Figure 6.5: Comparisons for non- uniform bottom heating at $Ra = 10^5$, $\phi = 0^0$ with Pr = 0.026 when $Ha = 0$ and $Ha = 50$.

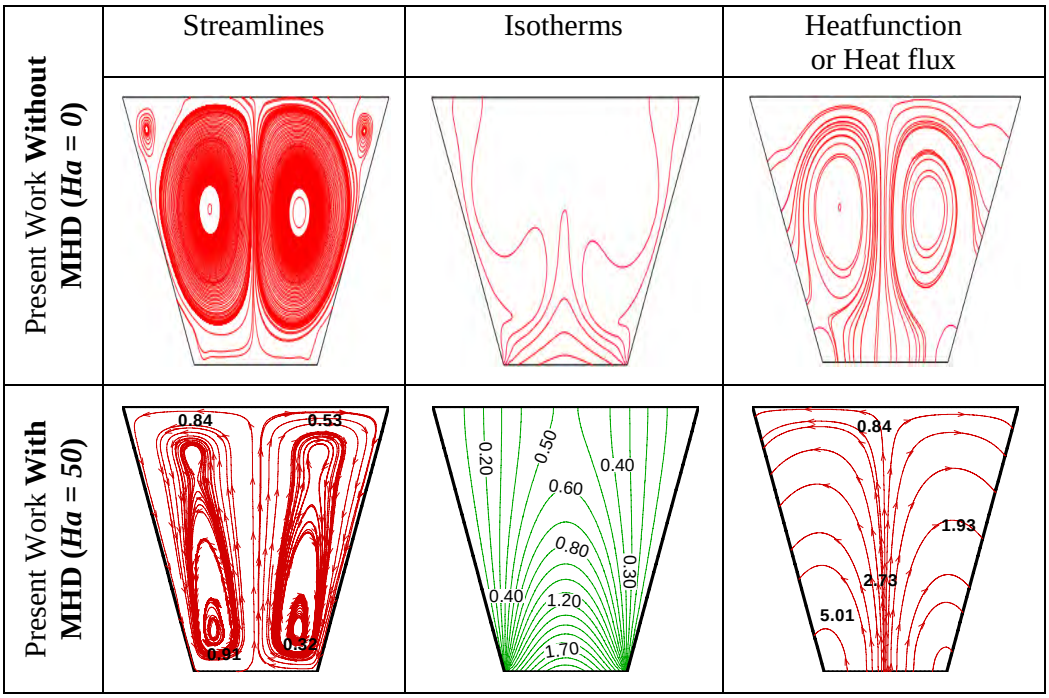

Figure 6.6: Comparisons for non- uniform bottom heating at $Ra = 10^5$, $\phi = 30^0$ with Pr = 0.026 when $Ha = 0$ and $Ha = 50$.

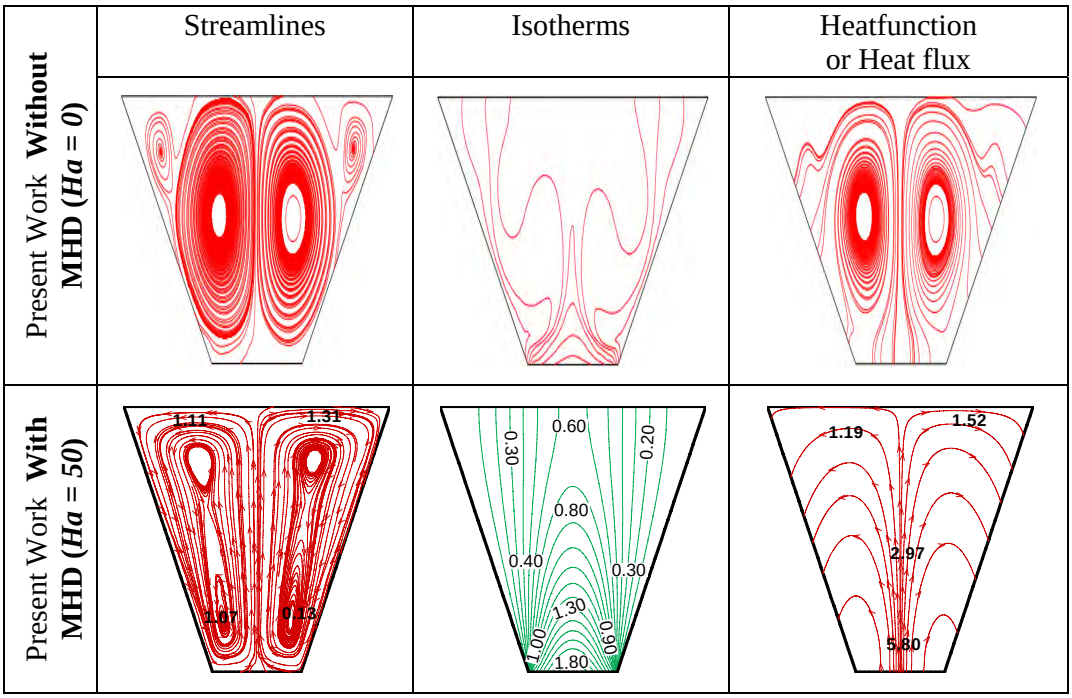

Figure 6.7: Comparisons for non- uniform bottom heating at *Ra* = 10^5, ϕ = 45^0 with Pr = 0.026 when *Ha* = 0 and *Ha* = 50.

6.4 Results and Discussion

After completing the code validation with those reported Basak et al. (March 2009), two dimensional laminar steady state on MHD free convection within trapezoidal cavity with non-uniformly heated bottom wall have also been studied numerically. Results are obtained on non-uniform heat flow for parametric study for the wide range of Rayleigh number, Ra = 10^3- 10^7 and Prandtl number, Pr = 0.026, 0.7, 1000 with various angles, ϕ = 45^0, 30^0, 0^0(square cavity).

6.4.1 Non-Uniform Heating of Bottom Wall

Figure 6.8 – 6.19 illustrate streamline (stream function), isotherms (temperature) and heatlines for Pr = 0.026, 0.7, 1000 on uniform heating of bottom wall for MHD free convection in presence of cold side walls.

Figure 6.8 illustrate that the magnitudes of streamfunction are considerably smaller and heat transfer are primarily due to conduction. For Ra = 10^3, Pr = 0.026 and ϕ = 0^0(square

cavity) isotherms (temperature) with $\theta = 0.10 - 0.20$ occur symmetrically along side (left or right) walls and with $\theta \geq 0.30$ are smooth curves symmetric with respect to vertical symmetrical line (Fig. 6.8a). For $Ra = 10^3$, $Pr = 0.026$ and $\phi = 30^0$ the temperature contours with $\theta = 0.10 – 0.40$ occur symmetrically near the side walls of the enclosure and with $\theta \geq 0.50$ are smooth curves symmetric with respect to central symmetrical line (Fig. 6.8b). Again for $Ra = 10^3$, $Pr = 0.026$ and $\phi = 45^0$ isotherms (temperature) with $\theta = 0.10 – 0.50$ occur symmetrically near the side walls of the enclosure and with $\theta \geq 0.60$ are smooth curves symmetric with respect to vertical symmetrical line (Fig. 6.8c).The heatlines or total heat flux or heat function are shown in panels of fig 6.8a-c. The heatlines illustrate similar feature that were observed for uniform heating cases.

It is interesting to note that at the bottom corner point $\phi = 0^0$(square cavity) is larger than for $\phi = 45^0$ and 30^0. It is evident that heatlines near the bottom portion of side walls are more dense for $\phi = 45^0$ and less dense for $\phi = 0^0$(square cavity). The dense heatlines is also indicating enhanced rate of heat transfer from the bottom to the side walls. Therefore isotherms with $\theta = 0.05 – 0.35$ are shifted for $\phi = 45^0$ toward the side walls. It ios also observed that heat transfer at the top portion of the cavity for $\phi = 45^0$ and 30^0 is higher compressed to $\phi = 0^0$(square cavity) based on value of heatfunction (Π). As the heat transfer is quite large at the corners of bottom wall, the thermal boundary layer was found to develop near the bottom edges and thickness of boundary layer is larger at the top portion of the cold wall signifying less heat transfer to the top portion.

Figure 6.9 and 6.10 point up that the magnitudes of streamfunction are smaller for $Ra = 10^4, 10^5$ when $Pr = 0.026$ and isotherms (temperature) with $\theta = 0.10 – 0.20$, $\theta = 0.10 – 0.40$, $\theta = 0.10 – 0.40$ occur symmetrically near the side walls of the enclosure and with $\theta \geq 0.30$, $\theta \geq 0.50$, $\theta \geq 0.65$ are smooth curves symmetric with respect to central symmetrical line for $Ra = 10^4, 10^5$, $Pr = 0.026$ and $\phi = 45^0, 30^0, 0^0$(square cavity) (Fig 6.9, 6.10a-c) and heatlines enhanced the rate of heat transfer from the bottom to side walls for $Ra = 10^4, 10^5$, $Pr = 0.026$.In contrast the non-uniform heating removes the singularity at the edges of bottom wall and provides a smooth temperature distribution in the entire enclosure. For $Ra = 10^4, 10^5$ the circulation pattern is qualitatively similar to the uniform heating case with the identical situation. However to this case isotherms and heatlines are more compressed near the bottom wall of the enclosure in case of non-uniform heating.

Figure 6.11 illustrate that the magnitudes of streamfunction at larger Ra = 10^7 with Pr = 0.026.It is interesting to detect that the stratification zone of temperature at the center vertical line near the bottom wall for Ra = 10^7 is suppressed whereas stratification zone of temperature is larger for Ra = 10^3 due to increased convection. It is also noted that stratification zone of temperature at bottom wall is thicker for $\phi = 0^0$(square cavity) due to less intense circulation near the top portion of the cavity. Isotherms (temperature) with θ = 0.10 – 0.1.20, θ = 0.10 – 1.20, θ = 0.10 – 1.10 occur symmetrically near the side walls of the enclosure and with $\theta \geq 1.30$, $\theta \geq 1.30$, $\theta \geq 1.20$ are smooth curves symmetric with respect to central symmetrical line for Ra = 10^7, Pr = 0.026 and $\phi = 45^0$, 30^0, 0^0(square cavity) respectively. Heatlines indicate the heat transfer from the hot wall to cold side walls and uniform heating flow circulation due to fluid circulation cells. Due to non-uniform heating of bottom wall the heating rate near to corners of the wall is generally lower and that induces less buoyancy effect resulting in less thermal gradient throughout the domain. Heatlines near the top portion of the side walls are oscillatory due to secondary circulation for $\phi = 45^0$ and 30^0. It is also observed that heatlines are quite dense near the central regime for $\phi = 45^0$ and 30^0 and implies enhance thermal mixing near the central to top portion of the cavity. This is due to the fact that strong primary circulations occur near to the corners to the bottom wall as like as uniform heating case.

Figure 6.12 – 6.15 represent that the magnitudes of streamfunction are circular or elliptical near the core but the streamlines near the wall is almost parallel to wall exhibiting large intensity of flow for Pr = 0.7 and Ra = 10^3 – 10^7. Also for Pr = 0.7 and Ra = 10^3 isotherms with θ = 0.10 – 0.20, θ = 0.10 – 0.40, θ = 0.10 – 0.50 and also θ = 0.10 – 0.20, θ = 0.10 – 0.50, θ = 0.10 – 0.60 for Pr = 0.7 and Ra = 10^4 and also θ = 0.10 – 0.50, θ = 0.10 – 1.00, θ = 0.10 – 1.00 for 0.7 and Ra = 10^5 and also θ = 0.10 – 0.90, θ = 0.10 – 0.80, θ = 0.10 – 0.80 for 0.7 and Ra = 10^7 occur symmetrically near the side walls of the enclosure and $\theta \geq 0.30$, $\theta \geq 0.50$, $\theta \geq 0.60$ and $\theta \geq 0.30$, $\theta \geq 0.60$, $\theta \geq 0.70$ and also $\theta \geq 0.60$, $\theta \geq 1.10$, $\theta \geq 1.10$ and $\theta \geq 1.00$, $\theta \geq 0.90$, $\theta \geq 0.90$ are smooth curves symmetric with respect to central symmetrical line for Ra = 10^3 - 10^7, Pr = 0.7 and $\phi = 45^0$, 30^0, 0^0(square cavity) respectively. It is also fascinating that multiple correlations are absent for Pr = 0.7 and Ra = 10^7. Due to enhanced flow circulations the isotherms are highly compressed near the side walls except near the bottom wall especially for $\phi = 45^0$ and 30^0.As Ra increases for Pr = 0.7 the the circulations near the central regime are stronger and consequently the bottom portion contours start getting stretched toward the central regime of the bottom

wall. Results indicate that the strength of circulations is more for non-uniform heating case than uniform heating case.

Figure 6.16 – 6.19 show streamline. Isotherms (temperature) and heatlines for Ra = 10^3 - 10^7, Pr =1000 and $\phi = 45^0, 30^0, 0^0$(square cavity) respectively. Also for Pr = 1000 and Ra = 10^3 isotherms with $\theta = 0.10 – 0.20$, $\theta = 0.10 – 0.50$, $\theta = 0.10 – 0.60$ and also $\theta = 0.10 – 0.40$, $\theta = 0.10 – 0.90$, $\theta = 0.10 – 1.00$ for Pr = 1000 and Ra = 10^4 and also $\theta = 0.10 – 0.90$, $\theta = 0.10 – 1.00$, $\theta = 0.10 – 1.00$ for 1000 and Ra = 10^5 and also $\theta = 0.10 – 0.80$, $\theta = 0.10 – 0.80$, $\theta = 0.10 – 0.90$ for 1000 and Ra = 10^7 occur symmetrically near the side walls of the enclosure and $\theta \geq 0.30$, $\theta \geq 0.60$, $\theta \geq 0.70$ and $\theta \geq 0.50$, $\theta \geq 1.00$, $\theta \geq 1.10$ and also $\theta \geq 1.00$, $\theta \geq 1.10$, $\theta \geq 1.10$ and $\theta \geq 0.90$, $\theta \geq 0.90$, $\theta \geq 1.00$ are smooth curves symmetric with respect to central symmetrical line for Ra = 10^3 - 10^7, Pr = 0.7 and $\phi = 45^0, 30^0, 0^0$(square cavity) respectively. As Pr incresses from Pr = 0.7 to 1000 the the flow intensity is found to be enhanced. Here it is seen that the magnitudes of streamlines is maximum and its shape is also circular or elliptical. It is also indicate that the values of stream functions of non-uniform heating case are almost similar to uniform heating cases due to the lower heat from bottom wall and the less intense heating effects near the central regime are attributed by less-dense heatline due to non-uniform heating effects.

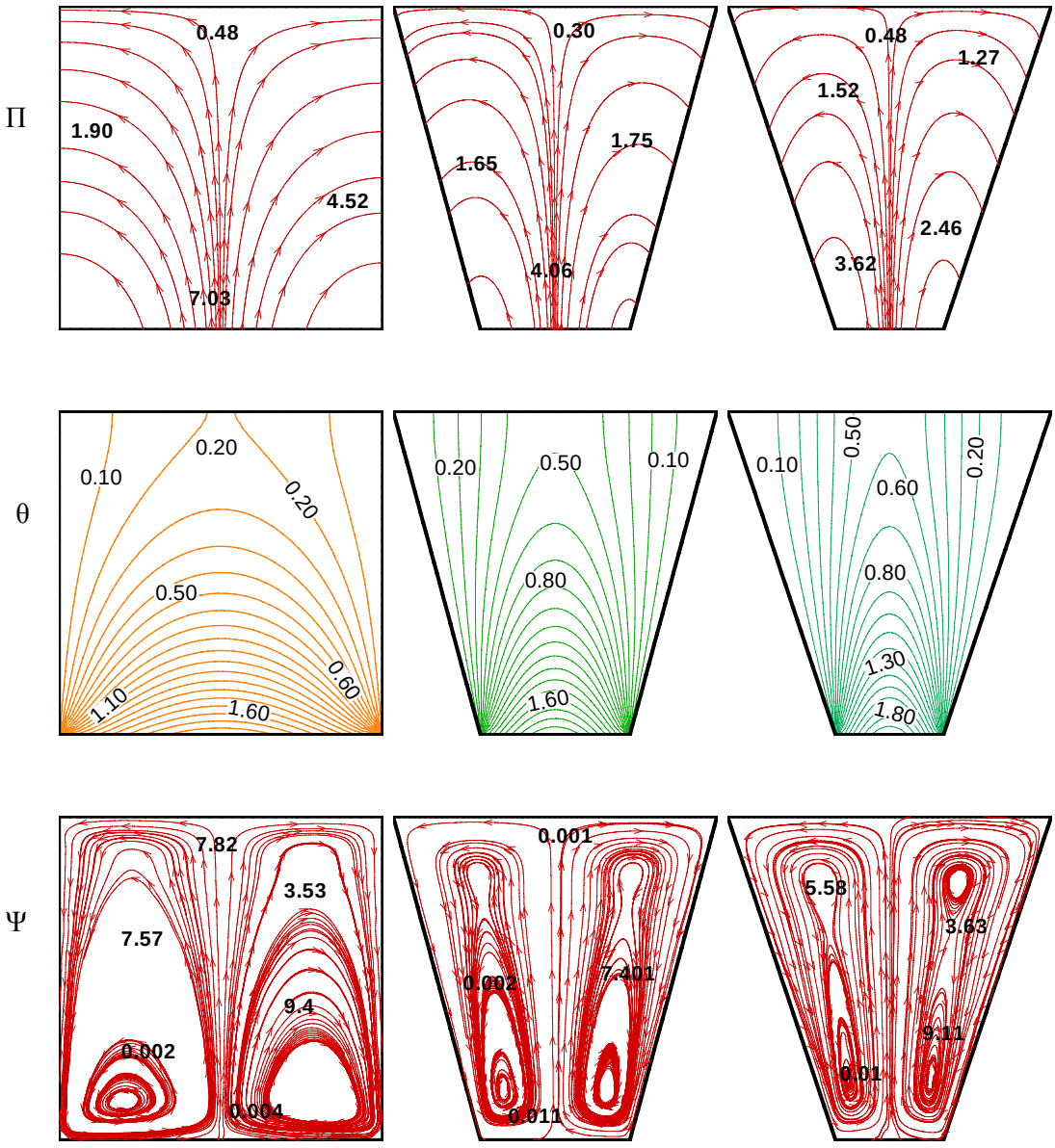

Figure 6.8: Stream function (Ψ), temperature (θ), heat function or total heat flux(Π) for non-uniform bottom heating θ(X,0) = sin(πx) with Pr = 0.026, Ha = 50 and Ra = 10^3 (a) Φ = 0^o
(b) Φ = 30^o (c) Φ = 45^o

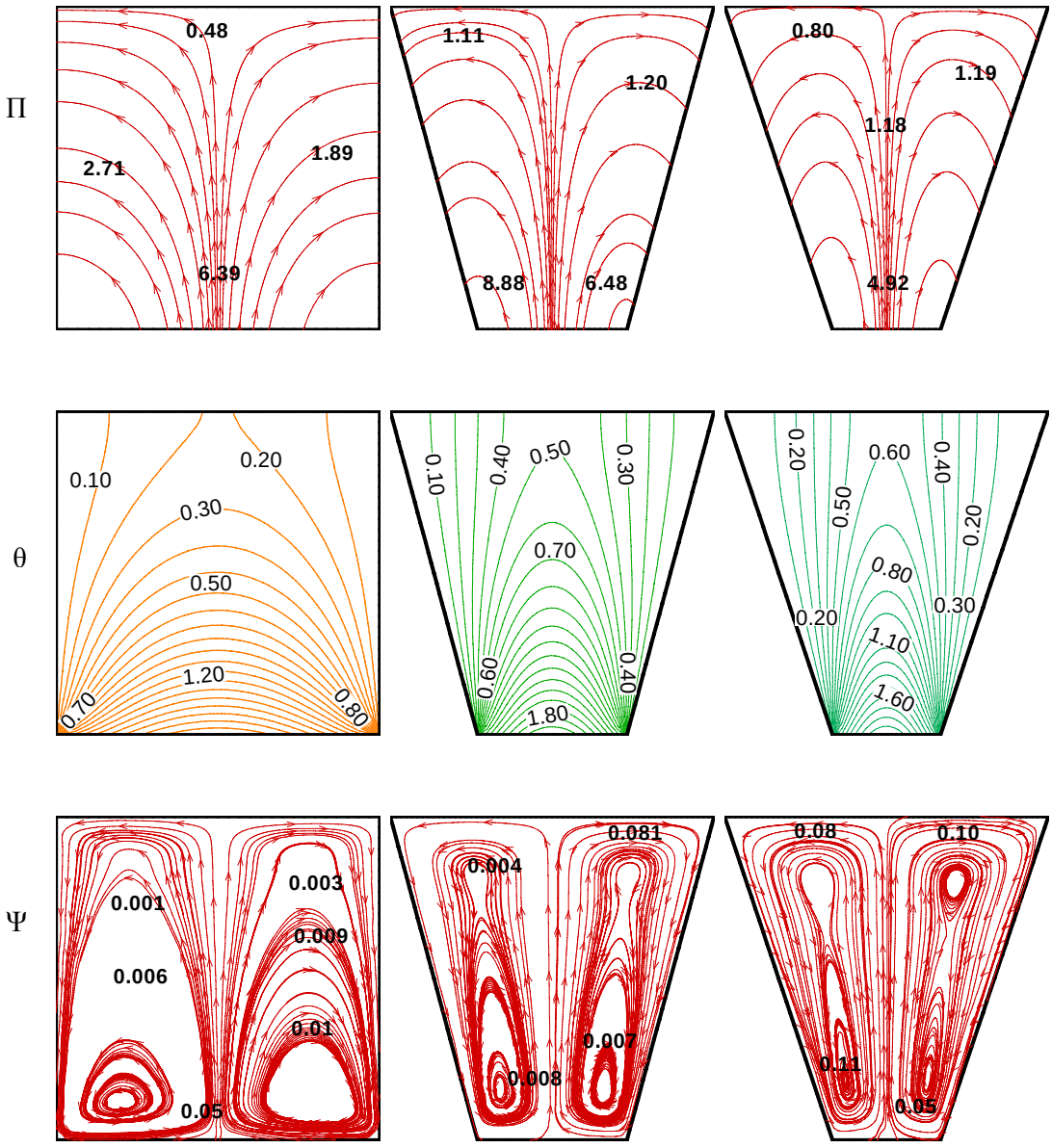

Figure 6.9: Stream function(Ψ), temperature(θ), heat function or total heat flux(Π) for non-uniform bottom heating θ(X,0) = sin(πx) with Pr = 0.026, Ha = 50 and Ra = 10^4 (a) Φ = 0^o (b) Φ = 30^o (c) Φ = 45^o

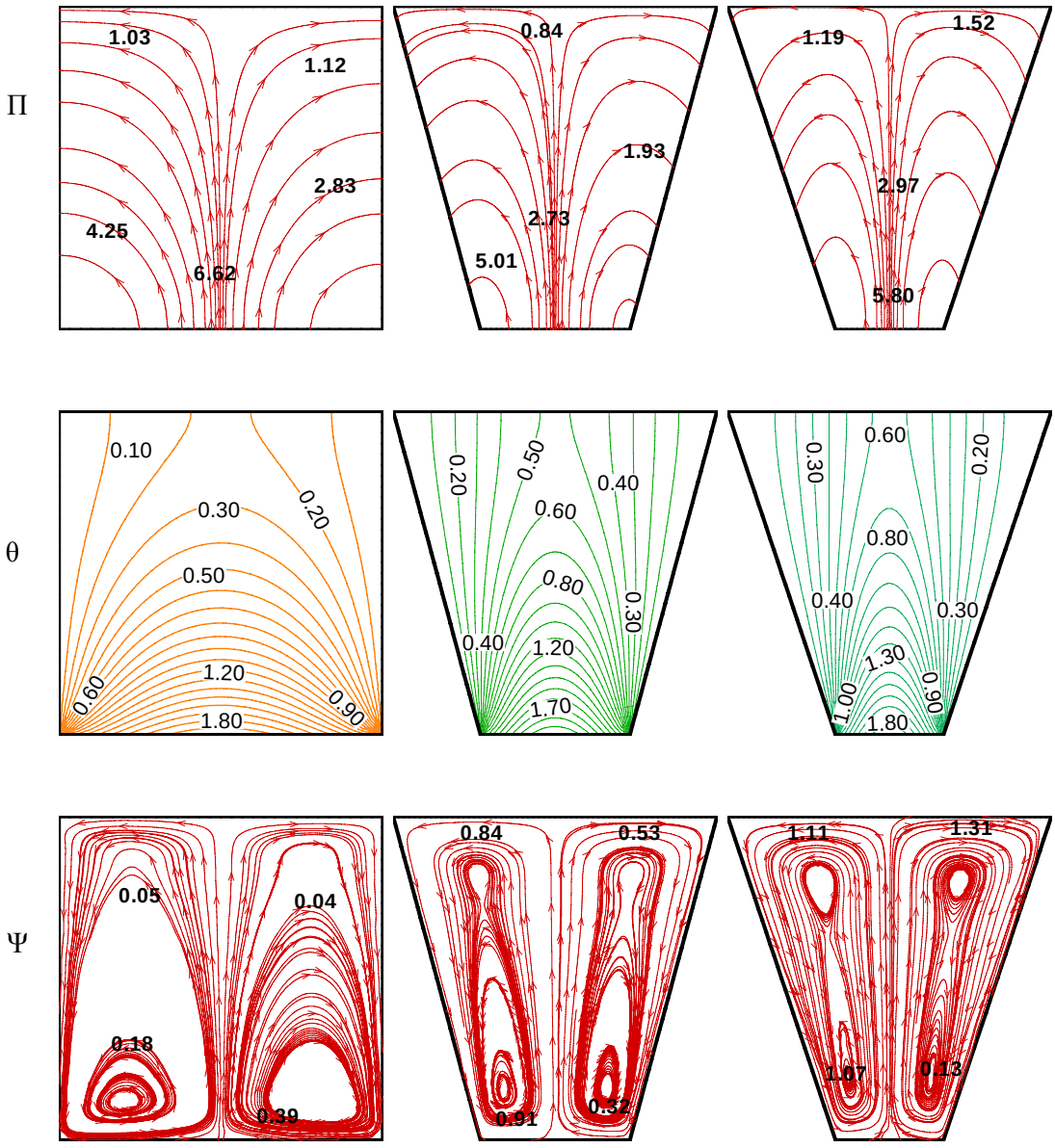

Figure 6.10: Stream function (Ψ), temperature (θ), heat function or total heat flux(Π) for non-uniform bottom heating θ(X,0) = sin(πx) with Pr = 0.026, Ha = 50 and Ra = 10^5 (a) Φ = 0^o (b) Φ = 30^o (c) Φ = 45^o

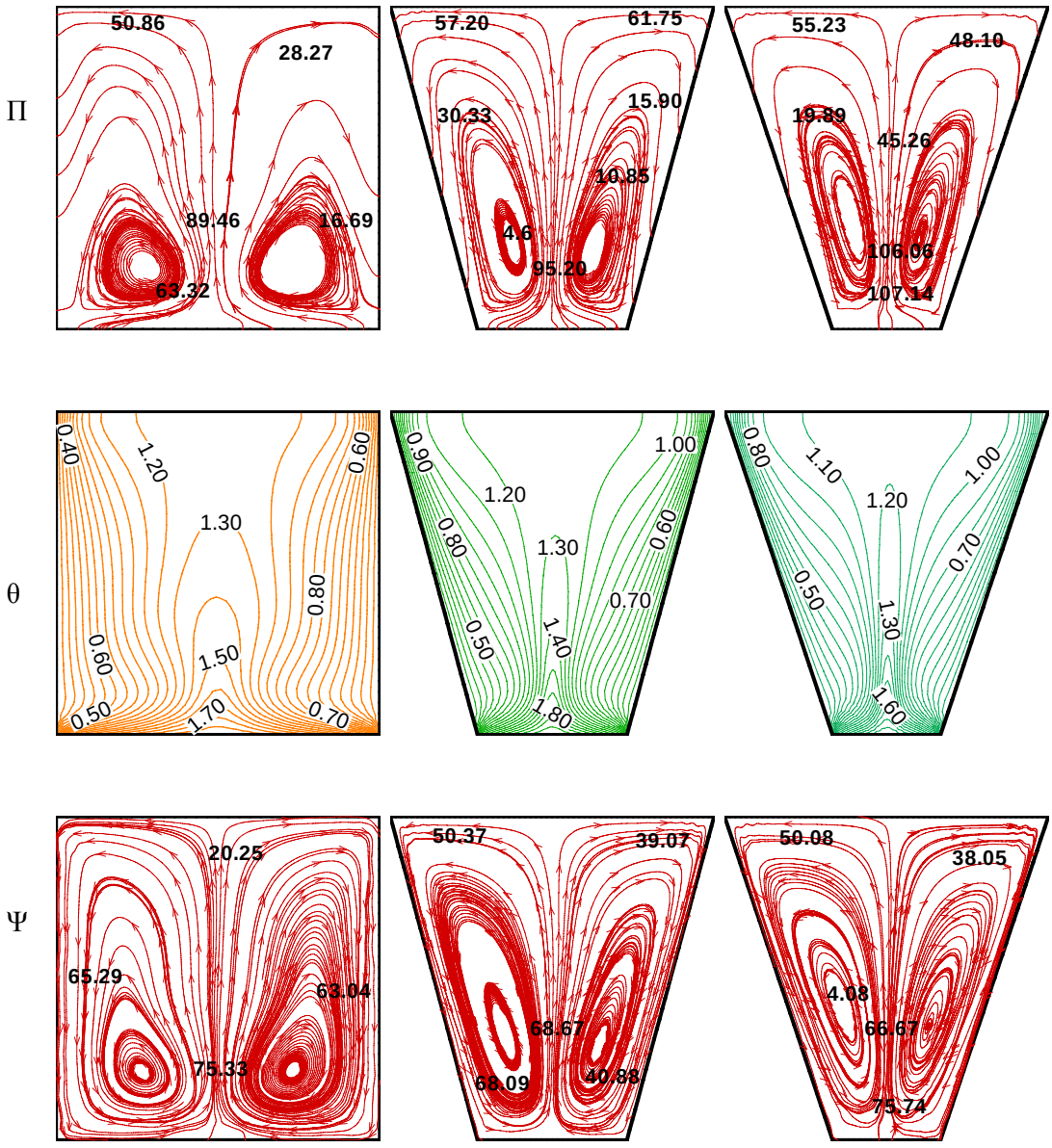

Figure 6.11: Stream function (Ψ), temperature (θ), heat function or total heat flux(Π) for non-uniform bottom heating θ(X,0) = sin(πx) with Pr = 0.026, Ha = 50 and Ra = 10^7(a) Φ = 0^o (b) Φ = 30^o (c) Φ = 45^o

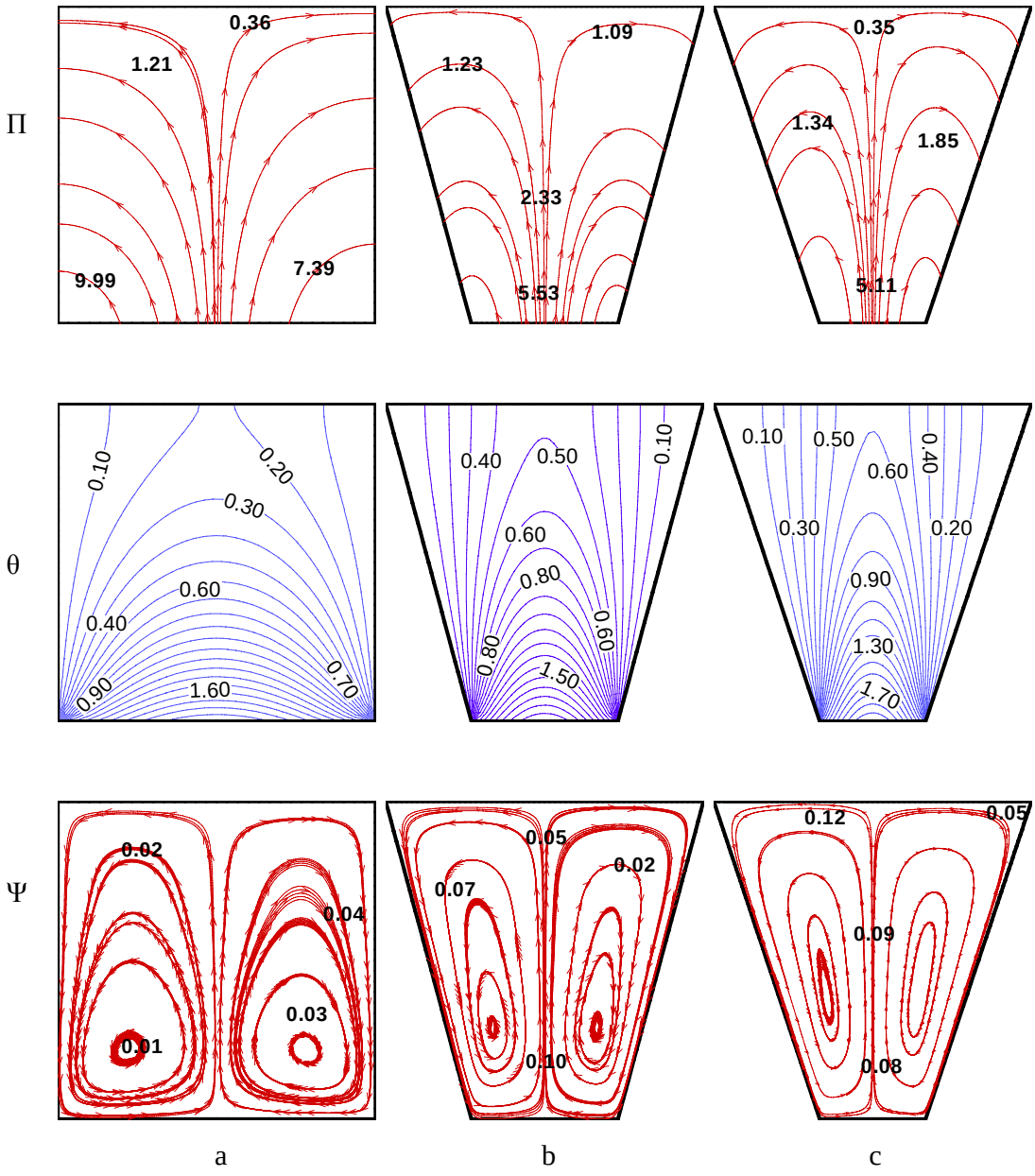

Figure 6.12: Stream function (Ψ), temperature (θ), heat function or total heat flux(Π) for non-uniform bottom heating θ(X,0) = sin(πx) with Pr = 0.7, Ha = 50 and Ra = 10^3 (a) Φ = 0^o (b) Φ = 30^o (c) Φ = 45^o

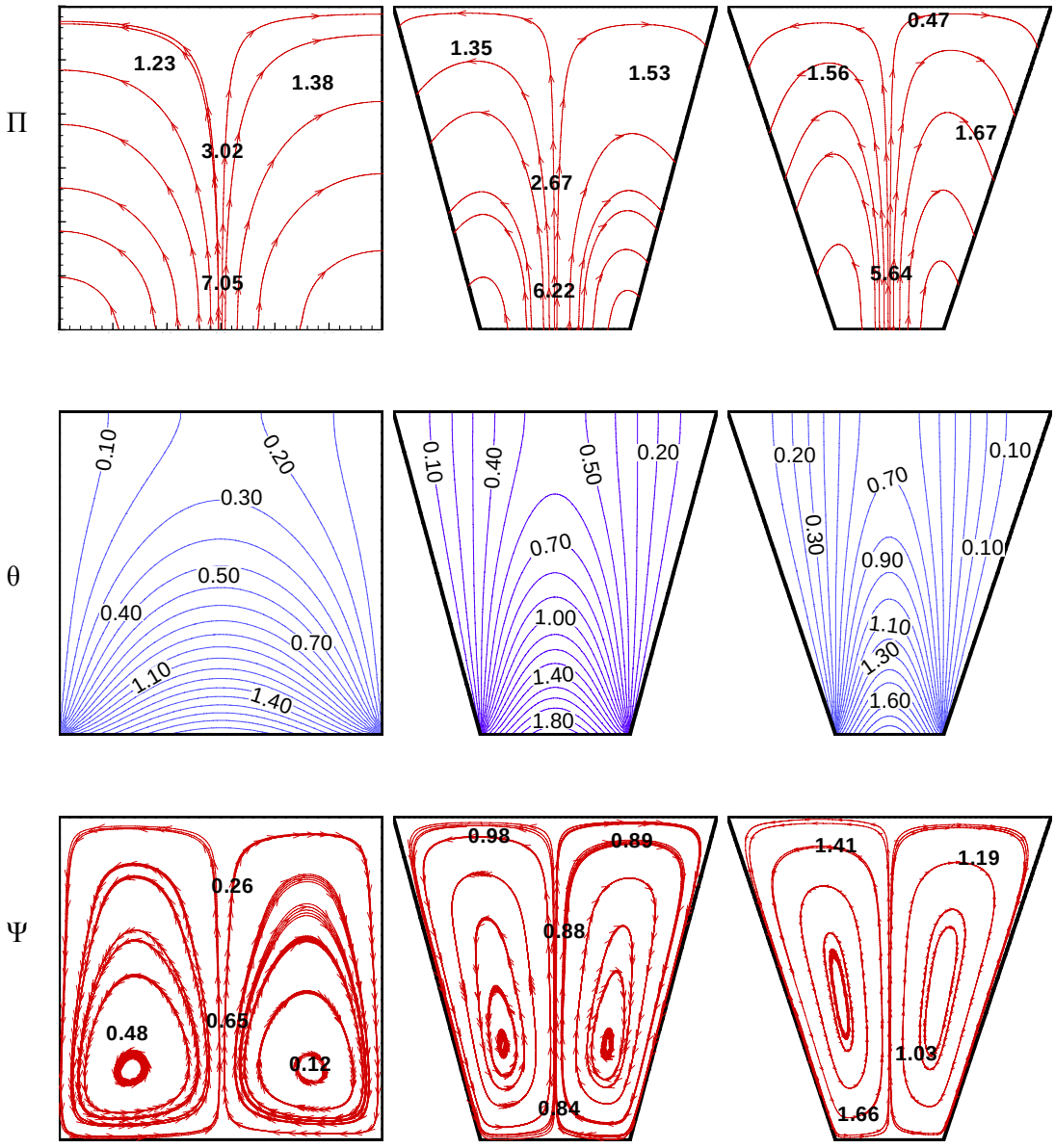

Figure 6.13: Stream function (Ψ), temperature (θ), heat function or total heat flux(Π) for non-uniform bottom heating θ(X,0) = sin(πx) with Pr = 0.7, Ha = 50 and Ra = 10^4 (a) Φ = 0^o (b) Φ = 30^o (c) Φ = 45^o

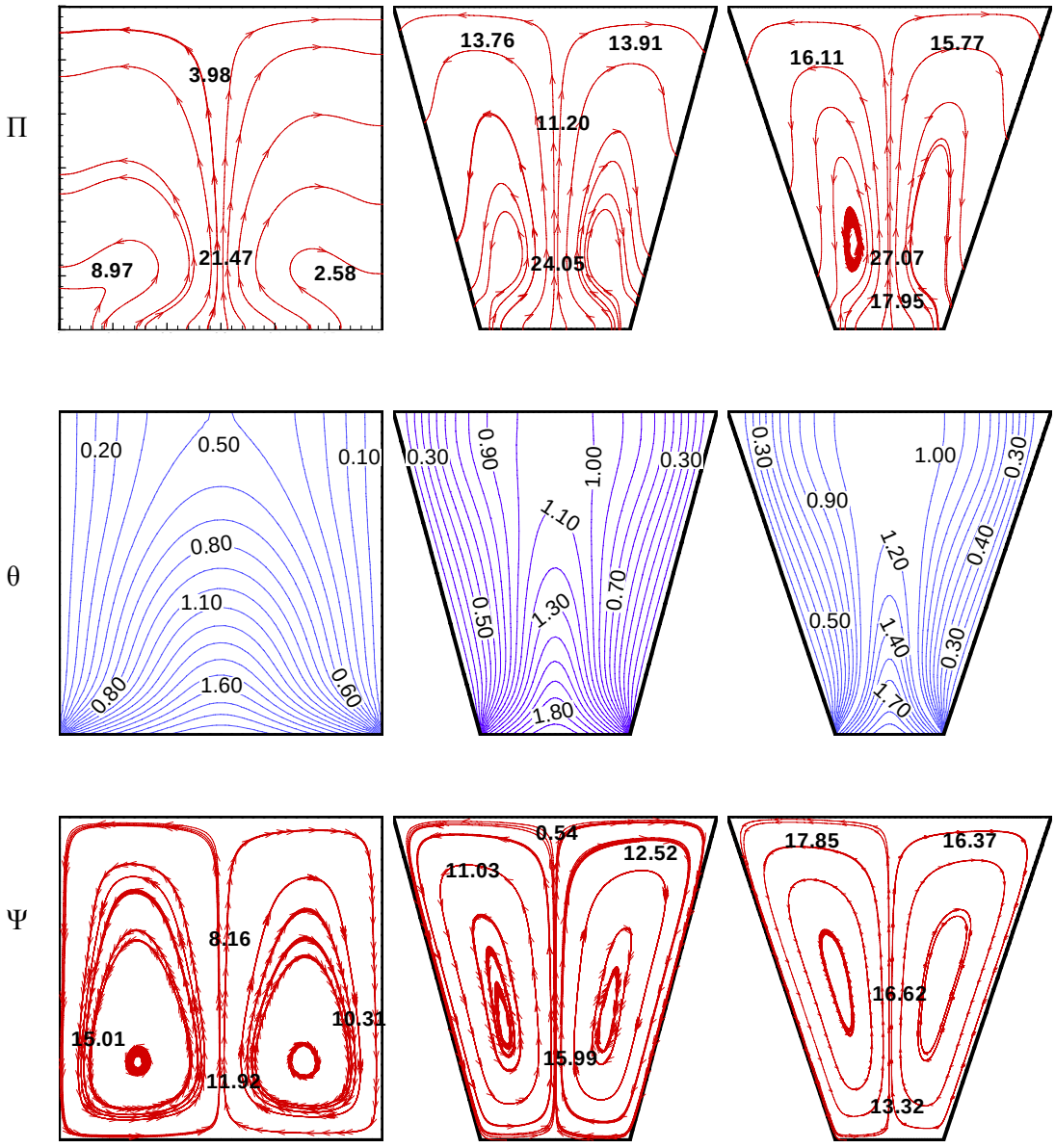

Figure 6.14: Stream function (Ψ), temperature (θ), heat function or total heat flux(Π) for non-uniform bottom heating θ(X,0) = sin(πx) with Pr = 0.7, Ha = 50 and Ra = 10^5 (a) Φ = 0^o (b) Φ = 30^o (c) Φ = 45^o

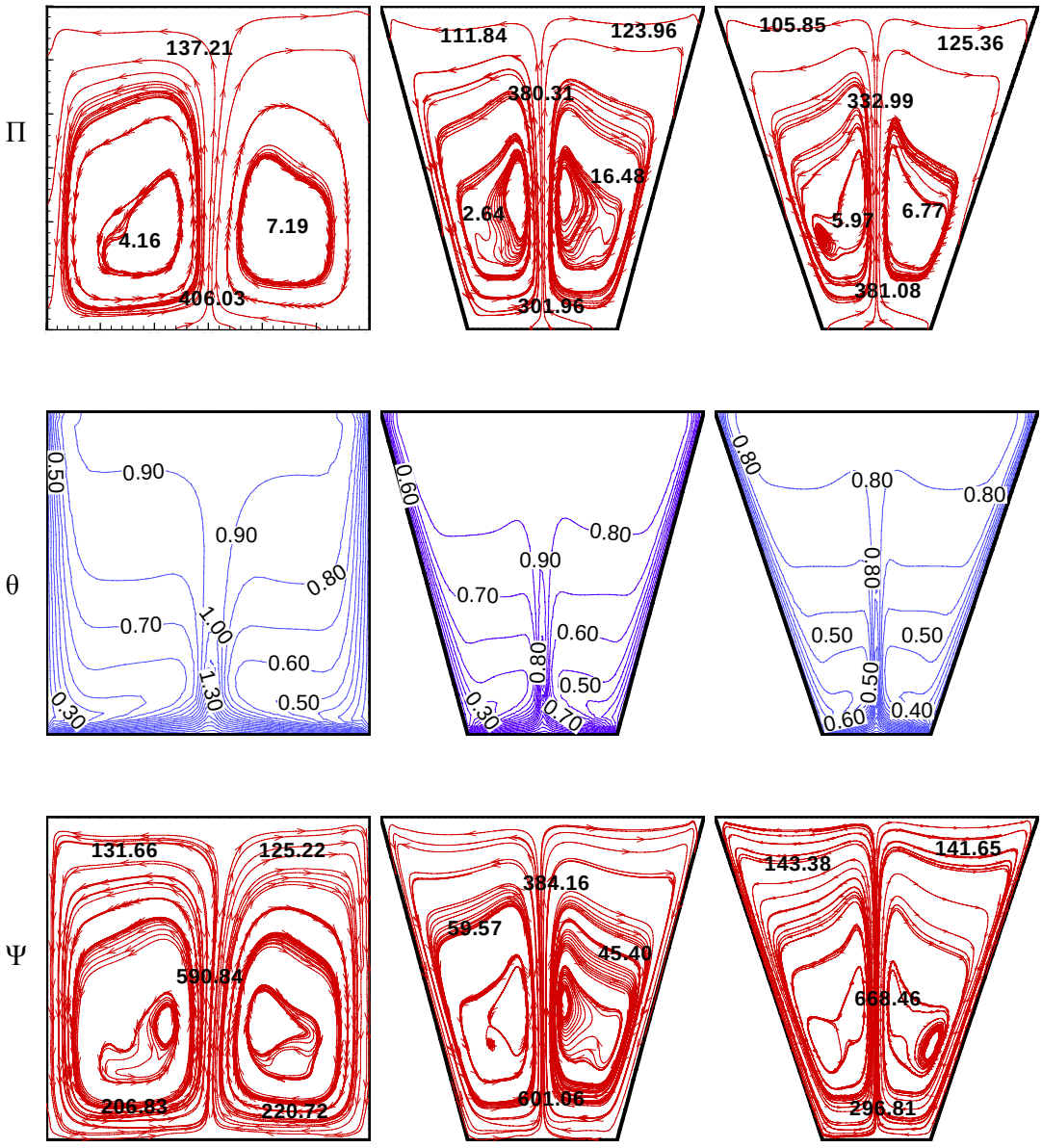

Figure 6.15: Stream function (Ψ), temperature (θ), heat function or total heat flux(Π) for non-uniform bottom heating θ(X,0) = sin(πx) with Pr = 0.7, Ha = 50 and Ra = 10^7 (a) Φ = 0^o (b) Φ = 30^o (c) Φ = 45^o

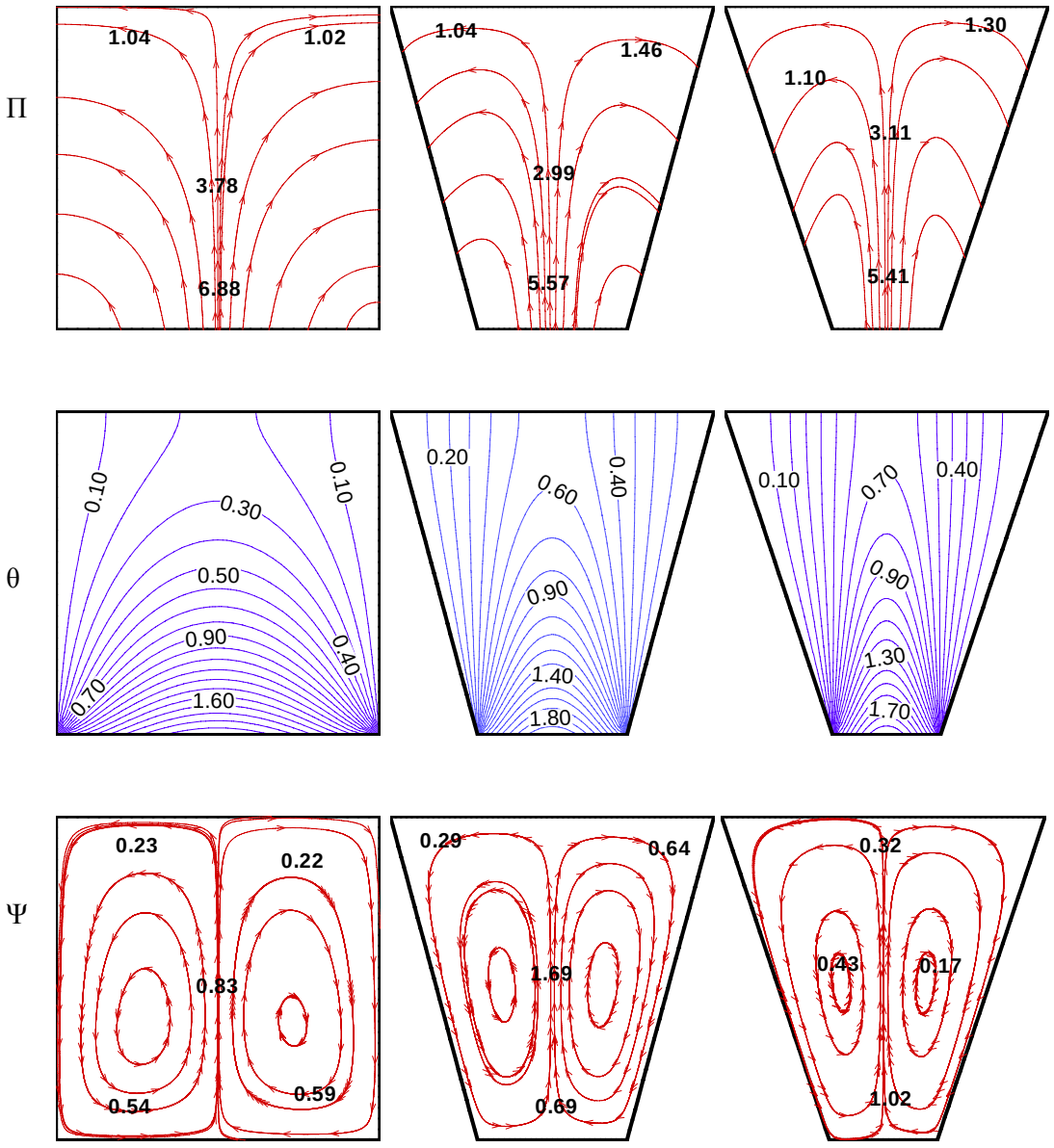

Figure 6.16: Stream function (Ψ), temperature (θ), heat function or total heat flux(Π) for non-uniform bottom heating θ(X,0) = sin(πx) with Pr = 1000, Ha = 50 and Ra = 10^3 (a) Φ = 0^o (b) Φ = 30^o (c) Φ = 45^o

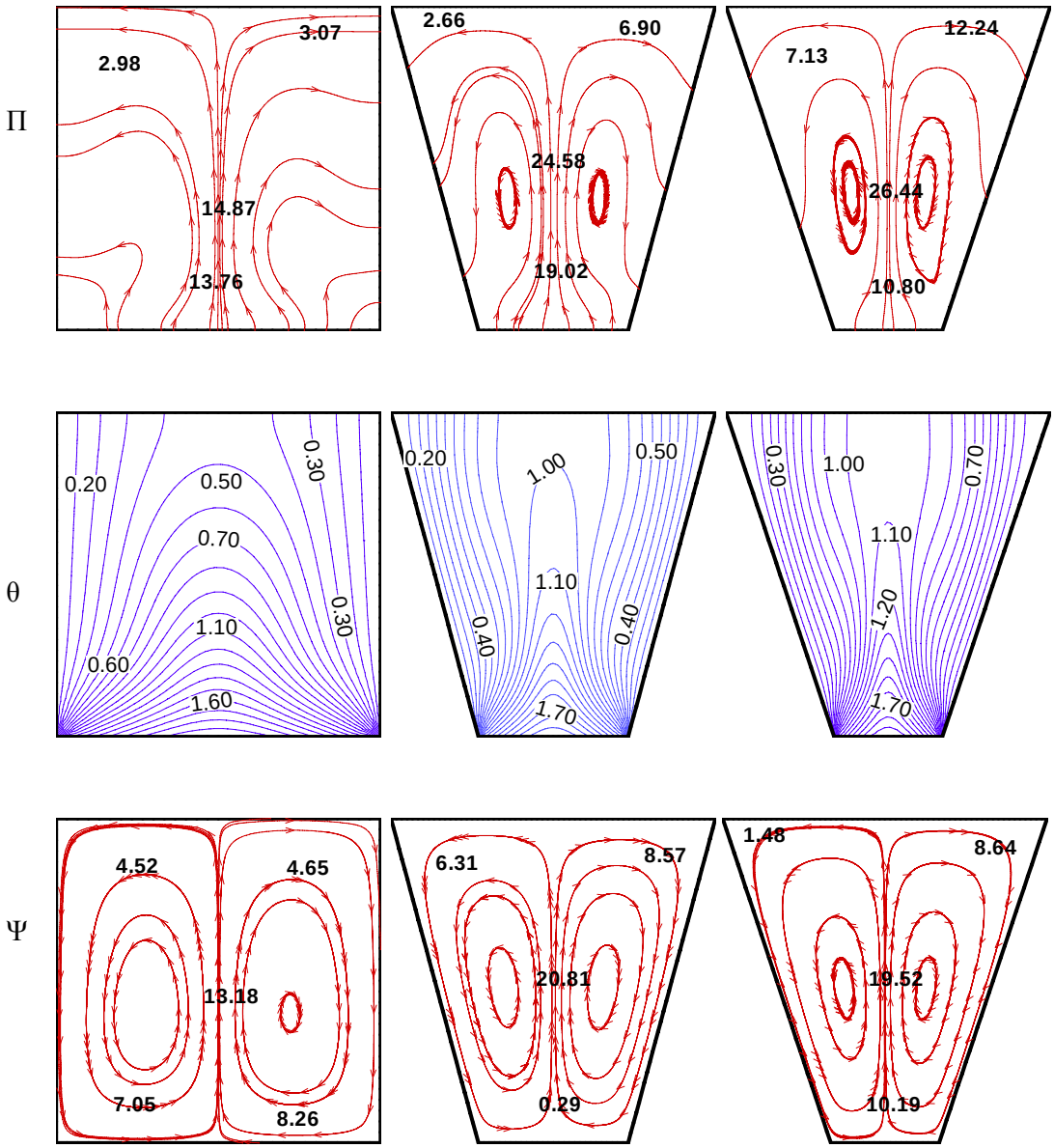

Figure 6.17: Stream function (Ψ), temperature (θ), heat function or total heat flux(Π) for non-uniform bottom heating θ(X,0) = sin(πx) with Pr = 1000, Ha = 50 and Ra = 10^4 (a) Φ = 0^o (b) Φ = 30^o (c) Φ = 45^o

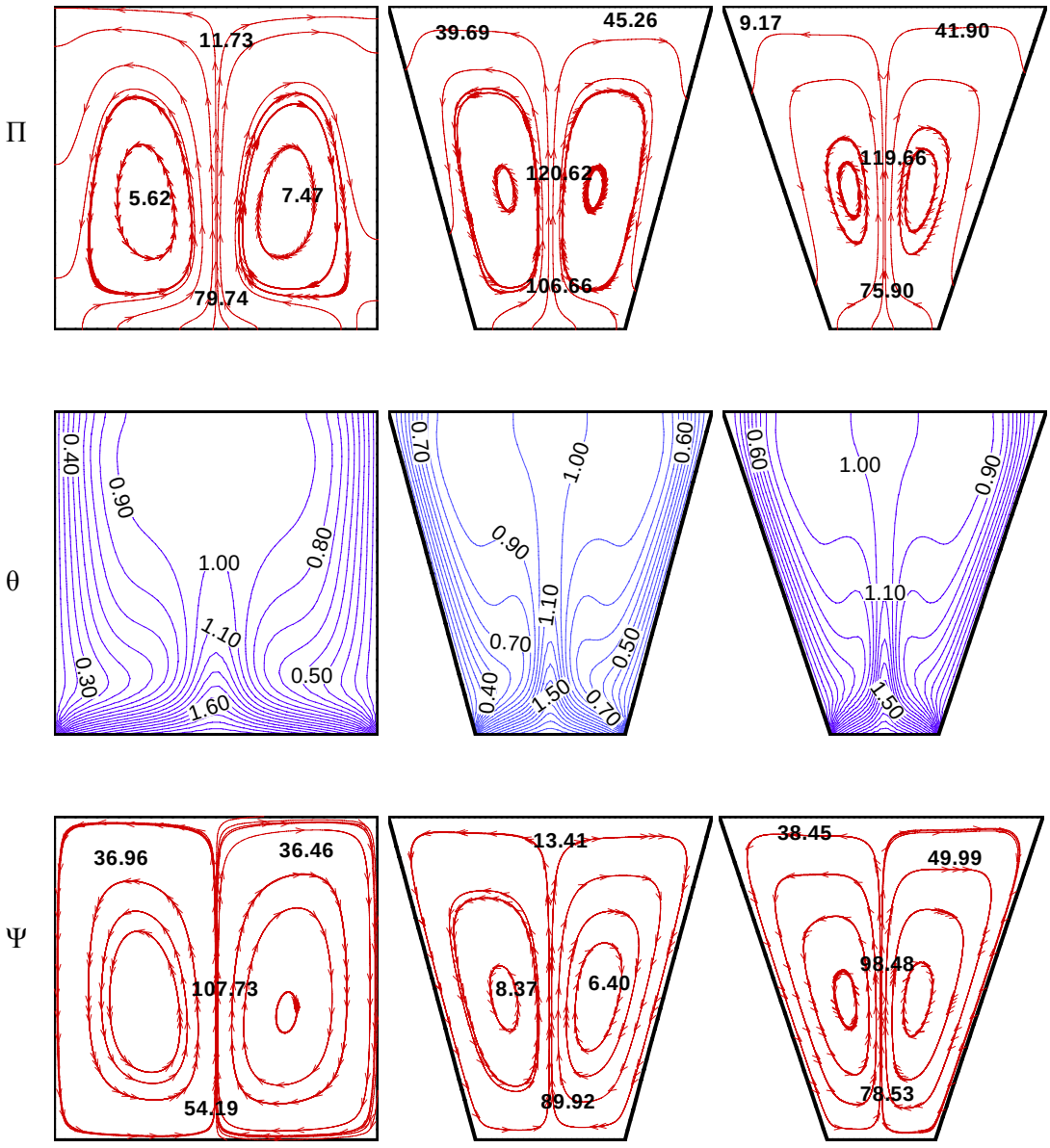

Figure 6.18: Stream function (Ψ), temperature (θ), heat function or total heat flux(Π) for non-uniform bottom heating θ(X,0) = sin(πx) with Pr = 1000, Ha = 50 and Ra = 10^5 (a) Φ = 0^o (b) Φ = 30^o (c) Φ = 45^o

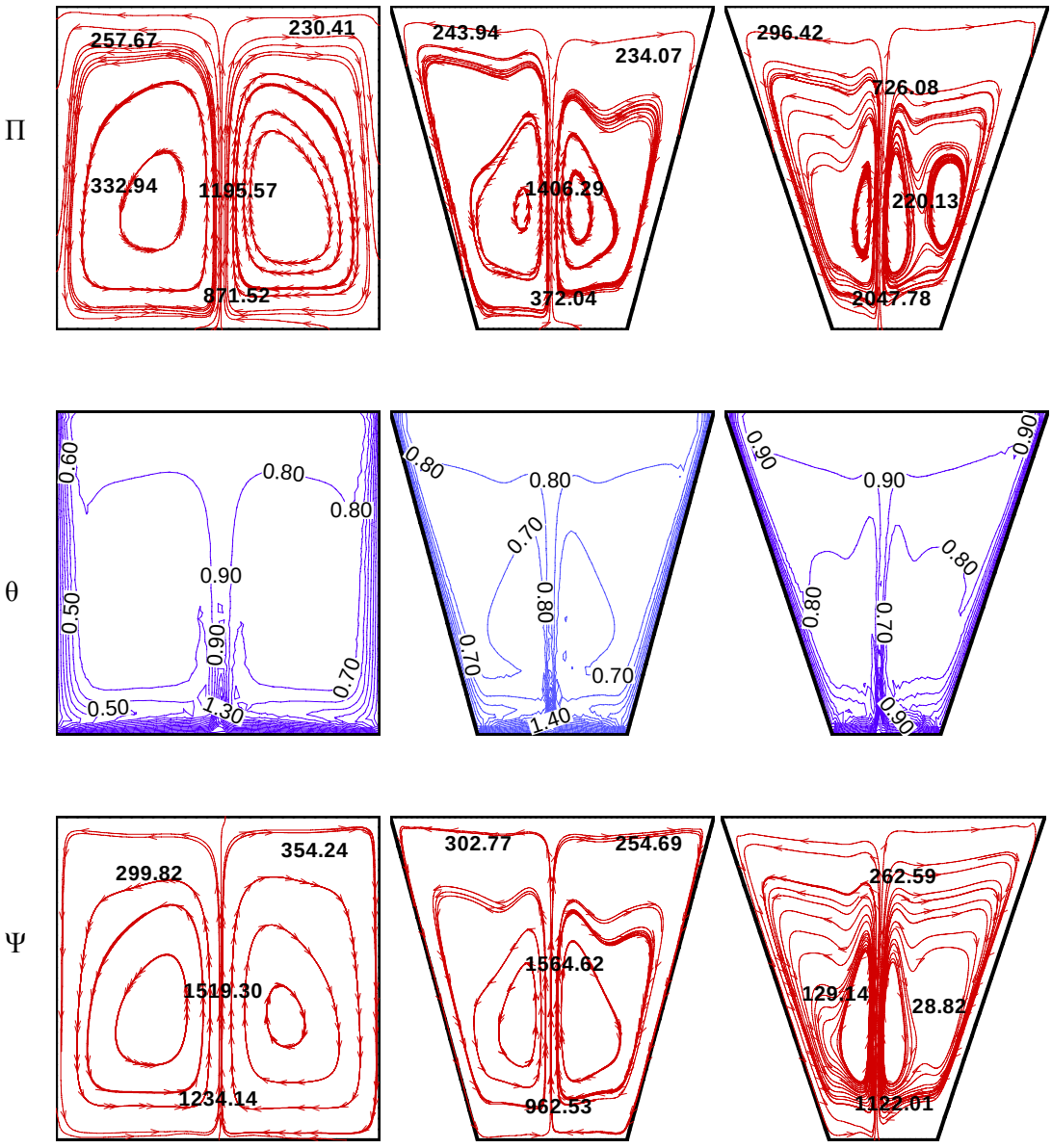

Figure 6.19: Stream function (Ψ), temperature (θ), heat function or total heat flux(Π) for non-uniform bottom heating θ(X,0) = sin(πx) with Pr = 1000, Ha = 50 and Ra = 10^7 (a) Φ = 0^o (b) Φ = 30^o (c) Φ = 45^o

6.4.2 Heat Transfer Rates: Local Nusselt Number vs distance for various Prandtl Number, Rayleigh Number and inclination angles in case of non-uniform heating

Figure 6.20 show the effects of local heat transfer rates (Nu_b) for various inclinations of angles i.e. for i) $\phi = 0^0$, ii) $\phi = 30^0$, iii) $\phi = 45^0$, for non-uniform of bottom wall with Pr = 0.026. Here the hat transfer rates are shown for $Ra = 10^3$. It is observed that heat transfer rate is maximum near edge of the wall and the rate is step down from left side and then it is straightly moving and then also it goes up to right side. The heat transfer rate is changing for the effect of Grashof number because Prandtl number is fixed. Here the heat transfer rates are almost same for $\phi = 30^0, 45^0$ except $\phi = 0^0$ [square cavity].Figure 6.21 and figure 6.22 also present similar effects of local Nusselt number with distance for various inclination tilt angles for Pr = 0.026 in case of non-uniform heating. But here the values of heat transfer rate increase a little and the heat transfer rates are shown for $Ra = 10^3, 10^4$.

Figure 6.23 detects the variation of local Nusselt number with distance for various inclination tilt angles i.e. i) $\phi = 0^0$,ii) $\phi = 30^0$, iii) $\phi = 45^0$,with Pr = 0.026 for non-uniform heating of bottom wall. Here heat transfer rates are discussed for $Ra = 10^7$. It is pragmatic that heat transfer rates is very high at corners and it reduce the heat transfer rates toward the middle of bottom wall as the comparison of temperature contours is minimum at the center of wall irrespective of ϕs with Pr = 0.026. Figure 6.24 explain the effects for various inclination angles when $Ra = 10^3$ and Pr = 0.7 in presence of non-uniform heating of bottom walls. Here it is seen that the value of heat transfer rates increases as Pr increases. It is also interesting to observe that the heat transfer rates (Nu_b) for $\phi = 30^0$, and $\phi = 45^0$ are almost alike except $\phi = 0^0$. It is also observed that thermal gradient is minimum at the center of bottom wall as seen from dispersed isotherm contours at the center of the wall for irrespective of ϕs.

Figure 6.25 – 6.27 epitomize that similar effects of various inclination angles $\phi = 45^0, 30^0, 0^0$ for $Ra = 10^4, 10^5, 10^7$ with Pr = 0.7 in presence of non-uniform bottom heating. Here we also see that, the heat transfer rate of left wall is very high at the top edge of left wall is very high and heat transfer rate is almost not uniform near the bottom edge of hot vertical wall. As Ra increases then the magnitudes of heat transfer rates increases. It is seen that the thermal gradient is minimum at the center of bottom wall for dispersed isothermal

contour for irrespective of ϕ. The larger heat transfer rate for $\phi = 0^0$ occurs due to highly compressed isotherms as seen figure 6.12a-c to figure 6.15a-c. Here it is also seen that the heat transfer rates for $\phi = 30^0$ and 45^0 are almost same except $\phi = 0^0$. But at larger Ra = 10^7 it is experiential that the oscillation of local heat transfer rates occur due to presence of secondary circulations which result of isotherm contours at various places of bottom wall of non-uniform heating.

Fig 6.28 – 6.31 illustrate that local heat transfer rate (Nu_b) vs distance for various inclination tilt angles i.e. for i) $\phi = 0^0$,ii) $\phi = 30^0$, iii) $\phi = 45^0$ when Pr = 1000 and for different Rayleigh numbers in presence of non-uniform heating of bottom wall. From figure 6.28, it is seen that heat transfer rates (Nu_b) are almost identical for $\phi = 30^0$, 45^0whereas $\phi = 0^0$ are larger. The larger heat transfer rates (Nu_b) are compressed due to strong circulations. The similar effects is shown in figure 6.29 – 6.31.But it is clear that when Ra increases then the magnitudes of local heat transfer rates (Nu_b) increases. As Ra increases then the strength of circulations is increased and consequently isotherm lines are compressed towards the hot wall. Hence the gradient increases near the wall. It is also seen the heat transfer rate is maximum near the edge of side wall and minimum near the center of bottom wall (See figure 6.28 – 6.31).

Figure 6.32 indicate local heat transfer rates vs distance for different Rayleigh numbers i.e. for Ra = 10^3 - 10^7 when Pr = 0.026 and $\phi = 0^0$ (square cavity).Here it is demonstrate that heat transfer rates are almost same for Ra = 10^3 – 10^5 except Ra =10^7. When Ra = 10^7 the local heat transfer rates (Nu_b) is larger and isotherms are distributed throughout the domain except near the center of bottom wall. Figure 6.33 – 6.34 show the similar effects of local heat transfer rates (Nu_b) for different Rayleigh numbers with $\phi = 0^0$ and Pr = 0.7, 1000 respectively. Here it is shown that when Pr increases from 0.026 to 0.7 (see figure 6.33) then the magnitudes of heat transfer rates (Nu_b) increases. It is also happen when Pr increase to 1000 (see figure 6.34). At higher Pr (Pr = 0.7 - 1000) the isotherms near the center of bottom wall are highly compressed due to strong circulations.

Figure 6.35 – 6.37 represents the same effects of local heat transfer rates vs distance for different Ra with $\phi = 30^0$ and Pr = 0.026 – 1000 respectively. Here we see that hat transfer rate are almost same (figure 6.35) for Ra = 10^3 – 10^5 and is more large for Ra = 10^7 when Pr = 0.026. When Pr increases (see figure 6.36 and 6.37) then the magnitudes of local heat transfer rates is also increased.

Figure 6.38 – 6.40 exemplify that the effects of local heat transfer rates for various Ra when $\phi = 45^0$ and Pr = 0.026 – 1000 is considered. Figure 6.38 display that the effects of local heat transfer rates (Nu_b) are identical for Ra = 10^3 and $10^4$with Pr = 0.026. As Ra increases then the heat transfer rates increases. When Pr [Pr = 0.7] increases (figure 6.39) then it is seen that the magnitudes of heat transfer rates increases. Here we also see that local Nusselt numbers have wavy distribution for Pr = 0.7. This is due to strong primary circulations. When Pr also increases (Pr = 1000 and see figure 6.40) then it is shown that the heat transfer rates are not almost identical for different Ra. As Ra increases then the strength of circulations is increased and local heat transfer rate (Nu_b) is also larger. Here also we see that local Nusselt numbers have also more wavy distributions (figure 6.40) for Pr = 1000. It is interesting to note that local Nusselt number has a high value for Pr = 1000 due to large temperature gradient resulting increased intensity of circulations for non-uniform hating case of bottom wall.

Figure 6.41 – 6.44 also show the effect of local heat transfer rates (Nu_s) vs distance for various inclination tilt angles i.e. for $\phi = 0^0$, 30^0, 45^0 when Ra = 10^3 and Pr = 0.026 for non-uniform heating of side wall. It is observed that local heat transfer rate is maximum at the bottom edge of side wall and thereafter decreases sharply upto a point which is very near to the bottom edge(see figure 6.41). It is seen that Nu_s increase upto a point near to the top wall and also decreases with distance near to the bottom wall. The boundary layer starts to form at the bottom edge of the side wall and the boundary layer thickness is quite large near the bottom wall for all ϕs. Due to large intensity of convection at Ra = 10^3 the thickness of the boundary layers are small at the middle portions of side walls and is found to be larger near the top portion. But also figure 6.42-6.43 shows the similar effects of local heat transfer rates (Nu_s) with distance for same Pr and different Ra respectively. As Ra increases then the magnitudes of local heat transfer rates become smaller and maximum heat transfer occur near the top portion. It is also seen from figure 6.44 that the magnitude of heat transfer rate becomes quite smaller due to dominant heat conduction mode.

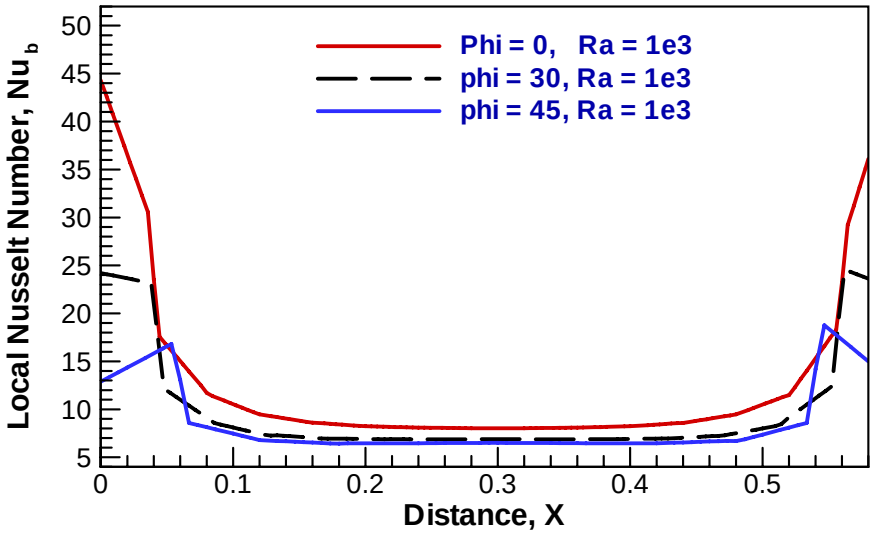

Figure 6.20: Variations of local Nusselt numbers (Nu_b) with distance for Pr = 0.026, Ra = 10^3 and for various inclination of angles (a) $\Phi = 0^o$ (b) $\Phi = 30^o$ (c) $\Phi = 45^o$ in presence of non-uniform heating of bottom walls.

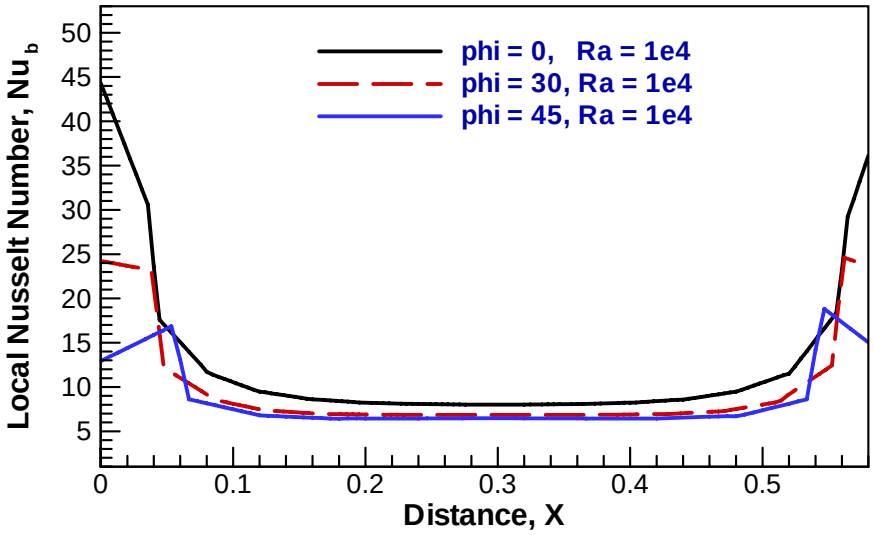

Figure 6.21: Variations of local Nusselt numbers (Nu_b) with distance for Pr = 0.026, Ra = 10^4 and for various inclination of angles (a) $\Phi = 0^o$ (b) $\Phi = 30^o$ (c) $\Phi = 45^o$ in presence of non-uniform heating of bottom walls.

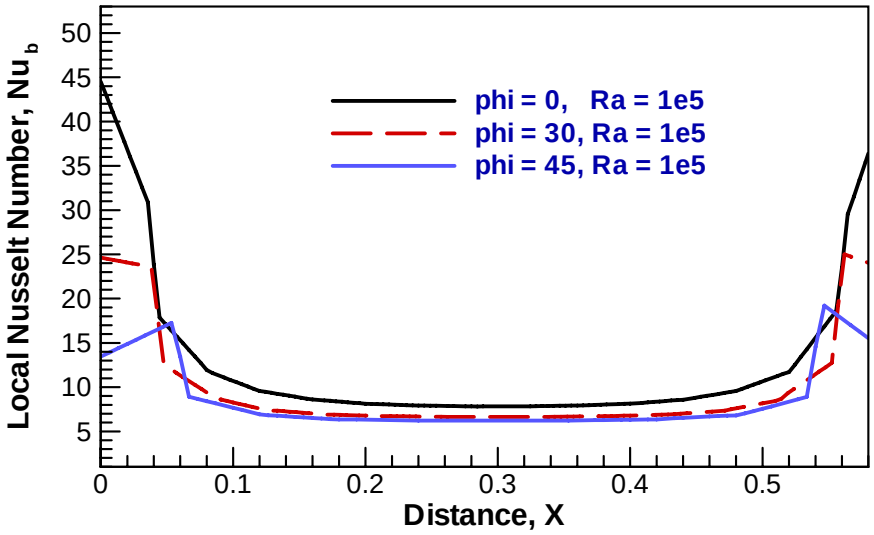

Figure 6.22: Variations of local Nusselt numbers (Nu_b) with distance for Pr = 0.026, Ra = 10^5 and for various inclination of angles (a) $\Phi = 0^o$ (b) $\Phi = 30^o$ (c) $\Phi = 45^o$ in presence of non-uniform heating of bottom walls.

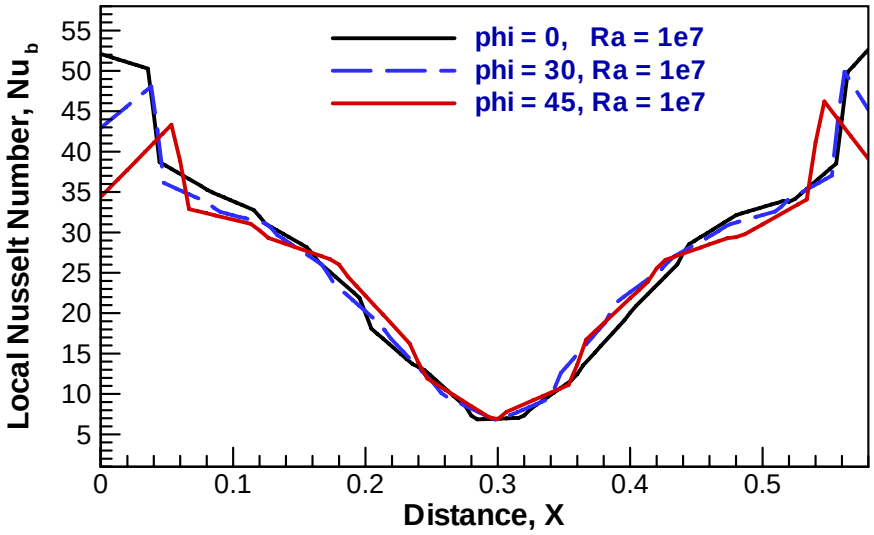

Figure 6.23: Variations of local Nusselt numbers (Nu_b) with distance for Pr = 0.026, Ra = 10^7 and for various inclination of angles (a) $\Phi = 0^o$ (b) $\Phi = 30^o$ (c) $\Phi = 45^o$ in presence of non-uniform heating of bottom walls.

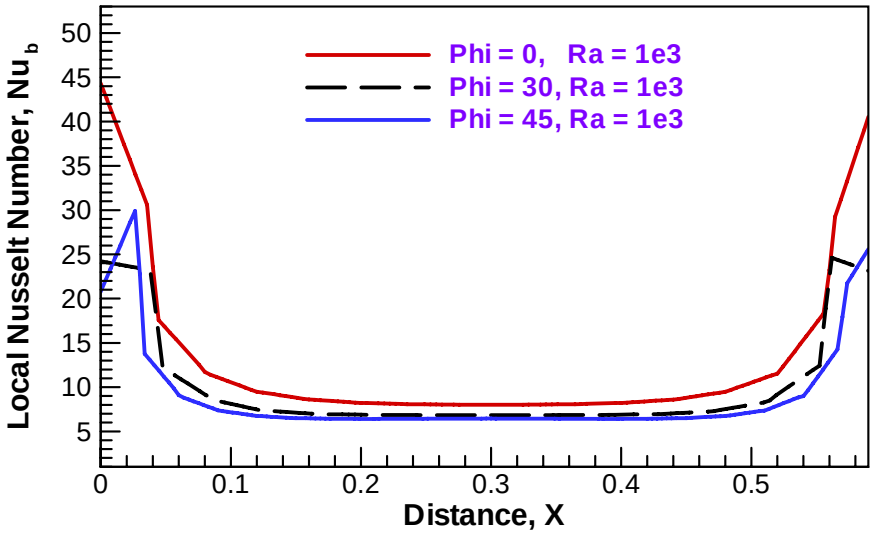

Figure 6.24: Variations of local Nusselt numbers (Nu_b) with distance for Pr = 0.7, Ra = 10^3 and for various inclination of angles (a) $\Phi = 0^o$ (b) $\Phi = 30^o$ (c) $\Phi = 45^o$ in presence of non-uniform heating of bottom walls.

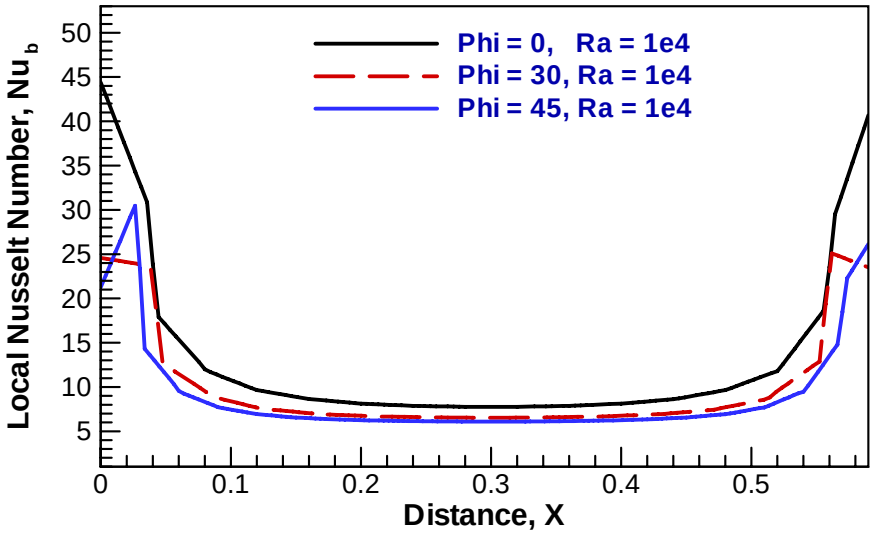

Figure 6.25: Variations of local Nusselt numbers (Nu_b) with distance for Pr = 0.7, Ra = 10^4 and for various inclination of angles (a) $\Phi = 0^o$ (b) $\Phi = 30^o$ (c) $\Phi = 45^o$ in presence of non-uniform heating of bottom walls.

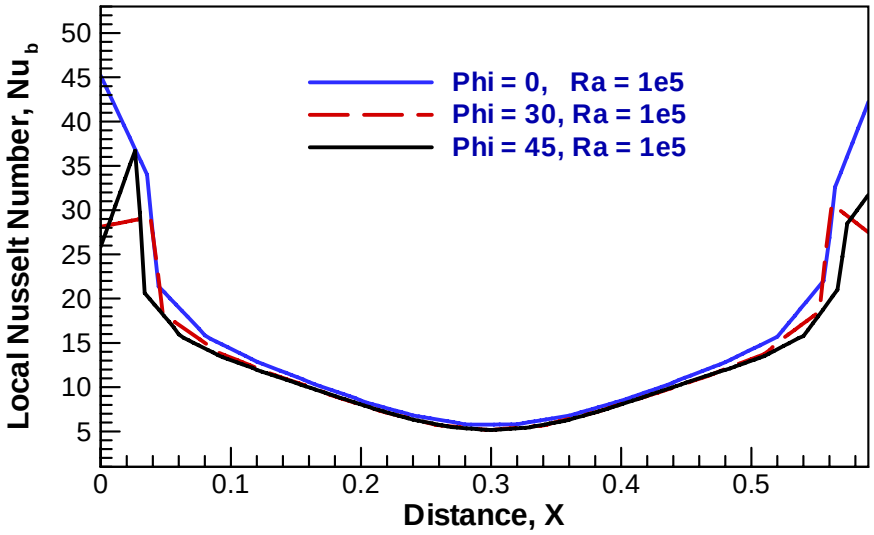

Figure 6.26: Variations of local Nusselt numbers (Nu_b) with distance for Pr = 0.7, Ra = 10^5 and for various inclination of angles (a) $\Phi = 0^o$ (b) $\Phi = 30^o$ (c) $\Phi = 45^o$ in presence of non-uniform heating of bottom walls.

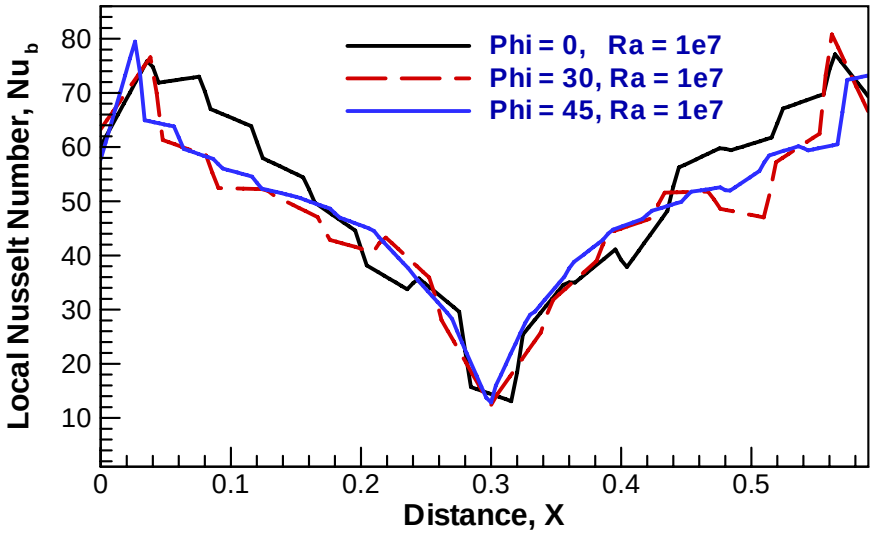

Figure 6.27: Variations of local Nusselt numbers (Nu_b) with distance for Pr = 0.7, Ra = 10^7 and for various inclination of angles (a) $\Phi = 0^o$ (b) $\Phi = 30^o$ (c) $\Phi = 45^o$ in presence of non-uniform heating of bottom walls.

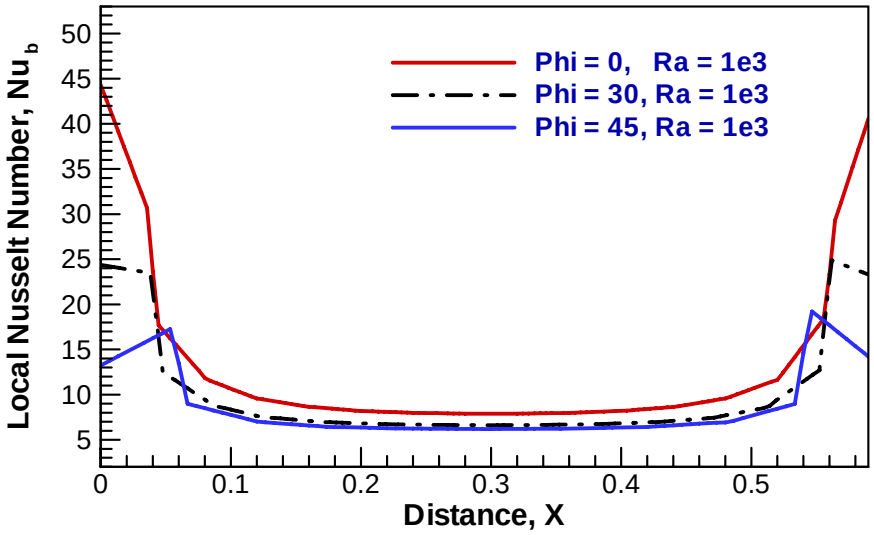

Figure 6.28: Variations of local Nusselt numbers (Nu_b) with distance for Pr = 1000, Ra = 10^3 and for various inclination of angles (a) $\Phi = 0^o$ (b) $\Phi = 30^o$ (c) $\Phi = 45^o$ in presence of non-uniform heating of bottom walls.

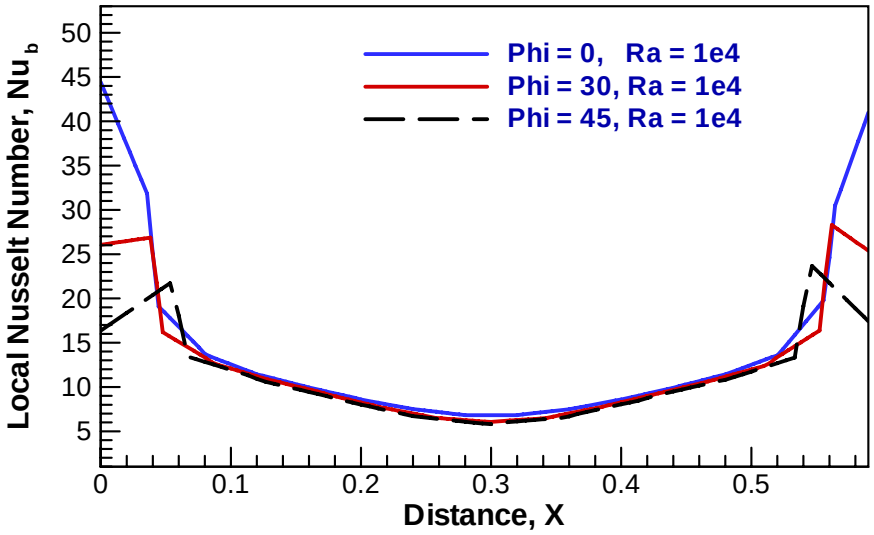

Figure 6.29: Variations of local Nusselt numbers (Nu_b) with distance for Pr = 1000, Ra = 10^4 and for various inclination of angles (a) $\Phi = 0^o$ (b) $\Phi = 30^o$ (c) $\Phi = 45^o$ in presence of non-uniform heating of bottom walls.

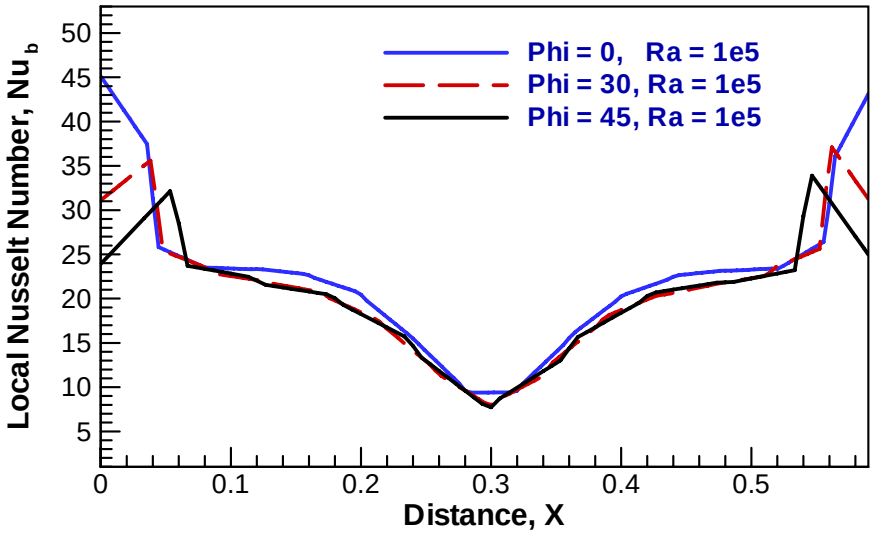

Figure 6.30: Variations of local Nusselt numbers (Nu_b) with distance for Pr = 1000, Ra = 10^5 and for various inclination of angles (a) $\Phi = 0^o$ (b) $\Phi = 30^o$ (c) $\Phi = 45^o$ in presence of non-uniform heating of bottom walls.

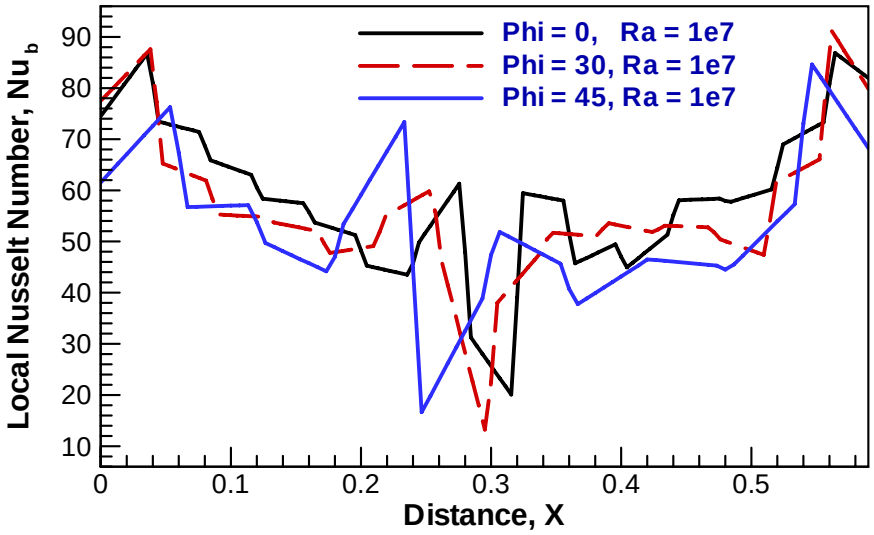

Figure 6.31: Variations of local Nusselt numbers (Nu_b) with distance for Pr = 1000, Ra = 10^7 and for various inclination of angles (a) $\Phi = 0^o$ (b) $\Phi = 30^o$ (c) $\Phi = 45^o$ in presence of non-uniform heating of bottom walls.

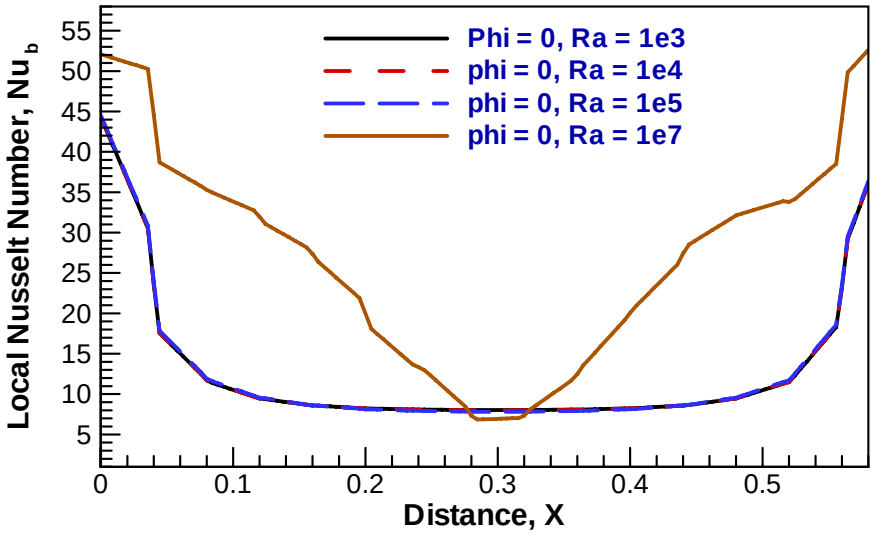

Figure 6.32: Variations of local Nusselt numbers (Nu_b) with distance for Pr = 0.026, $\Phi = 0^o$ and for various Rayleigh numbers (a) Ra = 10^3 (b) Ra = 10^4 (c) Ra = 10^5 (d) Ra = 10^7 in presence of non-uniform heating of bottom walls.

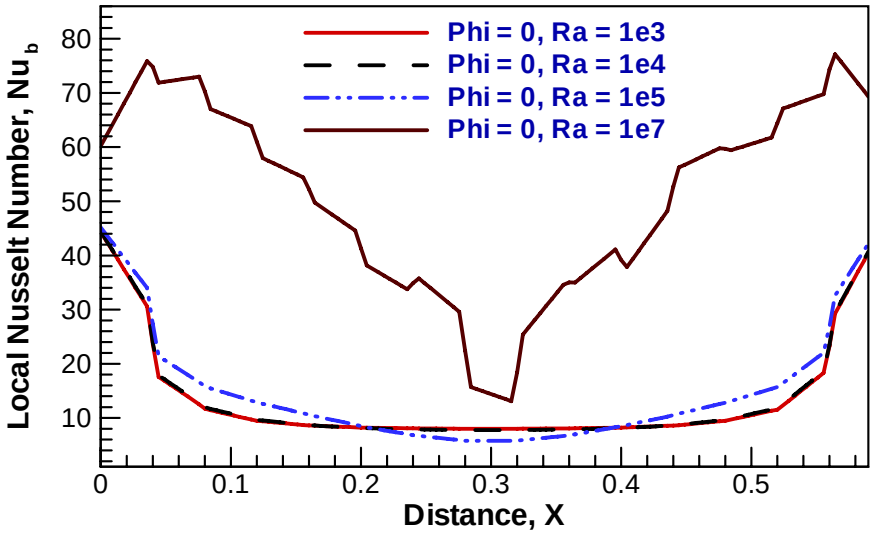

Figure 6.33: Variations of local Nusselt numbers (Nu_b) with distance for Pr = 0.7, $\Phi = 0^o$ and for various Rayleigh numbers (a) Ra = 10^3 (b) Ra = 10^4 (c) Ra = 10^5 (d) Ra = 10^7 in presence of non-uniform heating of bottom walls.

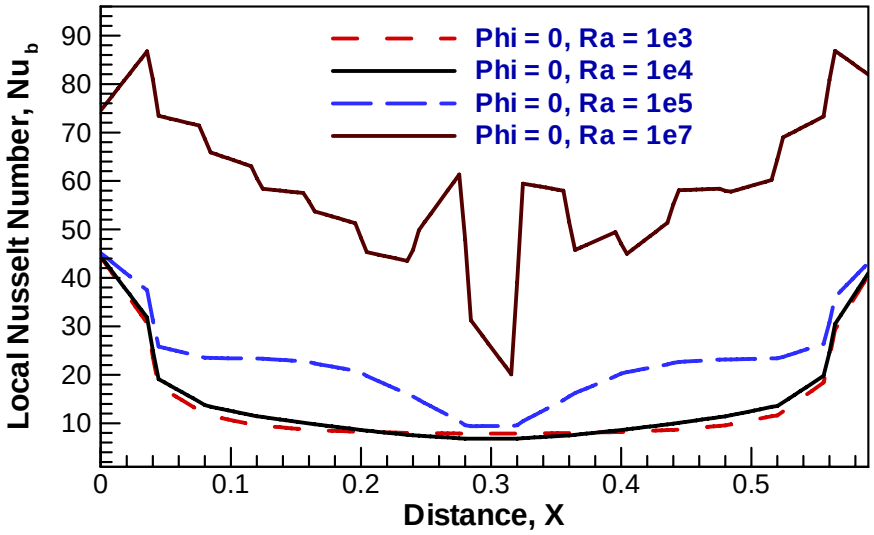

Figure 6.34: Variations of local Nusselt numbers (Nu_b) with distance for Pr = 1000, $\Phi = 0^o$ and for various Rayleigh numbers (a) Ra = 10^3 (b) Ra = 10^4 (c) Ra = 10^5 (d) Ra = 10^7 in presence of non-uniform heating of bottom walls.

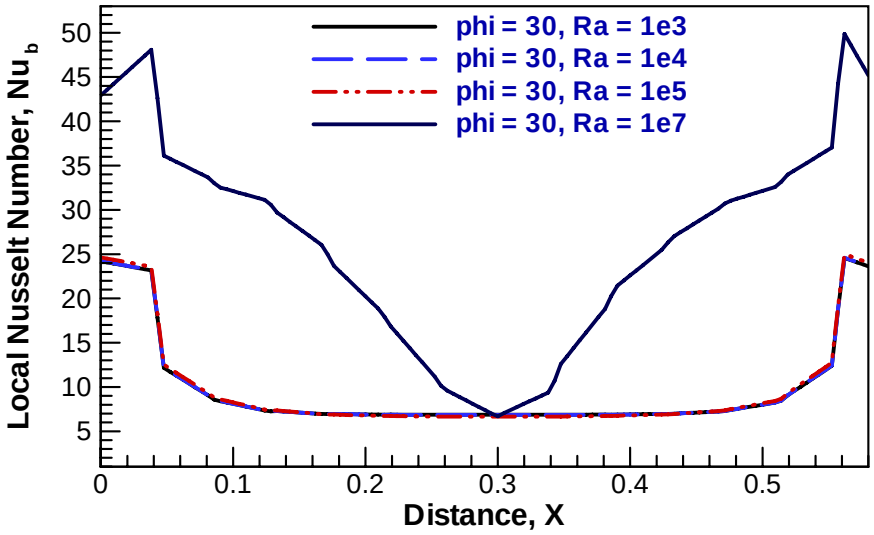

Figure 6.35: Variations of local Nusselt numbers (Nu_b) with distance for Pr = 0.026, $\Phi = 30^o$ and for various Rayleigh numbers (a) Ra = 10^3 (b) Ra = 10^4 (c) Ra = 10^5 (d) Ra = 10^7 in presence of non-uniform heating of bottom walls.

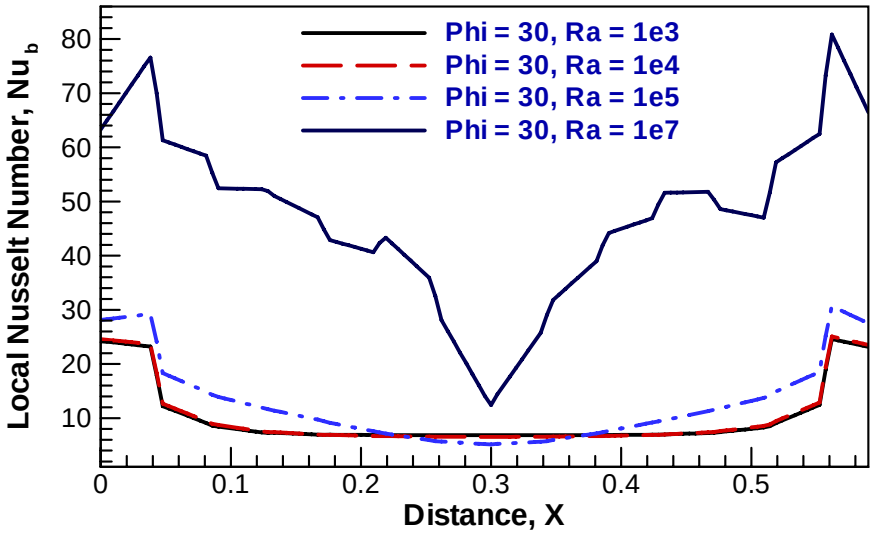

Figure 6.36: Variations of local Nusselt numbers (Nu_b) with distance for Pr = 0.7, Φ = 30° and for various Rayleigh numbers (a) Ra = 10^3 (b) Ra = 10^4 (c) Ra = 10^5 (d) Ra = 10^7 in presence of non-uniform heating of bottom walls.

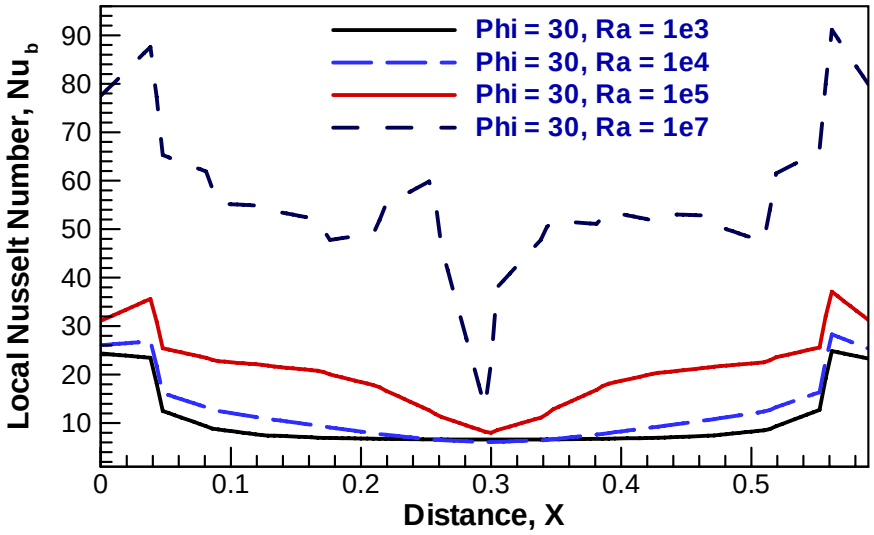

Figure 6.37: Variations of local Nusselt numbers (Nu_b) with distance for Pr = 1000, Φ = 30° and for various Rayleigh numbers (a) Ra = 10^3 (b) Ra = 10^4 (c) Ra = 10^5 (d) Ra = 10^7 in presence of non-uniform heating of bottom walls.

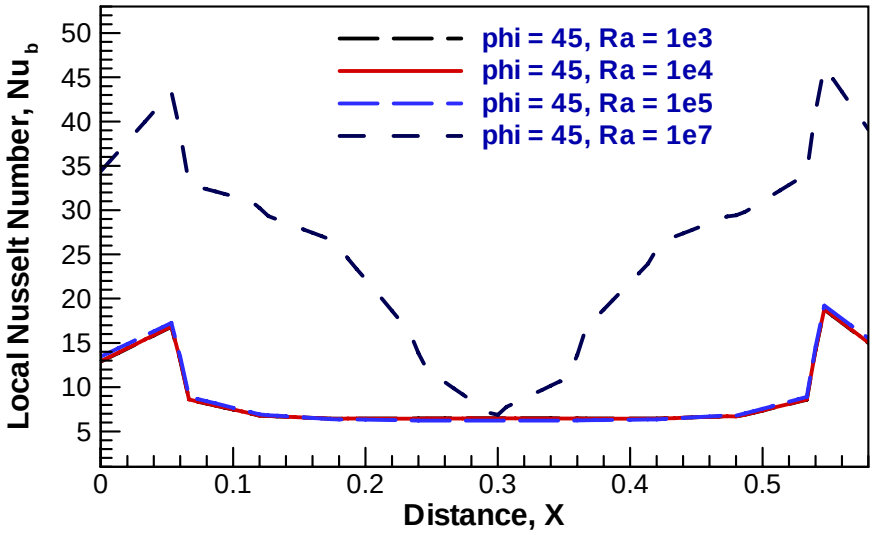

Figure 6.38: Variations of local Nusselt numbers (Nu_b) with distance for Pr = 0.026, Φ = 45° and for various Rayleigh numbers (a) Ra = 10^3 (b) Ra = 10^4 (c) Ra = 10^5 (d) Ra = 10^7 in presence of non-uniform heating of bottom walls.

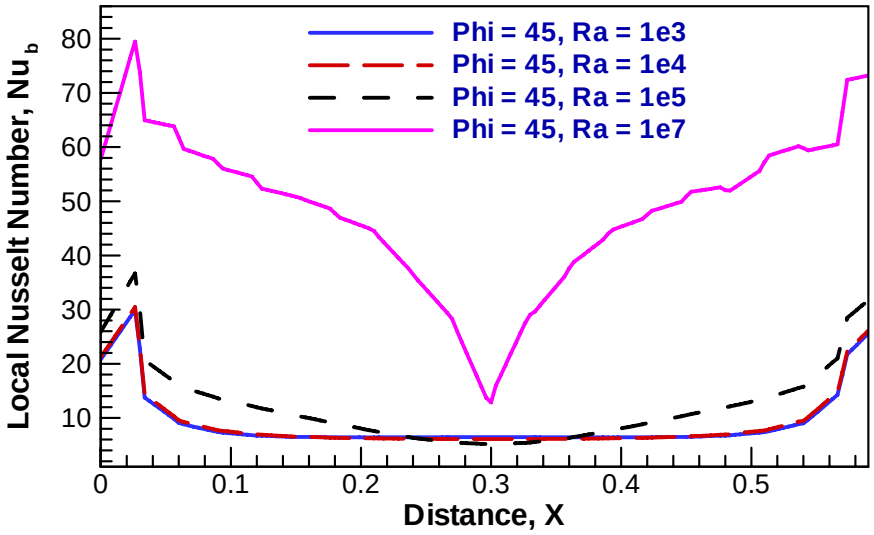

Figure 6.39: Variations of local Nusselt numbers (Nu_b) with distance for Pr = 0.7, Φ = 45° and for various Rayleigh numbers (a) Ra = 10^3 (b) Ra = 10^4 (c) Ra = 10^5 (d) Ra = 10^7 in presence of non-uniform heating of bottom walls.

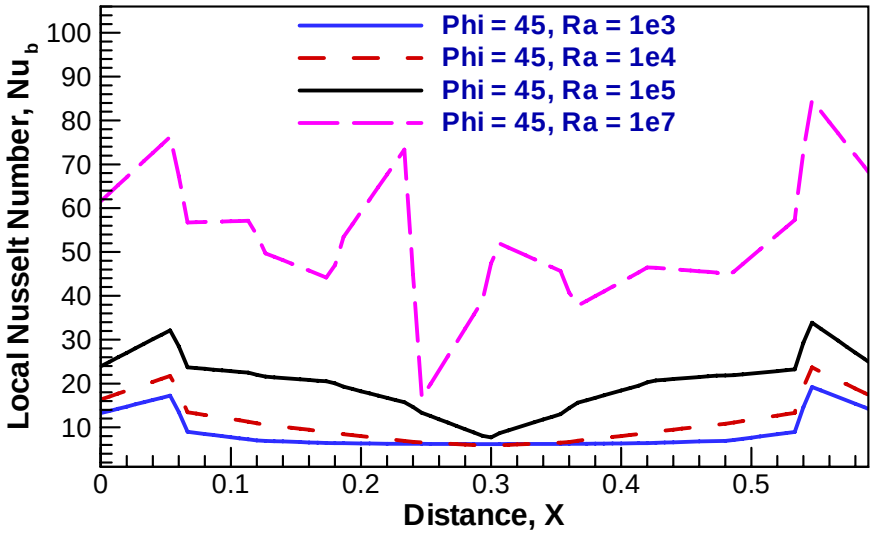

Figure 6.40: Variations of local Nusselt numbers (Nu_b) with distance for Pr = 1000, $\Phi = 45^o$ and for various Rayleigh numbers (a) Ra = 10^3 (b) Ra = 10^4 (c) Ra = 10^5 (d) Ra = 10^7 in presence of non-uniform heating of bottom walls.

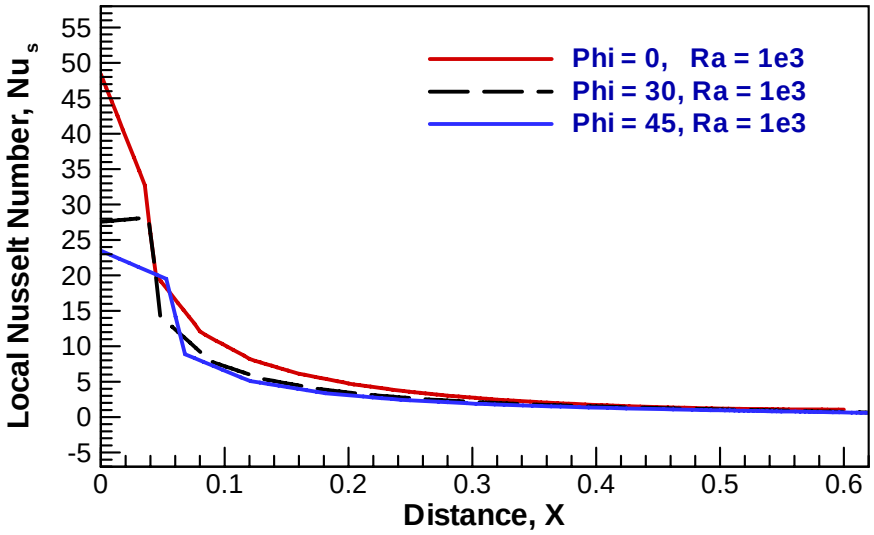

Figure 6.41: Variations of local Nusselt numbers (Nu_s) with distance for Pr = 0.026, Ra = 10^3 and for various inclination of angles (a) $\Phi = 0^o$ (b) $\Phi = 30^o$ (c) $\Phi = 45^o$ in presence of non-uniform heating of side walls.

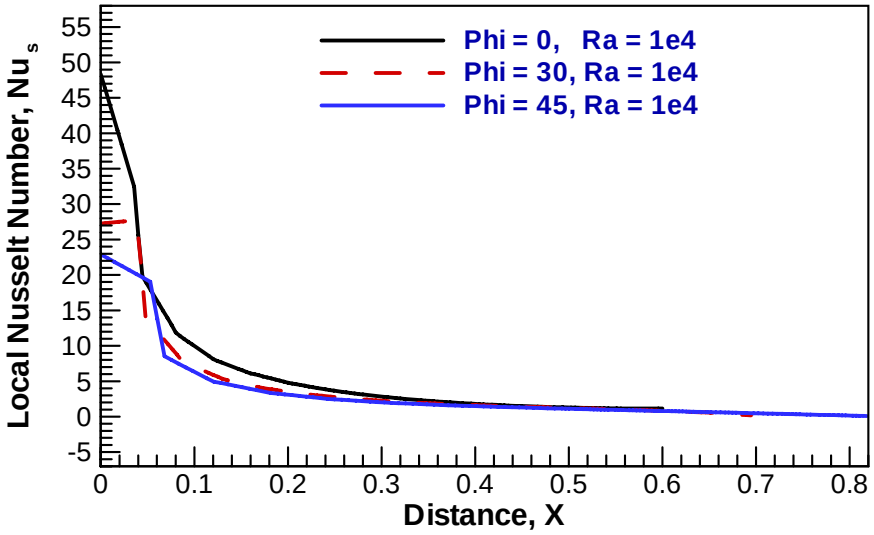

Figure 6.42: Variations of local Nusselt numbers (Nu_s) with distance for Pr = 0.026, Ra = 10^4 and for various inclination of angles (a) $\Phi = 0^o$ (b) $\Phi = 30^o$ (c) $\Phi = 45^o$ in presence of non-uniform heating of side walls.

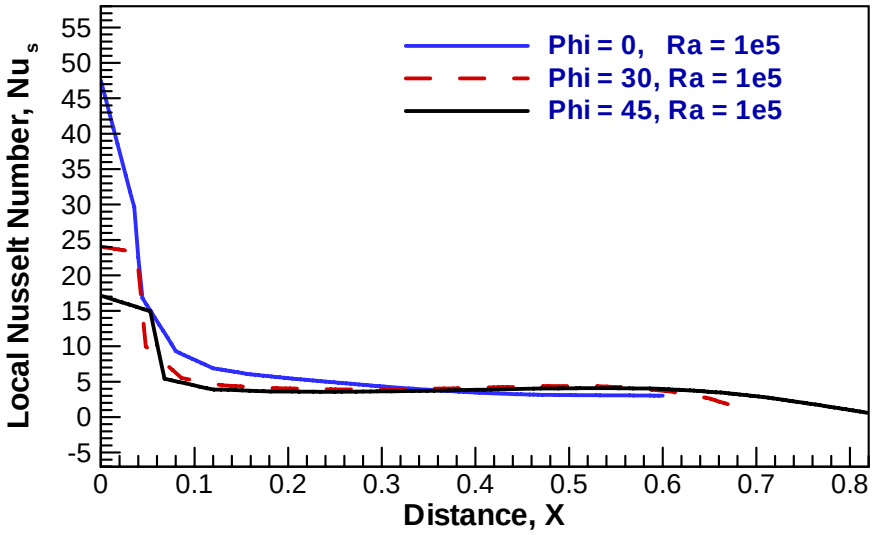

Figure 6.43: Variations of local Nusselt numbers (Nu_s) with distance for Pr = 0.026, Ra = 10^5 and for various inclination of angles (a) $\Phi = 0^o$ (b) $\Phi = 30^o$ (c) $\Phi = 45^o$ in presence of non-uniform heating of side walls.

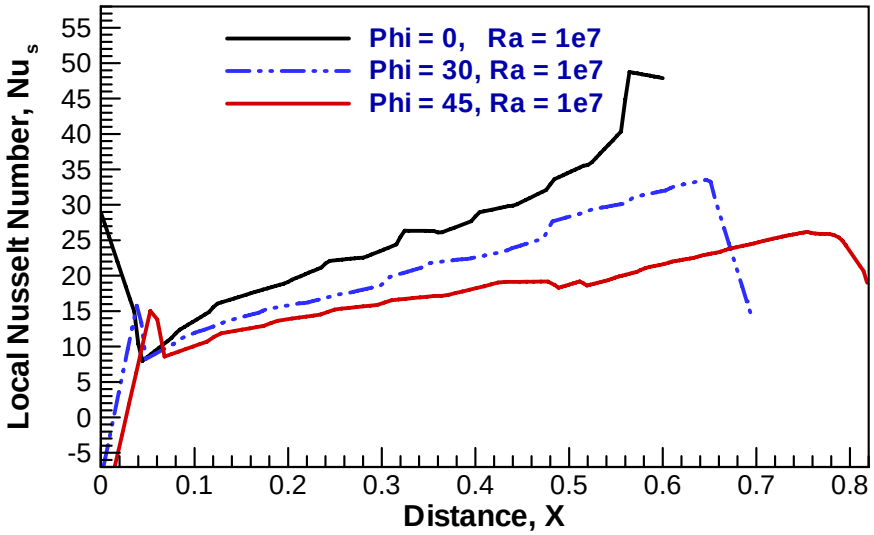

Figure 6.44: Variations of local Nusselt numbers (Nu_s) with distance for Pr = 0.026, Ra = 10^7 and for various inclination of angles (a) $\Phi = 0^o$ (b) $\Phi = 30^o$ (c) $\Phi = 45^o$ in presence of non-uniform heating of bottom walls.

6.4.3 Heat Transfer Rates: Average Nusselt Number vs Rayleigh Number for different Prandtl Number, and inclination angles in case of non-uniform heating

The effects upon the heat transfer rates are presented in figure 6.45 – 6.47 and 6.48 – 6.50, where distributions of average Nusselt number of bottom and side wall respectively are plotted vs the logarithmic Rayleigh number. Here figure 6.45 – 6.47 and figure 6.48 – 6.50 illustrate non-uniform heating of bottom wall and side wall respectively. It may be noted that average Nusselt number is obtained by considering temperature gradient. It also be noted that as Ra increases then the average Nusselt number increases. It is seen in figure 6.45 that as Ra increases from 10^3-10^6 then average Nusselt number is straightly moving but as Ra increases more, then average Nusselt number is increasing for Pr = 0.026. As Pr increases (figure 6.46) then conduction dominant heat transfer is narrowed down. It also seen from figure 6.47 that, as Pr increases more than from non-uniform heating case it is analyzed that average Nusselt number for bottom wall remain constant during the entire Rayleigh number regime. This illustrates that the conduction dominant heat transfer for different Prandtl number regime irrespective of Ra. As Pr increases then for conduction dominant heat transfer, the average Nusselt number is generally constant irrespective of Ra. It is observed that Nub at the middle portion of bottom wall for $\Phi = 0^o$ is larges for

non-uniform heating case whereas for $\Phi = 30^o$ and 45^o heat transfer rates are identical. It is also seen that Nu_s is largest near the bottom corner of side walls for $\Phi = 0^o$. At larges Pr (Pr= 1000) of non-uniform bottom heating it is seen that as Ra increase from 10^3 to 10^6, then average heat transfer rates (Nu_b) increases. After crossing $Ra = 10^6$ then it is also seen average heat transfer rates are decreasing. After that when Ra goes to 10^7 then average heat transfer rate is also increasing because of highly viscous of Pr. Figure 6.48 – 6.50 show the similar effects of average Nusselt number with non-uniform heating of side walls. Here it is interesting to note that the heat transfer rates (Nu_{av}) of side wall is less than non-uniform heating of bottom wall and it effects only for highly viscous of Prandtl number. Also magnitudes of average Nusselt number of non-uniform heating is less than uniform heating because of less heating effects. Besides this, the average Nusselt number with Rayleigh number are also shown in table (6.4 – 6.6) and table (6.7 – 6.9) for non-uniform heating of bottom wall and side walls respectively.

Ra	Average Nusselt Number, (Nu_{av})		
	$\phi = 0^0$	$\phi = 30^0$	$\phi = 45^0$
10^3	4.361202	3.505918	3.156808
10^4	4.36162	3.506366	3.157198
10^5	4.365935	3.511142	3.161605
10^6	4.42462	3.594347	3.267077
10^7	6.607187	6.452412	6.467831

Table 6.4: Average Nusselt Number vs Rayleigh number for non-uniform heating of bottom wall with Pr = 0.026

Ra	Average Nusselt Number, (Nu_{av})		
	$\phi = 0^0$	$\phi = 30^0$	$\phi = 45^0$
10^3	4.361568	3.506399	3.157268
10^4	4.365658	3.51229	3.163712
10^5	4.464063	3.729079	3.474017
10^6	7.399533	7.046409	6.97625
10^7	13.37451	12.753801	11.54703

Table 6.5: Average Nusselt Number vs Rayleigh number for non-uniform heating of bottom wall with Pr = 0.7

Ra	Average Nusselt Number, (Nu_{av})		
	$\phi = 0^0$	$\phi = 30^0$	$\phi = 45^0$
10^3	4.362899	3.510216	3.162099
10^4	4.408609	3.720888	3.438032
10^5	6.128158	5.68537	5.47684
10^6	9.797762	9.409716	9.372445
10^7	15.887965	15.346189	14.772105

Table 6.6: Average Nusselt Number vs Rayleigh number for non-uniform heating of bottom wall with Pr = 1000

Ra	Average Nusselt Number, (Nu_{av})		
	$\phi = 0^0$	$\phi = 30^0$	$\phi = 45^0$
10^3	2.106961	1.639905	1.441976
10^4	2.107064	1.640082	1.442203
10^5	2.108158	1.641997	1.444725
10^6	2.126783	1.678744	1.500528
10^7	3.160948	3.096726	3.144749

Table 6.7: Average Nusselt Number vs Rayleigh number for non-uniform heating of side wall with Pr = 0.026

Ra	Average Nusselt Number, (Nu_{av})		
	$\phi = 0^0$	$\phi = 30^0$	$\phi = 45^0$
10^3	2.10711	1.640168	1.442333
10^4	2.10876	1.643219	1.446786
10^5	2.154179	1.755563	1.618798
10^6	3.615316	3.418606	3.3888467
10^7	6.597279	6.32338	5.729601

Table 6.8: Average Nusselt Number vs Rayleigh number for non-uniform heating of side wall with Pr = 0.7

Ra	Average Nusselt Number, (Nu_{av})		
	$\phi = 0^0$	$\phi = 30^0$	$\phi = 45^0$
10^3	2.107811	1.642566	1.446052
10^4	2.131016	1.756123	1.602623
10^5	2.99983	2.749447	2.638332
10^6	4.807219	4.553474	4.531588
10^7	7.94031	7.857242	8.291167

Table 6.9: Average Nusselt Number vs Rayleigh number for non-uniform heating of side wall with Pr = 1000

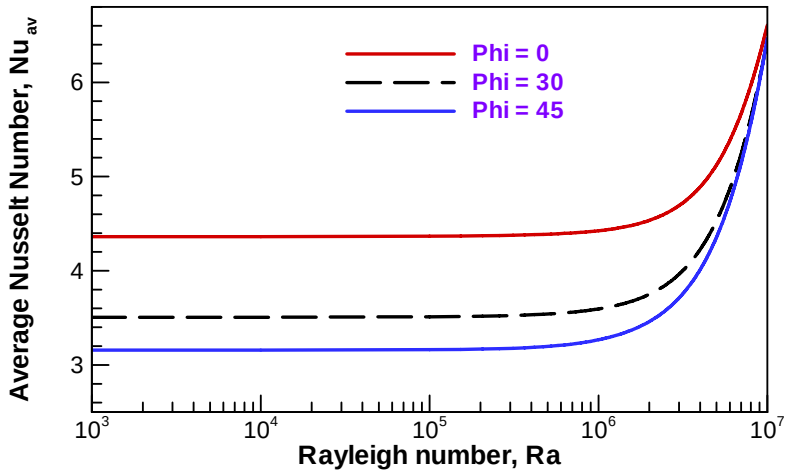

Figure 6.45: Average Nusselt Number vs Rayleigh number for non-uniform heating of bottom wall with Pr = 0.026

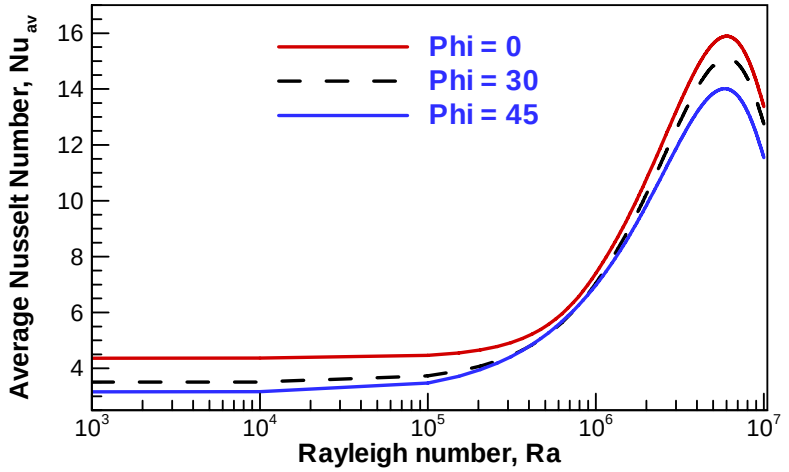

Figure 6.46: Average Nusselt Number vs Rayleigh number for non-uniform heating of bottom wall with Pr = 0.7

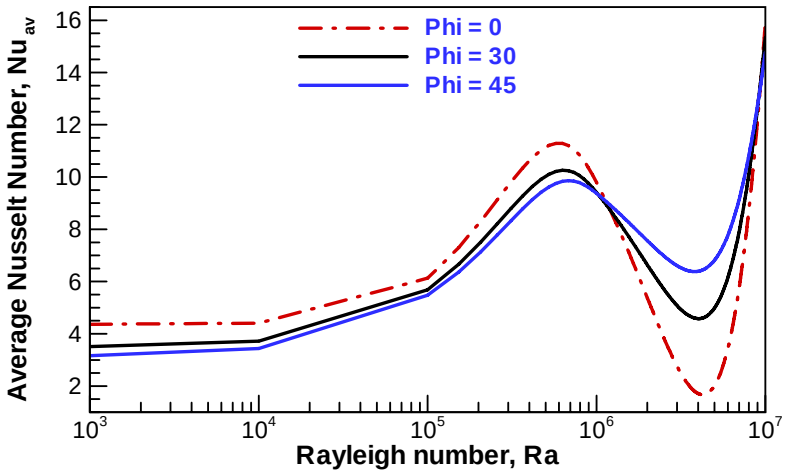

Figure 6.47: Average Nusselt Number vs Rayleigh number for non-uniform heating of bottom wall with Pr = 1000

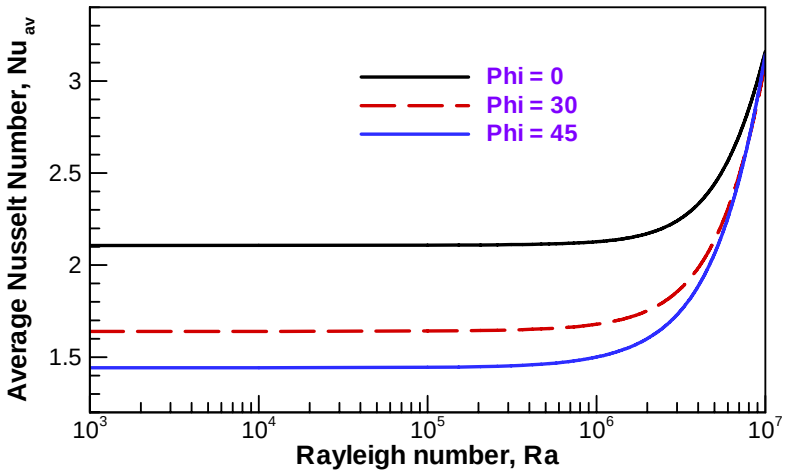

Figure 6.48: Average Nusselt Number vs Rayleigh number for non-uniform heating of side wall with Pr = 0.026

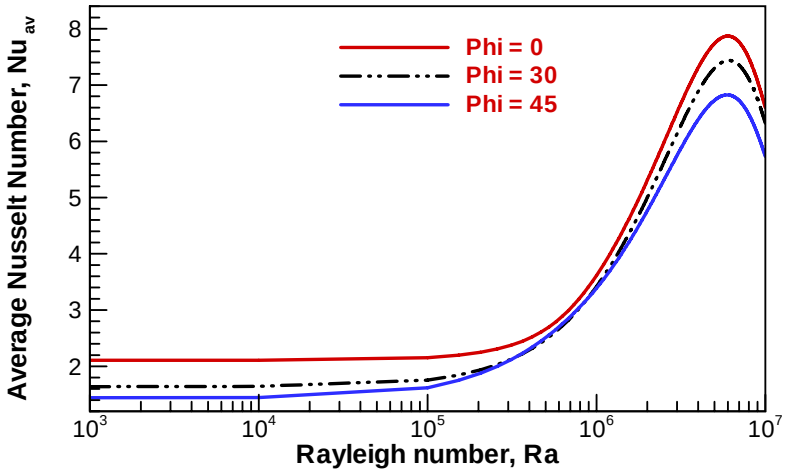

Figure 6.49: Average Nusselt Number vs Rayleigh number for non-uniform heating of side wall with Pr = 0.7

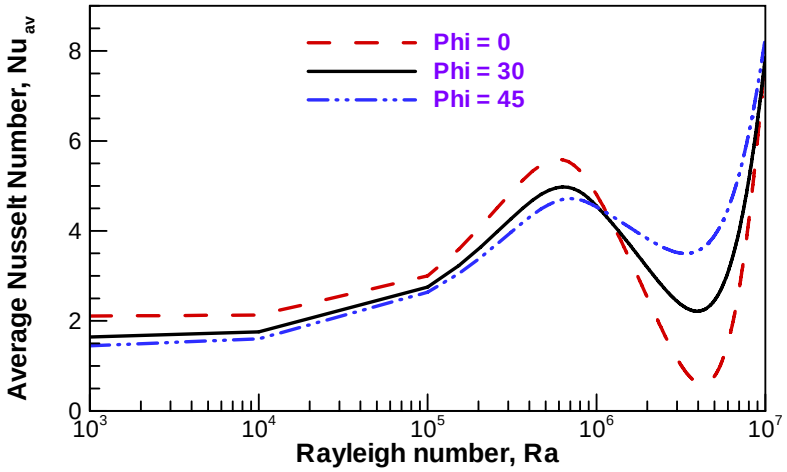

Figure 6.50: Average Nusselt Number vs Rayleigh number for non-uniform heating of side wall with Pr = 1000

6.5 Chapter Summary

Two-dimensional laminar steady state MHD free or natural convection within trapezoidal cavity for non-uniformly heated of bottom wall has been analyzed with heatlines concept. A finite element method for steady-state incompressible MHD free or natural convection flow is presented. The finite element equations were derived from the governing flow equations that consist of the conservation of mass, momentum, and energy equations. The derived finite element equations are nonlinear requiring an iterative technique solver. The Newton-Raphson iteration method has applied to solve these nonlinear equations for solutions of the nodal velocity component, temperature, and pressure by considering Prandtl numbers of 0.026, 0.7, 1000, Hartman numbers of 50 and also Rayleigh numbers of 10^3 to 10^7. The results show that

- The heat transfer rate is maximum near the edge of the wall and the rate is minimum near the center of the wall irrespective of all angles (ϕ) for non-uniform heating of the bottom wall for Rayleigh number 10^3 to 10^7 gradually.

- Heat transfer depends on Prandtl number and heat transfer rate is maximum near the edge of the wall and the rate is minimum near the center of the wall irrespective of all angles (ϕ) for non-uniform heating of the bottom wall.

- ❖ Thermal boundary layer thickness is thinner for increasing of Rayleigh number due to upsurge of convective heat transfer rate.
- ❖ Local Nusselt number for non-uniform bottom heating is largest at the bottom edge of the side wall, and thereafter that decreases sharply upto a point which is very near to the bottom edge.
- ❖ The heat transfer rate average Nusselt Number, Nu_{av} increases with the increase of Rayleigh number, Ra, for non-uniform heating of bottom wall.
- ❖ The heat transfer rate average Nusselt Number, Nu_{av} increases with the increase of Rayleigh number, Ra, for non-uniform heating of side wall.
- ❖ Various vortices entering into the flow field and secondary vortex at the vicinity boundary wall and bottom wall of the cavity is seen in the streamlines.

CHAPTER 7

CONCLUSIONS

The conjugate effects of conduction and MHD free or natural convection flow in a trapezoidal cavity with some possible boundary conditions are the fundamental objective of this work. The overall work can be summed up through the subsequent conclusions.

7.1 Summary of the Major Outcomes

In this authentication, the effect of conduction on free or natural convection flow and the significance of conduction on MHD free convection within trapezoidal cavity with uniformly and non-uniformly heated bottom based on heatline concept have been studied. In cases of uniform heating, the stream line, Total heat flux and thermal fields as well as characteristics of heat transfer process particularly its expansion has been evaluated in chapter 4. On the basis of the analysis the following conclusions have been drawn:

- The heat transfer rate is maximum near the edge of the wall and the rate is minimum near the center of the wall irrespective of all angles (ϕ) for uniform heating of the bottom wall for Rayleigh number 10^3 to 10^7 gradually.

- The average Nusselt number (*Nu*) at the uniform heating of bottom wall is the highest for the angle 0^0 when Rayleigh number 10^7, whereas the lowest heat transfer rate for the angle $45^0$when Rayleigh number 10^3. Moreover, the average Nusselt number, the uniform heated bottom wall is higher than those obtained with the non-uniform heated bottom wall for different angle.

- The average Nusselt number (*Nu*) at the uniform heating of side wall is the highest for the angle 0^0 when Rayleigh number 10^7, whereas the lowest heat transfer rate for the angle 45^0 when Rayleigh number 10^3. Moreover, the average Nusselt number, the uniform heating of side wall is higher than those obtained with the non-uniform heating of side wall for different angle.

- Heat transfer depends on Prandtl number and heat transfer rate is maximum near the edge of the wall and the rate is minimum near the center of the wall

irrespective of all angles (ϕ) for uniform heating of the bottom wall for different prandtl number.

- ❖ Thermal boundary layer thickness is thinner for increasing of Rayleigh number due to upsurge of convective heat transfer rate.
- ❖ Local Nusselt number for uniform bottom heating is largest at the bottom edge of the side wall, and thereafter that decreases sharply upto a point which is very near to the bottom edge.
- ❖ The heat transfer rate average Nusselt Number, Nu_{av} increases with the increase of Rayleigh number, Ra, for uniform heating of bottom wall.
- ❖ The heat transfer rate average Nusselt Number, Nu_{av} increases with the increase of Rayleigh number, Ra, for uniform heating of side wall.
- ❖ Various vortices entering into the flow field and secondary vortex at the vicinity boundary wall and bottom wall of the cavity is seen in the streamlines.

In cases of non- uniform heating, the stream line, Total heat flux and thermal fields as well as characteristics of heat transfer process particularly its expansion has also been evaluated in chapter 4. On the basis of the analysis the following conclusions have been drawn:

- ❖ The heat transfer rate is maximum near the edge of the wall and the rate is minimum near the center of the wall irrespective of all angles (ϕ) for non-uniform heating of the bottom wall for Rayleigh number 10^3 to 10^7 gradually.
- ❖ The average Nusselt number (*Nu*) at the non-uniform heating of bottom wall is the highest for the angle 0^0 when Rayleigh number 10^7, whereas the lowest heat transfer rate for the angle $45^0$when Rayleigh number 10^3. Moreover, the average Nusselt number, the non-uniform heating of bottom wall is lower than those obtained with the uniform heating of bottom wall for different angle.
- ❖ The average Nusselt number (*Nu*) at the non-uniform heating of side wall is the highest for the angle 0^0 when Rayleigh number 10^7, whereas the lowest heat transfer rate for the angle 45^0 when Rayleigh number 10^3. Moreover, the average Nusselt number, the uniform heating of side wall is higher than those obtained with the non-uniform heating of side wall for different angle.

- ❖ Heat transfer depends on Prandtl number and heat transfer rate is maximum near the edge of the wall and the rate is minimum near the center of the wall irrespective of all angles (ϕ) for non-uniform heating of the bottom wall for different prandtl number.

- ❖ Thermal boundary layer thickness is thinner for increasing of Rayleigh number due to upsurge of convective heat transfer rate.
- ❖ Local Nusselt number for non-uniform bottom heating is largest at the bottom edge of the side wall, and thereafter that decreases sharply upto a point which is very near to the bottom edge.

- ❖ The heat transfer rate average Nusselt Number, Nu_{av} increases with the increase of Rayleigh number, Ra, for non-uniform heating of bottom wall.
- ❖ The heat transfer rate average Nusselt Number, Nu_{av} increases with the increase of Rayleigh number, Ra, for non-uniform heating of side wall.
- ❖ Various vortices entering into the flow field and secondary vortex at the vicinity boundary wall and bottom wall of the cavity is seen in the streamlines.

7.2 Comparison of Uniform and Non-Uniform Heating

The streamlines, isotherms and heatlines have been influenced by MHD free convection within trapezoidal cavity with uniformly and non-uniformly heated bottom wall. The heat transfer rate for uniform heating of bottom and side wall is higher than non-uniform heating of bottom and side wall at different Rayleigh number, Ra. The average Nusselt number increases with the increases of Rayleigh number, Ra = 10^3 – 10^7 for uniform and non- uniform heating of bottom and side wall. In order to validate the numerical code, free or natural convection with Pr = 0.7 in a trapezoidal cavity has been solved. The results are compared for uniform and non- uniform heating. Table 6.1 show comparison of the results for uniform and non- uniform heating of bottom wall with Pr = 0.7 and table 6.2 show comparison of the results for uniform and non- uniform heating of side wall with Pr = 0.7. The reason for large difference at high Ra = 10^7 is explained by the fact that the heat transfer is dominated by convection regime.

Ra	Average Nusselt Number, (Nu_{av})					
	Uniformly Heated bottom wall			Non-uniformly Heated bottom wall		
	$\phi = 0^0$	$\phi = 30^0$	$\phi = 45^0$	$\phi = 0^0$	$\phi = 30^0$	$\phi = 45^0$
10^3	5.685321	4.46249	3.892641	4.361568	3.506399	3.157268
10^4	5.686197	4.463856	3.893894	4.365658	3.51229	3.163712
10^5	5.753017	4.666547	4.2141	4.464063	3.729079	3.474017
10^6	8.796366	8.230399	8.011008	7.399533	7.046409	6.97625
10^7	15.497432	14.561562	12.946846	13.37451	12.753801	11.54703

Table 7.1: Comparison of the results for uniform and non- uniform heating of bottom wall with Pr = 0.7.

Ra	Average Nusselt Number, (Nu_{av})					
	Uniformly Heated side wall			Non-uniformly Heated side wall		
	$\phi = 0^0$	$\phi = 30^0$	$\phi = 45^0$	$\phi = 0^0$	$\phi = 30^0$	$\phi = 45^0$
10^3	2.859967	2.239549	1.96883	2.10711	1.640168	1.442333
10^4	2.859702	2.240199	1.970905	2.10876	1.643219	1.446786
10^5	2.88603	2.341693	2.148533	2.154179	1.755563	1.618798
10^6	4.39259	4.125596	4.102104	3.615316	3.418606	3.388847
10^7	7.742302	7.407918	6.794414	6.597279	6.32338	5.729601

Table 7.2: Comparison of the results for uniform and non-uniform heating of side wall with Pr = 0.7.

7.3 Further Works

The following recommendation can be put forward for the further work on this present research.

- In the future, the study can be extended by dissimilar physics like radiation effects, heat generation and tube effects.
- Effect of conduction on heat flow for MHD free convection within a trapezoidal cavity with a circular and square cylinder block
- Effect of conduction on heat flow for MHD free convection within a trapezoidal cavity with joule heating effect.

- Effect of conduction on heat flow for MHD free convection within a trapezoidal cavity with a heat conducting circular and square cylinder.
- Effect of conduction on heat flow for MHD free convection within a trapezoidal cavity with a heated circular and square cylinder block.
- Effect of conduction on heat flow for MHD free convection within a trapezoidal lid-driven cavity for different boundary conditions
- Investigation can be performed by using magnetic fluid within the porous medium and changing the boundary conditions of the cavity's walls.
- Effect of conduction on heat flow for MHD free convection within a trapezoidal double lid-driven cavity for different boundary conditions.
- Two-dimensional fluid flow and heat transfer has been analyzed in this thesis. So this consideration may be extended to three-dimensional analyses to explore the effects of parameters on flow fields and heat transfer in cavities. In addition, the problem of fluid flow and heat transfer along with heat generating cylinder may be studied in three-dimensional cases.

REFERENCES

Aggarwal S.K., Manhapra A., Use of heatlines for unsteady buoyancy-driven flow in a cylindrical enclosure, J. Heat Trans. – Trans. ASME, Vol. 111, pp. 576–578, 1989.

Al-Amiri A.M., Khanafer K.M., Pop I., Numerical simulation of combined thermal and mass transport in a square lid-driven cavity, Int. J. Thermal Sci., Vol.46 Issue 7, pp. 662–671, 2007.

Anandalakshmi R., Basak T., "Heat flow visualization for natural convection in rhombic enclosures due to isothermal and non-isothermal heating at the bottom wall", International Journal of Heat and Mass Transfer, Vol. 55, Issue 4, pp. 1325-1342, 31 January 2012,.

Baez E. and Nicolas A., "2D natural convection flows in tilted cavities: Porous media and homogeneous fluids", Int. J. Heat and Mass Transfer, vol. 49, pp. 4773-4785, 2006.

Basak T., Anandalakshmi R., Kumar Pushpendra, Roy S., "Entropy generation vs energy flow due to natural convection in a trapezoidal cavity with isothermal and non-isothermal hot bottom wall", Energy, Vol. 37, Issue 1, pp. 514-532, January 2012.

Basak T., Ramakrishna D., Roy S., Matta A., Pop I., "A comprehensive heatline based approach for natural convection flows in trapezoidal enclosures: Effect of various walls heating", International Journal of Thermal Sciences, Vol.50, Issue 8, pp. 1385-1404, August 2011.

Basak T., Roy S, Pop I., Heat flow analysis for natural convection within trapezoidal enclosures based on heatline concept, Int.J. Heat Mass Transfer, Vol.52, pp. 2471-2483, March 2009.

Basak T., Roy S., Balakrishnan A.R., Effects of thermal boundary conditions on natural convection flows within a square cavity, Int. J. Heat Mass Transfer, Vol.49 Issues 23-24, pp. 4525-4535, 2006.

Basak T., Roy S., Matta A. , Pop I., “Analysis of heatlines for natural convection within porous trapezoidal enclosures: Effect of uniform and non-uniform heating of bottom wall” International Journal of Heat and Mass Transfer, Vol. 53, Issues 25–26, pp. 5947-5961, December 2010.

Basak T., Roy S., Singh A., Balakrishnan A.R., “Natural convection flows in porous trapezoidal enclosures with various inclination angles”, International Journal of Heat and Mass Transfer, Vol. 52, Issues 19–20, pp. 4612-4623, September 2009 (a).

Basak T., Roy S., Singh A., Pandey B. D., “Natural convection flow simulation for various angles in a trapezoidal enclosure with linearly heated side wall(s)”, International Journal of Heat and Mass Transfer, Vol. 52, Issues 19–20, pp. 4413-4425, September 2009(b).

Basak T., Roy S., Singh A., Pop I., “Finite element simulation of natural convection flow in a trapezoidal enclosure filled with porous medium due to uniform and non-uniform heating”, International Journal of Heat and Mass Transfer, Vol.52, Issues 1–2, pp. 70-78, 15 January 2009.

Basak T., Roy S., Singh S. K., Pop I., “Finite element simulation of natural convection within porous trapezoidal enclosures for various inclination angles: Effect of various wall heating”, International Journal of Heat and Mass Transfer, Vol. 52, Issues 19–20, pp. 4135-4150, September 2009(c).

Basak T.,Roy S., Finite element analysis of natural convection flows in a square cavity with non-uniformly heated wall(s), Int. J. Eng. Sci., vol. 43 Issues 8-9, pp. 668-680, 2005.

Baytaş A.C., Pop I., “Natural convection in a trapezoidal enclosure filled with a porous medium”, International Journal of Engineering Science, Vol.39, Issue 2, pp. 125-134 January 2001.

Bejan A., Convection Heat Transfer, third ed., Wiley, New York, 2004.

Bello-Ochende F.L., A heat function formulation for thermal convection in a square cavity, Int. Comm. Heat Mass Transfer, Vol. 15, pp. 193–202, 1988.

Boussaid M., Djerrada A., Bouhadef M., Thermosolutal transfer within trapezoidal cavity, Num. Heat Transfer A, Vol. 43, pp. 431–448, 2003.

Boussaid M., Mezenner A., Bouhadef M., “Convection naturelle de chaleur et de masse dans une cavité trapézoïdale”, International Journal of Thermal Sciences, Vol. 38, Issue 4, pp. 363-371, April 1999.

Chattopadhyay H., Dash S.K., Numerical visualization of convective heattransfer from a sphere-with and without radial mass efflux, Int. J. Num. Meth. Heat Fluid Flow, Vol. 5 Issue 8, pp. 705–716, 1995.

Costa V.A.F., Bejan’s heatlines and masslines for convection visualization and analysis, Appl. Mech. Rev., vol. 59 Issue 3, pp. 126–145, 2006.

Costa V.A.F., Heatline and massline visualization of laminar natural convection boundary layers near a vertical wall, Int. J. Heat Mass Transfer, Vol. 43 No. 20, pp. 3765-3774, 2000.

Costa V.A.F., Unification of the streamline, heatline and massline methods for the visualization of two-dimensional transport phenomena, Int. J. Heat Mass Transfer, Vol. 42 No.1, pp. 27-33, 1999.

Costa V.A.F., Unified streamline, heatline and massline methods for the visualization of two-dimensional heat and mass transfer in anisotropic media, Int. J. Heat Mass Transfer, Vol. 46 No.8, pp. 1309-1320, 2003.

Deng Q.H., Tang G.F., Numerical visualization of mass and heat transport for conjugate natural convection/heat conduction by streamline and heatline, Int. J. Heat Mass Transfer, Vol. 45 Issue 11, pp. 2373–2385, 2002.

Eyden J.T.V.D., Meer Th.H. V. D., Hanjalić K., Biezen E., Bruining J., “Double-diffusive natural convection in trapezoidal enclosures”, International Journal of Heat and Mass Transfer, Vol. 41, Issue 13, pp. 1885-1898, July 1998.

Fusegi T., Hyun J.M., Kuwahara K., Natural convection in a differentially heated square cavity with internal heat generation, Num. Heat transfer A, Vol. 21, pp. 215-229, 1992.

Hall J.D., Bejan A., Chaddock J.B., Transient natural convection in a rectangular enclosure with one heated side wall, Int. J. Heat Fluid Flow, vol. 9, pp. 396-404, 1988.

Ho C.J., Lin Y.H., Natural-convection of cold water in a vertical annulus with constant heat-flux on the inner wall, J. Heat Transfer – Trans. ASME, Vol. 112 Issue 1, pp. 117–123, 1990(a).

Ho C.J., Lin Y.H., Thermal-convection heat-transfer of air water layers enclosed in horizontal annuli with mixed boundary-conditions, Warme und Stoffubertragung – Thermo Fluid Dyn., Vol 24 Issue 4, pp. 211–224, 1989.

Ho C.J., Wu M.S., Jou J.B., Analysis of buoyancy-aided convection heat-transfer from a horizontal cylinder in a vertical duct at low Reynolds-number, Warme und Stoffubertragung – Thermo Fluid Dyn., Vol. 25 Issue 6, pp. 337–343, 1990(b).

Hooman K., Gurgenci H., Heatline visualization of natural convection in a porous cavity occupied by a fluid with temperature-dependent viscocity, J.heat Transfer-Trans. ASME 130, Article Number : 012501, 2008.

Hung C. I., Tsai J. S. and Chen C. K., “Nonlinear stability analysis of magnetohydrodynamic condensate film flow down a vertical plate with constant heat flux”, Int. J. Heat and Mass Transfer, vol. 39, no. 4, pp. 877-884, 1996.

Hyun J.M., Lee J.W., Numerical solutions of transient natural convection in a square cavity with different sidewall temperature, Int. J. Heat Fluid Flow, Vol. 10, pp. 146–151, 1989.

Kahveci K., Öztuna S., MHD natural convection flow and heat transfer in a laterally heated partitioned enclosure, European Journal of Mechanics - B/Fluids, Vol.28 No.6, pp. 744-752, (November-December) 2009.

Karyakin Y.E., Transient natural convection in prismatic enclosures of arbitrary cross-section, Int. J. Heat Mass Transfer, Vol. 32, pp. 1095–1103, 1989.

Kimura S., Bejan A., The heatline visualization of convective heat-transfer, J.Heat Transfer – Trans. ASME, Vol. 105 Issue 4 , pp. 916–919, 1983.

Kumar B.V. Rathish, Kumar Bipin., “Parallel computation of natural convection in trapezoidal porous enclosures”, Mathematics and Computers in Simulation, Vol. 65, Issue 3, pp. 221-229, 22 April 2004.

Kumar Subodh, “Natural convective heat transfer in trapezoidal enclosure of box-type solar cooker”, Renewable Energy, Vol. 29, Issue 2, pp. 211-222, February 2004.

Kuyper R.A., Hoogendoorn C.J., Laminar natural convection flow in trapezoidal enclosures, Num. Heat transfer A, Vol. 28, pp. 55 – 67, 1995.

Lage J.L., Bejan A., The Ra–Pr domain of laminar natural convection in an enclosure heated from the side, Num. Heat Transfer A, Vol. 19, pp. 21–41, 1991.

Lage J.L., Bejan A., The resonance of natural convection in an enclosure heated periodically from the side, Int. J. Heat Mass Transfer, Vol. 36, pp. 2027–2038, 1993.

Littlefield D., Desai P., Buoyant laminar convection in a vertical cylindrical annulus, J. Heat Transfer – Trans. ASME, Vol. 108 Issue 4, pp. 814–821, 1986.

Lyican L., Bayazitoglu Y., An analytical study of natural convective heat transfer within trapezoidal enclosure, ASME Trans. J. Heat transfer, Vol. 102, pp.640-647, 1980.

Mobedi M., Conjugate natural convection in a square cavity with finite thickness horizontal walls, Int. Commun. Heat Mass Transfer, Vol. 35 No. 4, pp. 503-513, 2008.

Nasrin Rehena, Parvin Salma, “Investigation of buoyancy-driven flow and heat transfer in a trapezoidal cavity filled with water–Cu nanofluid”, International Communications in Heat and Mass Transfer, Vol. 39, Issue 2, pp. 270-274, February 2012,.

Natarajan E., Basak T., Roy S., “Natural convection flows in a trapezoidal enclosure with uniform and non-uniform heating of bottom wall”, International Journal of Heat and Mass Transfer, Volume 51, Issues 3–4, pp. 747-756, February 2008.

Natarajan S. K., Reddy K.S., Mallick T. K., “Heat loss characteristics of trapezoidal cavity receiver for solar linear concentrating system”, Applied Energy, Vol.93, pp. 523-531, May 2012.

Nicolette V.F., Yang K.T., Lloyd J.R., Transient cooling by natural convection in a two-dimensional square enclosure, Int. J. Heat Mass Transfer, Vol. 28, pp. 1721–1732, 1985.

Papanicolaou E., Belessiotis V., “Double-diffusive natural convection in an asymmetric trapezoidal enclosure: unsteady behavior in the laminar and the turbulent-flow regime”, International Journal of Heat and Mass Transfer, Vol. 48, Issue 1, pp. 191-209, January 2005,.

Patterson J., Imberger J., Unsteady natural convection in a rectangular cavity, J. Fluid Mech., Vol. 100, pp. 65–86, 1980.

Peric M., Natural convection in trapezoidal cavities, Num. Heat transfer A,Vol.24, pp. 213 – 219, 1993.

Ram G.and Mishra R. S., “Unsteady flow through magnetohydrodynamic porous media”, Indian J. Pure Appl. Maths., vol. 8, pp. 637-647, 1977.

Raptis A. and Perdikis C., “Magnetohydrodynamics effects on mass transfer flow through porous medium”, Astrophys. Space Sci., vol. 113, pp. 53-58, 1985.

Rudraiah N., Ramaiah B. K. and Rajasekhar B. M., “Hartmann flow over a permeable bed”, Int. J. Engng. Sci., vol. 13, pp. 1-24, 1975.

Saha L.K., Hossain M.A., Rama Subba Reddy Gorla, Effect of Hall current on the MHD laminar natural convection flow from a vertical permeable flat plate with uniform surface temperature, Int. J. Thermal Sci., Vol. 46 No.8, pp. 790-801, August 2007.

Saleh H., Roslan R., Hashim I., “Natural convection heat transfer in a nanofluid-filled trapezoidal enclosure”, International Journal of Heat and Mass Transfer, Vol. 54, Issues 1–3, pp. 194-201,15 January 2011.

Saleh H., Roslan R., Hashim I., “Natural convection in a porous trapezoidal enclosure with an inclined magnetic field”, Computers & Fluids, Vol. 47, Issue 1, pp. 155-164, August 2011,.

Singh P. L., Sarviya R.M., Bhagoria J.L., “Heat loss study of trapezoidal cavity absorbers for linear solar concentrating collector”, Energy Conversion and Management, Vol. 51, Issue 2, pp. 329-337, February 2010.

Singh, S., and Sharif, M. A. R., “Mixed convective cooling of a rectangular cavity with inlet and exit openings on differentially heated side walls”. Numer. Heat Transfer, Part A Vol. 44, pp. 233–253, 2003.

Tawil M. A. E. and Kamel M. H., “MHD flow under stochastic porous media”, Energy Conserv. Mgmt., vol. 35, pp. 991-997, 1994.

Varol Y., “Natural convection for hot materials confined within two entrapped porous trapezoidal cavities”, International Communications in Heat and Mass Transfer, Vol. 39, Issue 2, pp. 282-290, February 2012,.

Varol Y., “Natural convection in divided trapezoidal cavities filled with fluid saturated porous media”, International Communications in Heat and Mass Transfer, Vol. 37, Issue 9, pp. 1350-1358, November 2010,.

Varol Y., Oztop H. F., Pop I., “Entropy analysis due to conjugate-buoyant flow in a right-angle trapezoidal enclosure filled with a porous medium bounded by a solid vertical wall”, International Journal of Thermal Sciences, Vol. 48, Issue 6, pp. 1161-1175, June 2009.

Varol Y., Oztop H. F., Pop I., “Maximum density effects on buoyancy-driven convection in a porous trapezoidal cavity”, International Communications in Heat and Mass Transfer, Vol. 37, Issue 4, pp. 401-409, April 2010.

Varol Y., Oztop H.F., Mobedi M., Pop I., Visualization of natural convection heat transport using heatline method in porous non-isothermally heated triangular cavity, Int. J. Heat Mass Transfer, Vol. 51 Issues 21–22, pp. 5040–5051, 2008(a).

Varol Y., Oztop H.F., Pop I., Natural convection in right-angle porous trapezoidal enclosure with partially cooled frominclined wall. Int. Commun. Heat Mass Transfer, Vol. 36 No. 1, pp. 6-15, 2009.

Varol Y., Oztop H.F., Pop I., Numerical analysis of natural convection in an inclined trapezoidal enclosure filled with a porous medium, Int. J. Thermal Sci., Vol. 47 No.10, pp. 1316-1331, 2008(b).

Wallace W. E., Pierce C. I. and Swayer W., “Experiments on the flow of mercury in porous media in a transverse magnetic field”, Tech. Rep. TN23, U7, no. 7259, US Bureau of Mines, (1969, digitized 19 Mar 2009).

Xia C., Murthy J.Y., Buoyancy-driven flow transitions in deep cavities heated from below, ASME Trans. J. Heat Transfer, Vol. 124, pp. 650–659, 2002.

Yih K. A., “The effect of uniform suction/ blowing on heat transfer of magnetohydrodynamic Hiemenz flow through porous media”, Acta Mechanics, vol. 130, pp. 147-158, 1998.

Zhao F.Y., Liu D., Tang G.F., Natural convection in an enclosure with localized heating and salting from below, Int J. Heat Mass Transfer, Vol. 51 Issues 11-12, pp. 2889-2904, 2008.

Zhao Fu-Yun, Liu Di, Tang Guang-Fa, Application issues of the streamline, heatline and massline for conjugate heat and mass transfer, Int. J. Heat Mass Transfer, Vol. 50, pp. 320–334, 2007.

Zienkiewicz, O. C., and Taylor, R. L., “The finite element method”, Fourth Ed., McGraw-Hill, 1991.